Poly(fluoroalkyl methacrylates) from trifluoroethene: synthesis & properties

Watson, Michael Steven

Poly(Fluoroalkyl Methacrylates) from Trifluoroethene:

Synthesis & Properties

Michael Steven Watson

St.Aidan's College

University of Durham

A thesis submitted for the Degree of Doctor of Philosophy to the

University of Durham

December 1997

Abstract

Poly(Fluoroalkyl Methacrylates) from Trifluoroethene: Synthesis and Properties

This work combines two technologically important areas of polymer science, namely polymer blends and fluoropolymers.

New fluoroalkyl methacrylate polymers have been synthesised making use of the telomerisation of trifluoroethylene, to give a partially fluorinated sidechain on a methacrylate backbone.

After characterisation, these materials were mixed with poly(methyl methacrylate), and the bulk phase behaviour and surface properties of these blends was investigated.

Using differential scanning calorimetry and small angle neutron scattering, it has been established that these materials are in a state of incipient phase separation.

Surface energetics of films of these blends have been investigated using contact angle measurements, and the near surface depth profile has been studied using neutron reflectivity and Rutherford backscattering spectrometry

Acknowledgements

As ever, these few words seem totally inadequate in expressing my gratitude to my supervisor, Randal Richards, for his support over the past three years, and perhaps more importantly, the confidence he had in me in awarding me the studentship in the first place. I wonder if he'd do it again, given the chance?

For the existence of the studentship in the first place and the financial support that came with it, I am indebted to Dr Dick Powell of ICI KLEA, Runcorn. While the results of the work weren't entirely what was expected, I do hope I've offered good value for money at least. The British hi-fi industry and a number of classic car restoration firms have also benefited greatly from this fund.

I must also thank Anwar Gilani and Professor Dick Chambers for supply of materials and any number of useful discussions.

I have worked here in the IRC in Polymer Science and Technology in Durham for quite a long time now (on and off). My memories of this place are only of happiness, and this is a great credit to Jim Feast, Randal, Jean and Helene for keeping the place running smoothly allowing science to be done in the best possible environment. A major part of this environment are the people involved in the operation; fellow postgraduates, postdocs, technicians etc. I couldn't have wished for a more friendly, supportive group of people to share the trials and tribulations this kind of work throws up every day. In particular, I must thank Helen Thompson and Foggy for getting me through the hell that is the Rutherford lab.

Oh yes! The Rutherford lab...I was trying to forget that! Well, like most "Randalites" (a name coined by a former inmate here) I have served my sentence at the delightful place that is the Rutherford lab. Breakfast times spent with a strange empathy with the myxomatosis-ridden rabbits outside, having spent the night changing samples, hurtling round the bleak Oxfordshire countryside feeling like Steve McQueen in "The Great Escape", and the delicious buns which come out of the machine in the instrument hall all make for a most memorable experience. I am, of course, extremely grateful to the instrument scientists and technicians down there for keeping me supplied with neutrons and correcting my

mistakes. Particular thanks must go to Drs Steve King and David Bucknall for their specific assistance in the execution of the small angle scattering and reflectivity experiments, although I must add that if I ever see a reflectometer again, it might be too soon! No offence meant, David.
Finally as far as work goes, I must acknowledge Dr Tony Clough and colleagues of the University of Surrey for the backscattering spectrometry work. I must also thank Tony for introducing me to pigeon in chocolate and strawberry sauce, an amazing dish at an equally amazing watering hole.

My residence in St.Aidan's College, Durham, has been a source of continuous pleasure, amazement and incredulity over the past years, particularly the last three as a member of the senior common room. The SCR itself has done well to contain the enormous animosity which resident members feel for one another, and violence had seldom, if ever, erupted. In particular, I feel I must mention one of our newest members, Sam, for his expertise in dismembering certain game birds for later consumption, and Mischief the cat for her ever cheerful and hungry presence. The rest of you lot are mentioned implicitly; thanks for the good times.

Finally, a couple of specific mentions for some very special people. I am eternally grateful to Joanna Greenwood and Catherine Short for their love, support and friendship over the years since that fateful day in Langdale. I must also thank Ed Lacey for his wonderfully laid-back attitude on life, many a late night discussing metaphysics over a bottle of port, and helping to develop many of the eccentricities that make me what I am. I count myself very lucky to have such wonderful friends. Last, but certainly the most, I must thank my parents and family back home in the 'shire, without whose love, nurture and, most of all, money, all this would have been impossible.

Mike Watson. Durham 1997.

Memorandum

The work reported in this thesis was carried out in the chemistry laboratories of the Interdisciplinary Research Centre in Polymer Science & Technology, University of Durham, the ISIS facility at the Rutherford Appleton Laboratory and the ion beam facility of the University of Surrey physics department between October 1994 and September 1997. This work has not been submitted for any other degree either in Durham or elsewhere and is the original work of the author except where acknowledged by means of appropriate reference.

Statement of Copyright

Financial Support

The author gratefully acknowledges the financial support from ICI KLEA, Runcorn

Units & Symbols

SI units have been used throughout this work, with the exception of the use of the gram (g) rather that the unwieldy kilogram, the Angstrom (Å) as a unit of length ($1x10^{-10}$m) in reference to small angle neutron scattering and neutron reflectivity and the litre (l, $1x10^{-3}m^3$) is used as the unit of volume. The spectroscopist's unit of frequency, cm^{-1}, is also used where relevant. Currently accepted abbreviations have been used to signify the order of magnitude applicable to the unit in question, *e.g.* μm signifies a length of the order of $1x10^{-6}$m.

Abbreviations

AIBN	α,α, bis azoisobutyronitrile
CMC	Critical Micelle Concentration
DSC	Differential Scanning Calorimetry
eV	Electron Volt (=$1.609x10^{-19}$ Joules)
FT-IR	Fourier Transform-Infrared Spectroscopy
LCST	Lower Critical Solution Temperature
MEK	Methyl Ethyl Ketone (Butanone)
NMR	Nuclear Magnetic Resonance Spectroscopy
NR	Neutron Reflectometry
PDI	Polydispersity index
P(EthTelMA)	Ethanol-telomer derived methacrylate polymer
P(MeTelMA)	Methanol-telomer derived methacrylate polymer
PMMA	Poly(Methyl Methacrylate)
PTFEMA	Poly(3,3,3, Trifluoroethyl Methacrylate)
RBS	Rutherford Backscattering Spectrometry
RPA	Random Phase Approximation
SANS	Small Angle Neutron Scattering
TGA	Thermogravimetric Analysis
UCST	Upper Critical Solution Temperature
(MW)96/40	Copolymer 7:1 MMA:MeTelMA

Roman Symbols

a	Statistical segment length
A	Area
b	Scattering length
B_{inc}	Incoherent scattering intensity
$C_{p,i}$	Heat capacity, component i
d	Distance between scatterers
e	Charge on electron = 1.609×10^{-19} C
E	Particle energy
f_i	Free volume fraction of component i
G	Gibbs' free energy
H	Enthalpy
I(Q)	Scattering intensity as a function of Q
k_B	Boltzman's Constant = 1.38066×10^{-23} J.K^{-1}
k	Rate constant
m_i	degree of polymerisation of component i
M	Molecular weight, Particle mass
M_n	Number-average molecular weight
M_w	Weight-average molecular weight
M	Molar (concentration in g.l^{-1})
n_i	number of moles of substance i
N_i	Number of molecules of substance i
P(Q)	Form factor as a function of Q
Q	Magnitude of scattering vector
r	Number of polymer repeat units
R	Gas constant = 8.31451 J.K^{-1}.mol^{-1}
$R_g i$	Radius of gyration of polymer i
S	Entropy
S(Q)	Interparticle scattering factor
T	Absolute temperature
T_g	Glass transition temperature
v	Particle velocity, kinetic chain length

V_i	Volume of component i
V_0	Reference volume: $V_i = m_i V_0$
w_i	Weight fraction of component i
W	Number of thermodynamic microstates
W	Work of adhesion
x_i	Mole fraction of component i
z	Coordination number, Flory-Huggins lattice
z^*	Surface excess
Z	Atomic number

Greek Symbols

α	Cubic expansion coefficient; scaling exponent
γ	Surface energy
Γ	Surface concentration
δ	Scattering length density, solubility parameter
Δ	Change in variable; heat
ε	Exchange energy, Stopping cross section
θ	Plane angle
λ	Wavelength
μ	Chemical potential
ν	Neutron refractive index
ρ	Bulk density
σ	Scattering cross section
ϕ	Volume fraction
χ, $\chi_{F\text{-}H}$	Flory-Huggins interaction parameter
χ_{eff}	Effective Flory-Huggins interaction parameter
Ω	Solid angle

Contents

Chapter One

Introduction

1.1. Introduction

Since Staudinger's concept of the macromolecule was finally accepted by a sceptical scientific community in the 1930s, polymer science has undergone a staggering expansion. Early efforts were concentrated on the production of new molecular structures, which would enable improvements to be made in performance or manufacturing techniques. These seminal works drew on the seemingly endless supply of new monomers. With advances in polymer synthesis, the variety of new polymers was further increased by the advent of the block- and graft copolymers, whose composition and properties could be varied by changing the monomer ratios within the chains. While the number of new avenues in polymer synthesis is far from exhausted, the development of a new polymer for every new application has become an expensive and time-consuming business.

Alloying of metals has been known for thousands of years, and attempts were made to exploit this conceptually simple and attractive idea using polymer mixtures. The idea was almost stillborn; in 1953, Flory[1] wrote

"*The critical value of the interaction free energy is so small for any pair of polymers of high molecular weight that it is permissible to state as a principle of broad generality that two high polymers are mutually compatible with one another only if their free energy of interaction is favourable i.e. negative. Since the mixing of a pair of polymers, like the mixing of simple liquids, in the great majority of cases is endothermic, incompatibility of chemically dissimilar polymers is observed to be the rule and compatibility is the exception. The principle exceptions occur among pairs in possession of polar substituents which interact favourably with one another*"

Notwithstanding Flory's prophecy, efforts to exploit the desirable concept of a polymer-polymer mixture have been considerable, and many examples have now been found. For a comprehensive, [if slightly outdated] list, see Sonja Krause's chapter in Paul's book[2]. Specific interactions (*e.g.* hydrogen-bonding[3]) have been identified in many of these cases, so again Flory's words ring true.

1.1.1. Nomenclature

Before the discussion of polymer blends is taken any further, there is a degree of ambiguity in the nomenclature used to discuss these systems which must be addressed. According to the source of a given piece of work, a blend may be described as miscible or compatible, or conversely, immiscible or incompatible. The term "compatible" has been used to describe a number of "blending effects", ranging from those characteristic of a thermodynamically miscible blend to simply describing a material which is commercially useful. In the simplest case, this means that the material shows no signs of gross phase separation, *e.g.* has mechanical properties which are essentially the weighted average of those of its components, a single glass transition, possesses optical clarity etc. Although it is argued that polymer blends do not display true solubility (*i.e.* random mixing on the molecular level)[4], "mutual solubility" is the most rigorous description of a single phase polymer blend.

Miscible polymer blends find considerable technological application where a compromise between the properties of the blends constituents is required. For example, a material with a "tailor-made" refractive index can be made if two miscible polymers can be blended and quenched into an optically transparent state.

A new application which has emerged in the past few years is the use of polymer blends in polymeric light emitting diodes[5]. By blending polymers each emitting at a given wavelength, the emission of the device as a whole can be tuned by varying the composition of the blend[6].

At the opposite end of the "spectrum", a compatible blend may show gross phase separation with poor mechanical cohesion, but the material so produced fulfils a specific role or desired function.

One example in which polymer blending is employed to improve macroscopic properties involves the combination of a rubber or polyolefin with a glassy polymer. In this case, phase separation occurs to produce ductile inclusions within a glassy matrix, with a result that a stiff composite material is produced with enhanced toughness relative to that of the glassy polymer alone.[7]

Another example of a situation where phase separation is employed is an attempt to improve properties of insulation for electrical cables. When exposed to moisture, plastics and rubber absorb water, despite their intrinsically hydrophobic nature. In the case of medium voltage cables, water may diffuse into the insulating material and, under the influence of the electric field, aggregate to form extended water filled dendritic structures known as water-trees[8]. In time, these defects grow across the dielectric and may ultimately cause electrical breakdown and failure of the cable.

One approach that has been adopted with the aim of restricting water tree growth is to add a second incompatible (immiscible) polymer containing hydrophilic groups to the normal dielectric material. This results in the formation of a disperse second phase within the insulation which effectively acts as a sink for

diffusing water molecules so inhibiting their aggregation within the main insulation itself.

In all of the above examples, these blends could be described as "compatible", even though their desirable properties of the latter two stem from their being thermodynamically immiscible.

1.1.2. Determining Polymer-Polymer Miscibility

In the discussion above, a number of references have been made to the physical properties which may be displayed by a particular polymer blend. Therefore, by studying these properties, one can characterise the miscibility of a blend.

Perhaps the most common criterion used to establish the miscibility of a given polymer blend is the detection of a single glass transition temperature. This technique is described in chapter 4 of the current work, and the reader is also referred to texts such as Turi[9] and Mathot[10]. A single glass transition is indicative of miscibility on the same scale as the molecular motion responsible for the glass transition *i.e.* ~0.1μm. Other techniques include viscometry[11] and NMR[12].

To put the terms "miscible" or "immiscible" on a more quantitative basis, the following section will consider the formulations which have been produced to characterise and predict the phase behaviour of polymer blends.

1.2.1. Ideal Polymer Solution Thermodynamics

Solution theory considers a polymer placed on contiguous sites on a hypothetical lattice, which can then be surrounded by solvent molecules or another polymer to give a solution or polymer blend, respectively. See figure 1.1.

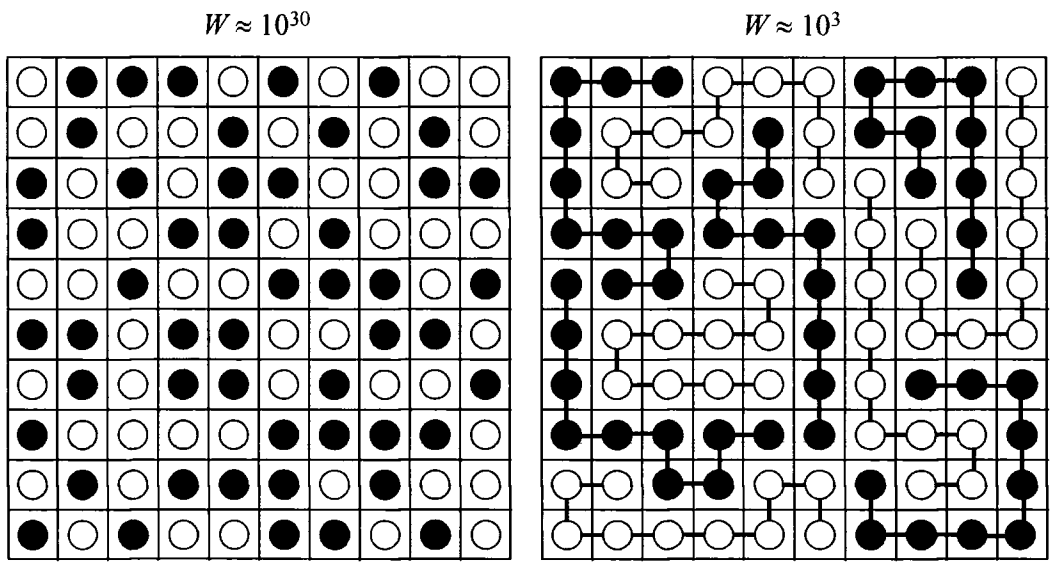

Figure 1.1. Lattice Formalism for Entropy of Mixing Calculations

The entropy of the system is then calculated by applying statistical mechanics, and calculating the entropy of each of the microstates using the Boltzmann law:

$$S = k_B \ln W \qquad \textbf{[1.1]}$$

where S is the entropy of the state, k_B is the Boltzmann constant and W is the number of statistical microstates available to the system.

This gives the following expression:

$$S_C = k_B \ln\left(\frac{N_0!}{N_1!\,N_2!}\right) \qquad \textbf{[1.2]}$$

where the c-subscript denotes combinatorial entropy, N_1 is the number of molecules of component 1, etc., and $N_1 + N_2 = N_0$, the number of cells on the hypothetical lattice.

For large values of N, Stirling's approximation can be applied to the factorial expressions to give:

$$S_C = k_B\left(N_0 \ln N_0 - N_0 - N_1 \ln N_1 + N_1 - N_2 \ln N_2 + N_2\right) \qquad \textbf{[1.3]}$$

which, on dividing by N_0 becomes

$$S_C = -k_B\left[N_1 \ln\left(\frac{N_1}{N_0}\right) + N_2 \ln\left(\frac{N_2}{N_0}\right)\right] \qquad \textbf{[1.4]}$$

Now, (N_i/N_0) is the mole fraction of component i, x_i and $R = k_B N_A$. Therefore

$$S_C = -R\left(n_1 \ln x_1 + n_2 \ln x_2\right) \qquad \textbf{[1.5]}$$

where n_i is the number of moles of component i.

For the pure component, $x_i = 1$. Now ΔS_{mix}, the entropy of mixing, is given by

$$\Delta S_{mix} = S_C - S_1 - S_2 \qquad \textbf{[1.6]}$$

so, for a two component system, we can write:

$$\Delta S^{id}_{mix} = -R\left(n_1 \ln x_1 + n_2 \ln x_2\right) \qquad \textbf{[1.7]}$$

The expression is derived assuming the change in volume on mixing is zero, the molecules are all the same size, all the particles have the same energy *i.e.* $\Delta H = 0$ and the motion of the components about their equilibrium position remains unchanged on mixing. Thus, the free energy of mixing is given by

$$\Delta G^M = -T\Delta S^M = RT(n_1 \ln x_1 + n_2 \ln x_2) \qquad \textbf{[1.8]}$$

i.e., the mixing of small molecules is a spontaneous, entropically driven process.

1.2.1. Flory-Huggins Theory

The above describes an ideal solution, but this is a rare occurrence in solutions of low molecular weight solutes, and even more so in macromolecular systems. Flory[13] and Huggins[14] arrived (independently) at an expression which could correct for deviations from ideality by replacing the mole fractions in equation 7 with volume fractions:

$$\Delta S_{mix} = -RV\left(\frac{\phi_1}{V_1}\ln\phi_1 + \frac{\phi_2}{V_2}\ln\phi_2\right) \qquad \textbf{[1.9]}$$

The volume of a given component can be conveniently expressed in terms of a reference volume V_0, such that $V_i = m_i V_0$ where m_i is the degree of polymerisation of component *i*. The final expression is:

$$\Delta S_{mix} = -\frac{RV}{V_0}\left[\frac{\phi_1}{m_1}\ln\phi_1 + \frac{\phi_2}{m_2}\ln\phi_2\right] \qquad \textbf{[1.10]}$$

Considering this expression, we see that for a simple liquid mixture where $m_1 = m_2 = 1$, the combinatorial entropy attains its ideal value. For solutions where one or both components are macromolecular species, the entropy is reduced from the ideal value in a way which is directly proportional to the degree of polymerisation of the species.

The above derivations consider the free energy of mixing of an *athermal solution* where the entropy deviates from ideal behaviour but the enthalpy of mixing is zero. However, polymer blends come under the description of an *irregular solution*, where there is also an enthalpic contribution to the free energy. Therefore, an expression is needed to account for this enthalpic contribution. We assume this enthalpy term to originate from the formation of new interactions between the solvent and the polymer solute *i.e.* some pure solvent (1-1) and pure

polymer (2-2) interactions will be replaced by solvent-polymer (1-2) interactions[15,16]. If the change in internal energy of the system is ΔU_{mix}

$$\Delta U_{mix} = \Delta\varepsilon_{12} = \varepsilon_{12} - 1/2\left(\varepsilon_{11} + \varepsilon_{12}\right) \qquad \textbf{[1.11]}$$

At constant volume $\Delta U_{mix} = \Delta H_{mix}$, so for q new contacts,

$$\Delta H_{mix} = q\Delta\varepsilon_{12} \qquad \textbf{[1.12]}$$

The number of contacts can be estimated from the lattice model by assuming that the probability of having a lattice cell occupied by a solvent molecule is the volume fraction ϕ_1. This means that each molecule is surrounded by $\phi_1 rz$ solvent molecules. z is the co-ordination number of the lattice and r is the reduced volume per monomer segment. For N_2 polymer molecules:

$$\Delta H_{mix} = rzm_1 N_2 \phi_1 \Delta\varepsilon_{12} \qquad \textbf{[1.13]}$$

From the definition of ϕ_2, we have:

$$rN_2\phi_1 = N_1\phi_2 \qquad \textbf{[1.14]}$$

hence

$$\Delta H_{mix} = zm_1 N_1 \phi_2 \Delta\varepsilon_{12} = zm_1 n_1 \phi_2 \Delta\varepsilon_{12} N_A \qquad \textbf{[1.15]}$$

This is the van Laar expression derived for regular solutions, and shows that this approach can be applied to polymer systems. z is eliminated by introducing a dimensionless parameter χ per solvent molecule, defined as

$$\chi_{12} = \frac{z\Delta\varepsilon_{12} N_A}{RT} \qquad \textbf{[1.16]}$$

which is the difference in energy of a solvent molecule when immersed in pure polymer and when immersed in pure solvent. χ_{12} can be positive or negative, and is theoretically inversely proportional to temperature.

The final expression is:

$$\Delta H_{mix} = RT\chi_{12} m_1 n_1 \phi_2 N_A \qquad \textbf{[1.17]}$$

Using equation 1.17 for ΔH_{mix} and the expression for the combinatorial entropy [1.7], one arrives at the following expression for the free energy of mixing, ΔG_{mix}:

$$\Delta G_{mix} = RT\left(n_1 \ln\phi_1 + n_2 \ln\phi_2 + m_1 n_1 \chi_{12}\phi_2\right) \qquad \textbf{[1.18]}$$

The components of the above equation are separable into the respective enthalpic and entropic contributions to the Gibb's free energy as indicated below:

$$\frac{\Delta G_{mix}}{RT} = \underbrace{m_1 n_1 \chi_{12}\phi_2}_{\text{enthalpic}} + \underbrace{\left(n_1 \ln\phi_1 + n_2 \ln\phi_2\right)}_{\text{entropic}} \qquad \textbf{[1.19]}$$

1.2.2. Effect of Molecular Weight

The unique factor affecting the thermodynamics of polymer blends when compared to other systems is the large molecular weight of the components. The major difference between polymer blends and solutions of small molecules is that the entropy of mixing of a polymer blend will be very small due to the small number of moles of each polymer in the blend. Recasting equation 1.19 in terms of molar volumes, we obtain:

$$\Delta G_{mix} = RTV\left\{\frac{\phi_1 \ln \phi_1}{\tilde{V}_1} + \frac{(1-\phi_1)\ln(1-\phi_1)}{\tilde{V}_2} + \tilde{\chi}_{12}\phi_1\phi_2\right\} \qquad \textbf{[1.20]}$$

ϕ_i is the volume fraction and V_i the molar volume of component *i*. $\tilde{\chi}_{12}$ is the interaction parameter per unit volume. By assuming that both components of the blend have the same molecular weight, M and density ρ, we can replace $\tilde{\chi}_{12}$ with an equivalent parameter $2\rho/M_{cr}$. M_{cr} is a *critical molecular weight*. Making these assumptions, equation 1.20 can be re-written:

$$\Delta G_{mix} = \frac{\rho VRT}{M_{cr}}\left\{\frac{M_{cr}}{M}\left[\phi_1 \ln \phi_1 + (1-\phi_1)\ln(1-\phi_1) + 2\phi_1(1-\phi_1)\right]\right\} \qquad \textbf{[1.21]}$$

For an arbitrary value of the prefactor, this function is shown in figure 1.2:

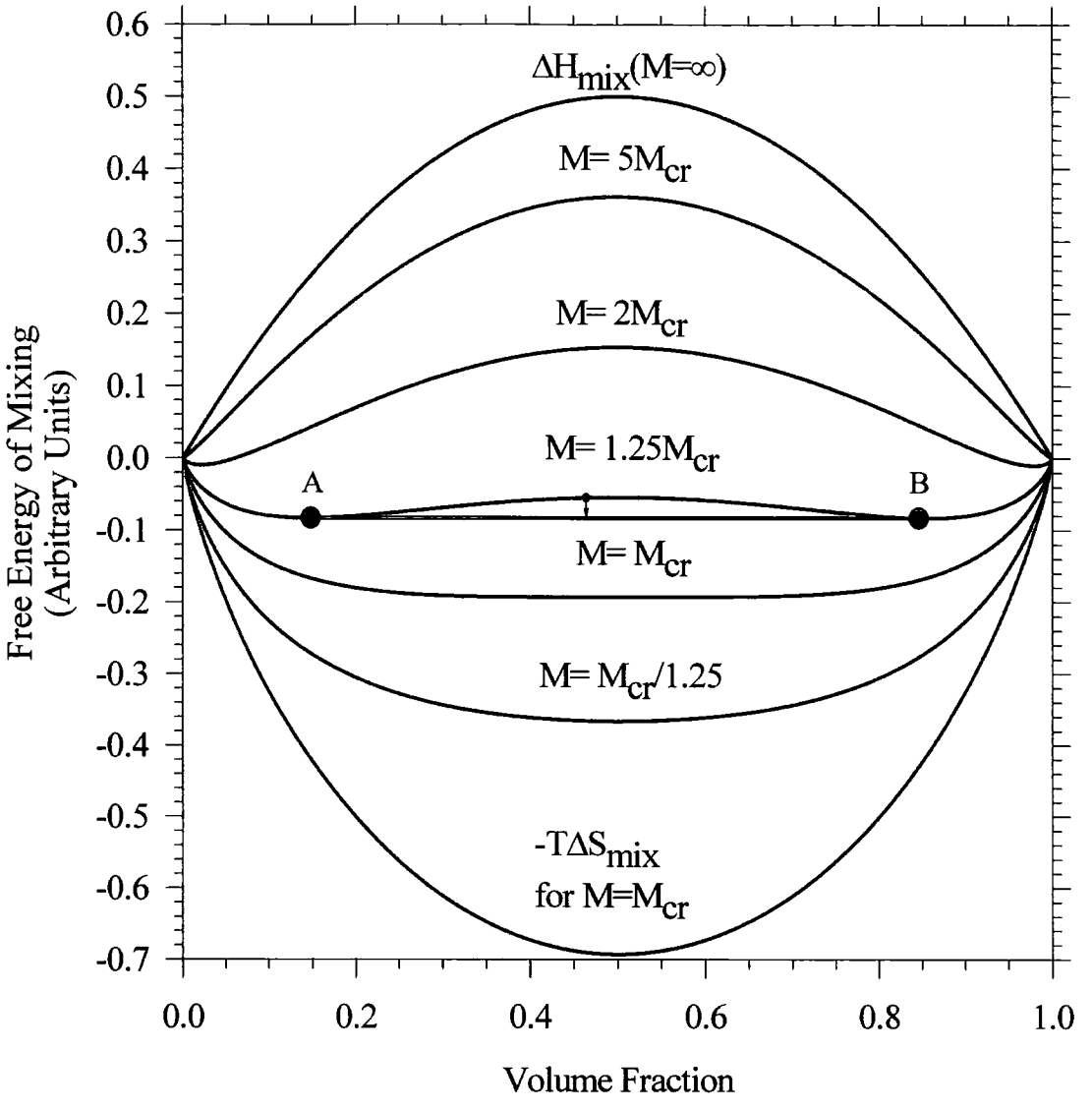

Figure 1.2. Free Energy of Mixing of Two Polymers with the same molecular weight, M, computed from equation 21.

From figure 1.2, one can see the increasing tendency for there being a positive (unfavourable) free energy of mixing as the molecular weight of the blend components increases. Of particular note are the curves where *M* is only slightly higher than the critical molecular weight. We see here that while a blend with a composition lying between A and B is thermodynamically stable with respect to the pure polymers, it is possible for such a blend to reduce its free energy further by separating into phases with compositions A and B. This consideration means

that a negative free energy of mixing is not a sufficient criterion for a polymer blend to be thermodynamically miscible. The second criterion is expressed in equation 1.22:

$$\left(\frac{\partial^2 \Delta G_{mix}}{\partial \phi_i^2}\right)_{T,p} > 0 \qquad \textbf{[1.22]}$$

It is this condition which is violated for some compositions as M exceeds M_{cr}. We see from fig 1.2 that regions of miscibility exist at the extremities of composition, but these become smaller as M increases further.

For cases where $M_1 \neq M_2$, the free energy curves shown in fig 1.2 would be skewed towards the side of the lower molecular weight component, rather than symmetrical as they appear.

1.2.3. Limitations of Flory-Huggins Theory

While the lattice-based theories remain popular because of their innate simplicity, it is also this same simplicity which limits its success in describing the phase behaviour of polymer blends. The "Equation of State" approach seeks to address these failings by relating the thermodynamic variables of temperature, pressure and volume together into a single partition function.

Before any further discussion on the equation of state theories, which in any case will be kept brief, the features of a generic polymer blend phase diagram must be discussed.

As mentioned already, the necessary criteria for a given polymer blend to be miscible at a particular temperature and composition are that the free energy of mixing must be negative, and the second derivative of the free energy with respect to composition must be positive.

In the absence of specific intermolecular interactions, mixing is, in general, an endothermic process *i.e.* $\Delta H_{mix} > 0$. We also see from figure 1.2 that the entropic contribution to the free energy of mixing decreases with increasing molecular weight. If the enthalpic factor outweighs the entropic factor, thermodynamics favours a phase separated system.

The enthalpy of mixing is generally regarded as being independent of temperature, and remains constant for a given specific pairwise interaction. However, the entropic contribution to the free energy of mixing is directly proportional to the absolute temperature, and therefore, this term becomes increasingly favourable towards mixing with an increase in temperature.

Applying these considerations to a polymer blend system, we see that a blend is expected to be immiscible at low temperatures, and miscible above a certain temperature. This is known as upper critical solution temperature (UCST) behaviour, and is shown in figure 1.3.

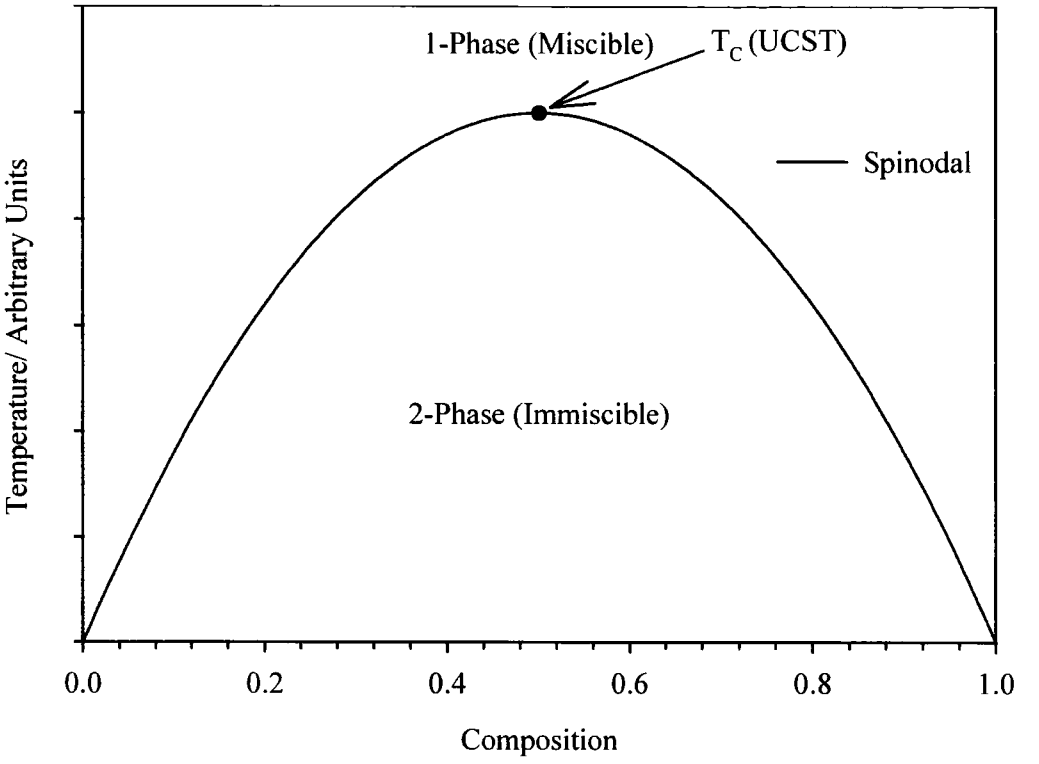

Figure 1.3. Phase Diagram: UCST Behaviour

The original Flory-Huggins theory predicts that χ_{12} decreases monotonically with an increase in temperature [1.16], which means that the miscibility of a polymer-polymer system increases with temperature. This means that the lattice theory can only explain UCST behaviour, and anything that falls outside this behaviour also falls outside the scope of the simple lattice theory.

Such behaviour was first demonstrated by Freeman and Rowlinson[17]. These workers observed phase separation in a polymer solution as the temperature was raised above a critical value, the lower critical solution temperature (LCST). To

account for these observations, the free energy of mixing must increase with temperature.

In general, it is uncommon to observe both UCST and LCST behaviour in one blend system. LCST behaviour is found in systems where there is a favourable enthalpic contribution to the free energy of mixing, *i.e.* where there are specific interactions between the blend constituents. In these systems, it is the reduction in the entropy of mixing which exceeds a critical value, and the favourable enthalpic interactions are cancelled out. UCST behaviour is uncommon in these systems.

UCST behaviour is normally observed in blends of low molecular weight components which have positive values for ΔH_{mix}. In these cases, the phase boundary represents the locus of compositions where the large, favourable entropic contributions overcome the unfavourable enthalpic factor. Conversely, LCST behaviour is uncommon in these systems.

These observations are indicative of a fundamental difference between high- and low molecular weight polymer blends. An UCST results from there being a positive enthalpy of mixing in low molecular weight systems, whereas LCST behaviour is due to a negative entropic contribution in high molecular weight blends.

It is this negative entropic contribution which is difficult to explain within the confines of the lattice theory. The disorder of the system, *i.e.* the combinatorial and excess entropy contributions, would be expected to be favourable towards mixing. As the combinatorial entropy can only be positive, it is the excess entropy term which is responsible for the observed LCST behaviour.

This discrepancy stems from the assumptions made in the formulation of the lattice theory. These assumptions are as follows:

1. The placement of the polymer chains is purely statistical, and that chain flexibility is unchanged on going from the solid to solution states, one can see that the entropy of the system is limited to combinatorial effects, and any contribution to the excess entropy from the flexing of a chain in solution is ignored.
2. A second limitation results from the assumption that there are no specific interactions between the constituent polymers (or, originally, between solvent and polymer). Such interactions could lead to ordering of the solvent in the vicinity of the polymer chain with subsequent reduction in entropy. The implication of point 2 is that polar solutions (or blends) are not adequately represented by the theory. Given that most miscible blends consist of polar constituents, this is a major failing of the lattice approach.
3. Finally, the definition of χ [1.16] shows no composition dependence, a feature which is not borne out by experiment. Evidence is available from small angle neutron scattering and infrared spectroscopy[3,18] to this effect.

The limitations detailed in point 3, above, can to some extent be remedied by recognising that χ is a free energy parameter made up of contributions from the enthalpy and entropy of mixing, *viz.*, $\chi_{12} = \chi_H + \chi_S$, where $\chi_H = -T\frac{d\chi_{12}}{dT}$ and

$$\chi_S = \frac{d(T\chi_{12})}{dT}$$

1.2.4. The Equation of State Approach.

In an attempt to describe more correctly the phase behaviour of polymer blends, an "equation of state" theory has been built up around the original ideas of Prigogine[19]. This approach assumes that a single function containing appropriate reduced variables of temperature, pressure and volume can describe the thermodynamic state of all liquids and liquid solutions. A polymer blend can be considered to be a liquid if all constituents are non-crystalline.

With considerable effort and very precise experimental data, Flory and co-workers modified and applied such a theory to mixtures of poly(ethylene) and poly(isobutylene)[20]. The advent of the personal computer has meant equation of state theories are now becoming a more common way of describing the thermodynamics of polymer solutions and blends.[21-23]

The major drawback with such an approach, particularly over the lattice theory, is its complexity and its need for considerable amounts of precise data. This combines with the findings of McMaster[24], in which the differences between the Flory-Huggins lattice theory and the equation of state theories are found to be small when the values of the reduced variables for both polymers are similar. In simple terms, Flory-Huggins theory works quite well when both polymers have similar thermal expansion coefficients.

1.3. Measurement of the Interaction Parameter.

The measurement of the interaction parameter is considered to be an important technique for assessing the miscibility of high molecular weight polymer systems, since for them to be miscible the interaction parameter must be small or negative. Several techniques have been employed by previous workers to establish values of χ. These include the use of low molecular weight analogues[25], melting point depression of a crystalline component of the blend[1], solvent vapour sorption[2] and small angle neutron scattering (SANS).

The heat of mixing of low molecular weight materials can be measured directly. For high polymers, one can measure the heat of mixing in the presence of a solvent, and if the heat of dissolution of the base polymers is known, Hess's law can be used to extract the value of the interaction parameter. Such a procedure has inherent problems in that the errors accumulate throughout the experiment, and the final result (heat of mixing) is a small value resulting from the difference between much larger numbers. The differences in chemical nature and density of the low molecular weight analogues also lead to difficulties.

The depression of the melting point of a crystalline component can be used to determine the value of χ. In practice it is difficult to determine the thermodynamic equilibrium temperature due to inhomogeneity and diffusion limitation in heating measurements. Supercooling during cooling measurements also causes problems hence the results are dependent on the rate of heating and cooling. Morphological changes must also be taken into consideration. The expression derived by Flory is as follows:

$$[\Delta H_u (T_m^\circ - T_m)/\phi_1 R T_m^\circ] - [T_m/M_1] - [\phi_1 T_m/M_2] = [C/R] - [\chi_{12}\phi_1 T_m] \quad \textbf{[1.25]}$$

where T_m° is the melting point of the pure polymer and T_m is that in the blend. The expression assumes that the morphological contribution is proportional to ϕ_1 with a proportionality constant C. M_1 and M_2 are the molecular weights of the components.

The use of small angle neutron scattering (SANS) for polymer blend studies is described in chapter 5 [*q.v.*].

1.4. Predicting Polymer-Polymer Miscibility.

1.4.1. The Solubility Parameter

Aside from actual experimental methods for determining χ, it is possible to estimate the interaction parameter for a polymer blend by considering the *solubility parameters* of the respective components.

The concept of the solubility parameter was formalised in 1950 by Hildebrand and Scott[26], who proposed the square root of the *cohesive energy density* as a parameter characterising the behaviour of a given material (polymer) in a given solvent. This parameter was given the symbol δ.

The cohesive energy density is defined as the increase in internal energy per mole of substance per unit volume if all the intermolecular forces are eliminated. The solubility of a given polymer in various solvents is determined largely by its chemical structure, the general rule being that "*like dissolves like*", *i.e.* structural similarity between solvent and solute favours solubility.

The physical state of the polymer also has a bearing on the solubility properties. Crystalline polymers are relatively insoluble compared to amorphous ones, and they often dissolve only at temperatures slightly below their crystalline melting points. Furthermore, solubility generally decreases with increasing molecular weight, a feature which is utilised in the fractionation of polymers.

1.4.2. Calculation of the Solubility Parameter

As mentioned above, the solubility parameter is defined as the square root of the cohesive energy density. This property has been the subject of considerable research efforts since the late 1920's, when Dunkel [27] proposed that it was an additive property and went on to calculate group contributions to the cohesive energy for a series of homologous liquids at room temperature. Since then, a number of workers have refined the theories and applied their findings to polymer solubility. Extensive tabulations of these group contributions can be found in Van Krevelen's book[28].

Having arrived at a value for the solubility parameter for a given material and a given solvent, one can relate their solubility parameters to the enthalpy of mixing as follows:

$$\Delta h_{mix} = \phi_1 (1 - \phi_1)(\delta_1 - \delta_2)^2 \qquad \textbf{[1.26]}$$

where Δh_{mix} is the enthalpy of mixing per unit volume, ϕ_1 is the volume fraction of component 1 and δ_i is the solubility parameter of component *i*. Equation 1.26 predicts that Δh_{mix} is zero for $\delta_1 = \delta_2$, so two substances with equal solubility

parameters should be mutually soluble due to the favourable entropic factor. As the difference in the solubility parameter increase, the tendency for solubility decreases.

Finally, we see from the work of Scott[29] that the interaction parameter can be expressed in terms of solubility parameters as follows:

$$\chi_{12} = \frac{V_r}{RT}(\delta_1 - \delta_2)^2 \qquad \textbf{[1.27]}$$

It should be emphasised that this approach is valid only for non-polar polymers. A number of workers have extended the simple theories to account for intermolecular interactions, such as hydrogen-bonding, by separating the cohesive energy into components corresponding to various types of interaction forces. In doing this, the attractive simplicity of the concept of the solubility parameter is diminished, and the gains in accuracy are not always worth the additional effort, particularly noting that the contributions to the cohesive energy cannot be determined directly from experiment. For a fuller critique on these methods, the interested reader is referred to the relevant section of Van Krevelen's book[28] and the references contained therein.

Sample calculations of solubility parameters and predictions of miscibility are included in the appendix.

1.5. Fluoropolymers

The second aspect of this work is the synthesis of a fluoroalkyl methacrylate polymer, which can then be blended and studied as above. The new fluoroalkyl methacrylate was prepared from the products of a *telomerisation* reaction of trifluoroethene with a simple alcohol. [*q.v.*]

The scientific and patent literature gives testimony to the wide range of uses and applications in which fluoropolymers are found. The properties and applications of the early (per)fluoropolymers (such as poly(tetrafluoroethylene), PTFE) are well known. PTFE is a highly chemical resistant, thermally stable material with a low surface energy, making it an important material for bearings, seals and release agents. Its release properties and thermal stability are epitomised by its use in non-stick cookware.

Unfortunately, it is the chemical and thermal properties of PTFE that make it extremely difficult and expensive to process. PTFE is not melt processable, and dissolves only in a limited number of solvents at very high temperatures. Overcoming such properties has meant the development of new fluoropolymers with different structures, such as fluorinated ethylene propylene (FEP), perfluoroalkoxy (PFA), poly(chlorotrifluoroethylene) (PCTFE), ethylene-co-tetrafluoroethylene (ETFE), ethylene-co-chloro-trifluoroethylene, and poly(vinylidene fluoride) (PVDF).

FEP is a random copolymer of tetrafluoroethylene and hexafluoropropylene; the hexafluoropropylene usually being about 10-12% by weight. It has a lower melting point than PTFE and is hence processable in the melt by extrusion and

injection moulding. The mechanical properties of FEP are inferior to those of PTFE, although its chemical resistance is similar.

Perfluoroalkoxy (PFA) is a recent development in the field of fluoropolymers. It is a copolymer of tetrafluoroethylene and perfluoroalkoxy monomer. The repeat unit is as follows:

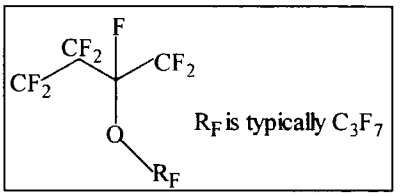

The material is melt processable, with a high melting point and better properties than PTFE at high temperature. In common with other fluoropolymers, it offers good chemical resistance, and finds use in the semiconductor industry in pumps, pipes, fittings and filtration systems[30].

Narrowing the field of view somewhat, fluoroalkyl methacrylates have attracted considerable attention from a number of interested concerns, and, most notably, a large number of references may be found in the Japanese patent literature.

Perhaps the most widespread application for these materials (judging by the number of "hits" in Chemical Abstracts ON-LINE) is their use in optical fibres and optical coatings. This application makes use of the low refractive index of fluorinated polymers, which enhances the already favourable properties of methacrylates[31,32]. Considering radiation properties in general, a number of fluoroalkyl methacrylates have also been investigated for use as lithographic resists. See, for example, the work of Pittman *et al* [33].

The use of fluoropolymers as coatings has already been alluded to, and fluoroalkyl methacrylates also find considerable application here as antifouling, anti-stain or anti-static formulations. The use of the methacrylate variants is favoured here due to their solubility in common solvents *c.f.* perfluoropolymers, which are insoluble. This solubility allows the coating of thermally sensitive materials, or can simply reduce the costs of such a treatment. It should be noted, however, that such a coating is less robust than a similar treatment by a perfluoropolymer.

The hydrophobic/lipophobic nature of fluoropolymers also gives them interesting properties when they come into contact with the body. Considerable effort is being given to this field, and the early developments are highly successful. Many patents have been filed for the use of fluoroalkyl methacrylates as both soft and hard contact lenses, products which also benefit from the optical properties and oxygen permeability of these materials.

Finally, fluoroalkyl methacrylates are subject to research on more exotic properties such as liquid crystal behaviour and solution surfactancy. The widely differing solubility requirements of the fluoroalkyl sidechain from the hydrocarbon backbone can lead to the production of mesophases and other aggregates[34,35].

In summary, fluoropolymers are employed to take advantage of their many desirable properties; *viz.* those of high thermal and chemical stability, low wettability and low refractive index relative to hydrogenous polymers. Applications vary from contact lenses to pump impellers.

1.6. Methacrylate Polymers

The methacrylate family of polymers has been known since the 1930's, and forms a wide-ranging group of commercially valuable materials. The properties of the polymers depend strongly upon the nature of the side chain, which can readily be varied by simple reactions early in their manufacture. The glass transition temperature is particularly sensitive to the length and chemical identity of the side chain, for example, poly(methyl methacrylate) (atactic) has a T_g of 378K (105°C), descending to 293K (20°C) for the *n*-butyl derivative. The specifying of the tacticity of the polymer also implies a dependence, which is in fact very strong. *viz.* 378K, 433K and 316K for atactic, syndiotactic and isotactic PMMA, respectively[36]. Methacrylate polymers are stiff, hard, brittle glasses below their T_g, becoming soft, limp and stretchable above it. PMMA is most commonly encountered as a transparent plastic used as an alternative to silicon glasses, but its hydrolytic stability and low toxicity mean that it also finds use in medical applications, and particularly as a bone cement. The ease with which it may be moulded makes it attractive for use in lenses, prisms and more recently optical fibres, a feature for which fluoroalkyl derivatives are particularly attractive. The low refractive index imparted by the fluorination of the side chains make fluoroalkyl methacrylates especially suitable for optical materials, and a body of work on their synthesis and use is building up in the literature.

1.7. Telomerisation

The new system has been made possible by the telomerisation of trifluoroethene with methanol, to yield a new fluoroalcohol. Telomerisation is defined[37] as "*the process of reacting, under polymerisation conditions, a molecule YZ (a telogen) with more than one unit of a polymerizable compound having ethylenic unsaturation (a taxogen), to form products called telomers having formula* $Y(A_n)Z$ *wherein* $(A)_n$ *is a divalent radical formed by chemical union, with the formation of new carbon bonds, of n molecules of the taxogen, the unit A being called the taxomon, n being any integer greater than one, and Y and Z being fragments of the telogen attached to the terminal taxomons*". In general:

$$n\,A + YZ \rightarrow Y\text{-}(A)_n\text{-}Z \qquad \textbf{[1.28]}$$

and specifically

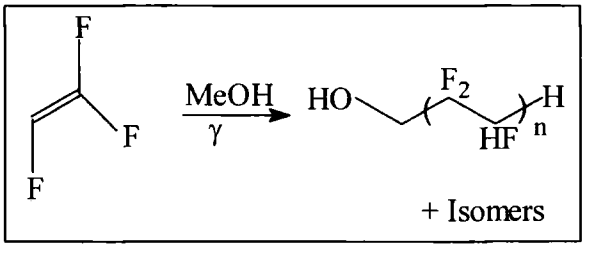

Figure 1.4. Methanol-terminated Telomer of Trifluoroethene n≅2

Ethanol can also be used as the telogen, giving a secondary fluoroalcohol:

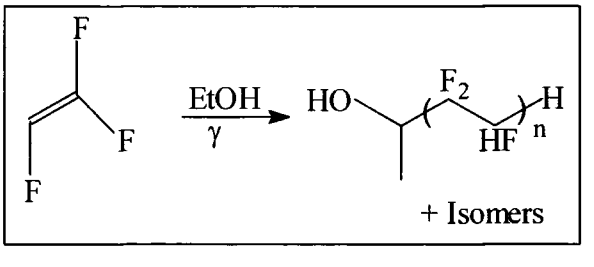

Figure 1.5. Ethanol-terminated Telomer of Trifluoroethene n≅2

The isomers as drawn are the most common, but the isomers with the CF_2H group at the end are also formed, *i.e.* head-tail isomerism.

The alcohols produced, and indeed (fluoro)alcohols in general can be reacted with methacrylic acid to give a methacrylate ester, which can then be polymerised to give the polymer:

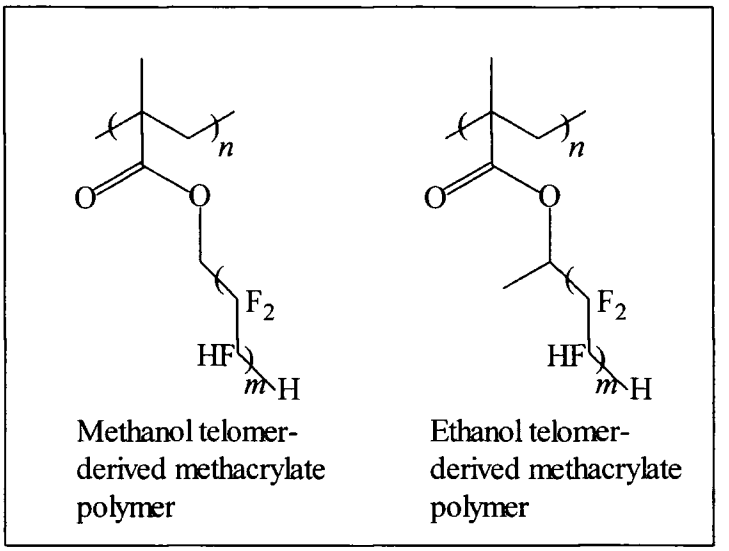

Figure 1.6. New Polymers from Telomers of Trifluoroethylene

1.8. Aims of the Current Work.

With the above considerations in mind, the aims of this work were to develop and characterise a new family of fluoroalkyl methacrylate polymers, and study their properties in blends with PMMA.

Such materials may find application in optical systems and coatings formulations which have a combination of the attractive properties of fluorinated polymers and methacrylate polymers.

1.8. References

1)Flory, P. J. *Principles of Polymer Chemistry*; Cornell University Press: New York, 1953.

2)Paul, D. R.; Newman, S. *Polymer Blends*; Academic Press Ltd: New York, 1978; Vol. 1.

3)Coleman, M. M.; Painter, P. C. "*Hydrogen Bonded Polymer Blends*" in Progress in Polymer Science; Pergamon: London, 1995; Vol. 20, pp 1-59.

4)Kaplan, D. S. *Journal of Applied Polymer Science* **1976**, *20*, 2615.

5)Pommerehne, J.; Vestweber, H.; Guss, W.; Mahrt, R. F.; Bassler, H.; Porsch, M. M. *Advanced Materials* **1995**, *7*, 551-554.

6)Granstrom, M.; Inganas, O. *Applied Physics Letters* **1996**, *68*, 147-149.

7)Wilfong, D. L.; Hiltner, A.; Baer, E. *Journal of Materials Science* **1986**, *21*, 2014.

8)Ku, C. C.; Liepins, R. *Electrical Properties of Polymers-Chemical Principles*; Hanser: Munich, 1987.

9) *Thermal Characterisation of Polymeric Materials*; 2 ed.; Turi, E., Ed.; Academic Press: San Diego, 1997; Vol. 1.

10)Mathot, V. B. F. *Calorimetry and Thermal Analysis of Polymers*; Hanser: Munich, 1994.

11)Danait, A.; Deshpande, D. D. *European Polymer Journal* **1995**, *31*, 1221-1225.

12)Kwei, T. K.; Nishi, T.; Roberts, R. F. *Macromolecules* **1974**, *7*, 667.

13)Flory, P. J. *Journal of Chemical Physics* **1941**, *9*, 660.

14)Huggins, M. L. *Journal of Chemical Physics* **1941**, *9*, 440.

15)Guggenheim, E. A. *Proceedings of the Royal Society (London)* **1944**, *A183*, 213.

16)Orr, W. J. C. *Transactions of the Faraday Society* **1944**, *40*, 320.

17)Freeman, P. I.; Rowlinson, J. S. *Polymer* **1959**, *1*, 20.

18)Leonard, C.; Halary, J. L.; Monnerie, L. *Polymer* **1985**, *26*, 1507-1513.

19)Prigogine, I. *The Molecular Theory of Solutions*; Wiley Interscience: New York, 1959.

20)Flory, P. J.; Eichinger, B. E.; Orwoll, R. A. *Macromolecules* **1968**, *1*, 278.

21)Zhong, C. L.; Wang, W. C.; Lu, H. Z. *Macromolecules* **1995**, *28*, 7737-7743.

22)Rudolf, B.; Cantow, H. J. *Macromolecules* **1995**, *28*, 6586-6594.

23)Rudolf, B.; Cantow, H. J. *Macromolecules* **1995**, *28*, 6595-6599.

24)McMaster, L. P. *Macromolecules* **1973**, *6*, 760.

25)Barlow, J. W. *Macromolecular Symposia* **1993**, *70/71*, 235-244.

26)Hildebrand, J. H.; Scott, R. L. *The Solubility of Non-Electrolytes*; 3 ed.; Reinhold Publishing: New York, 1950.

27)Dunkel, M. *Z. Phyzik. Chem* **1928**, *A138*, 42.

28)Van Krevelen, D. W. *Properties of Polymers*; 3 ed.; Elsevier Science: Amsterdam, 1990.

29)Scott, R. L. *Journal of Polymer Science* **1952**, *9*, 423.

30)Miller, W. A. *Chemical Engineering* **1993**, *4*, 163-168.

31)Boutevin, B.; Rousseau, A.; Bosc, J. *Journal of Polymer Science, Polymer Chemistry Edition* **1992**, *30*, 1279.

32)Takezawa, Y.; Tanno, S.; Taketani, N.; Ohara, S.; Asano, H. *Journal of Applied Polymer Science* **1991**, *42*, 3195-3203.

33)Pittman, C. U.; Chen, C.-Y.; Ueda, M.; Helbert, J. M.; Kwaitowski, J. H. *Journal of Polymer Science, Polymer Chemistry Edition* **1980**, *18*, 3413-3425.

34)Volkov, V. V.; Plate, N. A.; Takahara, A.; Kajiyama, T.; Amaya, N.; Murata, Y. *Polymer* **1992**, *33*, 1316.

35)Katano, Y.; Tomono, H.; Nakajima, T. *Macromolecules* **1994**, *27*, 2342-2344.

36)Brandrup, J.; Immergut, E. H. *Polymer Handbook*; 3 ed.; Wiley Interscience: New York, 1989.

37)Gordon, B. I.; Loftus, J. E. *Telomerization*; Mark, H.F., Bikales, N.M., Overberger, C.G. & Menges, G., Eds.; John Wiley & Sons: New York, 1989; Vol. 16, pp 533-544.

Chapter Two

Monomer Synthesis

2.1. Esterification Reactions

Methacrylate monomers have been synthesised on the laboratory scale by an esterification reaction between methacrylic acid (or a derivative) and an alcohol. The choice of reagents, particularly the acid derivative, depends on the reactivity of the system. The most common technique, however, is the acid or base catalysed reaction described in any basic organic chemistry textbook, *e.g.*:

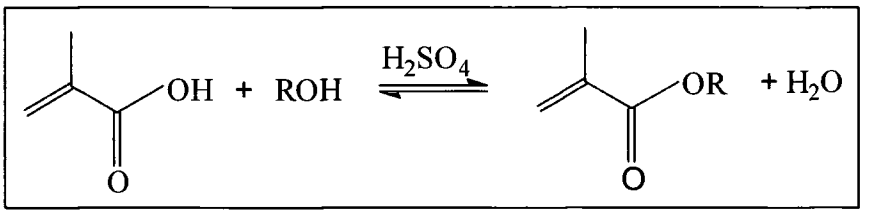

Figure. 2.01 Esterification (of Methacrylic Acid).

2.1.1. Esterification of Fluoroalcohols

Several workers[1-3] have commented on the difficulty found in the esterification of methacrylic and acrylic acids with fluoroalcohols such as those used in this work. This difficulty arises due to the acidic nature of fluoroalcohols in general, which in turn is due to the electron-withdrawing properties of fluorine, *viz.*

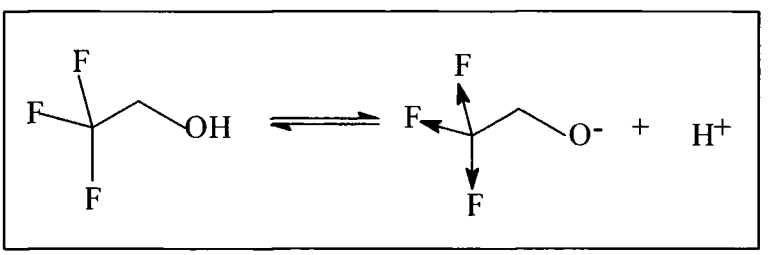

Figure 2.02 Acidity of Fluoroalcohols

This charge delocalisation enhances the stability of the fluoroalkoxy- species, and hence it is a better leaving group than the HO^- from methacrylic acid. The equilibrium position of the reaction lies on the side of the reagents rather than the desired products so, therefore, a number of strategies have been developed

specifically to enable the esterification reaction between acrylic derivatives and fluoroalcohols to take place with enhanced efficacy.

2.1.1.1. Trifluoroacetic Anhydride Route

The first of these is a general route[1], applicable to both acrylates and methacrylates, using trifluoroacetic anhydride, $(CF_3CO)_2O$ (I), as a promoter. In this synthesis, the trifluoroacetic anhydride is added to (meth)acrylic acid, to form, *in situ*, an activated mixed anhydride (II).

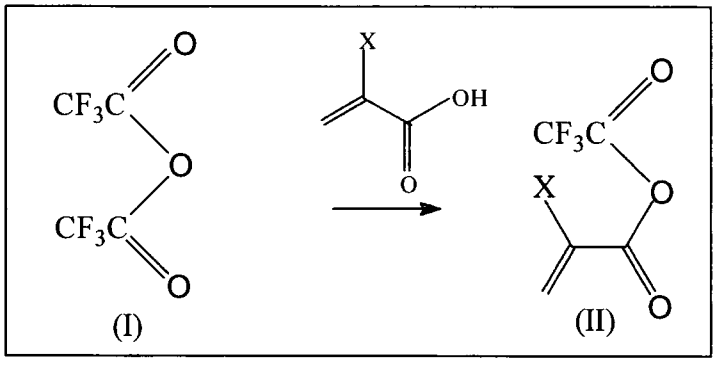

Figure. 2.03 Mixed Anhydride Synthesis. X = H, CH_3

Addition of the alcohol to the mixed anhydride gives exclusive formation of the ester of the non-fluorinated acid. This is attributed to the superior ability of the fluorinated species over the hydrogenous species to act as an anionic leaving group, *viz.* $CF_3CO_2^-$ *vs.* $CH_2CXCO_2^-$.

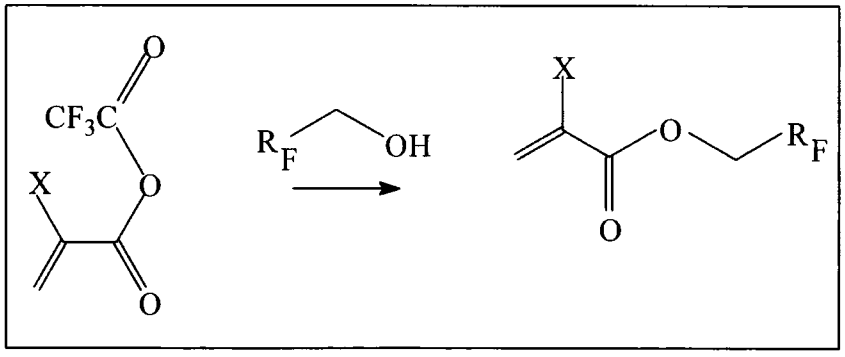

Figure 2.04 Ester Synthesis from Mixed Anhydride

R_F represents a fluoroalkyl chain, X= H, CH_3

2.1.1.2. Phosphorus Pentoxide (P_4O_{10}) Route

The second route, detailed in a patent[3], was described specifically for the synthesis of methacrylate esters; the reference states that a low yield was obtained when acrylic acid was used. The method involves the use of phosphorus (V) oxide, P_4O_{10}, which acts as a dehydrating agent removing water from the reaction as it is formed, thereby shifting the equilibrium position to favour the desired products.

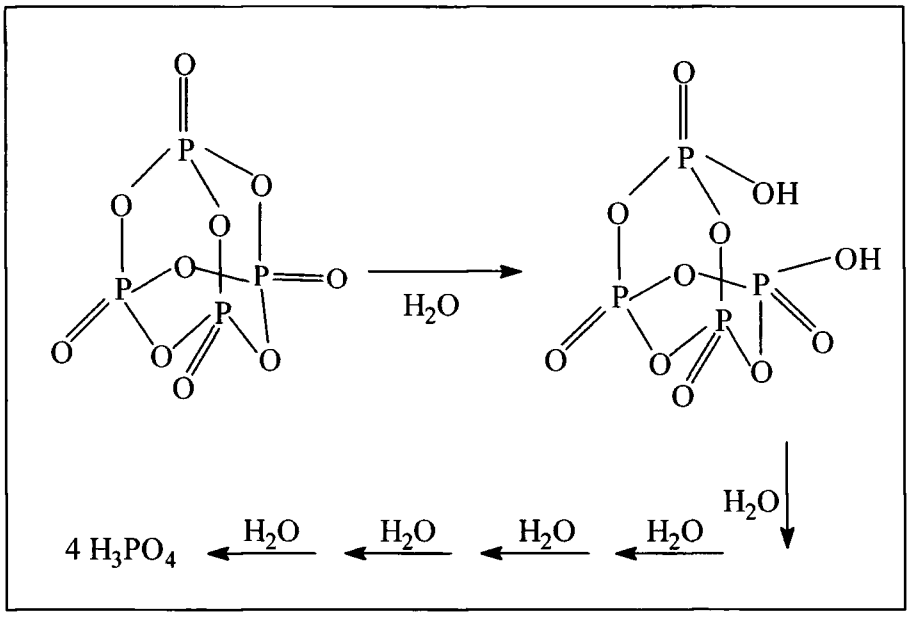

Figure 2.05 Dehydrating action of P_4O_{10}

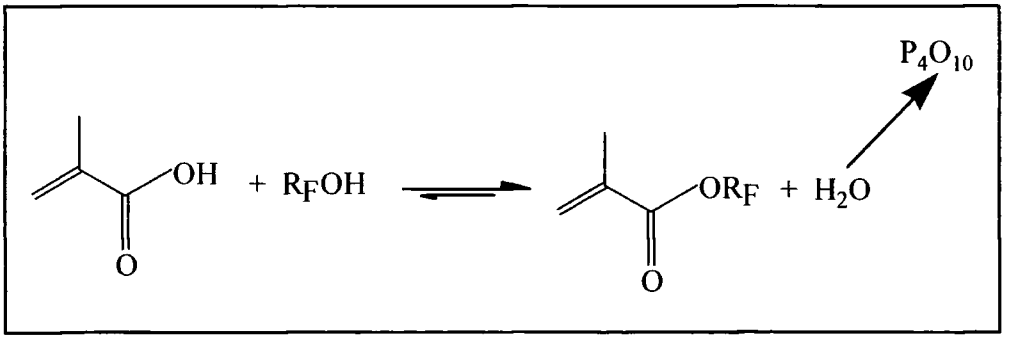

Figure 2.06 Action of P_4O_{10} to drive forward reaction

The reaction was carried out in the presence of polymerisation inhibitors, namely di-^{t}butyl-p-cresol.

2.1.2. Pilot Experiments

To test the efficacy of the synthetic methods described above, trials were conducted using some commercially available fluoroalcohols before using the telomeric alcohols (*q.v.*), which are laborious to synthesise. The commercial alcohols used were 2,2,2 Trifluoroethanol, 1H,1H,5H, Octafluoropentanol and 1,1,1,3,3,3, Hexafluoropropan-2-ol (Hexafluoroisopropanol; these names are used interchangeably). Trifluoroethanol is the shortest chain fluoroalcohol available. The longer chain derivative was used to model the effects of chain length, and the secondary alcohol to model the effects of chain branching.

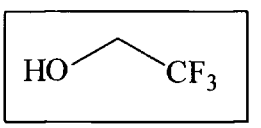

Figure 2.07 2,2,2 Trifluoroethanol.

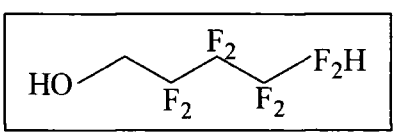

Figure 2.08 1H,1H,5H, Octafluoropentan-1-ol.

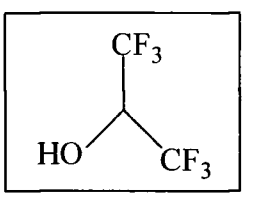

Figure 2.09 1,1,1,3,3,3, Hexafluoropropan-2-ol.

The primary alcohols react in good yields (~70%) by the trifluoroacetic anhydride method, but some difficulty was found in the isolation of the final product with the P_4O_{10} route. Attempts to esterify the secondary alcohol met with more problems, the product was difficult to purify and the yields were very poor. With this consideration, a more reactive system was sought for the secondary alcohols, and the route described by Strange[4] has been used with more success.

2.1.3. Experimental Details

1. Trifluoroacetic anhydride route:

Hydroquinone inhibited methacrylic acid (43g, 0.5 moles) was poured to a three-necked round-bottomed flask, which was then fitted with a reflux condenser, pressure equalised dropping funnel, magnetic stirrer bar and thermometer. The apparatus was immersed in an ice/water bath, before trifluoroacetic anhydride (105g, 0.5 moles) was added down the dropping funnel. The pure acid was observed to freeze in the flask, making stirring difficult, but the solid disappears after the addition of about half the anhydride. The rate of addition was adjusted such that the temperature throughout did not exceed 288K. Once addition was complete, stirring was continued for 15mins before trifluoroethanol (50g 0.5 moles) was added. The rate was adjusted such that the temperature did not exceed 298K.

The resulting mixture was stirred for a further 90 mins, before pouring into a separating funnel. Distilled water was added until the layers separated, and the bottom ester layer washed with alternating water/ 5% NaOH solution. Six washes of 150ml were used. The ester layer was finally removed, and distilled under reduced pressure to give 55.5g of a colourless liquid boiling at 317K@13332Pa. The formation of an ester was confirmed by FT-IR from the shift in the carbonyl absorption frequency and the disappearance of the alcohol signals. The yield with respect to the alcohol was 66%.

A similar procedure using 1H,1H,5H Octafluoropentan-1-ol (23g, 0.1 moles) resulted in the production of 20.46g (0.068moles) octafluoropentyl methacrylate. The product was distilled at reduced pressure, and had a boiling point of 338K@13332Pa. The yield was 68%.

2. P_4O_{10} Route

Methacrylic acid (130g, 1.5 moles), 0.5g t-butyl catchecol (polymerisation inhibitor), P_4O_{10} (32g, 0.12 moles) and trifluoroethanol (50g, 0.5 moles) were added to a flask equipped with stirrer, thermometer, and reflux condenser. The resulting mixture was stirred and heated to 333K for 1 hour.

After cooling, the mixture was poured into a separating funnel and washed with distilled water. Difficulties were experienced at this point in the separation of the phases, there being a large quantity of tar-like partially hydrated P_4O_{10} present. Only a small amount of the ester layer was finally separated. The brown coloration was removed by vacuum transfer. 6.8g of product was recovered, corresponding to a yield of 8%.

This route may be more effective on a large scale using a mechanical-type stirrer to achieve more efficient mixing. The interested reader may like to note the large scales on which the reaction was originally performed. On this scale, however, it would seem to be unsuitable.

3.Trifluoroacetic anhydride route on secondary alcohol

Using the same experimental conditions as described for trifluoroethanol, hexafluoroisopropanol was esterified. The quantities of reagents were as follows: 12.85g (0.15 moles) methacrylic acid, 31.50g (0.15 moles) trifluoroacetic anhydride and 25.02g (0.15 moles) hexafluoroisopropanol. The ester so produced had a mass of 3.30g, corresponding to a yield (w.r.t. alcohol) of 9%.

4. Methacryloyl Chloride Route

The poor yields seen above for the esterification of a secondary alcohol meant that another route needed to be found.

Hexafluoroisopropyl methacrylate has been prepared using the method described by Strange[4]. Freshly distilled methacryloyl chloride (26.5g, 0.25 moles) was poured into a rigorously dried three necked flask, fitted with reflux condenser, pressure equalising dropping funnel and thermometer well. Dry nitrogen was let into the apparatus through a long Pasteur pipette protruding through the thermometer well. The methacryloyl chloride was heated in the presence of hydroquinone (polymerisation inhibitor) to 348K, before the hexafluoro-isopropanol (42g, 0.25moles, distilled, dried over type 3Å molecular sieve) was added rapidly from the dropping funnel. The rapid addition prevents the formation of an unwanted side product, a fluoroalkyl β-chloro-α-methylpropionate ester:

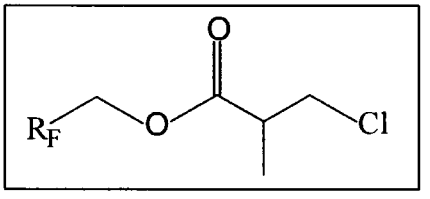

Figure 2.10 Side product from methacryloyl chloride route

The mixture was then heated to a gentle reflux at 393K overnight, and the resulting brown liquid distilled through a Hempel column packed with Raschig rings, to yield a number of fractions. The fraction boiling at 317K@13332Pa was identified by IR to be the desired product, and its structure confirmed by ^{1}H, ^{13}C and ^{19}F NMR. The yield with respect to the alcohol was 43%.

2.1.4. Comparison of the results of the various Strategies

It is of importance at this stage to consider the relative methods and drawbacks of the various synthetic methodologies considered above.

The efficacy of the trifluoroacetic anhydride route with primary alcohols makes it an attractive synthetic method, especially as the reaction takes place quickly at temperatures below room temperature. However, it is a most inefficient reaction; only half of the trifluoroacetic anhydride takes place in the desired reaction, the rest giving trifluoroacetic acid. On addition of the (fluoro)alcohol, a second mole equivalent of trifluoroacetic acid is liberated. These side products must be treated and recovered for safe disposal, adding further to the expense should the reaction be scaled up.

The opposite is true for the P_4O_{10} route. This reaction does not appear to work well on the small scales for which it has been used in this work. However, with more efficient stirring, this reaction could be highly successful and give a useful by-product, phosphoric acid.

The main difficulty with using methacryloyl chloride is handling the methacryloyl chloride itself. This material is highly toxic in both the vapour and liquid phases, and must also be kept dry to prevent degradation to the acid. This consideration also plays a part in the purity of the reagent; it must be distilled immediately before use.

Not withstanding these drawbacks, the enhanced reactivity of the acid chloride system to fluoroalcohols is a significant advantage, meaning one methodology may be used to prepare several materials.

2.2. Characterisation

All monomers were characterised by FT-IR and NMR (^{1}H, ^{13}C, ^{19}F). Fluorinated materials are not, in general, amenable to analysis by mass spectrometry, as the electronic properties of the fluorine atoms effect the ionisation and fragmentation of the sample. The purity was assessed by gas chromatography. Examples of spectra are included in the appendix, all are consistent with the structures proposed.

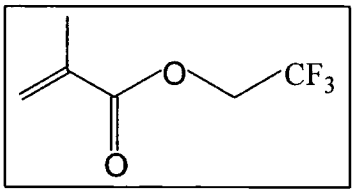

Figure 2.11 2,2,2 Trifluoroethyl Methacrylate

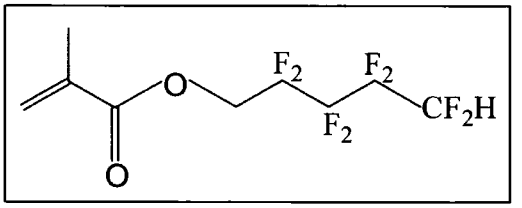

Figure 2.12 1H,1H,5H,Octafluoropentyl Methacrylate

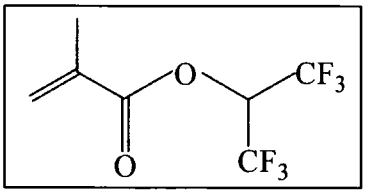

Figure 2.13 Hexafluoroisopropyl Methacrylate

2.3. Target Monomers

The target monomers (and polymers) are methacrylate esters of a novel fluoroalcohol produced by the *telomerisation* of trifluoroethene with an alcohol. The synthesis of the fluoroalcohols was performed by Anwar Gilani in the chemistry department, Durham University[5]

2.3.1. Telomerisation [6]

Telomerisation has been described as "the reaction under polymerisation conditions, between a *telogen* (molecule YZ) with more than one molecule of a polymerizable compound having ethylenic unsaturation (a *taxogen*) to form products called *telomers* having the formula $Y(A)_nZ$. A_n is a divalent radical formed by the chemical reaction between *n* molecules of the taxogen, the unit A being referred to as the *taxomon*, *n* being any number greater than one, and Y and Z being fragments of the telogen attached to the terminal taxomons"; *i.e.*

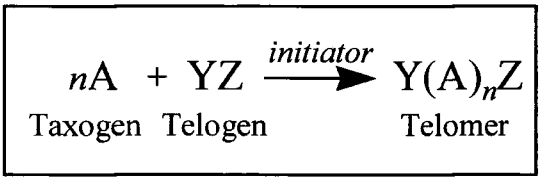

Figure 2.14 General Telomerisation Reaction.

In this work, the telogens used were methanol and ethanol, the taxogen being trifluoroethene, *i.e.*

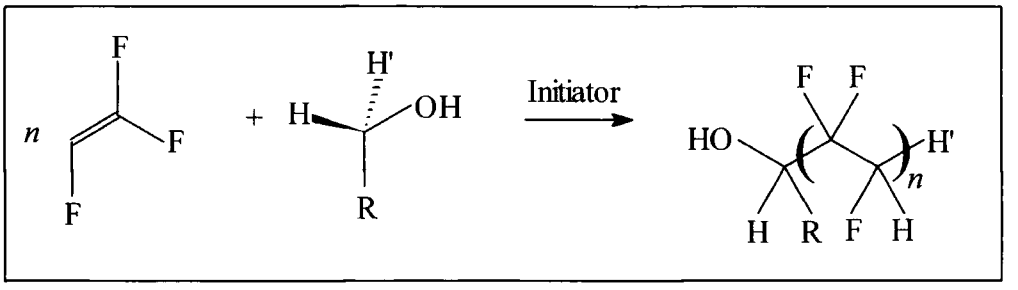

Figure 2.15 Telomerisation of Trifluoroethene with RCH_2OH. R = H, CH_3.

Note the origins of H'. It is interesting to mention briefly the regiochemistry of the above reaction. From the diagram above, it can be seen that the H' radical of the telogen is attached to a carbon bearing only one fluorine atom. This particular regiochemistry is seen in approximately 80% of the reaction products, the other 20% being of the other orientation, *i.e.* a head-tail defect. Stability of the respective propagating radicals is offered as the explanation for this observation; the interested reader is referred to the original work of Gilani[5].

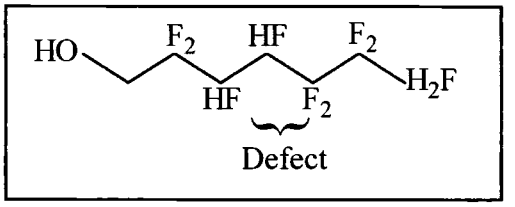

Figure 2.16 Heat-Tail Defect in n=3 Methanol-derived Telomer

Furthermore, in the case of the ethanol-derived telomer, there are stereochemical issues to be addressed. The carbon α- to the OH group is chiral, a feature which may effect the way it interacts with tactic, *i.e.* pseudo-chiral, chains of PMMA.

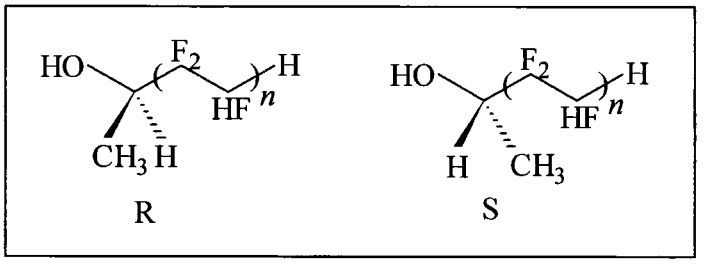

Figure 2.17 Stereoisomers of the Ethanol-Derived Telomer

2.3.2. Nomenclature

The telomer with methanol as the telogen has been dubbed the "methanol telomer"; the ethanol based variant is similarly described. Where appropriate, these have been abbreviated to MeTelOH and EthTelOH respectively. Similarly, the esters are called MeTelMA and EthTelMA.

2.3.3. Ester of Methanol Telomer, MeTelMA

Synthesis of MeTelMA *via* the trifluoroacetic anhydride route resulted in the isolation of very small amounts of the desired product. Therefore, the methacryloyl chloride route as described above was used to synthesise MeTelMA with three notable differences:

The stability of the telomeric materials is rather questionable. The telomeric alcohols as supplied were clear and colourless liquids. Although both MeTelOH and EthTelOH were refrigerated before use, a brown coloration was observed to develop with time. Therefore, purification of the alcohol was necessary before the esterification reaction, and this was achieved by room temperature vacuum transfer.

A second implication of the poor thermal stability is that the reaction temperature of the original reaction was unacceptably high. The reaction, using the methacryloyl chloride route described above, was performed in an inert, dry solvent (THF), with a reflux temperature of around 338K. This procedure resulted in yields of around 40% with respect to the fluoroalcohol.

Thirdly, distillation, even at reduced pressure, could be deleterious to the reaction products. Given the nature of the fluorinated alcohol and the similarities between its isomers, one would expect to collect a single fraction with a broad distribution of boiling points. While column chromatography does not suffer from the thermal disadvantages of distillation, the second point regarding the number of isomers is still valid. Therefore, the only viable purification technique was low temperature vacuum transfer, which allows the isolation of "pure" samples of the ester with minimal detrimental effects.

2.3.4. Ester of Ethanol Telomer

Noting the results of the trifluoroacetic anhydride synthesis of MeTelMA and the reduced reactivity of secondary alcohols in esterification reactions, the anhydride route was not tried for the synthesis of EthTelMA. The methacryloyl chloride route was again used with slightly lower yields than those reported for the methanol-derived variant, around 30-35% with respect to the fluoroalcohol.

2.4. Preparation of Deuterated Monomers

Small angle neutron scattering and neutron reflectometry experiments require the use of deuterated materials in order that the necessary contrast[†] may be achieved. It was necessary, therefore, to prepare deuterated monomers and polymers for use in these techniques. The use of methacryloyl chloride had been found to be the most efficient method of producing esters of the telomeric alcohols, but as deuterated methacryloyl chloride is not available, another route had to be sought.

2.4.1. Transesterification

A transesterification reaction takes place between an ester and an alcohol, the intention being to replace the alcohol residue from the ester with that from the free alcohol; *i.e.*:

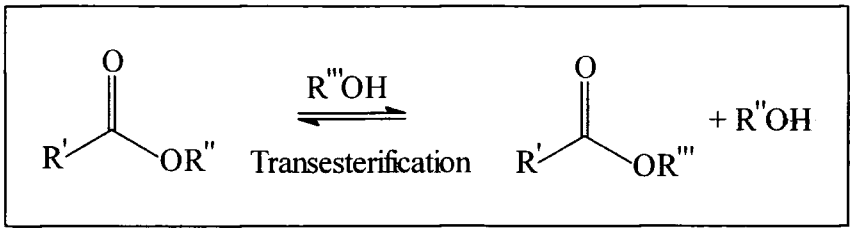

Figure 2.18 Transesterification Reaction

[†] See respective chapters for a fuller explanation

The reaction is catalysed by either acid or base, and both of these have been tried in order to optimise the reaction conditions.

Two strategies are available to produce a deuterated end product, *i.e.* polymer. One is to deuterate the monomer, such that when used in subsequent polymerisation reactions, a deuterated polymer is produced. The alternative is to perform the transesterification reaction on an existing polymer. Each route has its advantages and disadvantages.

The most obvious advantage to the former (monomer) approach is that the monomer can be purified before it is reacted to form the desired polymer. This is not possible using the polymer route; if the extent of the transesterification is less than 100%, a copolymer would result.

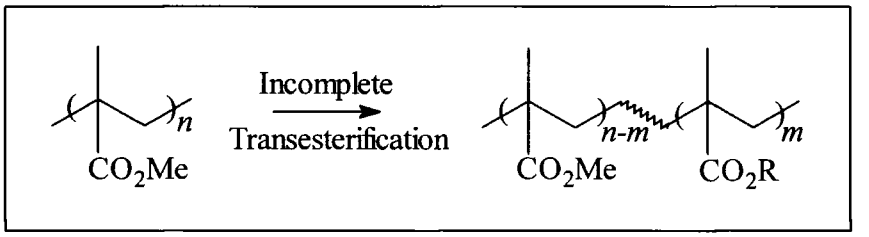

Figure 2.19 Copolymer resulting from Incomplete Transesterification

The polymer route has the significant advantage of having a pre-formed and possibly well defined polymer backbone on which to work. While this has no particular advantage in the transesterification stage, the nature (*i.e.* the molecular weight and polydispersity) of the polymer may be crucial at later experimental stages.

Weighing up the pros and cons of the two approaches, and also noting that judicious choice of polymerisation conditions can result in a well defined polymer from the deuterated monomer, efforts were concentrated on the synthesis of the monomer.

2.4.1.1. Base-Promoted Reaction

The base catalysed reaction was after the work of Meth-Cohn[7]. In this reaction, butyl lithium is added to the alcohol in solution in THF. The product of this reaction is a lithium alkoxide, which, when added to an α,β-unsaturated or aromatic methyl ester, gives the ester of the previously free alcohol.

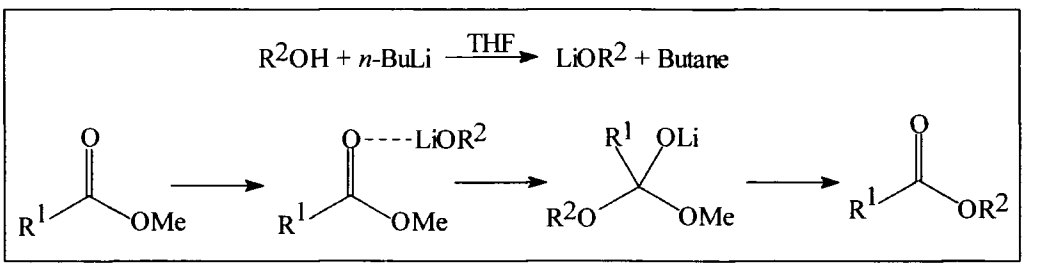

Figure 2.20 Reaction Scheme for Base-Promoted Reaction

A typical reaction was as follows:

MeTelOH(10g, $\bar{n}$ = 1.9, ~0.06 moles) was added to 100ml THF in a dry flask. To this solution were added 40ml *n*-butyl lithium (1.6M in hexanes, ~0.064moles) and MMA (6.5g, 0.065moles). With stirring, the reaction was allowed to proceed for 96hours before the mixture was washed, alternately with distilled water and ether. The organic layer was dried over 5Å molecular sieve, before the solvent was removed on a rotary evaporator. The resulting brown oil was vacuum transferred to give a final product of mass 6.23g. This corresponds to a yield of approximately 30%

2.4.1.2. Acid Catalysed Reaction

Noting the relative acidities of the fluoroalcohols to that of methanol (produced in the reaction) an acid catalysed reaction was attempted to take advantage of this. Also to be considered is the volatility of methanol and its density relative to the solvent (THF), which means that, in principle, a Dean & Stark trap which

returns the high density THF fraction and having facility to remove the methanol produced in the reaction could be used to drive the reaction to favour the production of the fluorinated ester. Therefore, an apparatus as shown in fig 2.21 was set up to explore the possibilities of this reaction:

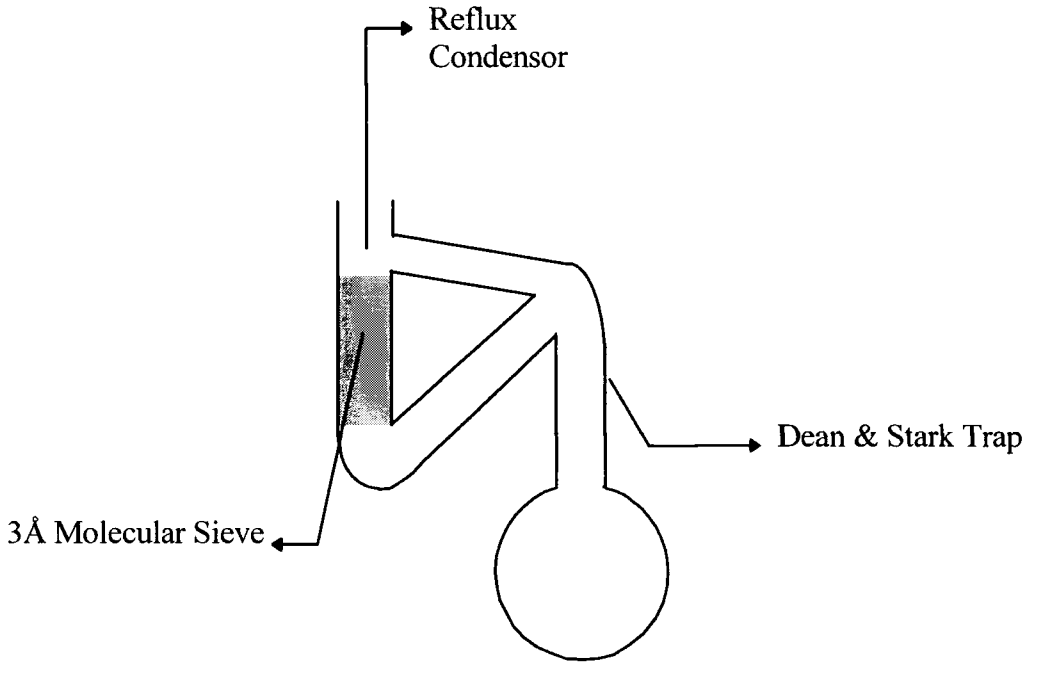

Figure 2.21 Apparatus for Acid Catalysed Transesterification Reaction

Using this apparatus, an equimolar mixture of fluoroalcohol and methyl methacrylate were refluxed in THF solution overnight with a catalytic amount of concentrated sulphuric acid. After the reaction had cooled, volatiles (residual MMA, THF) were removed on a rotary evaporator and the resulting oil was purified by vacuum transfer to obtain the "pure" (*q.v.*) fluorinated ester. Yields of 40-50% have been found.

This reaction had a drawback in that, on a number of occasions, a significant amount of polymer was recovered instead of monomer. THF is known to polymerise in dry acidic conditions, and the initial steps of such a reaction could bring about the polymerisation of the methacrylate monomers.

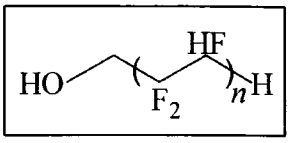

Figure 2.22 Methanol Telomer of TFE

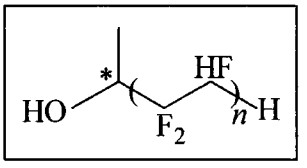

Figure 2.23 Ethanol Telomer of TFE. * denotes the chiral carbon

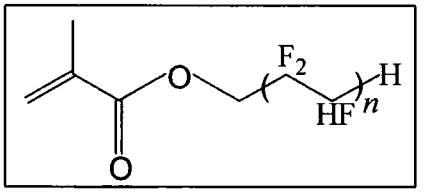

Figure 2.24 Methacrylate ester of methanol telomer

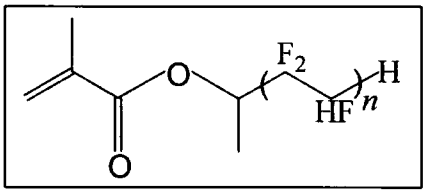

Figure 2.25 Methacrylate ester of ethanol telomer

2.5. Characterisation of Target Monomers.

The monomers as drawn above appear relatively simple molecules, but reference has already been made to the mix of species present in their reactions. Not only is there a distribution of side chain lengths, but also a number of possible (head-tail) isomers for a given degree of telomerization, *viz.*:

$$number\ of\ isomers = 2^n$$

Therefore, for a typical reaction mixture with an average degree of telomerization of ~2, there will be of the order of 10 different species, each of different concentration, in a "pure" monomer sample.

That the products of these reactions are complex mixtures has significant implications when it comes to their characterisation. Looking at the ^{13}C NMR spectrum of octafluoropentyl methacrylate, already the signals from the fluorine-bearing carbons are small and ill-resolved. The added complication that arises from having a mixture of products results in a confusion of multiplets and means that these signals are very difficult to observe against the instruments' background noise. Even the most powerful assignment aids such as 2D NMR fail to resolve or assign any of the signals attributable to the sidechain.

Similar difficulties arise in FT-IR. While the absorbances from the methacrylate-part of the molecule are easily seen, the absorbances from the C-F region of the spectrum are very broad. This confirms the fact that carbon-fluorine bonds are found in a number of different environments in these materials, which in a somewhat perverse way, helps in their characterisation.

2.6. Technological Considerations

As a brief aside, the technological interests driving this work should also be considered. Were the telomeric alcohols and downstream products (monomers and polymers) to be produced on a large (plant) scale, it would be most undesirable to have to separate out each fraction according to its side chain composition, at least unless a particular composition was found to have a particularly desirable property and subsequently offer extra added value. In this respect, it would seem that the separation and characterisation of pure single isomer products is not as desirable as it would be were the work purely curiosity driven.

It is also of technological interest to determine the properties of the mixture as a whole; heavy chemical production is not interested in producing high purity chemicals, simply ones which will do the job for which they are marketed.

2.7. References

1)Ahlbrecht, A. H.; Codding, D. W. *Journal of the American Chemical Society* **1955**, *75*, 984.

2)Codding, D. W.; Reid, T. S.; Ahlbrecht, A. H.; Smith Jr, G. H.; Husted, D. R. *Journal of Polymer Science* **1955**, *15*, 515.

3)Gregorio, G.; Roberti, L.; Strepparola, E. *Process for preparing methacrylates of Fluorinated Alcohols*; Gregorio, G.; Roberti, L.; Strepparola, E., Ed., 1990.

4)Strange, M. ;MSc Thesis.; University of Durham: Durham, 1978.

5)Gilani, A. H. S. ; PhD Thesis; University of Durham,: Durham,, 1997.

6)Gordon, B. I.; Loftus, J. E. *Telomerization*; 2 ed.; Gordon, B. I.; Loftus, J. E., Ed.; John Wiley & Sons: New York, 1989; Vol. 16, pp 533-544.

7)Meth-Cohn, O. *Journal of the Chemical Society, Chemical Communications* **1986**, 695-697.

Chapter Three

Polymerisation Techniques

3.1. Introduction

Methacrylate esters are amenable to polymerisation initiated by both free radical and anionic means.

A radical initiator can bring about the polymerisation of almost any double bond, but with scant regard for any control. Practically any substituent is capable of stabilising a radical species by delocalisation over several atoms, resulting in polymers with a broad spread of molecular weight (large polydispersity) and having no control over the tacticity.

By way of comparison, anionic initiation can be used to provide high degrees of stereospecificity in a polymerisation resulting from the stringent requirements for the stabilisation of the propagating species. Initiation by anionic initiators is a very fast reaction, meaning polydispersity can be kept small. By the appropriate choice of initiator and/or solvent conditions, it is possible to produce polymers ranging from highly syndiotactic to those which are isotactic[1].

The pros and cons of these techniques are discussed below.

3.2. Free Radical Polymerisation

Before discussing the practical aspects of radical polymerisation, it is important to look at the theoretical background. The interplay between kinetic and thermodynamic processes affects the outcome of free radical polymerisation reactions in a profound way, and some aspects of these will be discussed below.

Radical polymerisations are characterised by three reaction processes within the polymerisation *viz. Initiation, propagation* and *termination.*

Initiation is divided further into two steps. The first is the production of free radicals, which can take place by many means, but the most common is by homolytic dissociation of an initiating species I to give a pair of radicals R$^{\cdot}$

$$I \xrightarrow{k_d} 2R^{\cdot} \qquad \textbf{[3.1]}$$

where k_d is the rate constant for initiator dissociation. The second part of the initiation reaction involves the addition of this radical to the first monomer molecule to produce the chain initiating species $M_1^{\cdot}$

$$R^{\cdot} + M \xrightarrow{k_i} M_1^{\cdot} \qquad \textbf{[3.2]}$$

Propagation proceeds with the growth of $M_1^{\cdot}$ by the addition of successive monomer units, creating a new radical species each time. In general:

$$M_n^{\cdot} + M \xrightarrow{k_p} M_{n+1}^{\cdot} \qquad \textbf{[3.3]}$$

where k_p is the rate constant for polymerisation.

Propagation with growth of the chain to high polymer proportions takes place rapidly, until at some stage the polymer chain stops growing by the process of termination.

Termination occurs by bimolecular reactions between propagating radicals. Two radicals may react with each other by *combination*, or more rarely by

disproportionation. Combination is the reverse of homolytic cleavage, the free electrons of each radical forming a new carbon-carbon bond. Disproportionation can occur when there is a hydrogen atom β- to the propagating species. This hydrogen may transfer as a radical to another propagating radical, resulting in one saturated and one unsaturated polymer.

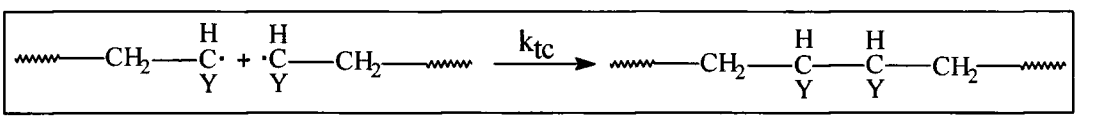

Figure 3.01 Termination by Combination

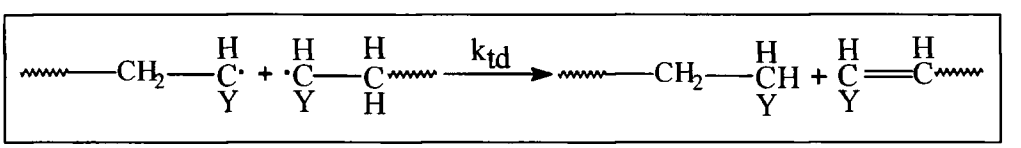

Figure 3.02 Termination by Disproportionation

where k_{tc} and k_{td} are the rate constants for termination by combination and disproportionation respectively. Methyl methacrylate is, in fact, one monomer for which disproportionation is a significant mode of termination. An increase in temperature increases the extent of termination by disproportionation; it is also more prevalent for sterically hindered monomers. The relative contributions of combination to disproportionation in methyl methacrylate polymerisations range from 67% disproportionation at 298K to 80% at 353K.

Termination takes place at a rate

$$k_t = k_{tc} + k_{td} \qquad [3.4]$$

3.2.1. Overall Rate Expression

To formulate an overall rate expression for chain growth polymerisation, it is necessary to make the assumption that the rates of propagation and termination are independent of chain length. This assumption is borne out experimentally[2]. Monomer is consumed in both the initiation and propagation steps, so the rate of monomer disappearance (which equals the rate of polymerisation) is given by:

$$\frac{-d[M]}{dt} = R_i + R_p \qquad [3.5]$$

where R_i and R_p are the rates of initiation and propagation, respectively. However, the number of monomer molecules reacting in the initiation steps are far less than the number reacting in the polymerisation steps so, to a good approximation, the former can be neglected. The rate of polymerisation is then simply given by

$$\frac{-d[M]}{dt} = R_p \qquad [3.6]$$

The rate of propagation is the sum of many individual propagation steps. Since the rate constants for all the propagation steps are the same, the rate of polymerisation is now given by

$$R_p = k_p[M^{\cdot}][M] \qquad \textbf{[3.7]}$$

where [M] is the overall monomer concentration and [M$^{\cdot}$] is the total concentration of all chain radicals, *i.e.* all radicals of size $M_1^{\cdot}$ and larger.

Equation 3.07, in containing a term for the concentration of radicals, is not directly usable to determine the rate of polymerisation. Radical concentrations are difficult to measure experimentally as their concentrations are very small due to the great reactivity of the species. The *steady state approximation* is used to eliminate the radical concentration from the expression. This assumes that the concentration of radicals remains constant throughout the reaction *i.e.* the rates of production and termination are equal:

$$R_i = 2k_t[M^{\cdot}]^2 \qquad \textbf{[3.8]}$$

The factor of 2 accounts for the destruction of radicals in pairs. Rearranging 3.8 for [M$^{\cdot}$] gives:

$$[M^{\cdot}] = \left(\frac{R_i}{2k_t}\right)^{1/2} \qquad \textbf{[3.9]}$$

Substituting for [M˙] into 3.9 gives the overall rate expression

$$R_P = k_P[M]\left(\frac{R_i}{2k_t}\right)^{1/2} \qquad \textbf{[3.10]}$$

Equation 3.10 presents the significant conclusion that the rate of polymerisation depends on the square root of the initiation rate. Doubling the rate of initiation increases the rate of polymerisation by a factor of $\sqrt{2}$ *i.e.* 1.414.

3.2.2. The Kinetic Chain Length

The rate of initiation also has a significant effect on the molecular weight of the resulting polymer, by way of the *kinetic chain length*, ν. The kinetic chain length is defined as the average number of monomer molecules consumed per radical by successfully initiating a polymer chain. This quantity is given by the ratio of the polymerisation rate to the initiation or termination rates, since the latter two rates are equal in the steady state approximation.

$$\nu = \frac{R_P}{R_i} = \frac{R_P}{R_t} \qquad \textbf{[3.11]}$$

Substituting for R_p and R_i from equations 3.07 and 3.08 gives:

$$\nu = \frac{k_p[M]}{2k_t[M^\bullet]} \qquad \textbf{[3.12]}$$

The substitution for the radical concentration from equation 3.9 finally yields:

$$\nu = \frac{k_p^2[M]^2}{2k_t R_P} \qquad \textbf{[3.13]}$$

Equations 3.12 and 3.13 display fundamental characteristics of radical chain polymerisation, notably, the kinetic chain length is inversely proportional to the radical concentration and the polymerisation rate.

The practical significance of these features are great; any attempt to increase the rate of polymerisation occurs at the expense of the molecular weight. The kinetic chain length at constant polymerisation rate is a characteristic of a particular monomer and is independent on the method of initiation.

3.2.3. Free Radical Polymerisation Initiators

There are a wide selection of molecules which may fulfil the role of a free radical polymerisation initiators, but in general they fall into three classes.

1. Molecules which form radicals by *thermally* promoted homolytic fission of a weak bond
2. Molecules which undergo *photolytically*-promoted dissociation or rearrangement.
3. Redox initiators

A fourth method, which does not need a separate initiator present, is the use of ionising radiation

In the first category are molecules such as peroxides and azo compounds, where thermally-induced homolysis results in the production of two radicals:

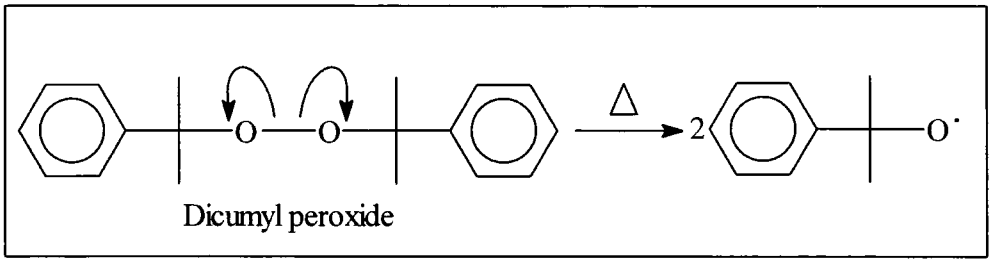

Figure 3.03 Thermally-Induced decomposition of a Peroxide Initiator

By judicious choice of the initiator used, the rate of decomposition can be controlled as a function of temperature such that optimal rates of reaction and/or degrees of polymerisation are attained

Metal Iodides, metal alkyls and azo compounds undergo photolysis to generate free radicals, *e.g.* α,α'-azobisisobutyronitrile (AIBN) decomposes by the action of light with a wavelength of 360nm.

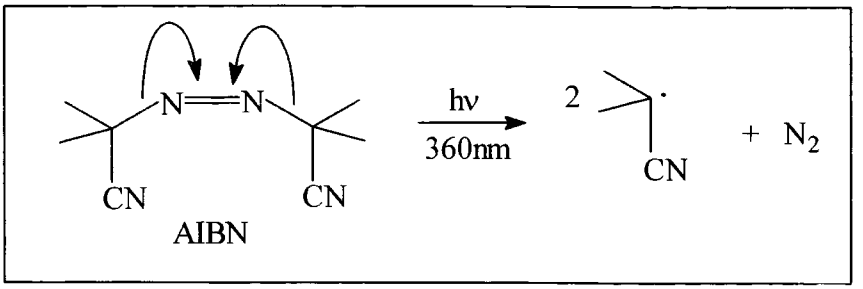

Figure 3.04 Photolytic Dissociation of AIBN

In both these types of reaction, a pair of radicals are normally produced per initiator molecule.

The classic example of a redox initiator is the reaction between ferrous ion and hydrogen peroxide to give a hydroxyl radical:

$$H_2O_2 + Fe^{2+} \rightarrow Fe^{3+} + OH^- + OH^\bullet$$

Figure 3.05 Ferrous Ion:H_2O_2 Redox Initiator System

Similarly, Cerium (IV) Sulphate oxidises an alcohol as follows:

$$RCH_2OH + Ce^{4+} \rightarrow Ce^{3+} + H^+ + RC(OH)H^\bullet$$

Figure 3.06 Oxidation of an Alcohol by Ce^{4+}

3.2.4. Types of Radical Polymerisation

Having established the initiation system, polymerisations are described by the state of the monomer in the reaction. It may be pure (*i.e.* a *bulk* reaction), in solution, or in a heterogeneous system such as in *precipitation* or *emulsion* polymerisation. Various factors determine which technique is used, and some of these are discussed below.

3.2.4.1. Bulk Polymerisation

Polymerisation in the bulk offers the simplest possible method of converting monomer to polymer, and has a distinct advantage in not requiring any other materials to be present in the reaction mixture. The resulting polymer can be utilised without the need for further purification. However, difficulties are experienced in bulk polymerisations due to the heat liberated by the polymerisation reaction (polymerisation reactions are always exothermic; two carbon-carbon single bonds are stronger than one carbon-carbon double bond) and the increasing viscosity as the reaction progresses. In the absence of powerful stirring devices, thermal inhomogeneities can result in "hot spots", causing polymer degradation, and difficulties with monomer transport can give polymer contaminated with unreacted monomer.

In spite of the problems discussed above, bulk polymerisation is a commercially important process, by which many polymers are made. Therefore, initial attempts at polymerisation were done in the bulk. Small volumes were used in pilot experiments, such that thermal inhomogeneities were kept to a minimum. No

attempt was made to stir the reaction. The container was a specially made tube of 10mm internal diameter, and fitted with a "Young's"-type tap at one end. Monomer, initiator (AIBN) and chain transfer reagent (1-octane thiol) were weighed into the tube according to the proportions reported by Koizumi *et al*[3], and then the liquid degassed by repeated freeze-vacuum-thaw cycles. The charged tube was then heated in an oil bath to 333K for 72 hours, after which the tube was broken to recover the polymer as a clear, colourless solid. In order to purify the polymers, they were dissolved in a suitable solvent (acetone) and reprecipitated into petroleum ether (40-60 fraction). The resulting polymers were dried *in vacuo* to constant weight.

This recipe was used with some success for trifluoroethyl and octafluoropentyl methacrylate, but attempts to reprecipitate polymers with longer side chains was marred by insolubility in common solvents. Also, noting the modest conversion (40%), bulk polymerisation was considered unsuitable for further use, and polymerisation in solution was attempted.

3.2.4.2. Solution Polymerisation

Given the poor conversion seen in the bulk polymerisation above, a polymerisation in solution was attempted. Again, trifluoroethyl methacrylate was used for the trials. The monomer was dissolved in butanone (MEK) (10% w/v). The resulting solution was deoxygenated by bubbling nitrogen through a glass sinter immersed in the liquid, which was then heated to reflux before the initiator (AIBN) was added. At the reflux temperature of butanone (353K), the half life of

the initiator is relatively short compared to its value at 333K, so no chain transfer reagent was added. An attempt was made to follow the reaction using the infra-red absorption of the double bond. The intensity of the absorption was taken at regular intervals, but no appreciable change was observed over 13 hours. After this time, more AIBN was added, to no apparent effect as seen by FT-IR. After a further 6 hours, the polymer was precipitated from MEK solution into petroleum ether (40-60 fraction), and dried *in vacuo*. The recovery of polymer was poor, only 35% by weight.

3.2.5. Emulsion Polymerisation

Emulsion polymerisations are seen to overcome most of the problems of the techniques mentioned above. They are known to go readily to high conversion,[4] and the presence of the dispersant eliminates the problems seen in early bulk methods such as those associated with viscosity and heat transfer. The most important difference, however, is that the molecular weight can easily be varied without the change in reaction rate seen in the techniques above. This is associated with a different reaction mechanism, and the different kinetics of that reaction.

A possible drawback of emulsion polymerisation is the presence of residual soap (sodium dodecyl sulphate) in the polymer. This could have an adverse effect on the determination of the surface energy of the material, so must be removed. Ion exchange and dialysis are possible techniques.

3.2.5.1. Qualitative Picture

The physical picture of emulsion polymerisation is based originally on the qualitative picture developed by Harkins[5]. Several other workers[6-8] have been responsible for the development of the quantitative description of the processes which occur in the reaction.

The main components of the process are the monomer(s), *dispersant, emulsifier*, and dispersant-soluble *initiator*. The dispersant is commonly water, and is the liquid in which the components are dispersed as an emulsion by the emulsifier. The emulsifier is often referred to as the *surfactant.* Other components, such as pH buffers, acid, alkalis and chain transfer reagents may be added to any particular system as required.

The locations of the various components require consideration. When the concentration of the emulsifier exceeds the *critical micelle concentration* (CMC), the excess surfactant molecules aggregate to form colloidal clusters called *micelles.* As the CMC is exceeded and the solution becomes a colloidal dispersion, heat is liberated (heat of solution) and there is a sharp fall in surface tension. In typical emulsion polymerisations, where the emulsifier concentration is around 2-3%, the CMC is exceeded by 1-3 orders of magnitude. Most of the emulsifier is therefore found in this micellar form.

When a water-insoluble or only slightly soluble monomer is added, a very small fraction dissolves and goes into solution. Of particular relevance to this work is the solubility of MMA, being 16g.dm^{-3} *c.f.* styrene, butadiene and vinyl chloride at 0.07, 0.8 and 7g.dm^{-3} respectively. A larger but still small portion of the monomer enters the interior of the micelles, they being of a hydrocarbon nature.

The largest portion, however, is dispersed as monomer droplets, the size of which is dependant on the intensity of agitation.

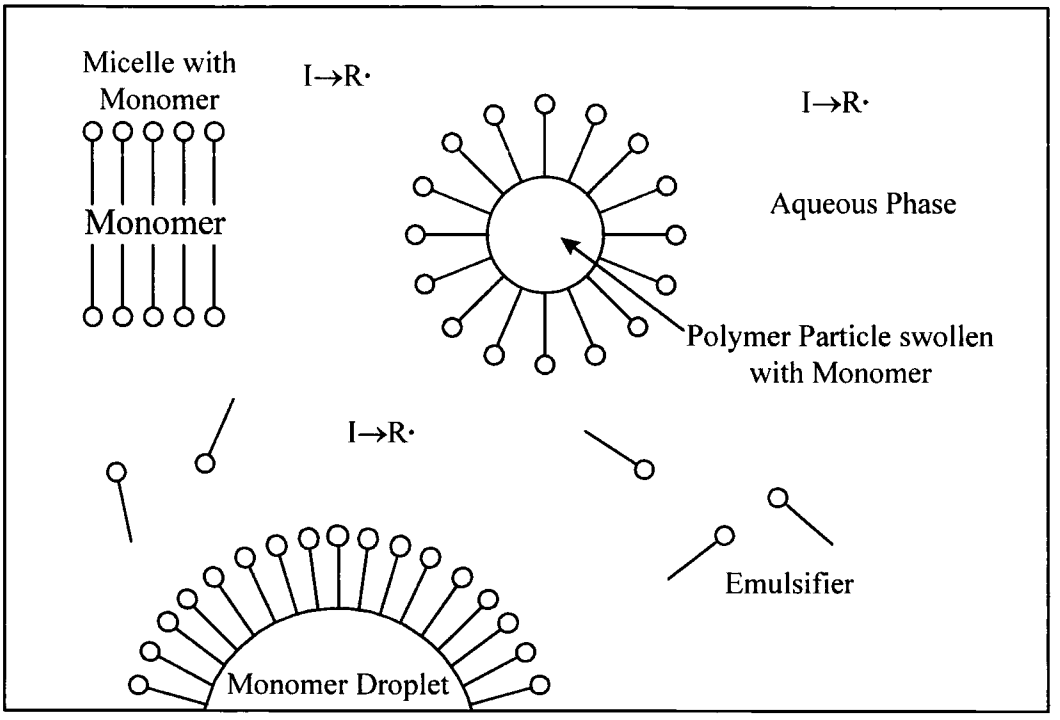

Figure 3.07 Qualitative Description of Emulsion Polymerisation

3.2.5.2. Progress of Polymerisation

A variety of behaviours are observed for the polymerisation rate *vs.* conversion, which are dependant on the relative rates of initiation, propagation and termination: these in turn are dependant on the reaction conditions and the monomer used. In all instances, however, there can be discerned three intervals (I, II, III), based on the number of particles (N = concentration of polymer particles, units: no. of particles/ml) and the existence of a separate monomer phase, *viz.* there is a separate monomer phase in intervals I and II, but not in III. The particle number is seen to increase in interval I, then remains constant in II and III. The nucleation of particles occurs during interval I, with the polymerisation rate increasing with time and the number of particles. As the

monomer present in the polymer particles reacts, it is replaced by monomer diffusing from the droplets. At some time during interval I, the particle number is seen to stabilise at some value, which is only a small percentage of the concentration of micelles initially present. Typical figures for N are of the order of 10^{13}-10^{15} particles per millilitre *c.f.* 10^{16}-10^{18} micelles per millilitre. As the polymerisation proceeds, the polymer particles, swollen with monomer, grow in size and adsorb more and more surfactant from that in solution to maintain stability. The surfactant concentration falls quickly, and soon drops below the CMC. At this point, the inactive micelles become unstable and break up with dissolution of the surfactant contained therein. By the end of interval I or very early in interval II, all or almost all of the surfactant has been adsorbed onto the polymer particles. Consequently, the monomer droplets, previously stabilised by the presence of surfactant, are unstable to coalescence unless vigorous stirring is maintained.

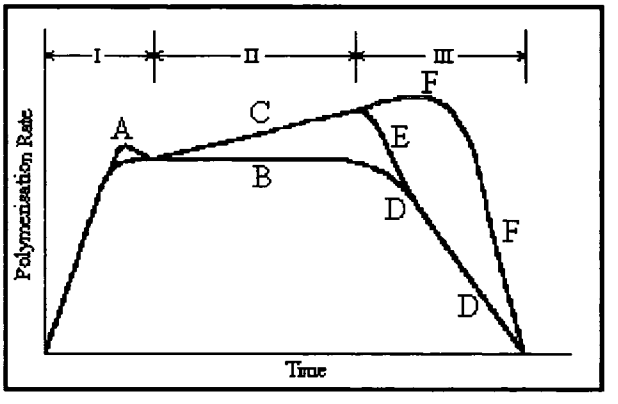

Figure 3.08 Progress of Emulsion Polymerisation

The duration of interval I is inversely proportional to the initiation rate, as this affects the time taken to attain a steady particle number. Monomers which display a high solubility in water also tend to complete interval I faster than less soluble monomers; this is attributed to the greater extent of homogeneous

nucleation in the soluble monomers, occurring alongside the "ordinary" micellar nucleation decreasing the time required to attain a steady particle number. The rate is seen to achieve a maximum at A, the proceeds with the rate either constant (B) or increasing slightly (C) during interval II.

The latter behaviour is a consequence of an autocatalysis phenomena called the *Trommsdorff effect*, which is a feature of many radical polymerisations. It results from the decrease in mobility of the polymeric radicals causing deviation in the steady state kinetics of the reaction. The rate of initiation remains constant, but the rate of termination is reduced as radicals are unable to get together in combination/disproportionation reactions.

The monomer concentration in the polymer particles is high; as much as 85% of the total monomer present is contained within the polymer particles. As the polymerisation proceeds during interval II, the polymer particles grow at the expense of the monomer droplets, the total disappearance of which heralds the beginning of interval III. The particle number remains the same during interval III as in II, but the monomer concentration drops with time as it is no longer being replenished by from the monomer droplets. The decrease in the volume fraction of monomer, ϕ_m, is slower in more water soluble monomers, as the monomers in solution act as a reservoir. The presence or absence of a Trommsdorff effect determines the behaviour in interval III, as represented in curve ED or F. Polymerisation continues at a steadily decreasing rate as ϕ_m decreases.

3.2.5.3. Kinetics of Emulsion Polymerisation

The rate expression for an emulsion polymerisation is derived by first considering the rate of reaction in a single polymer particle in which propagation is occurring, *i.e.*, a particle containing a radical, then the number of such particles. At the start of polymerisation, the typical concentration of micelles is 10^{18} per millilitre, and the initiation rate is 10^{13} radicals per millilitre-second. Therefore, a radical diffuses into a micelle every 10^{5} seconds at the start of interval I (*q.v.*). As the system progresses through interval I, this time period decreases dramatically, since the concentration of micelles is decreasing. A radical enters a particle every 10 seconds during interval II and III, where N is typically 10^{14} particles per millilitre. Once inside a micelle or polymer particle, the radical propagates in the usual way at a rate R_p dependent on the propagation rate constant k_p and the monomer concentration [M] in the particle.

$$R_p = k_p[M] \qquad \textbf{[3.14]}$$

The monomer concentration is usually quite high, since the equilibrium swelling of the particle by monomer is often of the order of 50-80% by volume. Values of [M] of 5*M* are not uncommon.

The next important event occurs when a radical enters a particle which already contains a propagating chain. For most reaction systems, the radical concentration in a polymer particle is $10^{-6}M$ or higher. This is a higher radical concentration than in homogeneous polymerisation systems, and the radical lifetime here is only a few thousandths of a second. Thus, the entry of a second

radical into the polymer particle results in immediate bimolecular termination. A polymer particle can therefore have zero or two radicals. The presence of two radicals is synonymous with zero radicals, as termination occurs so quickly. The particle is then dormant until another $(2n+1)$th radical arrives, after which it is activated and propagation proceeds until the next radical enters. The cycle of alternate growth and inactivity continues until the monomer conversion is essentially complete.

The rate of polymerisation at any instant is given by the product of the concentration of active particles [P$^{\cdot}$] and the rate of propagation in a particle.

$$R_p = k_p[M]\,[P^{\cdot}] \qquad \textbf{[3.15]}$$

[P$^{\cdot}$] is conveniently expressed by

$$[P\cdot] = \frac{10^3 N\bar{n}}{N_A} \qquad \textbf{[3.16]}$$

where N' is the concentration of micelles plus particles, $\bar{n}$ is the average number of radicals per micelle plus particle and N_A is Avogadro's number. The use of $10^3/N_A$ in eqn. 3.16 and subsequent equations expresses [P$^{\cdot}$] in moles/dm^3 and R_p in moles/dm^3.sec. Combining equations 3.15 and 3.16 gives the polymerisation rate as

$$R_p = \frac{10^3 N \bar{n} k_p [M]}{N_A} \qquad [3.17]$$

Interplay between the values of N' and $\bar{n}$ determine the rate of polymerisation throughout the reaction, the interested reader being referred to specific emulsion polymerisation texts for details, *e.g.* the Harkins reference already mentioned.

3.2.5.3.1. Kinetic Chain Length

As in other types of radical polymerisation, the kinetic chain length is synonymous with the degree of polymerisation. The number average degree of polymerisation for an emulsion polymerisation can be obtained by considering what occurs in a single polymer particle. The rate r_i at which primary radicals enter a polymer particle is given by:

$$r_i = \frac{R_i}{N} \qquad [3.18]$$

Since two radicals cannot coexist in the same particle, the rate of initiation is equal to the rate of termination. The degree of polymerisation is then the rate of growth of a polymer chain divided by the rate at which primary radicals enter the polymer particle. That is:

$$\bar{X}_n = \frac{r_p}{r_i} = \frac{N k_p [M]}{R_i} \qquad [3.19]$$

Comparing eqn. 3.17 and 3.19 with their analogues for homogeneous radical reactions shows the significant characteristics of emulsion polymerisation. In homogeneous polymerisations, the rate of polymerisation can be increased by increasing the rate of initiation at the expense of polymer molecular weight. The situation in emulsion polymerisation allows the rate and degree of polymerisation to be increased simultaneously by increasing the number of particles at constant initiation rate.

3.2.5.4. Experimental

The following "recipe" was used in early trials:

- Dispersant (water)
- monomer 10% v/v with water
- Emulsifier (Sodium Dodecyl Sulphate) 2% w/w with water
- Initiator (Potassium Persulphate) 1% w/w with monomer.

Dispersant and monomer were added to a suitable round-bottomed flask, and the emulsifier added as a solution in water. The resulting emulsion was deoxygenated by the bubbling of nitrogen through a glass sinter immersed in the liquid. The deoxygenated emulsion was then heated, with vigorous stirring, to 333K before the initiator was added, again as a solution in water.

As the polymerisation proceeds, the particle size grows and the emulsion becomes white and opaque. When no monomer can be detected (by smell), the heat is removed and the emulsion allowed to cool. The cooled emulsion was poured into pre-wetted dialysis tubing (BDH, 50.8mm diameter), knotted at each end, and immersed in distilled water. The water was changed regularly until no

soap bubbles persist on shaking of the "sausage". The polymer was seen to flocculate as the emulsifier concentration decreases. When dialysis was complete, the polymer was washed with methanol (this causes further flocculation), filtered, reprecipitated and dried *in vacuo* before characterisation and use. There is a noticeable decrease in the rate of flocculation between PMMA and the fluorinated polymers; this is attributed to the higher polarity of the fluoropolymers, making the soap "stick" to them more strongly.

Emulsion polymerisation is perhaps not the ideal technique for the polymerisation of MMA, as its comparatively high solubility in water means that the onset of the *Interval III* stage of polymerisation, where the rate of polymerisation decreases, occurs at around 25% conversion. Hence, if 100% conversion is required, the process will be lengthy. The hydrophobicity of the fluorinated monomers may reduce this effect

Another recipe has been described by Pittman *et al.*[9]

10g of monomer is added to a solution of 0.3g Sodium Dodecyl sulphate and 0.03g Potassium Persulphate (emulsifier and initiator respectively) in 25ml of water. This is deoxygenated by the passage of nitrogen, then, with vigorous stirring, heated to 60°C for 26 hours. The resultant latex is coagulated by pouring into rapidly stirred methanol (300ml), the polymer thus precipitated is filtered and dried *in vacuo* overnight. The yield is reported to be 85%.

The above procedure produced a material similar to that from the first, in 76.5% yield. However, the molecular weight of the polymer proved to be too great for analysis by GPC (calibration limit 1030000). Various unsuccessful attempts were

made to reduce the molecular weight, including variations in the emulsifier and initiator concentration. Another deviation from Pittman's original "recipe" was that dialysis was used to remove the emulsifier from the latex; the presence of emulsifier in the polymer is undesirable for the subsequent surface energy determination experiments.

3.3. Polymer Characterisation

Polymers were characterised by the standard techniques of polymer science *viz.* FT-IR, NMR (^{1}H, ^{13}C, ^{19}F), Size Exclusion (or Gel Permeation) Chromatography (SEC, GPC respectively) and DSC. The results from the DSC are discussed in a later section.

3.3.1. FT-IR Spectroscopy

The infra-red spectra of the polymers were taken as a solid in KBr. The resolution was $4cm^{-1}$, and 16 scans were taken. All spectra show a strong carbonyl absorption at around $1735cm^{-1}$ in PMMA and $1750cm^{-1}$ in the fluorinated polymers. The C=C vibration at around $1640cm^{-1}$ is seen to have disappeared. The fluorinated polymers all exhibit a strong absorption at $1170cm^{-1}$, attributable to C-F vibrations.

3.3.2. NMR Spectroscopy

NMR spectra were recorded at a frequency of 400MHz as a solution in D6-acetone. Proton and carbon spectra are seen to exhibit chemical shifts and splitting patterns conducive with the proposed structures. Fluorine NMR has been used to establish the presence of fluorine in the product, and lend further weight to the establishing of the structure.

3.3.3. SEC

Size exclusion, or gel permeation chromatography has been used to determine the molecular weight of the polymers produced. Polymer samples are dissolved in $CHCl_3$ or THF. Detection is by refractive index and viscosity, and the molecular weight calibrated against five polystyrene standards.

Sample	Solvent	M_w	M_n	PDI
Bulk PTFEMA	THF	$1.77x10^6$	$6.88x10^5$	2.56
Solution PTFEMA	THF	$1.98x10^5$	$5.21x10^4$	2.13
Emulsion PTFEMA	THF	$3.50x10^{6*}$	-	-
Emulsion PMMA	THF	$6.90x10^4$	$3.20x10^4$	2.18
P(MeTelMA), (solution)	THF	$1.10x10^5$	$4.85x10^4$	2.26
P(EthTelMA), (solution)	THF	$9.93x10^6$	$3.90x10^6$	2.55

* Peak molecular weight, beyond calibration limit.

3.4. Miscellaneous

Elemental analysis for sodium is extremely sensitive, the detection limit being in the parts per billion. The soap concentration decreased by the dialysis process, from 3% w/w (monomer) to 0.08% w/w(polymer). Dialysis for longer periods would further decrease the soap concentration, but a balance must be struck between adequate dialysis and the need for polymers for further experiments.

3.5. Anionic Polymerisation

Given the problems encountered with other (free radical) techniques, an attempt was made to prepare polymers using anionic initiators.

The major difference between free radical and anionically initiated polymerisation reactions is that, under ideal conditions (*q.v.*), one polymer chain is initiated per anionic initiator molecule, whereas radical centres readily undergo chain transfer to initiate several (many) polymer chains. The implications of this are quite significant, it means that polymer molecular weight should be controlled stoichiometrically, *i.e.* by the monomer to initiator ratio. Again given ideal conditions, it also means that the polydispersity of the polymer produced from such a reaction is low.

3.5.1. Ideal Conditions?

Anionic initiators, and indeed the propagating centre, exist as an ion pair, *i.e.* a closely associated pair of species of opposite charge.

Ideal conditions will depend on the monomer/initiator system used, but what is required is to solvate the ion pair sufficiently that the addition of monomer units to the propagating chain is very fast, and notably, much faster than any termination step. Under these conditions, the polymerisation reaction is described as being "living", and a propagating chain will continue to add monomer units until there are no more left to add. The living nature of a reaction can therefore be ascertained by the addition of further monomer, upon which the polymer chain will continue to grow. Under non-ideal conditions, there will be significant termination reactions, the living nature of the reaction will be destroyed and the molecular weight and polydispersity will be adversely affected.

3.5.2. Anionic Initiators

There are a number of species used to initiate anionic polymerisation reactions. These include covalent or ionic metal amides such as $NaNH_2$ and $LiNEt_2$, alkoxides, hydroxides, cyanides, phosphines, amines and organometallic compounds such as *n*-butyl lithium and Phenyl magnesium bromide. The common property of these reagents is their basicity, and initiation typically involves the addition of a nucleophilic (basic) initiator to a monomer, *i.e.*

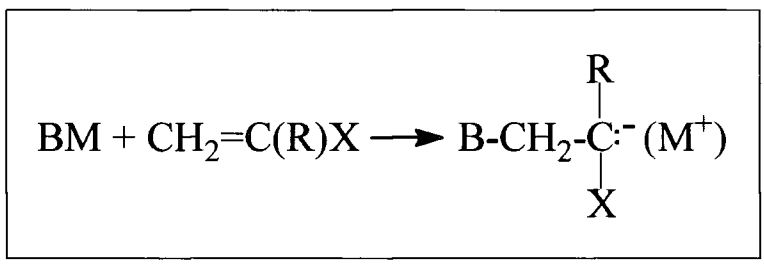

Figure 3.09 Initiation by Anionic Initiator

Propagation follows:

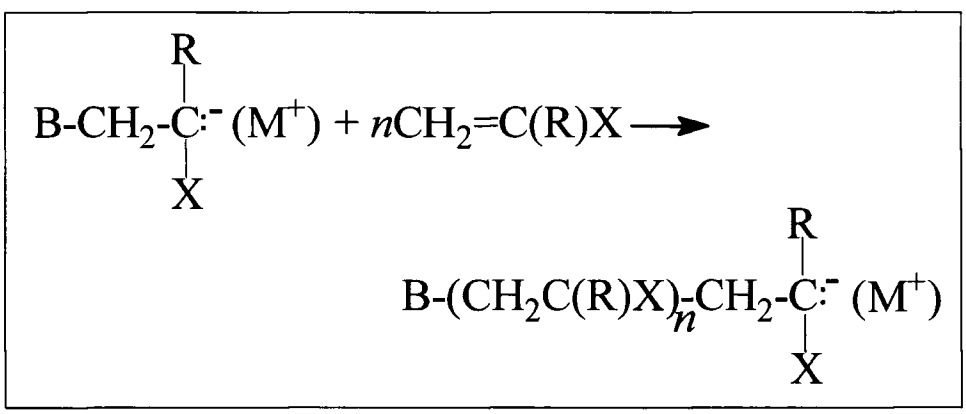

Figure 3.10 Propagation of Anionically-Initiated Chain

3.5.3. Experimental

3.5.3.1. Preparation of Initiators

3.5.3.1.1. Fluorenyl Lithium

Fluorenyl lithium was prepared by an exchange reaction between fluorene and *n*-butyl Lithium. 4.15g (0.025moles) of fluorene were weighed into a round-bottomed flask containing 35ml of dry THF. The solution was deoxygenated by the passage of nitrogen, before *n*-butyl lithium, (12ml, 2M in hexane) was added with stirring to give a deep orange solution. The concentration of fluorenyl lithium was ~0.5M.

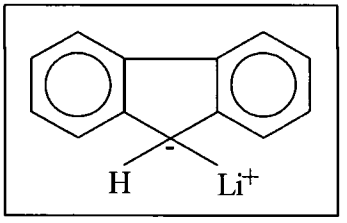

Figure 3.11. Fluorenyl Lithium

3.5.3.1.2. Sodium Naphthalene

6.4g Naphthalene (0.05moles) was dissolved into 50ml of dry THF in a round bottomed flask, then 1.2g (0.05moles) of sodium wire was added. The solution was stirred until the sodium wire had dissolved, upon which the solution became deep green in colour. The concentration of initiator solution was ~1M.

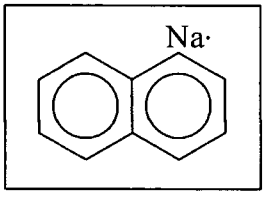

Figure 3.12 Sodium Naphthalene

3.5.3.2. Polymerisation Reactions

Anionic polymerisation is particularly sensitive to impurities, so extensive measures must be taken to purify the monomers before a reaction can be attempted. To this end, monomers were dried using $CaSO_4$, 3Å molecular sieve and CaH_2. Degassing was performed by repeated freeze-pump-thaw cycles.

Particular attention was paid to the removal of unreacted fluoroalcohol which may be present in the monomer. Anionic polymerisation reactions are often "killed" by the addition of methanol, so the presence of alcohols was considered to be especially deleterious to the reaction. These impurities were "mopped up" by the addition of trialkylaluminium species as recommended by McGrath[10], which complex strongly and irreversibly with alcohols to give aluminium alkoxide plus the corresponding alkane, *i.e.*

$$AlR_3 + R'OH \rightarrow Al(OR')_3 + 3RH$$

In this reaction, the aluminium species is added until a yellow coloration persists, in a similar manner to an acid-base titration with an indicator.

Polymerisation reactions were performed in a specially designed, multi-bulb apparatus similar to those used in the early work on living polymerisations[11]. Young's' taps were fitted between bulbs and the main "backbone" instead of thin seals. After evacuation, a benzene solution of polystyryl lithium (contained in one of the bulbs) was rinsed around the apparatus to remove any polymerisable contaminants present from previous uses. The vapour pressure of benzene is such that with the use of liquid air and the heat of ones hand, the polystryryl lithium solution can be distilled and washed back into its original bulb and confined by closing the tap.

The scrupulously clean apparatus was then attached to a vacuum line, and dried solvent (THF) introduced to the main bulb by vacuum transfer. An amount of monomer can then be added with a syringe though a septum into the main bulb. Initiator solution was added into a separate bulb through a septum. This procedure means that the monomer solution can be added rapidly to the initiator solution thereby helping to keep polydispersity to a minimum.

3.5.4. Results & Discussion

Noting the considerable benefits to be gained by the use of anionic initiators (notably polymers with well defined molecular weight and narrow polydispersity), it is somewhat disappointing to report the lack of success from these techniques. No polymerisation was affected by any of the reagents used in this work, recovering only monomer on the evaporation of the solvent. This is all the more disappointing noting the work of Narita *et al* [12-14], who has reported successes in the anionic polymerisations of various fluoroalkyl acrylates and methacrylates, along with a number of other fluorinated monomers.

The strong basicity of the initiators and comparative acidity of the hydrogens of the sidechain are implicated in the reasoning for the failure of these reactions. The hydgrogens make for an alternative (and favourable) site for the initiator to attack, *i.e.*

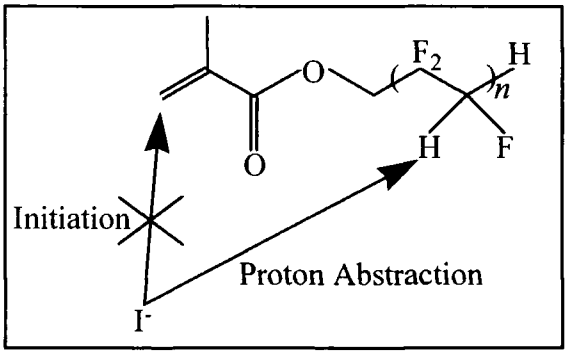

Figure 3.13 Competitive Initiation/ Proton Abstraction Reactions

3.6. References

1)Hatada, K.; Ute, K.; Tanaka, K.; Okamoto, Y.; Kitayama, T. *Polym J* **1986**, *18*, 1037.

2)Kerr, J. A. *Rate Processes in the Gas Phase*; Kochi,J.K., Ed.; Wiley: New York, 1973; Vol. 1.

3)Koizumi, S.; Tadano, K.; Tanaka, Y.; Shimidzu, T.; Kutsumizu, S.; Yano, S. *Macromolecules* **1992**, *25*, 6563.

4)Odian, G. G. *Principles Of Polymerisation*; 2 ed.; Wiley: New York, 1981.

5)Harkins, W. D. *J Am Chem Soc* **1947**, *69*, 1428.

6)Smith, W. V.; Ewart, R. W. *J Chem Phys* **1948**, *16*, 592.

7)Smith, W. V. *J Am Chem Soc* **1948**, *70*, 3695.

8)Gardon, J. L. *Emulsion Polymerisation,*; in "*Polymerisation Processes*".Schildknecht, C.E., Ed. with Skeist, I. ; Wiley-Interscience,: New York,, 1977.

9)Pittman, C. U. *et al. J Polym Sci, Polym Chem Ed* **1980**, *18*, 3413-3425.

10)McGrath, J. E.; Allen, R. D.; Long, T. E. *Polymer Bull* **1986**, *15*, 127-134.

11)Swarc, M. *Carbanions, Livuing Polymers and Electron Transfer Processes*; Interscience Publishers Inc:, 1968.

12)Narita, T.; Hagiwara, T.; Hamana, H. *Makromoleculaire Chemie, Rapid Communications* **1985**, *6*, 175-178.

13)Narita, T.; Hagiwara, T.; Hamana, H.; Goto, M. *Makromoleculaire Chemie* **1986**, *187*, 731-737.

14)Narita, T.; Hagiwara, T.; Hamanda, H.; Wakayama, A.; Hotta, T. *Makromoleculaire Chemie* **1987**, *188*, 273-279.

Chapter Four

Differential Scanning Calorimetry

4.1. Introduction

Differential Scanning Calorimetry, (DSC) is a commonly used technique which enables the determination of a number of thermal properties of a polymer. The technique is based on the observation that when a substance undergoes a physical or chemical change, there is an accompanying enthalpy change with heat flowing into or out of the system. The relevant changes which may be observed in a polymer system include melting and crystallisation, and also the glass transition. These processes all display characteristic DSC curves, making the technique ideal for their study.

4.1.1. Instrumental Information

The Perkin Elmer DSC7 is a power compensation instrument, measuring the differential change in heating power required to keep the sample (S) and a reference (R, empty sample pan) at the same temperature throughout a programmed heating profile. See fig 4.1. Data are presented as a trace plotting heat flow *vs.* temperature. Heat flowing into the sample (endothermic transition, *e.g.* melting) is represented by an increase in heat flow to the sample ("up", on the trace) and *vice versa* (*e.g.* crystallisation). The T_g manifests itself as a discontinuity in the baseline; see fig 4.2. This transition should always be endothermic, and care is needed when interpreting results from different workers where different instruments may have been used.

For more detailed information on the technique, the interested reader is referred to the excellent treatment in Turi's book[1]

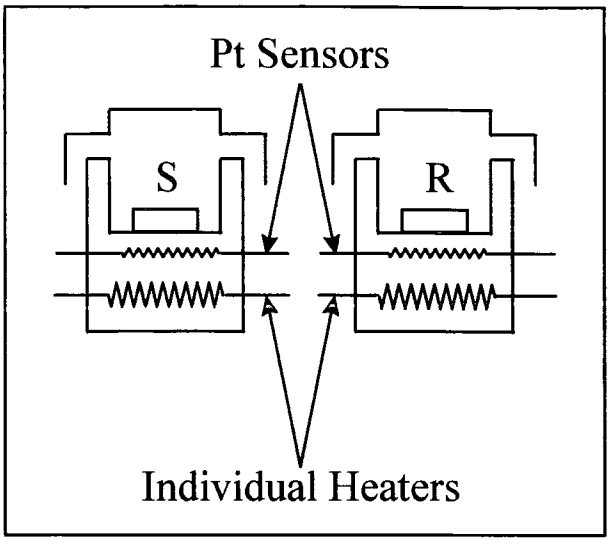

Figure 4.1 Schematic of DSC Instrument Head

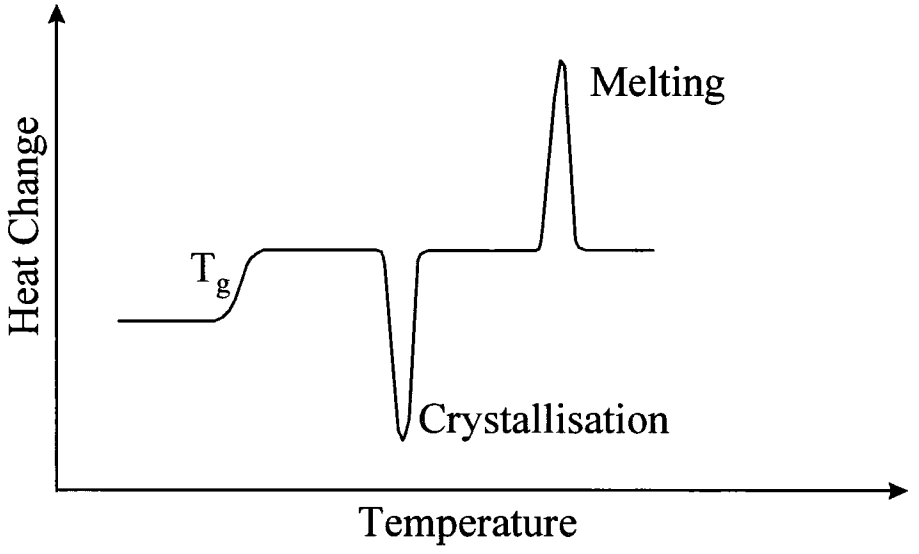

Figure 4.2 Idealised DSC Thermogram

The instrument was calibrated with samples of indium and zinc, noting their melting points (T_m) and the enthalpies of melting (ΔH_m). This enables the temperature to be placed on an absolute scale, and the enthalpy changes associated with the thermodynamic processes in the polymer to be evaluated in a quantitative manner.

The values given in the instruments' manual are:

Metal	T_m/K (Onset)	ΔH_m /J.g^{-1}
Indium	429.60	28.45
Zinc	692.47	108.37

Table 4.1 Expected Calibration Values for DSC7

Sample masses need to be kept small wherever possible to minimise thermal lag between the sample and the instrument. Typical sample masses are of the order of 2-7mg, although, in practice, some samples were larger to allow the necessary resolution to be achieved.

4.2. Thermogravimetric Analysis (TGA)

Prior to study by DSC, every sample was examined by thermogravimetric analysis (TGA) to assess its thermal stability and ascertain the presence of any residual solvent. This technique involves the pyrolysis of a small sample in an electric furnace in an inert atmosphere of nitrogen. The sample pan is suspended on one side of a sensitive balance, and a printout of mass loss *vs.* temperature is obtained.

TGA was used as a precautionary technique prior to DSC. By assessing the thermal stability of a sample, those with low thermal decomposition temperatures can be prevented from undergoing DSC analysis, as the condensation of any decomposition products onto the sensitive head of the instrument could be highly damaging to its performance and lifetime.

The technique may also be used to give a qualitative assessment of the state of mixing in a polymer blend[2-5]. A miscible blend is sometimes found to

decompose at a higher temperature than its constituent homopolymers; this is an example of a possible synergistic relationship between the properties of the constituents of a polymer blend resulting in improved performance of the blend over those of its separate components.

To confuse matters, there are also examples of blends in which one component has an adverse effect on the thermal stability of the blend as a whole, *e.g.* PVC:PMMA[6], PαMS:PS[7] and PVC:PVA[8] to name but a few. Furthermore, some pairs of polymers show no evidence of interaction in the thermal degradation of the blend, *e.g.* PS:PMMA[9]. Indeed, these systems also fall into the latter category

4.3. DSC and Polymer Blends

DSC has been used as a probe of the miscibility of polymer blends on numerous occasions; see for example,[10-17]. Immiscible polymer blends display the thermal characteristics of a simple intimate mixture, having individual glass transitions for each component of the blend. Binary miscible blends, on the other hand, display a glass transition temperature intermediate between the T_g of the two components.

Where a blend has a crystalline component, DSC can be used to measure the depression in the melting point of the crystalline polymer as a function of blend composition. This can be related to the strength of interaction between the constituent polymers of the blend, thereby giving an estimate of the Flory-Huggins interaction parameter, χ. As no crystallinity has been observed in the polymers used in this work, this technique was not available. Therefore the discussion will be centred on the glass transition behaviour of the materials.

4.3.1. Dependence of T_g with Blend Composition

A number of expressions have been formulated to predict the behaviour of the glass transition of polymer blends, the simplest of these being the "Rule-of-Mixtures" equation [4.1],

$$T_g = w_1 T_{g1} + w_2 T_{g2} \qquad \textbf{[4.1]}$$

where w_i is the weight fraction of pure homopolymer component i and T_{gi} is the corresponding glass transition temperature.

This expression assumes that the volume of the mixture is purely additive, and therefore the T_g of the blend increases monotonically with an increase in the weight fraction of the higher T_g polymer. However, it is often seen that there are deviations from a simple linear rise in T_g, indicating that the free volume of the blended system is not just the sum of the free volumes of its components, rather a more complex function which results in deviation from the behaviour predicted by equation 1. Prud'homme[18] and Painter[19] argue that the expression derived by Couchman and Karasz[20] is the most general of these, in that many of the other equations may be derived from this by making simplifying assumptions. The Couchman equation reads:

$$\ln T_g = \frac{w_1 \Delta C_{p1} \ln T_{g1} + w_2 \Delta C_{p2} \ln T_{g2}}{w_1 \Delta C_{p1} + w_2 \Delta C_{p2}} \qquad \textbf{[4.2]}$$

w_i and T_{gi} are defined above. ΔC_{pi} is the difference in specific heat between the glassy and liquid states at T_{gi}.

If it is assumed that $\Delta C_{p1} = \Delta C_{p2}$, then

$$\ln T_g = w_1 \ln T_{g1} + w_2 \ln T_{g2} \qquad \textbf{[4.3]}$$

which was proposed by Pochan *et al*[21]. Furthermore, if $T_{g2}/T_{g1} \approx 1$, the expansion of the logarithmic term in expression 3 can be limited to the first term, and Pochan's expression reduces to the Rule of Mixtures equation, [4.1]. The Flory-Fox equation[22] is derived from the rearrangement and expansion of the logarithm term in [4.3]:

$$\frac{1}{T_g} = \frac{w_1}{T_{g1}} + \frac{w_2}{T_{g2}} \qquad \textbf{[4.4]}$$

Again starting from [4.2], and instead of assuming $\Delta C_{p1} = \Delta C_{p2}$, (which is not a good assumption in most cases) a constant k is defined as $\Delta C_{p2}/\Delta C_{p1}$, one arrives at the Utracki expression[23]:

$$\ln T_g = \frac{w_1 \ln T_{g1} + k w_2 \ln T_{g2}}{w_1 + k w_2} \qquad \textbf{[4.5]}$$

Finally, limiting the expansion of the logarithm in eqn[4.2] to the first term, and with T_{g2}/T_{g1} close to unity:

$$T_g = \frac{w_1 T_{g1} + k w_2 T_{g2}}{w_1 + k w_2} \qquad [4.6]$$

which is the Gordon-Taylor equation, where k is defined as $\Delta\alpha_2 / \Delta\alpha_1$. $\Delta\alpha_i$ is the cubic expansion coefficient of polymer i. Both the "Rule of Mixtures" and Flory-Fox expressions are seen to be rather crude approximations. Equations 3, 5 and 6 are much better representations and are more generally applicable, especially 5 and 6 taking into account the ratios of specific heats.

All these expressions predict a continuous, monotonic dependence of T_g upon concentration:

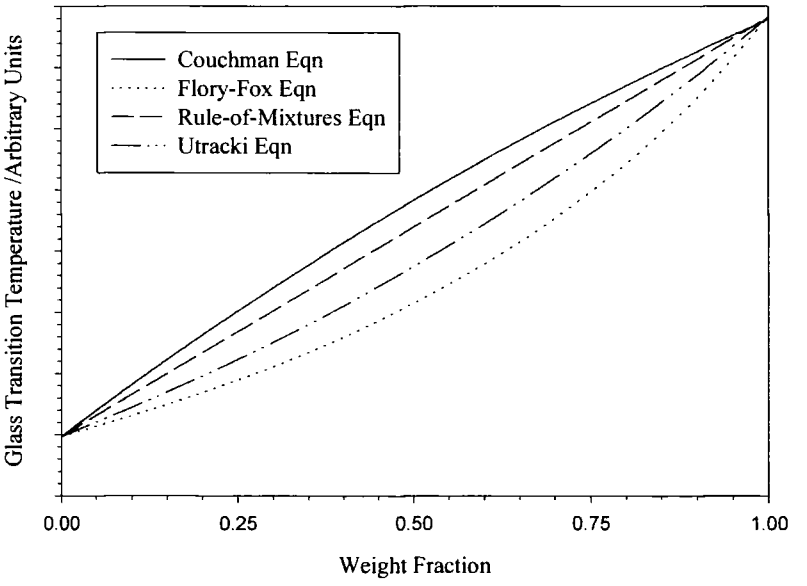

Figure 4.3 Graphical Comparison of a number of T_g:Composition Equations

It is common practice to use k as a fitting parameter, and using this approach, many experimental data can be fitted regardless of their deviations from linearity. Be'lorgey and Prud'homme related the "concavity" of the T_g-composition curve to the strength of interaction between constituent polymers in a blend[24]. When the interaction is very strong, such as effected by strong hydrogen bonds, blend T_gs higher than the weight averaged values can be observed[25].

However, where a discontinuity is found in the T_g:Composition behaviour, a more complex treatment is needed. Nandi *et al*[26] reported the existence of "cusps" in the T_g-composition diagram; that is, the curve displays discontinuities. They use the iso-free volume theory as modified by Kovacs[27] to arrive at complex expressions which allow the fitting of curves using the cubic expansion coefficients as the adjustable parameter:

$$T_g = T_{g,2} + \frac{f_{g,1}}{\Delta\alpha_2}\frac{\phi_1}{\phi_2} \qquad \textbf{[4.7]}$$

for $T<T_c$. T_c is the cusp point temperature. In their formulation $T_{g1}>T_{g2}$. Above T_c, the curve is expressed by the Kelley-Bueche equation:

$$T_g = \frac{\phi_1\Delta\alpha_1 T_{g,1} + \phi_2\Delta\alpha_2 T_{g,2}}{\phi_1\Delta\alpha_1 + \phi_2\Delta\alpha_2} \qquad \textbf{[4.8]}$$

The cusp point is given by:

$$T_c = T_{g,1} - \frac{f_{g,1}}{\Delta\alpha_1} \qquad \textbf{[4.9]}$$

and the composition at the cusp point by:

$$\phi_{2,c} = \frac{f_{g,1}}{\Delta\alpha_2\left(T_{g,2} - T_{g,1}\right) + f_{g,1}\left(1 - \Delta\alpha_2 / \Delta\alpha_1\right)} \qquad \textbf{[4.10]}$$

In the above equations, f_{gi} is the free volume fraction of polymer blend component i at their respective T_gs. According to the theory, f_{gi} has a value of 0.025. $\Delta\alpha_i$ is defined as above.

In spite of the apparent complexity of these expressions, they fail to fit T_g:composition data where there is a positive deviation from volume additivity, *i.e.* both parts of the expression predict negative deviations.

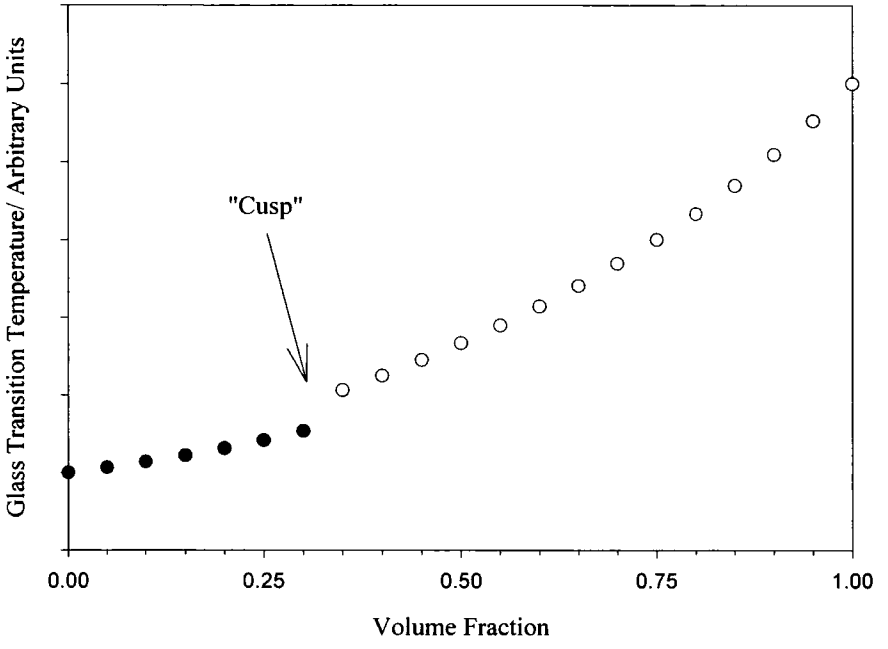

Figure 4.4 Glass Transition Temperature: Composition Behaviour after Nandi

An apparently simpler expression was proposed by Kwei[28]. S-Shaped curves were observed in blends of stereoregular (iso- and syndiotactic) PMMA with Novolac resins, and Kwei noted that the positive deviation from additivity was expressed by the product of the weight fractions and a fitting parameter. *i.e.* qw_1w_2.

The full expression reads:

$$T_g = \frac{w_1 T_{g1} + kw_2 T_{g2}}{w_1 + kw_2} + qw_1w_2 \qquad \textbf{[4.11]}$$

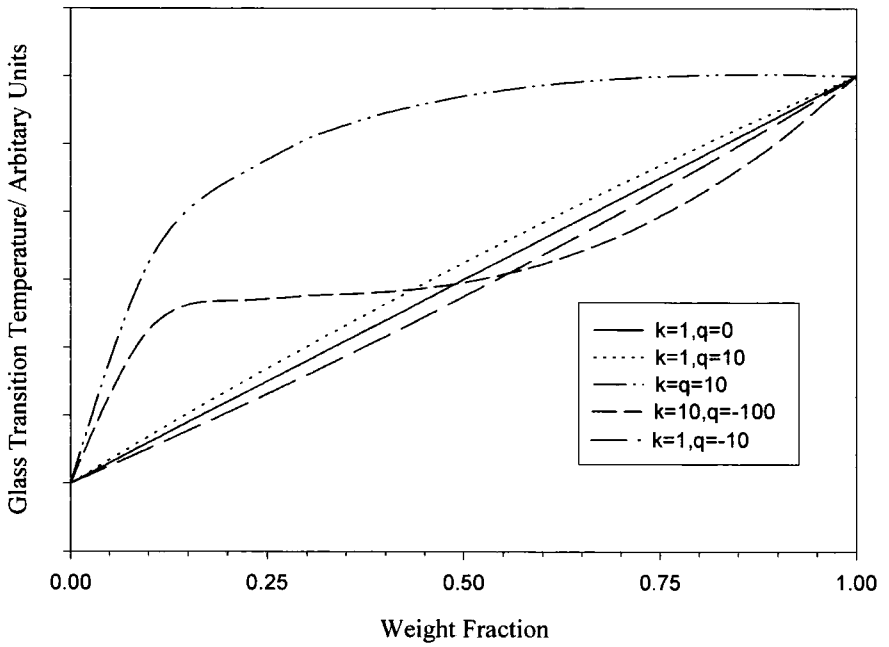

Figure 4.5 Interplay between the parameters *k* and *q* in the Kwei Equation

Fig 4.5 displays the inherent flexibility of Kwei's approach; through the appropriate choice of fitting parameters, their interplay means that a wide variety of curve shapes can be reproduced. This approach will be discussed further in terms of the results of this work.

Third Order Expressions

In the next strata of thermodynamic intricacy is the so-called "Third Order" expression proposed by Brekner *et al*[29]. Following a complex argument which combines the free volume theory of the simpler expressions with an extension of the solution theory of Flory, a powerful expression with two fitting parameters is obtained. The expression reads:

$$\begin{aligned}&\left(T_g - T_{g1}\right)/\left(T_{g2} - T_{g1}\right) = \\ &\left(1+K_1\right)\left\{\left[K'\left(T_{g1}/T_{g2}\right)w_2\right]/\left[w_1 + K'\left(T_{g1}/T_{g2}\right)w_2\right]\right\} \\ &-\left(K_1+K_2\right)\left\{\left[K'\left(T_{g1}/T_{g2}\right)\right]/\left[w_1 + K'\left(T_{g1}/T_{g2}\right)w_2\right]\right\}^2 \\ &+K_2\left\{\left[K'\left(T_{g1}/T_{g2}\right)\right]/\left[w_1 + K'\left(T_{g1}/T_{g2}\right)w_2\right]\right\}^3\end{aligned} \qquad \textbf{[4.12]}$$

The fitting parameters, K_1 and K_2, take values which depend on the contact energies in the local (binary) environment (K_2), and also the larger near neighbour interactions (K_1).

The constant K' is derived from free volume arguments similar to those of Gordon & Taylor, such that the equation is expressed as weight fractions rather than the less convenient volume fractions:

$$K = \frac{\rho_1 T_{g1}}{\rho_2 T_{g2}} = K'\frac{T_{g1}}{T_{g2}} \qquad \textbf{[4.13]}$$

This in itself stems from the application of the Simha-Boyer rule, assuming continuity of volume at T_g. Therefore, K' accounts for differences in density

between the components of the blend. As many polymers have similar densities, it is expected that $0.8 \leq K' \leq 1.2$. Should the disparity in the densities of the blend component fall outside this region, K should be used instead of K'.

Brekner applied this equation to a number of data, accurately reproducing the composition dependencies in blends of PS and PPO, PS and PVME and, perhaps most notably, the PMMA:Novolac blends studied by Kwei (*q.v.*)

4.3.2 Chi dependence on the Glass Transition

Extending further the significance of the fitting parameters from T_g:Composition equations is the work of Lu and Weiss[30]. This formulation gives a quantitative relationship between the T_g:composition behaviour of a polymer blend and the Flory-Huggins interaction parameter, χ.

A careful thermodynamic argument is followed, treating the glass transition formally as a second-order Ehrenfest transition, through which the thermodynamic state functions remain continuous, but their first derivatives undergo discontinuities.

Enthalpy is chosen as the thermodynamic parameter in the argument. The molar enthalpy of mixing of two polymers is given by:

$$H_M = x_1 H_1 + x_2 H_2 + \Delta H_{mix} \qquad \textbf{[4.14]}$$

where x_i is the mole fraction of component i in the blend and ΔH_{mix} is the excess enthalpy of mixing. A thermodynamic cycle was proposed for the mixing process:

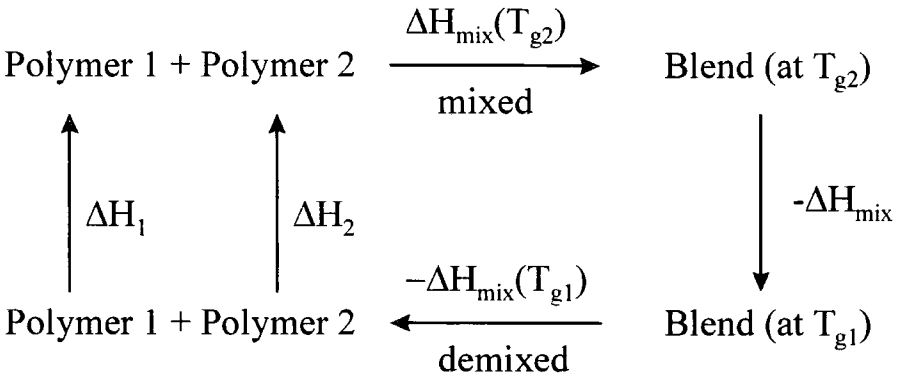

Figure 4.6 Proposed Thermodynamic Cycle for Polymer blending

Solving for ΔH_{mix} yields:

$$\Delta H_{mix} = x_1 \Delta H_1 + x_2 \Delta H_2 + \Delta H_{mix}\left(T_{g2}\right) - \Delta H_{mix}\left(T_{g1}\right) \qquad \textbf{[4.15]}$$

where ΔH_i and ΔH_{mix} are the enthalpy changes when the temperature is raised from T_{g1} to T_{g2} for component *i* and the blend respectively.

Now:

$$\Delta H_1 = \int_{T_{g1}}^{T_{g2}} c_{p1}^{l} dT \qquad \textbf{[4.16]}$$

$$\Delta H_2 = \int_{T_{g1}}^{T_{g2}} c_{p2}^{g} dT \qquad \textbf{[4.17]}$$

$$\Delta H_{mix} = \int_{T_{g1}}^{T_{gm}} c_{pm}^{g} dT + \int_{T_{g1}}^{T_{gm}} c_{pm}^{l} dT \qquad \textbf{[4.18]}$$

Here, c_{pi} is the isobaric specific heat of polymer *i*, and the superscripts g and l refer to the glassy and liquid states respectively. Experiment has shown[31] that the c_p of a blend is not given simply by the weighted average of the specific heats of its components, and Wolf *et al*[32] have proposed a quadratic cross term:

$$c_{pm} = x_1 c_{p1} + x_2 c_{p2} + x_1 x_2 \delta c_p \qquad \textbf{[4.19]}$$

δc_p is the specific heat change on blending. This is usually negative for a miscible blend[31].

Substituting the integral forms of the enthalpy into [15] and noting the result of [19], the following is obtained:

$$T_{gm} = \frac{x_1 T_{g1} + k x_2 T_{g2}}{x_1 + k x_2} - \frac{\Delta H_{mix}\left(T_{g1}\right)}{\left(x_1 + k x_2\right)\left(\Delta c_{p1} - x_2 \delta c_p^g\right)} \qquad \textbf{[4.20]}$$

where

$$k = \frac{\Delta c_{p2} - x_1 \delta c_p^l}{\Delta c_{p1} - x_2 \delta c_p^g} \qquad \textbf{[4.21]}$$

and

$$\Delta c_{pi} = c_{pi}^l - c_{pi}^g \qquad \textbf{[4.22]}$$

i.e. Δc_{pi} is the change in specific heat of species *i* at T_{gi}.

Using the Van Laar relationship for the enthalpy of mixing of a binary polymer blend, the following is obtained:

$$\Delta H_{mix}(T) = \chi R T \phi_1 \phi_2 \qquad \textbf{[4.23]}$$

where ϕ_i is the volume fraction of component *i*, R is the gas constant, T the absolute temperature and χ the Flory-Huggins interaction parameter, as required.

Substituting this expression into [4.20]

$$T_{gm} = \frac{x_1 T_{g1} + kx_2 T_{g2}}{x_1 + kx_2} - \frac{\chi R\left(T_{g2} - T_{g1}\right)\phi_1\phi_2}{\left(x_1 + kx_2\right)\left(\Delta c_{p1} - x_2 \delta c_p^g\right)} \qquad \textbf{[4.24]}$$

In general, χ is found to have a quadratic dependence on composition:

$$\chi = \chi_0 + \chi_1 w_2 + \chi_2 w_2^2 \qquad \textbf{[4.25]}$$

Considering this result, and redefining Δc_{pi} in terms of unit mass, an expression in terms of the more convenient weight fractions is obtained:

$$T_{gmix} = \frac{w_1 T_{g1} + kw_2 T_{g2}}{w_1 + kw_2} + \frac{A w_1 w_2}{\left(w_1 + kw_2\right)\left(w_1 + bw_2\right)\left(w_1 + cw_2\right)^2} \qquad \textbf{[4.26]}$$

where

$$A = \frac{-\chi R\left(T_{g2} - T_{g1}\right)c}{M_1 \Delta c_{p1}} \qquad \textbf{[4.27]}$$

and

$$k = \frac{\Delta c_{p2} - w_1 \delta c_p^l}{\Delta c_{p1} - w_2 \delta c_p^g} \qquad \textbf{[4.28]}$$

$c = \rho_1/\rho_2$, $b = M_2/M_1$, ρ_i is the density of polymer *i* and M_i the molar mass per chain segment of component *i*.

The work goes on to consider the interplay of the various parameters when the interactions between polymers in a blend are very weak, moderate and strong.

In the limit of very weak interactions, δc_p and χ (hence A) are very small, and may be neglected. The equation then simplifies to the well-known Couchman equation [4.2] (*q.v.*).

At the other extreme, where there are strong interactions between the blends' constituents, the importance of χ (A) becomes paramount, and the effects of δc_p may be neglected. This simplifies the k-parameter:

$$k = \frac{\Delta c_{p2}}{\Delta c_{p1}} \qquad \textbf{[4.29]}$$

This simplification means that in the strong interaction regime, the equation has no adjustable parameters; it is possible to determine A, b, c and k experimentally.

A number of these expressions will be used in the subsequent discussion in an attempt to fit and interpret the experimental results from this work. Of particular interest is the lattermost expression [4.26-28], enabling as it does an evaluation of the Flory-Huggins interaction parameter. It will then be possible to compare the results from DSC experiments directly with those obtained by small angle neutron scattering.

4.4. Experimental

Sample preparation involves the accurate weighing of the material into an aluminium sample pan, which is then closed with a lid and crimped to give a leak-proof package. The sample weight was carefully recorded as this is required in calculations of the enthalpy change seen in the various transitions observed on a "run".

In order to prepare samples of blended materials, they were first dissolved in a common solvent, and reprecipitated into a suitable non-solvent. Butanone and THF have been found to be suitable solvents for PMMA/PTFEMA, petroleum ether was used for the non-solvent (6ml 3% polymer solution into 50ml 40-60 petroleum ether). The rapid reprecipitation of the polymers in the blend means that there is insufficient time for them to separate should there be any propensity to do so, so on a gross scale at least, a homogeneous material is produced. Blends of PMMA with P(MeTelMA) and P(EthTelMA) were prepared in an identical manner. The blends are then dried *in vacuo* to constant weight, then a sample is weighed out into a pan as for the pure homopolymers.

Samples are heated at a rate of $10Kmin^{-1}$ from 293-423K, then quenched back to 293K at a rate of $200Kmin^{-1}$ before reheating as before. This heating profile is used to enhance the content of glassy polymer in a sample, as rapid quenching from the melt inhibits any tendency for the polymers to crystallise. T_g's were recorded from the reheat cycle of the heating profile.

4.5. Results and Discussion.

4.5.1. Homopolymers

The results from the DSC on the homopolymers are shown in table 4.2.

Polymer	T_g/K	ΔC_p/J/g.K
PMMA	401.20	0.05
PTFEMA	350.76	-
Poly(styrene)†	379.75	-
P(MeTelMA)	333.33	0.12
P(EthTelMA)	351.98	0.13

Table 4.2 Results from DSC Studies

†Poly(styrene) was run to check correct operation of instrument.

The value of T_g for the PMMA is quite high compared to the literature values (~378K), indicative of a high proportion of syndiotactic polymer. The tacticity of the PMMA has been verified by ^{13}C NMR, the analysis of which gave 61% rr dyads and 39% mr (= rm) dyads. Significantly, the number of mm dyads, corresponding to isotactic sequences, was negligible. Therefore, it can be concluded that the polymer is highly syndiotactic and the value of T_g is reasonable.

4.5.2. Blends of Model Polymers.

4.5.2.1. PMMA: PTFEMA

The running of a first blend (1:1 PMMA:PTFEMA) clearly shows two glass transitions, at positions similar to those found in the pure homopolymers. As stated earlier, this is indicative of an immiscible blend at this composition. This behaviour is found to persist across the whole composition range of this combination of polymers; there is very little variation in the T_g's of either component of the blend: see Fig 4.5

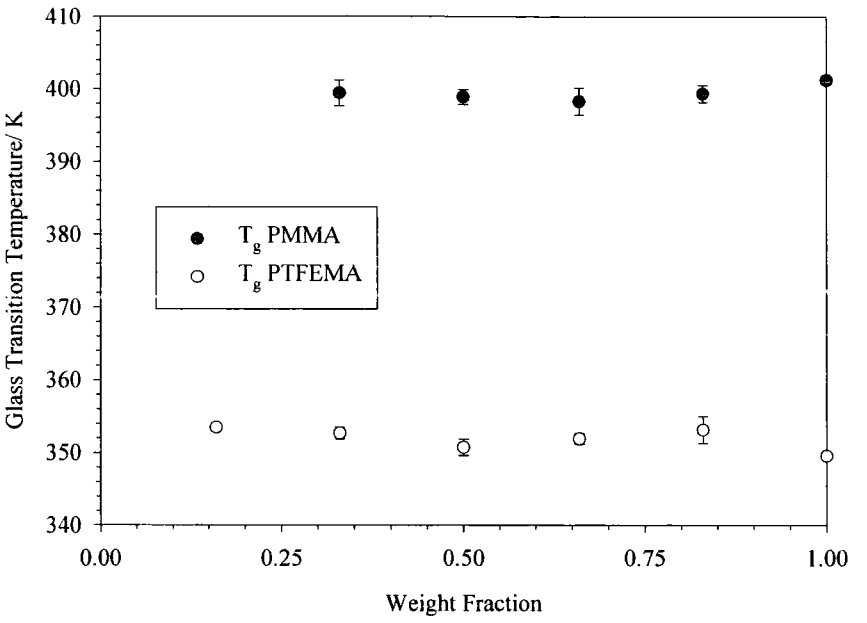

Figure 4.7 Variation of Glass Transition Temperature with Composition: PMMA: PTFEMA

note: no T_g for PMMA was resolved in the 16% PMMA blend. The transition was probably too small to be resolved by the instrument

4.5.2.2. PMMA: P(OFPMA)

Attempts to prepare blends of PMMA with poly(octafluoropentyl methacrylate) were unsuccessful, in that the poly(octafluoropentyl methacrylate) was found to be insoluble and co-precipitation was impossible. It is suspected that the fluorinated polymer had crosslinked during the polymerisation reaction, as a number of solvents were observed to swell the polymer, but dissolution was never achieved.

4.6. Target Polymers

4.6.1. PMMA:Methanol Telomer Methacrylate P(MeTelMA)

The T_g-composition diagram for PMMA:P(MeTelMA) is shown below. The most obvious trait of the system is the complex deviation from linearity. Sigmoidal curves have been discussed above. Positive deviation from linearity is attributed to the decreased free volume caused by a strong interaction between the blend components. Such interactions behave as crosslinks in the blend, inhibiting molecular motion and hence increasing the T_g. The negative deviations in the high PMMA weight fraction region of the curve represent the more normal behaviour. While a single T_g is still observed, the volume additivity of the blend in this region follows the more normal positive deviation. Theories describing the state of the blend in this region will be presented later after more data have been considered.

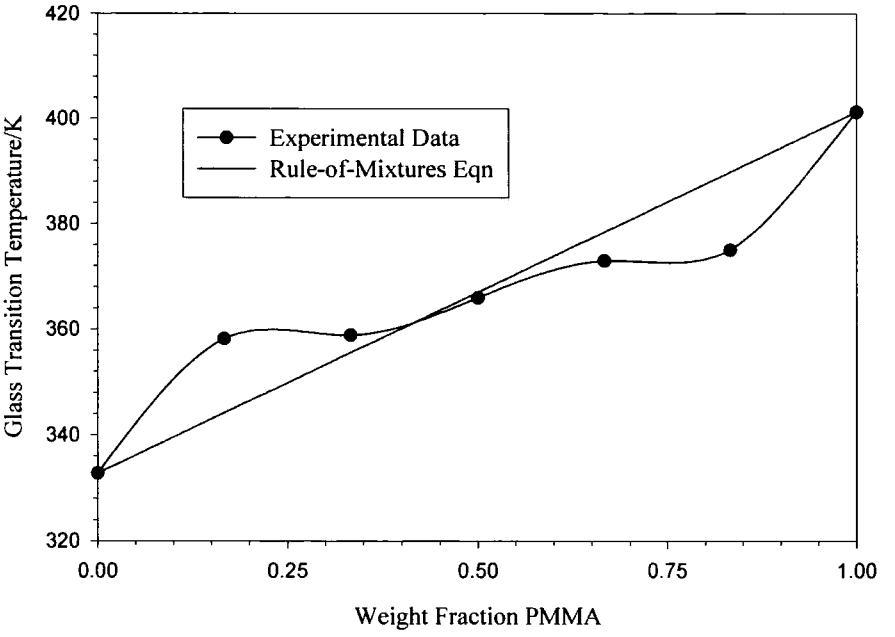

Figure 4.8 Variation of Glass transition temperature with composition: PMMA: P(MeTelMA)

4.6.2. Ethanol Telomer Methacrylate P(EthTelMA)

Again, the T_g/composition diagram of PMMA:P(EthTelMA) is shown below. It is readily noticeable that the behaviour of this blend is rather different to that of the blend containing P(MeTelMA). Most noticeable is the negative deviation from rule-of-mixtures behaviour. The size of the deviation should also be emphasised; the negative deviation seen in this blend is markedly smaller than that observed in either sense in the PMMA:P(MeTelMA) blend. The apparent positive deviations are probably more to do with the spline routine used to generate the guiding line through the data rather than any physical process in the blend itself. The reasons behind the negative deviation have been discussed above, but it seems most interesting that the methyl group (being the difference between the two sidechains) has such a profound effect on the miscibility behaviour of the blends.

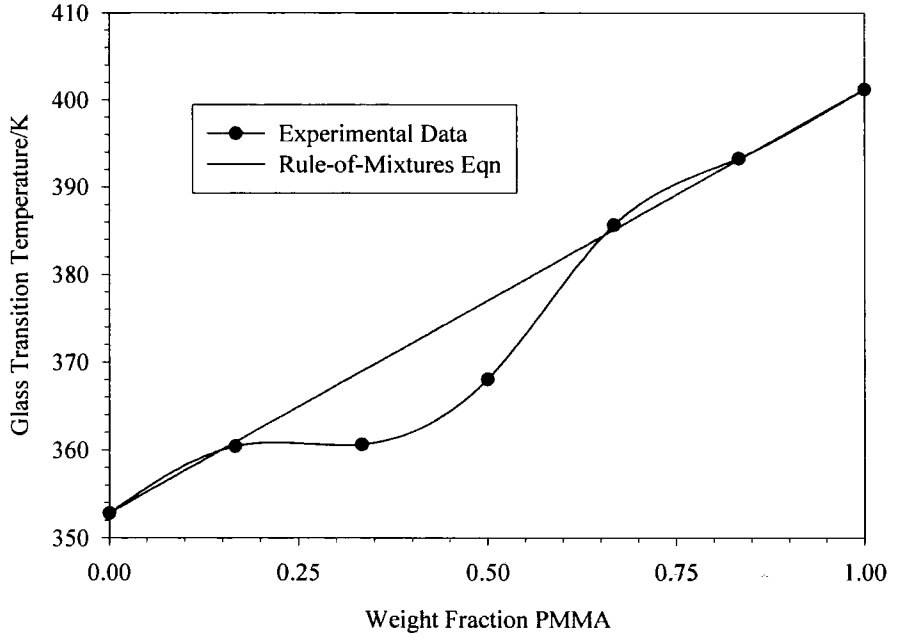

Figure 4.9 Variation of Glass Transition temperature with composition: PMMA: P(EthTelMA)

By recourse to the earlier studies on blends of PMMA with poly-(trifluoroethylmethacrylate), it is immediately apparent that the interactions between the groups β-to the carbonyl carbon are not the limiting factor in determining the miscibility behaviour of these blends, *viz.*;

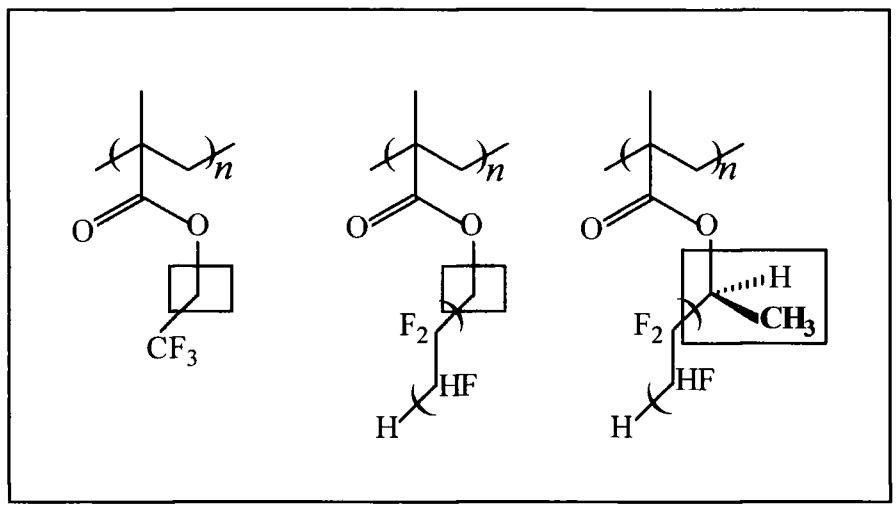

Figure 4.10 Comparison of the Groups β-to the Carbonyl Carbon

The more electron-deficient hydrogen atoms further down the sidechain are clearly more important, as their interactions with the carbonyl groups of the PMMA are stronger that the comparatively electron-rich sites nearer the ether-type oxygen.

The chirality of the carbon β-to the carbonyl in the P(EthTelMA) has already been hinted at. This may effect the interactions between the fluorinated sidechain and the tactic PMMA.

4.6.3. Fitting to the Kwei Equation

As mentioned earlier, Kwei[28] observed sigmoidal curves in blends of PMMA with Novolac resins, which are described by the equation

$$T_g = \frac{w_1 T_{g1} + k w_2 T_{g2}}{w_1 + k w_2} + q w_1 w_2 \qquad \textbf{[4.11]}$$

The fits to the data are shown in the figures below:

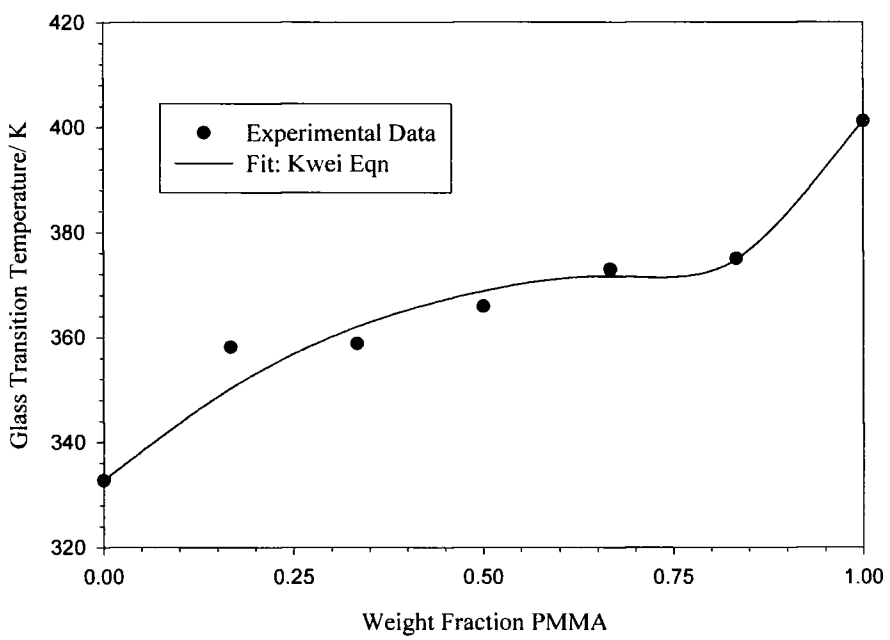

Figure 4.11 PMMA:P(MeTelMA): Fit by Kwei Equation

k= 0.12, q = 114.07

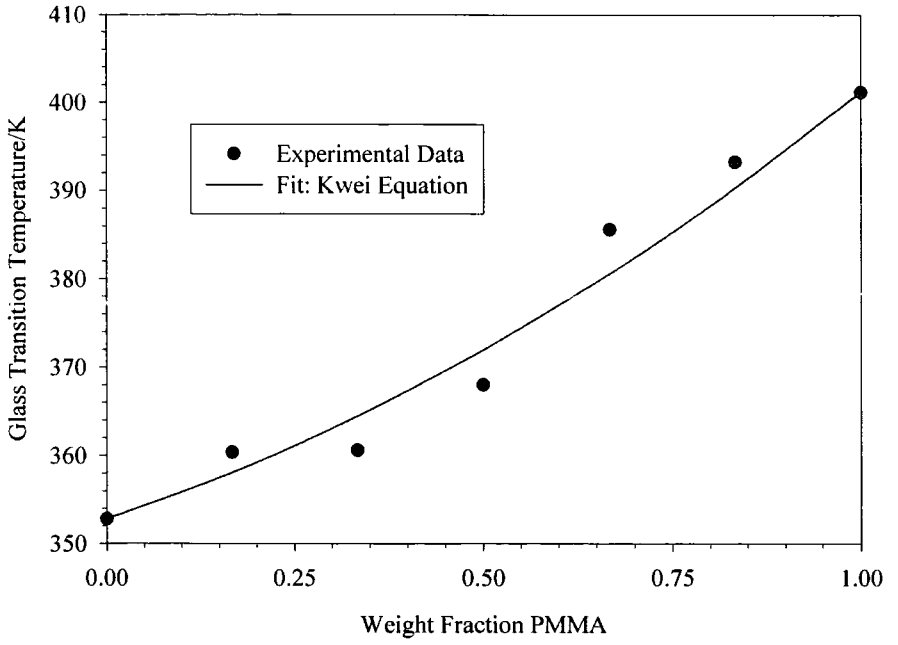

Figure 4.12 PMMA: P(EthTelMA): Fit by Kwei Equation

k = 1.0, q = -20.27

The Kwei expression gives a reasonable account of the behaviour of the PMMA:P(MeTelMA) blend, although the fit is far from perfect. Lin *et al* [33] propose a physical interpretation of the fitting parameters in the Kwei equation [4.11], *viz.* k & q.

This equation may be rewritten in terms of the weight fraction of the component with the higher T_g:

$$T_g = \frac{T_{g1} + w_2\left(kT_{g2} - T_{g1}\right)}{1 + w_2(k-1)} + q\left(w_2 - w_2^2\right) \qquad \textbf{[4.30]}$$

Differentiating with respect to w_2 and rearranging, for the case where k = 1, the following is obtained:

$$w = \frac{T_{g2} - T_{g1} + q}{2q} \qquad \textbf{[4.31]}$$

and the second derivative is:

$$\left.\frac{d^2 T_g}{dw^2}\right|_{k=1} = -2q \qquad \textbf{[4.32]}$$

For k = 1, the function will have its extremum at the value given by equation 4.32, and there will be no point of inflexion. The extremum will be a minimum for q<0, and a maximum for q>0.

The case where k = 1 also allows consideration of the physical interpretation of q. Again, when k = 1, equation 4.11 simplifies to:

$$T_g = \left(w_1 T_{g1} + w_2 T_{g2}\right) + q w_1 w_2 \qquad \textbf{[4.33]}$$

The terms in the brackets represent the weighted mean of the T_g's of the components of the blend, and the quadratic term gives the deviation of the blend's T_g from this value. It is widely accepted that the glass transition is associated with the inchoate motion of the polymer backbone. The product $k_B T_g$ is the average thermal energy which is just sufficient to overcome the energy barriers which, below T_g, immobilise the backbone. Therefore, the product $k_B q w_1 w_2$ is the excess energy by which the average stabilisation of the backbone

is moderated from the weight-averaged value for the homopolymers. If q is positive, the excess stabilisation means that the T_g of the blend will be higher than the weighted mean value; the converse is also true.

The forces which inhibit the motion of the backbone are ultimately governed by the contact interactions formed between the backbones, be they homo- or heterocontacts. Using a simple lattice model, Lin arrives at the following for the excess stabilisation energy:

$$k_B q w_1 w_2 = \phi_{11} E_{11} + \phi_{22} E_{22} + \phi_{12} E_{12} - 0.5\left(E_{11} + E_{22}\right) \qquad \textbf{[4.34]}$$

This expression is similar to that for the enthalpy of mixing of a (polymer) solution. ϕ_{ij} is equal to the probability of finding an *ij*-contact in the mixture, and this probability will clearly be related to the composition. To estimate this probability in the lattice model, only the near neighbours will be considered. A co-ordination number must also be assumed; 6 is the value used by Lin. If a backbone segment is surrounded by (6) other segments, connectivity constraints mean that two adjacent sites must be occupied by members of the same chain. The remaining sites will be occupied by other segments, statistically distributed between homo- and hetero- segments. Therefore, the probability of a component 1 segment forming a heterocontact is:

$$\phi_{12} = \frac{4}{6} w_2 \qquad \textbf{[4.35]}$$

and the probability that such a contact will be found anywhere throughout the system is:

$$\phi_{12} = \frac{4}{6} w_1 w_2 \qquad \textbf{[4.36]}$$

These primitive statistics only apply if the polymer segments are distributed randomly throughout the system. Clearly, this does not accurately represent a polymer:polymer mixture, and to compensate for this discrepancy, a dispersion factor f is introduced:

$$\phi_{12} = f \frac{2}{3} w_1 w_2 \qquad \textbf{[4.37]}$$

Rearranging [4.34] and eliminating ϕ_{11} and ϕ_{22}:

$$q = \frac{2f}{3k_B}\left[E_{12} - 0.5\left(E_{11} + E_{22}\right)\right] \qquad \textbf{[4.38]}$$

It is now possible to consider the implications of obtaining various values for the fitting parameters k and q.

k = 1 and q = 0:

$$E_{11} = E_{12} = E_{22} \qquad \textbf{[4.39]}$$

i.e. the energy of the heterocontacts is the same as the energy of the homocontacts. In this case, the blend will display a T_g:composition behaviour which is linear in all terms, *i.e.* it will be the weighted mean value.

There is, however, another explanation for this behaviour; the enhanced stabilisation of one component may be (almost) exactly balanced by the destabilisation of the other component. In this case, E_{12} is the arithmetic mean of the energies of the homocontacts.

k = 1 and q > 0:

Here, $E_{12} > 0.5(E_{11} + E_{22})$. The interaction between hetero- segment pairs is strong, and the blend T_g is higher than the arithmetic mean of its components.

k = 1 and q < 0

Given this set of parameters and considering the result above, it would seem at first that a negative value of q would imply that the blend should be immiscible. This is not necessarily the case; while the free energy of mixing overall must be negative for a blend to be miscible, the interplay between the enthalpy and entropy is to be considered. In this regime, it seems that the enthalpy factor is not so dominant, and it is an increase in entropy resulting from the disruption in

packing of the high T_g polymer which makes an important contribution to the miscibility of the blend. The enthalpy is still an important consideration; there must still be a weak favourable interaction to allow the co-ordination of the blends' components.

At this point, it is instructive to calculate the magnitudes of these energies under consideration. If a 1:1 blend is taken, with the (large) q-value of 50, the molar excess stabilisation energy Rqw_1w_2 has a value of 0.104 kJ.mol^{-1}. Contrast this with the value of the backbone stabilisation, RT_g, which equals 3.121 kJ.mol^{-1}. Even with the large value of q used in this calculation, the excess stabilisation energy is still only of the order of 3% of the backbone stabilisation energy. The glass transition is a very sensitive monitor of changes in the stabilisation energy in a polymer blend.

$k \neq 1$ and $q \neq 0$

Finally, the case where both k and q deviate from the simple relations is considered. In this regime, the system changes from one which is stabilised relative to additivity to one which is destabilised. In the amorphous matrix, this must correspond to a change in molecular morphology.

Such systems are normally predisposed to phase separation, and Lin's interpretation centres on a phase behaviour similar to that observed in segmented block copolymers. These systems can only support hetero-interactions across

phase boundaries, and these interactions tend to maximise interfacial area and minimise the volumes of the individual phases.

To get back to the fits to the data from this work, for the PMMA:P(MeTelMA) blend, values of $k = 0.12$ and $q = 114.07$ are found. Clearly, this is a very large value for q, and the significance of having a k-value differing from unity has also been explained. These values fall into the regime in which the system is considered to be in a state of microphase separation. That the DSC experiment finds a single glass transition temperature reflects simply on the resolution of the technique. The length scale over which the changes thought responsible for the glass transition take place are on the micrometer scale. One must therefore assume that the phase separation in this system is on a smaller length scale.

The values for k and q found for the PMMA:P(EthTelMA) are 1.0 and -20.27, respectively. These values fall into the regime in which a weak interaction is implied, and the blend T_g is moderated by the entropic considerations discussed above. Put in simple terms, the low T_g component acts as a lubricant between chains of the high T_g polymer thereby reducing the T_g of the blend as a whole.

4.6.4. Evaluation of the Flory-Huggins Interaction Parameter (χ) from T_g: Composition Behaviour

The expression derived by Lu & Weiss[30] has also been used here to give a quantitative analysis of the behaviour of these blends. Equation 26 was applied to the data generated from the DSC experiment, and solved for A. Noting the large q value obtained for the PMMA:P(MeTelMA) blend from the use of the Kwei

equation, Lu's expression was applied with the strong interaction assumptions detailed in equation 29.

The graph produced by this approach is shown in figure 4.13:

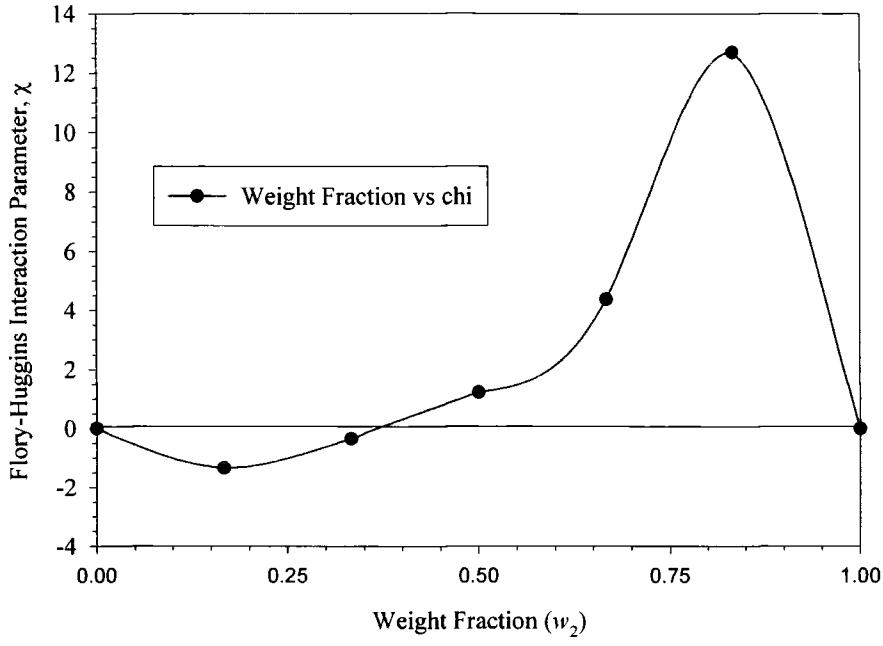

Figure 4.13 Variation of χ with Composition PMMA:P(MeTelMA)

Two things are worthy of mention from this; the first is that the χ-dependence mirrors the T_g data. This is to be expected. As mentioned earlier, a T_g above the weighted mean value is indicative of a strong interaction between the components of the blend, therefore, a negative value for χ is obtained. The converse of this is also true; where the T_g falls below the weighed mean value, the strength of interaction is weak or unfavourable giving a positive χ.

The second, and perhaps more important point to note is the magnitude of χ. P(HMMA): P(DMMA) (a weakly interacting polymer blend) show χ-values of the order of $^{-}1\text{-}2\text{x}10^{-2}$, similarly, PEO:PMMA ranges from $^{-}1.5\text{-}\ ^{-}4\text{x}10^{-2}$. Noting these results, and comparing them with the extremum of fig 4.6, *i.e.* $^{+}12.7$, the data clearly should not be taken on its absolute values. Notwithstanding this, the

trends shown give useful information as to the physical state of the blend, and lend weight to the theories of Lin in predicting the likelihood of phase separation at high weight fractions of PMMA.

Again bearing in mind the value of q obtained from the Kwei expression, the data for the PMMA:P(EthTelMA) blend was analysed using the theory of Lu and Weiss. This time, the weak interaction expression was used. This approximates to the Gordon-Taylor expression (*q.v.*), but with a value of k' given by:

$$k' = k + \frac{A}{T_{g2} - 1} \qquad \textbf{[4.40]}$$

Figure 4.7 shows the fit to the data by the Lu equation:

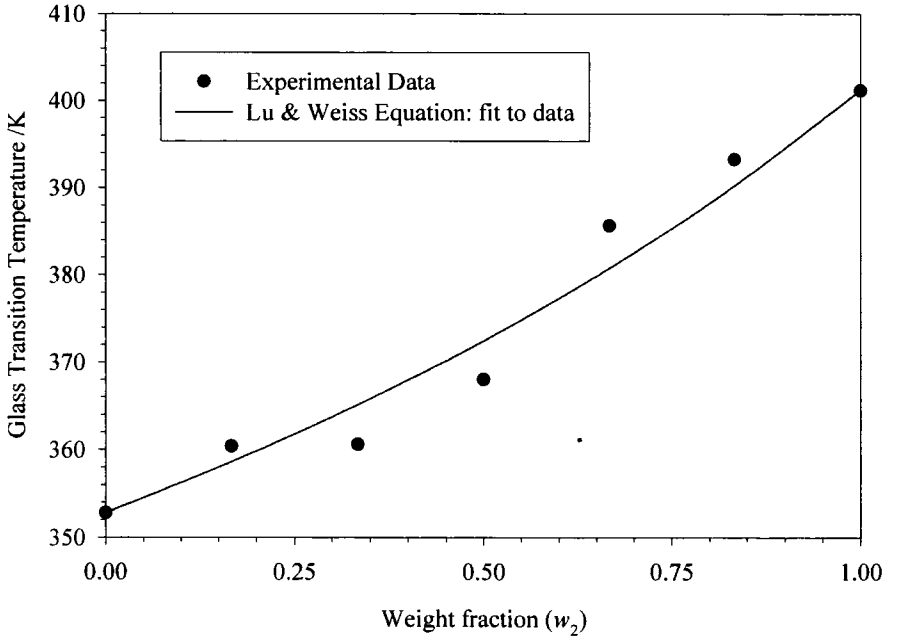

Figure 4.14 PMMA: P(EthTelMA) Fit by Lu & Weiss Eqn.

$k = 1.3, A = 151.90$

The fit is of a similar quality to that obtained by the Kwei equation, see fig 4.12. While again this is far from perfect, it should be pointed out that the deviations

from additivity in this blend are much smaller than those seen in the PMMA:P(MeTelMA) blend; the maximum deviation being less than 5K. The composition dependence of χ is shown in figure 4.8:

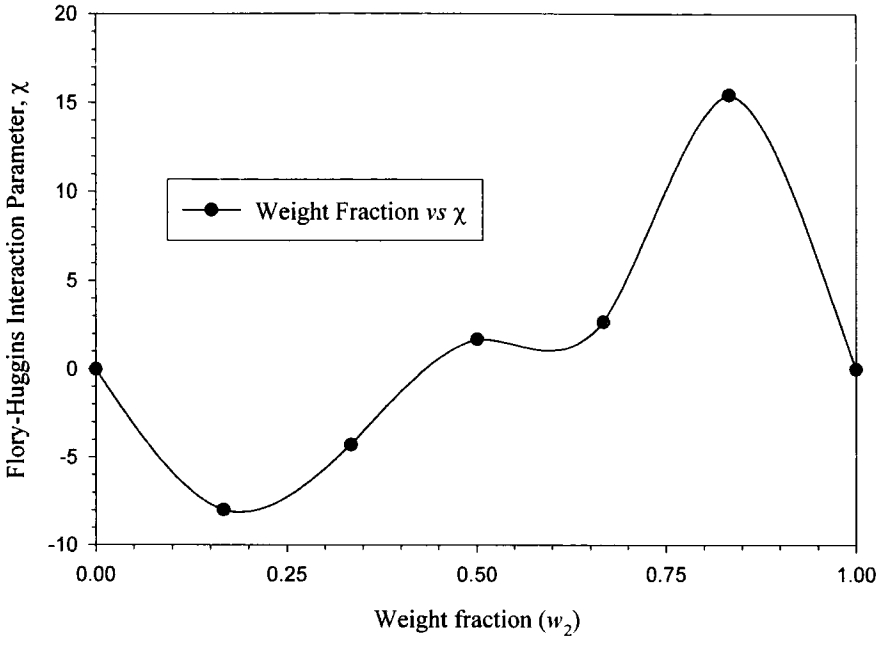

Figure 4.15 Variation of χ with Composition PMMA:P(EthTelMA)

note: the secondary minimum around w_2 = 0.6 is a feature of the spline routine used to generate the curve.

Considering the differences seen in the T_g: composition behaviours of the two blends, this seems to be remarkably similar in shape to fig 4.13. However, it is of note to mention the magnitudes of χ at the two extremities of the curve, being -8.0 at the minimum and 15.45 at the maximum. Both these values are, again, very large compared to values for weakly interacting polymers. That a system can switch from being so strongly stabilised toward blending to being so predisposed towards phase separation is indeed remarkable.

Perhaps more remarkable when considering the large positive χ values is that there are no visual signs of phase separation. It was mentioned in the discussion

of the MeTelMA blend that the resolution of the DSC experiment is of the order of $1x10^{-6}$m, *i.e.* the length scale of the glass transition. For a phase separated blend to appear cloudy, the size of phase would have to be of the order of the wavelength of light, *i.e.* 400-700nm. It is therefore possible to "pin down" the scale of phase separation in these blends to a level of the order of $1x10^{-7}$m or smaller.

4.7. References

1)Gallagher P. K.; *Thermoanalytical Instrumentation, Techniques and Methodology*; in *Thermal Characterization of Polymeric Materials.* 2 ed.; Edith A Turi, Ed.; Academic Press: San Diego, 1997; Vol. 1, pp 73-112.

2)Dodson, B.; McNeill, I. C. *J. Polym.Sci., Polym. Chem Ed* **1976**, *14*, 353.

3)Fernandes, E. G.; Giolito, I.; Chiellini, E. *Thermochim Acta* **1994**, *235*, 67-79.

4)Smith, S. D.; Long, T. E.; McGrath, J. E. *J Polym Sci Part A-Polym Chem Ed* **1994**, *32*, 1747-1753.

5)Vega, D.; Villar, M. A.; Failla, M. D.; Valles, E. M. *Polym Bull* **1996**, *37*, 229-235.

6)McNeill, I. C.; Neil, D. *Eur. Polym. J.* **1970**, *6*, 143.

7)Richards, D. H.; Salter, D. A. *Polymer* **1967**, *8*, 127.

8)Jamieson, A.; McNeill, I. C. *J. Polym. Sci., Polym. Chem Ed* **1974**, *12*, 387.

9)Grassie, N.; McNeill, I. C.; Cooke, I. *J. Appl. Polym. Sci.* **1968**, *12*, 831.

10)Das, G.; Banerjee, A. N.; Mitra, B. C. *Eur Polym J* **1996**, *32*, 179-184.

11)Guo, M. M. *Abstracts of Papers of the American Chemical Society* **1996**, *211*, 316-POLY.

12)Hammiche, A.; Song, M.; Pollock, H. M.; Hourston, D. J. *Abstracts of Papers of the American Chemical Society* **1996**, *212*, 186-PMSE.

13)Ou, C. F.; Lin, C. C. *J Appl Polym Sci* **1994**, *54*, 1223-1231.

14)Pollock, H. M.; Hammiche, A.; Song, M. *Abstracts of Papers of the American Chemical Society* **1996**, *212*, 246-POLY.

15)Vazqueztorres, H.; Cruzramos, C. A. *Polym Bull* **1994**, *33*, 673-680.

16)Xie, R.; Yang, B. X.; Jiang, B. Z. *J Polym Sci Part B-Polym Phys Ed* **1995**, *33*, 25-32.

17)Mathot, V. B. F. *Calorimetry and Thermal Analysis of Polymers*; Hanser: Munich, 1994.

18)Aubin, M.; Prud'homme, R. E. *Macromolecules* **1988**, *21*, 2945-2949.

19)Painter, P. C.; Graf, J. F.; Coleman, M. M. *Macromolecules* **1991**, *24*, 5630-5638.

20)Couchman, P. R.; Karasz, F. E. *Macromolecules* **1978**, *11*, 1156.

21)Pochan, J. M.; Beatty, C. L.; Pochan, D. F. *Polymer* **1979**, *20*, 879.

22)Fox, T. G. *Bulletin of the American Physics Society* **1956**, *2*, 1.

23)Utracki, L. A. *Advances in Polymer Technology* **1985**, *5*, 33.

24)Be'lorgey, G.; Prud'homme, R. E. *J Polym Sci, Polym Phys Ed* **1982**, *20*, 191.

25)Ting, S. P.; Pearce, E. M.; Kwei, T. K. *J Polym Sci, Polym Lett Ed* **1980**, *18*, 201.

26)Nandi, A. K.; Bandal, B. M.; Bhattacharyya, S. N.; Roy, S. K. *Polym Comm* **1986**, *27*, 151-154.

27)Kovacs, A. J. *Advances in Polymer Science* **1963**, *3*, 394.

28)Kwei, T. K. *J. Polym. Sci.: Polym. Lett. Ed* **1984**, *22*, 307-313.

29)Brekner, M.-J.; Schneider, H. A.; Cantow, H.-J. *Polymer* **1988**, *29*, 78-85.

30)Lu, X.; Weiss, R. A. *Macromolecules* **1992**, *25*, 3242-3246.

31)Allard, D.; Prud'homme, R. E. *Appl Polym Sci* **1982**, *27*, 559.

32)Wolf, M.; Wendorff, J. H. *Polym Comm* **1990**, *31*, 226.

33)Lin, A. A.; Kwei, T. K.; Reiser, A. *Macromolecules* **1989**, *22*, 4112-4119.

Chapter Five

Small Angle Neutron Scattering

5.1. Introduction

In a small angle neutron scattering (SANS) experiment, a neutron beam is incident on the sample under study. Elastically scattered radiation is collected, and the resulting angular distribution of scattered intensity is analysed to provide information about the size, shape and orientation of some component of the sample. Most notably in the case of polymer blends, the radius of gyration and the *effective binary interaction parameter*, χ_{eff}, can be determined. From the temperature and composition dependence of χ_{eff}, the type of phase diagram (LCST, UCST) may be determined and spinodal temperatures predicted[1-3].

The properties of the neutron also give the technique considerable utility and advantage over other methods for determining various material properties. Firstly, the strength of the neutron interaction varies irregularly with atomic number Z; this *neutron scattering cross section* varies even between isotopes of the same element. The most significant isotopic variation occurs when Z=1. As a consequence of this, neutrons are not only able to "see" hydrogen atoms, moreover they can distinguish between the different isotopes, *i.e.* ^{1}H, ^{2}D. This is in contrast to light and *X*-ray scattering where the scattering arises from electrons and hence preferentially "sees" heavier atoms.

Secondly, the interactions of neutrons with matter are weak and the absorption of neutrons by most materials is correspondingly small. This means that neutrons can be used to determine bulk properties of samples with a pathlength of a couple of centimetres or, alternatively, samples with a shorter pathlength but contained inside complex pieces of apparatus *e.g.* cryostats, furnaces, pressure cells, shear apparatus *etc.*

A third difference of considerable importance to the study of polymer blends is the different resolution of SANS over other techniques of polymer characterisation. For example, melting point or glass transition-based methods can only observe miscibility (changes) on a macroscopic scale. The *thermal concentration fluctuations* "seen" by SANS characterise the degree of random mixing in a polymer blend and, in that respect, the resolution of the SANS experiment is on the molecular level. These fluctuations arise according to the distribution of scattering centres (polymer segments) from an arbitrarily chosen origin. Their distribution will depend upon the conformation of the polymer chains, which in turn depends on the balance of intermolecular and intramolecular forces.

5.1.1. Nomenclature

The interdisciplinary nature of SANS means that different texts and different users tend to use different nomenclature and symbols for the same properties. This work will use the nomenclature defined and used in the manuals of the LoQ diffractometer at the ISIS facility, Rutherford-Appleton Laboratory.[4]

5.1.2. The Sample Polymers

It is necessary to discuss briefly the sample polymers used for this study. The fluoropolymer used (sample code MW96/40 [*q.v.*]) was a random copolymer of deuterated MeTelMA and deuterated MMA. The composition by elemental analysis was 1MeTelMA:7MMA. The matrix polymer was hydrogenous syndiotactic PMMA with M_w = 132000 and a polydispersity of 1.39.

5.2. Theory

5.2.1. Thermodynamics

Applying the Flory-Huggins lattice theory to a binary polymer mixture results in the following expression for the Gibbs free energy of mixing, ΔG_{mix}:

$$\frac{\Delta G_{mix}}{RT} = \frac{\phi_1}{m_1}\ln\phi_1 + \frac{\phi_2}{m_2}\ln\phi_2 + \phi_1\phi_2\chi_{FH} \qquad \textbf{[5.1]}$$

Blend components 1 and 2 are assumed to have equal segment volumes. ϕ_i is the volume fraction and m_i is the number average degree of polymerisation of component *i*, R is the gas constant, T is the absolute temperature and χ_{FH} is the Flory-Huggins interaction parameter. The second differential with respect to the volume fraction is given by:

$$\frac{\partial^2}{\partial\phi_1\partial\phi_2}\left(\frac{\Delta G_{mix}}{RT}\right) = \frac{1}{m_1\phi_1} + \frac{1}{m_2\phi_2} - 2\chi_{FH} \qquad \textbf{[5.2]}$$

At the spinodal:

$$\frac{\partial^2}{\partial\phi^2}\left(\frac{\Delta G_{mix}}{RT}\right) = 0 \qquad \textbf{[5.3]}$$

and therefore

$$\chi_S = \frac{1}{2m_1\phi_1} + \frac{1}{2m_2\phi_2} \qquad \textbf{[5.4]}$$

χ_S is the value of the Flory-Huggins interaction parameter at the spinodal. The original formulation assumed that χ_{FH} was purely enthalpic in origin, and has no dependence on molecular weight or blend composition. However, the χ from small angle neutron scattering is an *effective interaction parameter*, χ_{eff}, which may display dependencies on molecular weight and/or blend composition. Clearly when such dependencies are not observed, $\chi_{eff} = \chi_{FH}$. Such dependencies have prompted a number of discussions and reviews, *e.g.*[5-12]

5.2.2. Neutron Scattering [4,13]

From Bragg's Law, the wavelength of the incident radiation must be comparable to the distance between scattering centres for scattering to occur. The scatterers in question in this work are (segments and agglomerations of) polymer molecules, and therefore the wavelength of the radiation must be of the order of polymeric dimensions, *i.e.* 10-100Å. By varying the *scattering vector*, Q, [*q.v.*] the SANS experiment can observe structures which range from atoms through molecular segments to (assemblies of) complete molecules.

The objective of a SANS experiment is to determine the (microscopic) *differential cross-section*, $d\sigma/d\Omega(Q)$, since it is this function which contains all the information on the shape, size and interactions of the scattering bodies. This is given by:

$$\frac{d\sigma}{d\Omega}(Q) = N_p V_p^2 (\Delta\delta)^2 P(Q) S(Q) + B_{inc} \qquad \textbf{[5.5]}$$

where N_p is the number concentration of scattering bodies (subscript "p" refers to "particles"), V_p is the volume of one scattering body, $(\Delta\delta)^2$ is the square of the difference in *neutron scattering length density* and is commonly referred to as *contrast*. The function $P(Q)$ is known as the *form* or *shape factor*, and $S(Q)$ is the *interparticle structure factor*. Q is the modulus of the *scattering vector*, and B_{inc} is the isotropic background signal due to incoherent scattering. It is worthy of note that some texts refer to the *macroscopic differential cross section*, $d\Sigma/d\Omega(Q)$, which is the product of the microscopic cross section and the number of scatterers, N_p.

The terms in equation 5 shall now be considered individually.

5.2.2.1. The Scattering Vector ,Q

In scattering experiments (light, *X*-rays, neutrons), the essential experimental parameter is the *scattering vector*, Q. For two scatterers A and B, separated by a distance r_{AB}, there is a phase difference $(\mathbf{k}-\mathbf{k_0})r_{AB}$, where $\mathbf{k_0}$ and $\mathbf{k}$ are wavevectors parallel to the incident and scattered neutron directions respectively. In the following discussion, vector quantities are represented by bold text; scalars are written in regular font. For elastic scattering, the magnitudes of $\mathbf{k_0}$ and $\mathbf{k}$ are equal. Schematically:

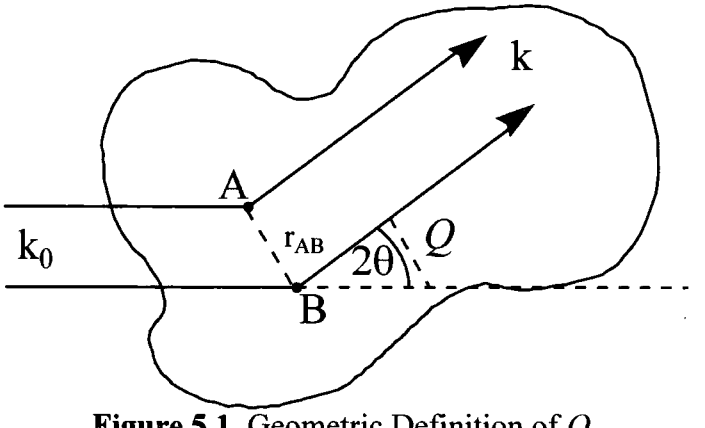

Figure 5.1. Geometric Definition of Q

Q is the magnitude of the vector difference between $\mathbf{k}_0$ and $\mathbf{k}$:

$$Q = |\boldsymbol{Q}| = |\mathbf{k} - \mathbf{k}_0| = 4\pi\sin\theta/\lambda \qquad \textbf{[5.6]}$$

where λ is the wavelength of the incident radiation.

From Bragg's law,

$$\lambda = 2d\sin\theta \qquad \textbf{[5.7]}$$

where d is the distance between scatterers. Substituting for λ in equation 6, we obtain:

$$d = 2\pi/Q \qquad \textbf{[5.8]}$$

By considering equation 8, above, one is able to configure the instrument such that its Q-range is sufficient to look at the system one wishes to study. A typical SANS instrument will have a Q-range between 0.005 and 0.2Å^{-1}, enabling the study of scattering bodies with spacing 30-1250Å. This range is ideal for the study of colloidal-type systems, including polymer blends.

5.2.2.2. The Factors P(Q) and S(Q)

The scattering experiment responds to the density-density correlation function between any two points r_A and r_B. This function takes the form:

$$S_{12}(r_A - r_B) = \langle \phi_1(r_A)\phi_2(r_B) \rangle - \langle \phi_1 \rangle \langle \phi_2 \rangle \qquad \textbf{[5.9]}$$

ϕ_i is the volume fraction of component i, < > denotes the thermal average and S_{12} denotes the *scattering power*. Equation 9 describes how $d\sigma/d\Omega(Q)$ is modulated by interference effects from radiation scattered by different scattering centres. The structure factor may be divided into terms arising from scattering within the same particle and that which results from interference from scattering centres on other molecules or particles within the bulk sample. In the nomenclature used at the ISIS facility, these are given the symbols P(Q) and S(Q) respectively.

1) The Form Factor

P(Q) is commonly referred to as the *form factor*, and gives information on the shape of an individual scattering body. The general form of P(Q) is given by Van der Hulst's expression:

$$P(Q) = \frac{1}{V_p^2}\left| \int_0^{V_P} \exp\left[if(Q\alpha)\right] dV_P \right| \qquad \textbf{[5.10]}$$

where α is a shape dependent parameter. A number of analytical expressions exist for many common shapes, and a pertinent selection of these are given in table 5.1, below.

i) Sphere of radius R_p	$P(Q) = \left[\frac{3\left(\sin(QR_P) - QR_P\cos(QR_P)\right)}{(QR_P)^3}\right]^2$
ii) Debye Function for monodisperse Gaussian Chain	$P(Q) = \left(\frac{2}{U^2}\right)\left(\exp^{-U} + U - 1\right)$ $U = Q^2 R_{gi}^2$
iii) Gaussian random coil with z-average radius of gyration R_g, polydispersity (Y+1) and $U = \frac{(QR_g)^2}{(1+2Y)}$	$P(Q) = \frac{2\left[(1+UY)^{-1/Y} + U - 1\right]}{(1+Y)U^2}$

Table 5.1 Form Factors for a variety of Molecular Shapes

In the limit of Y→0, *i.e.* the polymer has a polydispersity of 1, equation *iii*, above, reduces to the Debye equation, (*ii*). Figure 5.2 demonstrates these effects graphically:

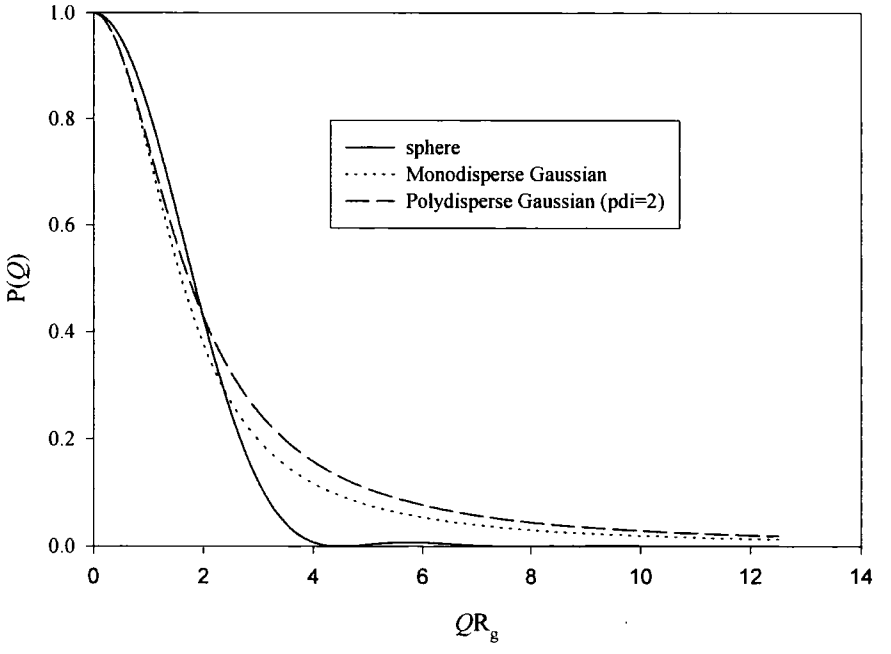

Figure 5.2 Form Factors for a Sphere and a Gaussian chain with R_g = 50Å

2) The Scattering Power

$S(Q)$ is the scattering power (S_{12}) at a given value of Q and describes how $d\sigma/d\Omega(Q)$ is affected by interparticle interference. Therefore, $S(Q)$ gives information on the order arising from interactions between the different scattering bodies in a sample.

5.2.2.3. The Contrast Term: Deuteration

The scattering length density which appears in the contrast term in the neutron scattering experiment is obtained by summing the scattering lengths of the component atoms in the repeat unit:

$$\delta = \frac{\rho N_A}{M_w} \sum_i b_i \qquad \textbf{[5.11]}$$

δ is the *neutron coherent scattering length density*, b_i is the coherent scattering length of atom i in the repeat unit, ρ is the bulk density of the polymer , N_A is Avogadro's number and M_W is the molecular weight of the scatterer (considered to be a monomer-like segment for polymers).

Table 5.2. gives values for *coherent scattering lengths*, b_i and *neutron scattering cross section*, σ for several important nuclei:

Atomic Nucleus	b_{coh} / $1x10^{-15}$m	σ_{coh} / barns‡
^{1}H	-3.741	1.76
^{2}D	6.671	5.59
C	6.646	5.55
O	5.803	4.23
F	5.70	4.02

Table 5.2 Coherent Scattering Lengths and Neutron Scattering Cross Sections

From Table 5.2. it can be seen that δ can be negative or positive. The contrast term is simply the difference in the scattering length densities of the constituents of the blend all squared, *i.e.* $(\Delta\delta)^2 = \left(\delta_p - \delta_m\right)^2$, where subscripts p and m refer to the polymer of interest and the matrix polymer, respectively. Clearly, if Δδ is zero, there can be no coherent scattering. The majority of polymers are made up of carbon, hydrogen and oxygen in similar relative proportions, and there is therefore a potential contrast problem in using SANS to look at polymers.

This problem can be overcome by noting the anomalously large difference between the neutron scattering cross sections of the hydrogen isotopes ^{1}H and ^{2}D, being 1.76 and 5.59 barns, respectively. Selective deuteration of a particular component of a blend allows the deuterated polymer to be "seen" against a background of invisible† hydrogenous "matrix." The opposite is also true, but this

‡ 1Barn = $1x10^{-27}m^2$ = $1x10^{-24}cm^2$

† The matrix polymer is invisible in that it doesn't contribute to the coherent scattering. However, hydrogen has a very large incoherent scattering cross section.

represents the less attractive idea of looking for the absence, rather than the presence, of a particular scatterer.

5.3. Data Analysis

The main data analysis method applied to the scattering data obtained was the de Gennes' Random Phase Approximation (RPA)[14] calculation for polymer blends near to their critical points. In this approach, the correlation functions for a given value of Q are expressed in terms of the degrees of polymerisation and volume fractions of the components, combined with the Debye function[15], $g_D(R_{gi},Q)$ for the scattering by a Gaussian polymer chain and the effective interaction parameter χ:

$$\frac{1}{S(Q)} = \frac{1}{m_1\phi_1 g_D\left(R_{g1},Q\right)} + \frac{1}{m_2\phi_2 g_D\left(R_{g2},Q\right)} - 2\chi \qquad \textbf{[5.12]}$$

where

$$g_D\left(R_{gi},Q\right) = \left(\frac{2}{u^2}\right)\left(\exp^{-u} + u - 1\right) \qquad \textbf{[5.13]}$$

and

$$u = Q^2 R_{gi}^2 \qquad \textbf{[5.14]}$$

This expression was fitted to the corrected scattering data [*q.v.*] using R_{g2} and χ as adjustable parameters. R_{g1}, the radius of gyration of the matrix polymer (HPMMA), was calculated from literature values of characteristic ratios [16]and held constant.

Equation 12 is cast in the same form as the expression for the second derivative of the Gibbs free energy at the spinodal (equation 2), and indeed, in the limit of Q tending to zero, these expressions are identical. It follows from this that S(Q) will be infinite at the spinodal.

The expressions shown above are general expressions which may be used for fitting to data across a wide range of Q. Where Q is small, more particularly when $QR_g<1$, the expression for the inverse intensity may be simplified by the expansion of the Debye function at small Q. This is referred to as the Guinier regime.[17]

$$g_D\left(R_{gi},Q\right)=1-\frac{Q^2R_{gi}^2}{3} \qquad \textbf{[5.15]}$$

$$R_{gi}^2=\frac{m_i a_i^2}{6} \qquad \textbf{[5.16]}$$

where a_i is the statistical step length of the polymer molecule. Using this simplified Debye function, we obtain:

$$S(Q)=\frac{1}{2(\chi_s-\chi)(1+Q^2\xi^2)} \qquad \textbf{[5.17]}$$

This is known as the Ornstein-Zernike expression. χ_s is the value of the interaction parameter at the spinodal. ξ is the average concentration fluctuation length in the miscible state:

$$\xi=\frac{a_i}{6}\left[\phi_1\phi_2(\chi_s-\chi)\right]^{-1/2} \qquad \textbf{[5.18]}$$

De Gennes' random phase approximation has been used on many occasions to describe successfully the phase behaviour of a number of polymer-polymer blends. However, the RPA assumes a Gaussian distribution for the radius of gyration. While this assumption has been borne out in innumerable cases, *e.g.*[18-22], that is not to suggest that the assumption can be made without due consideration. Therefore, in order to verify (or indeed refute) these assumptions, a more general approach may be used, which assumes no *a priori* knowledge of the shape of the scattering bodies in the system.

The radius of gyration of a polymer as a function of its degree of polymerisation (m) is a characteristic of its molecular shape, irrespective of its chemical composition. Table 5.3. shows the so-called *scaling exponents* for a number of different polymer architectures:

Gaussian Chain	$\overline{R}_g \approx m^{1/2}$
Chain with Excluded Volume	$\overline{R}_g \approx m^{3/5}$
Rigid Rod	$\overline{R}_g = L = m^1$

Table 5.3 Scaling Relationships as a function of R_g

In general, $\overline{R}_g \approx m^a$. If we neglect intermolecular interactions, which is a good assumption at high Q:

$$S(Q) = Nm^2 P(QR_g) \qquad \textbf{[5.19a]}$$

or in terms of volume fractions

$$S(Q) = V\phi mP(QR_g) \qquad \textbf{[5.19b]}$$

Substituting for R_g as a function of m in Eqn 19b:

$$S(Q) = V\phi m(Qm^a)^{-\alpha} = V\phi Q^{-\alpha} m^{(1-a\alpha)} \quad \textbf{[5.20]}$$

For $S(Q)$ to be independent of m (which it is at high Q), the power at which m is taken in eqn 20 must be zero. Therefore:

$$a = \frac{1}{\alpha} \quad \textbf{[5.21]}$$

and $S(Q)$ should vary as $Q^{-1/a} = Q^{-\alpha}$.

These considerations hold true for linear objects, and by extending the theories to include 2- and 3-dimensional objects, a series of exponents can be built up, each of which are characteristic of a given shape.

Rigid Rod	1
Linear Gaussian Chain	2
Chain with Excluded Volume	5/3
Randomly Branched Gaussian Chain	16/7
Smooth 3-D Objects e.g. sphere	4

Table 5.4 Scaling Exponents

Therefore, by fitting the data to an expression of the form $S(Q) = AQ^{-\alpha}$ and comparing the value of α with those listed above, the shape of the scatterers may be determined independently of any assumptions made by the fitting of analytical form factors.

A third method, similar to the free form fitting, is to plot the data at high Q on two logarithmic axes. The log-log approach enables the scaling exponent to be evaluated from the slope of a linear regression through the data points.

The results from these methods will be discussed below.

5.4. Experimental

1.Sample Discs

The samples used for this work took the form of a disc 15mm diameter x 1mm thick. Polymers (HPMMA, MW96/40 [*q.v.*]) were weighed out to give a total mass of approximately 0.2g per disc when blended. Blending was achieved by dissolving individual components in THF and mixing the solutions to give compositions of 2, 5, 7.5, 10 and 15% w/w fluorinated polymer. This gave a clear, single phase solution indicative of solution miscibility. The mixed solutions were poured into light petroleum ether to precipitate the solids, which were then thoroughly dried *in vacuo*.

The sample discs were prepared in a SPECAC press coupled with a SPECAC heating jacket. This apparatus accepts a 15mm die, in which the samples are contained between polished steel plates; the die can also be evacuated.

Having weighed the appropriate amount of polymer into the die, vacuum was applied and the jacket heated to around 393K [approximately the T_g of the blend]. The bolster of the press was tightened to hand pressure for about 5minutes, before the vacuum was turned off and both pressure and temperature increased to 2 kPa and 423K, respectively. This was maintained for approximately 1hour, before the pressure was released and the heating turned off. It was found that the

apparatus was best disassembled hot, as it proved easier to remove the sample disc from the plates. The sample discs so produced were clear and colourless, with the exception of a pure fluoropolymer disc, which was brown in colour.

The discs were then placed in a sample holder such as they could be subsequently mounted in the instrument. These consist of a brass die closed with a brass sealing ring, in which the sample is contained between quartz discs and PTFE washers:

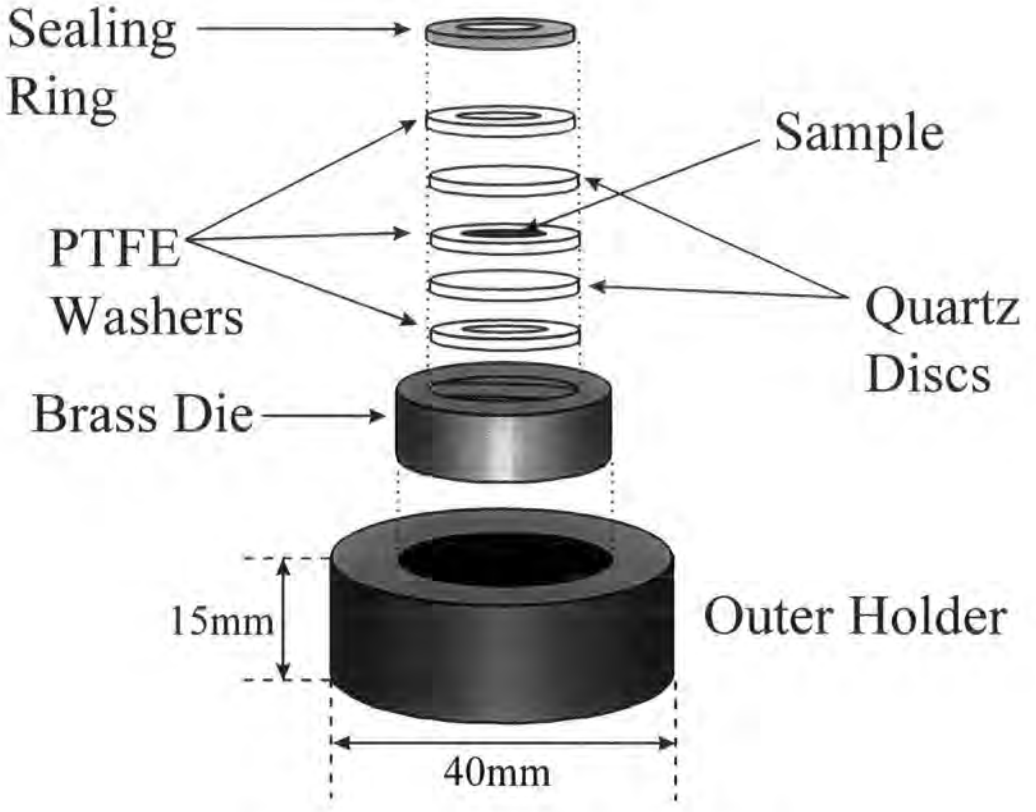

Figure 5.3 Sample Container for SANS

In order to ensure thermodynamic equilibrium and relieve any internal stresses caused by the processing, samples mounted in their sample holders were then annealed at 448K for 4days. Over this time, some coloration developed and bubbles formed. Thermal decomposition of the fluorinated polymer has been noted earlier, and is blamed for these effects.

The sample area of the LoQ instrument (*q.v.*) at the ISIS facility allows sufficient room for a number of different sample environments including furnaces, refrigerators, magnets, flow cells, as well as other user-supplied apparatus. This work has followed in the path of a number of recent workers in using the heated "Durham rack." This rack is a large piece of brass machined so as to accept up to nine sample cells as a given time, and also contains an electrical heater which may be controlled by a remote instrument enabling a wide range of temperatures to be explored. The rack is mounted on a computer-controlled sample changer to allow any one of the sample positions to sit in the beam for study.

2. Neutron Scattering.

The neutron scattering experiments documented in this work took place at the ISIS facility, Rutherford-Appleton Laboratory, using the LoQ Diffractometer. The ISIS facility is a pulsed neutron source, in which neutrons are produced by the process of "spallation" or chipping. A proton beam is produced in a linear accelerator and synchrotron, and this beam is then incident on a tantalum target. This process releases approximately 25 neutrons for every incident proton. The neutron beam is then moderated by liquid hydrogen at 25K before passing down the flight tube to the sample. The detector is placed at a distance of 4.05m from the sample position, and has a sensitive area of 640x640mm. The available Q range of the instrument is from 0.008-0.24Å^{-1}

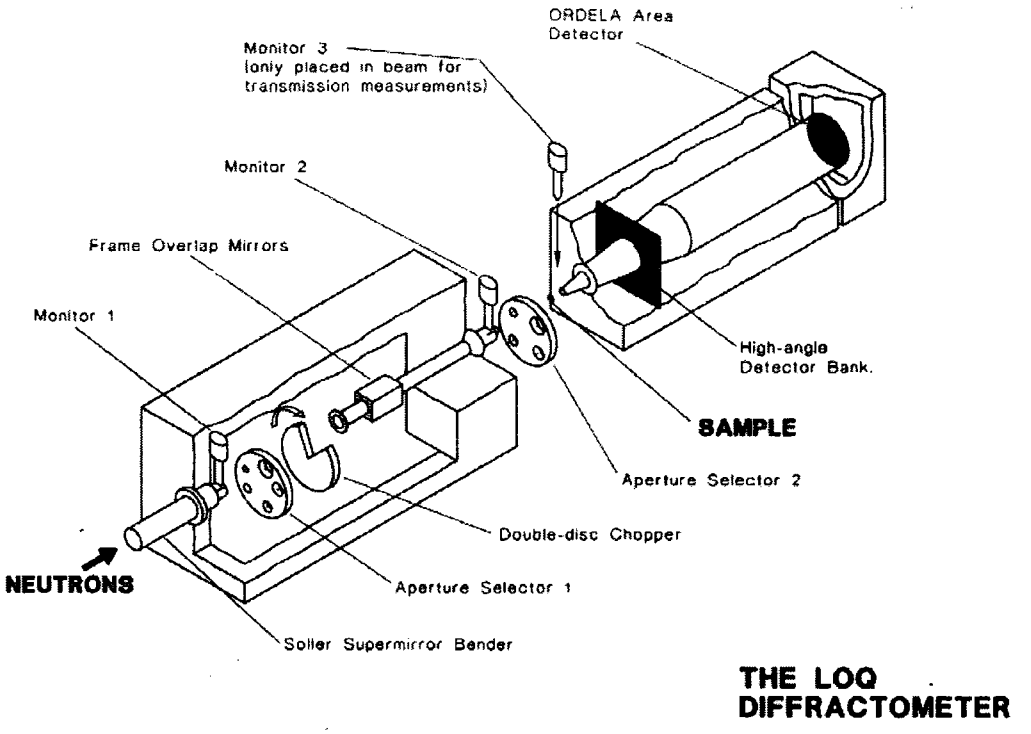

Figure 5.4 The LoQ Diffractometer

Before data can be collected on the samples, the diffractometer must be calibrated, such that instrumental parameters such as the incident flux are known. This is achieved by the use of the various monitors along the beamline. The effects of the sample container are also accounted for in this manner.

Data reduction requires the contributions to the incoherent background scattering from each polymer to be known. Hence, scattering intensities were also recorded for pure HPMMA and pure MW96/40.

Finally, in order to fix the scattering intensities on an absolute scale, the instrument is calibrated using a blend of deuterated and hydrogenous poly(styrene). The molecular weights and composition of this blend have been accurately determined by other methods. The incoherent background of the blend was obtained using a random copolymer of hydrogenous and deuterated polystyrene of the same composition and molecular weight as the calibrant mixture.

5.5. Results & Discussion

A typical data set before background subtraction is shown in figure 5.5. The Random Phase Approximation (RPA) fit to the data is shown in figure 5.6.

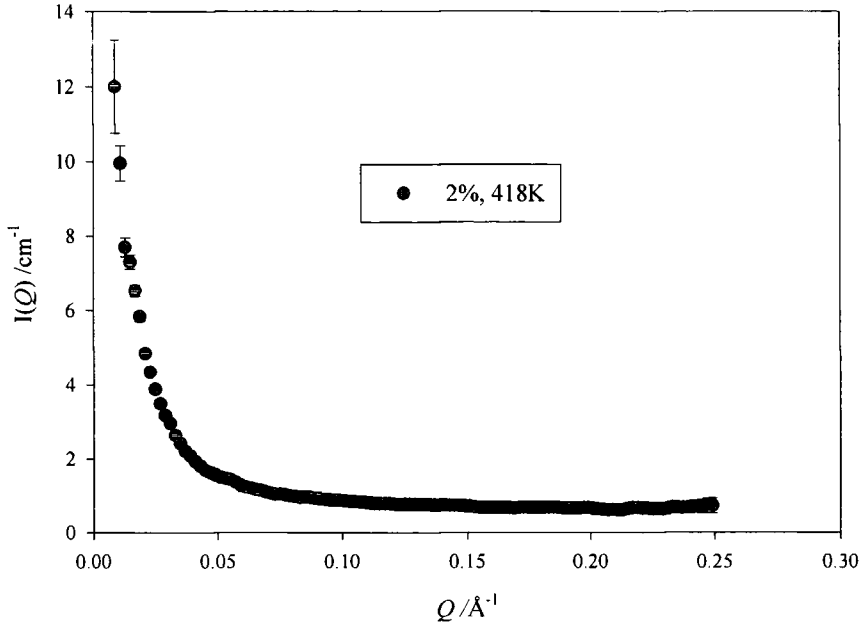

Figure 5.5 Typical Scattering Pattern

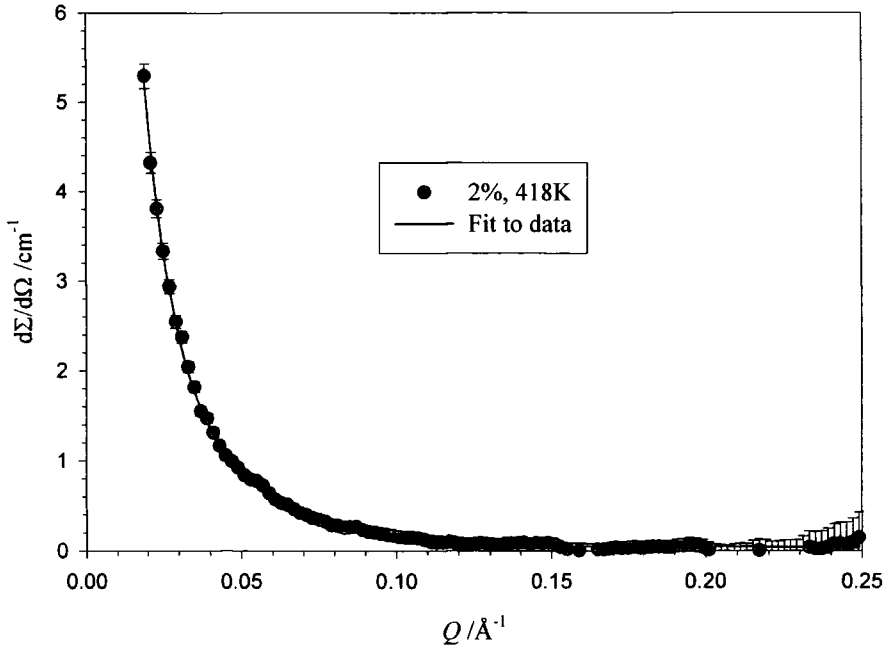

Figure 5.6 Data after Background Subtraction and Fitting

Looking at these particular data sets, it can be seen that fitting to the RPA is a fairly successful procedure, in that the quality of fit is reasonable. Not

withstanding the efficacy of this fitting routine, the expression which has been used only caters for a monodisperse chain. The form factor for a chain with polydispersity Y is given in table 5.1., and the effects of increasing polydispersity are demonstrated in figure 5.2. [*q.v.*]

Figure 5.2. demonstrates two important points:

a) scattering intensity is relatively insensitive to the effects of polydispersity (note the small Q-range), and

b) polydispersity results first in a decrease then an increase in scattering intensity as Q becomes smaller. At high Q-values, the effects of polydispersity become insignificantly small.

Looking at plots of the residual values from a fit, we see that the RPA tends to overestimate the value of the scattering intensity. See Figure 5.7 A-E.

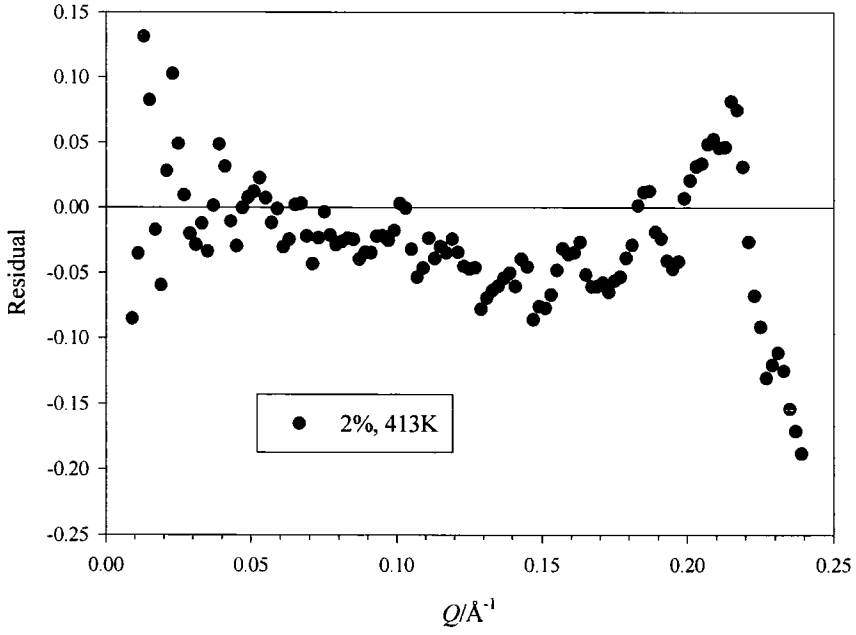

A

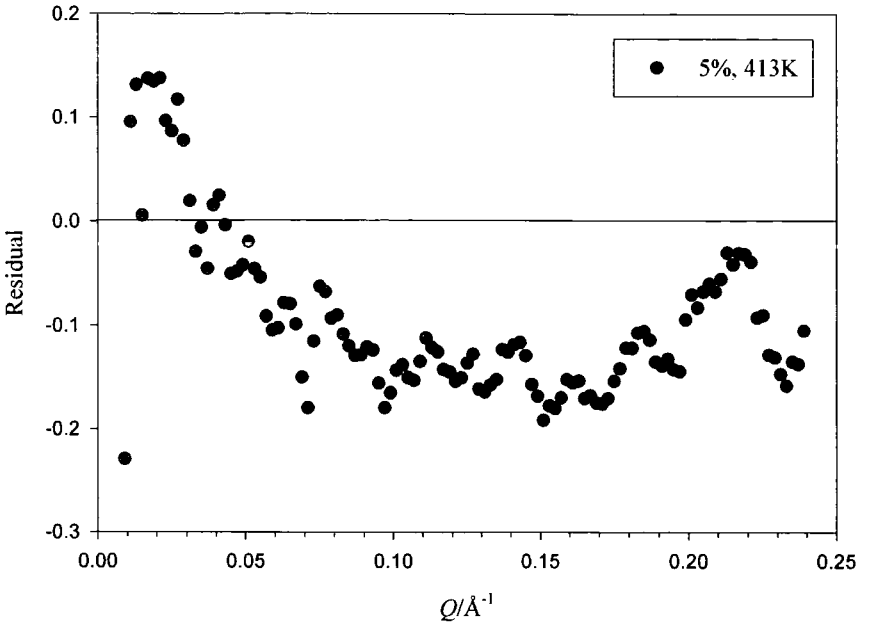
5%, 413K
Residual
0.2
0.1
0.0
-0.1
-0.2
-0.3
0.00
0.05
0.10
0.15
0.20
0.25
Q/Å-1

B

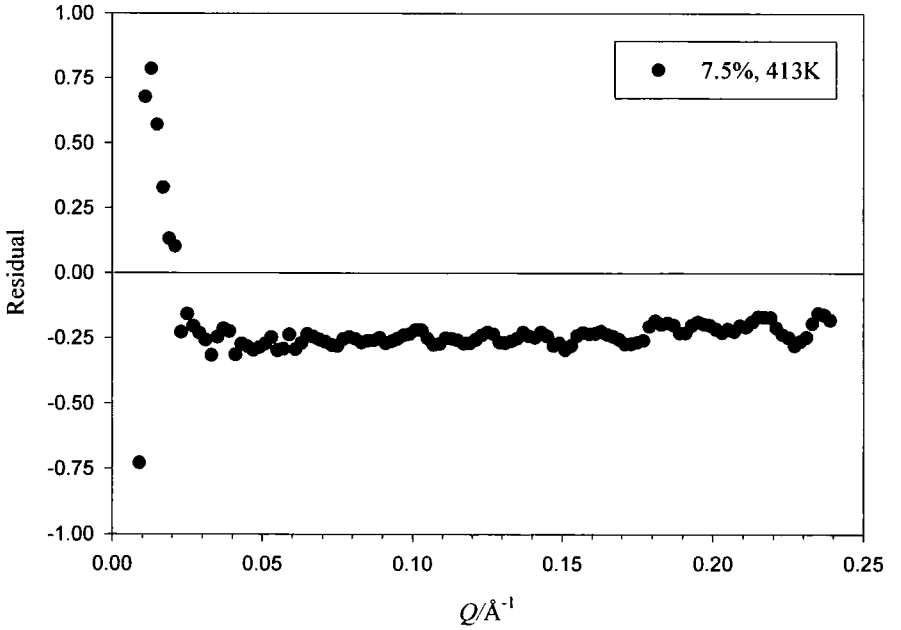
7.5%, 413K
Residual
1.00
0.75
0.50
0.25
0.00
-0.25
-0.50
-0.75
-1.00
0.00
0.05
0.10
0.15
0.20
0.25
Q/Å-1

C

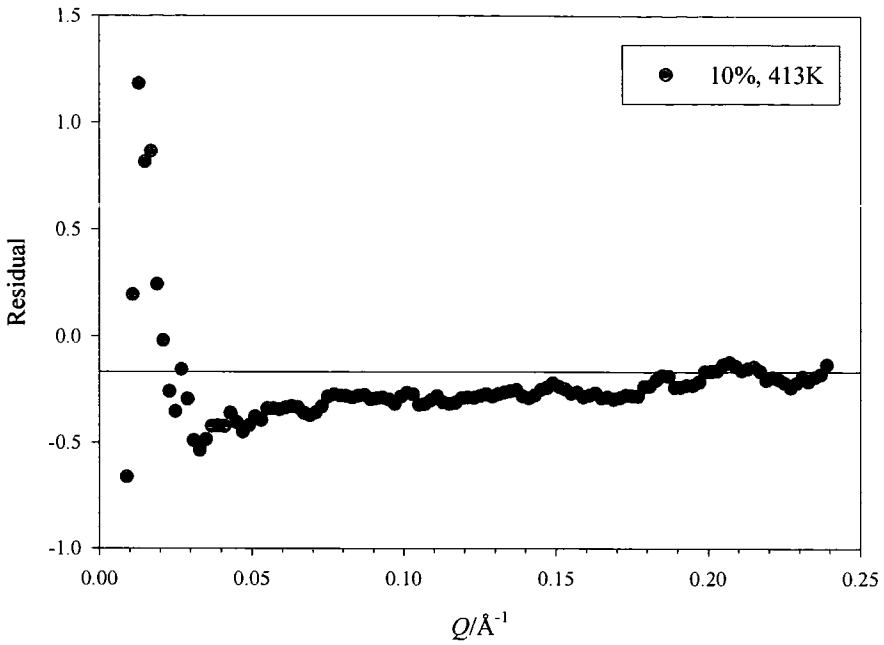

D

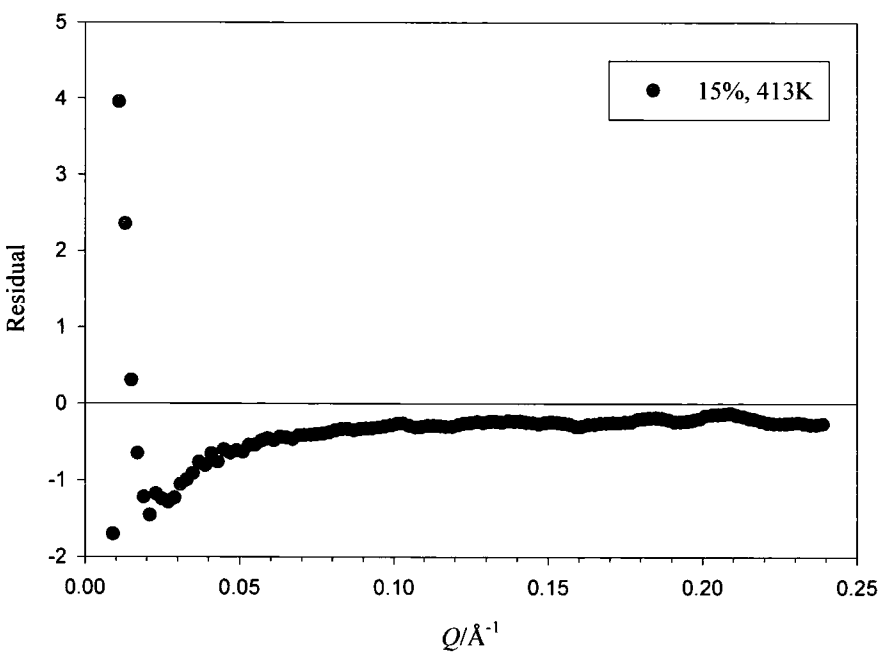

E

Figure 5.7 A-E: Residual Plots at T = 413K

The absolute values of the residuals grow with increasing fluoropolymer concentration, but as the overall scattering intensity also increases significantly with fluoropolymer concentration, the relative values remain small.

Clearly, polydispersity effects can account for some of this discrepancy, and are likely to be responsible for the change in sign of the residual at low Q values. Figure 5.8 demonstrates the sensitivity of the fitting procedure to χ as a function of Q The data is plotted in the Kratky form to enhance the differences in the scattering:

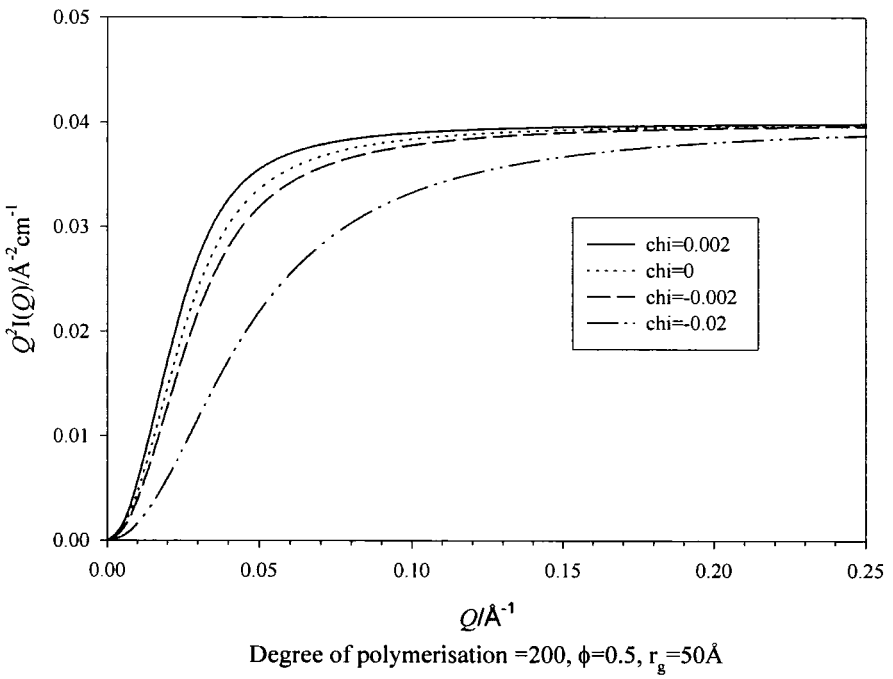

Figure 5.8 Scattering from Blends with $R_{g1}=R_{g2}=50Å$,

Degree of polymerisation = 200, volume fraction = 0.5 for differing values of χ

From this, we can see that an increase in χ causes a small increase in the scattering intensity. However, as figure 5.9 shows, the change in scattering intensity is not uniform over the range of Q.

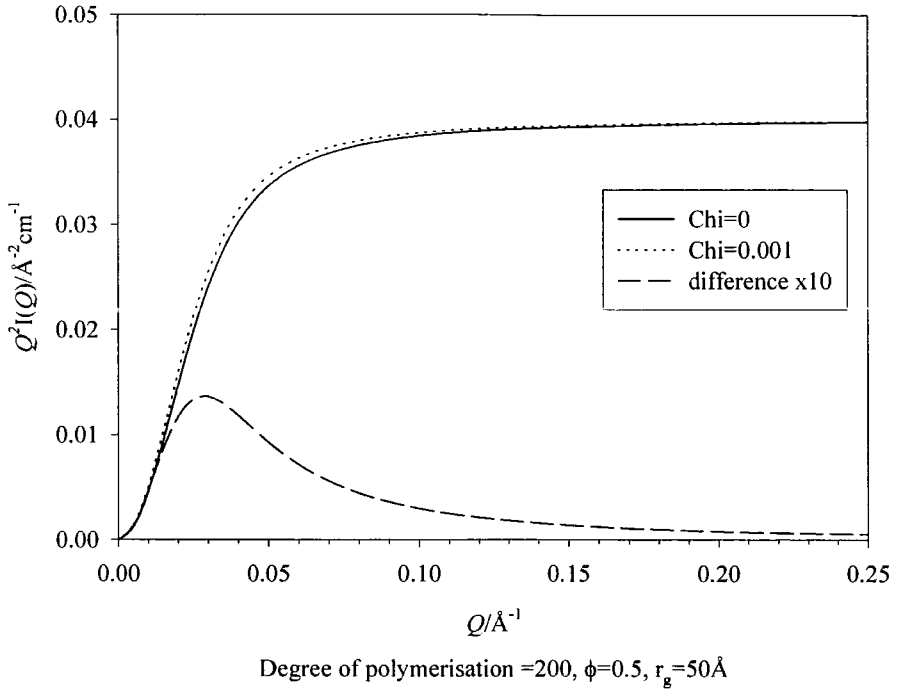

Figure 5.9 Sensitivity of the RPA to χ as a function of Q

Figure 5.9 clearly demonstrates that the RPA is more sensitive to changes in the value of χ at lower Q than when Q is larger. Therefore, given the propensity of the RPA analysis to overestimate the scattering intensity, we must also conclude that there is a propensity to overestimate the value of the interaction parameter.

Bearing these considerations in mind, the RPA analysis across the whole composition and temperature range enables the evaluation and interpretation of the composition and temperature dependence of the Flory-Huggins interaction parameter to be established for this blend. The values of the interaction parameter obtained from fits to the data are shown graphically in figures 5.10. and 5.11., respectively:

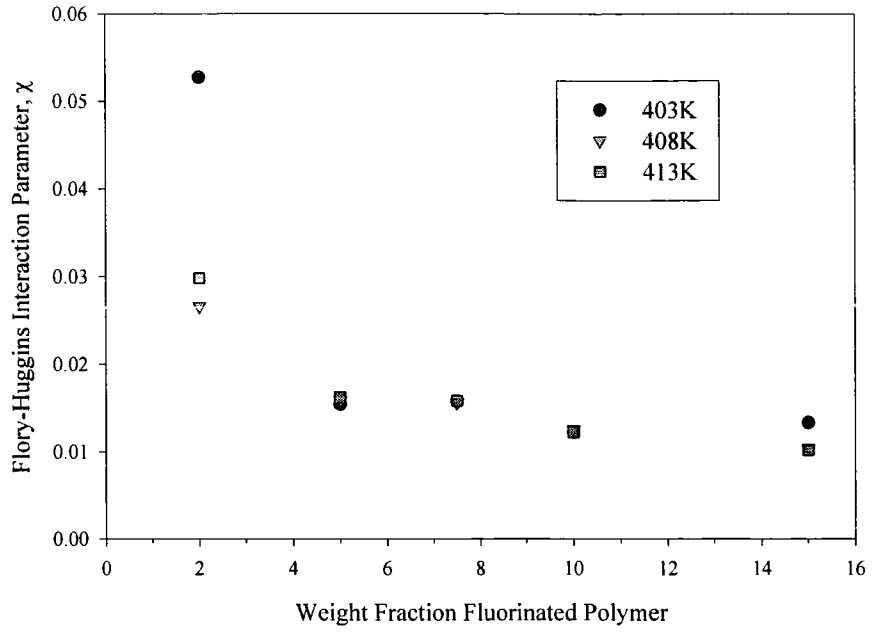

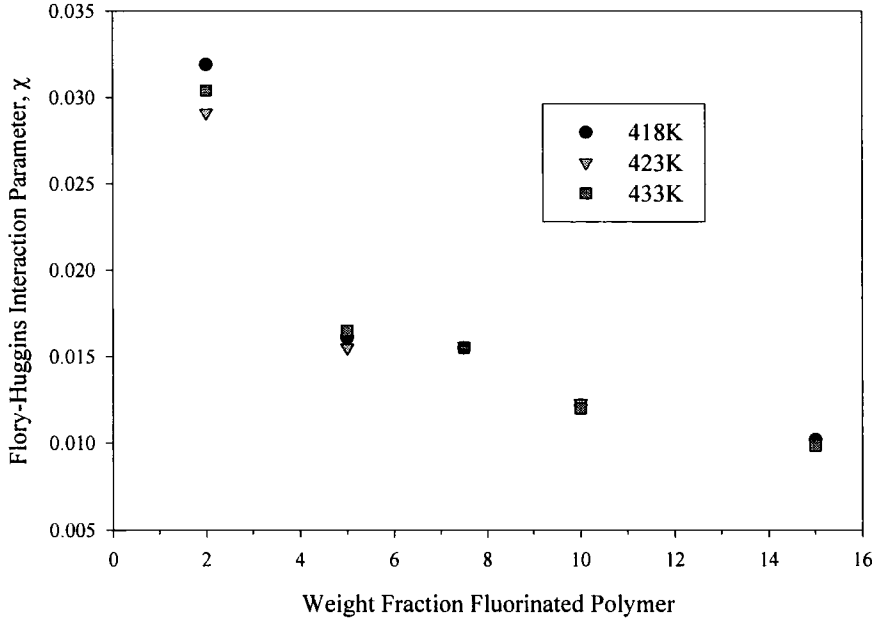

Figure 5.10 Composition dependence of χ_{eff}

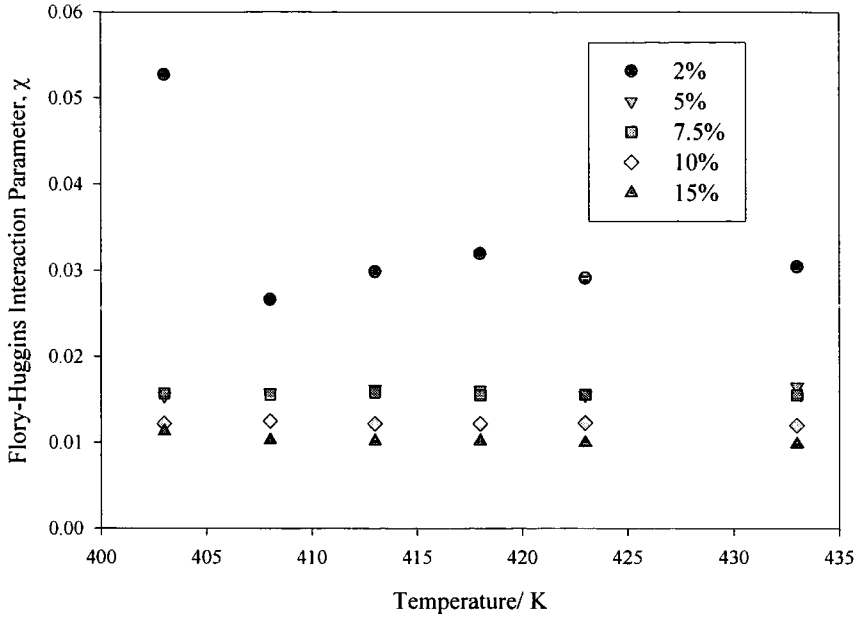

Figure 5.11 Temperature dependence of χ_{eff}

The most obvious point to note from the above figures is that χ has a positive value as was found from the DSC studies on this blend (described earlier). Substituting the values for the degrees of polymerisation and composition into the expression for the critical value of χ at the spinodal (eqn 4), the following curve is obtained:

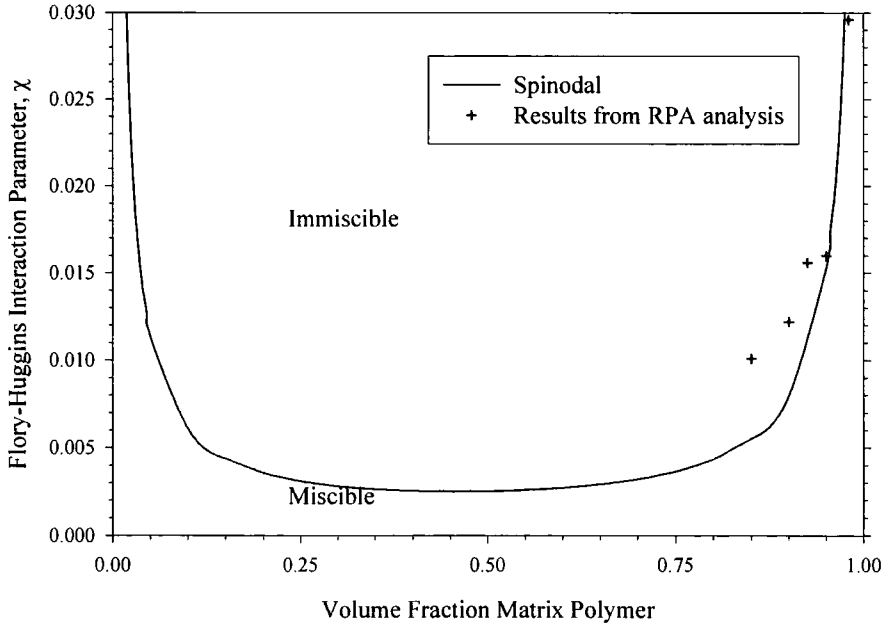

Figure 5.12 Spinodal Curve for HPMMA:MW96/40

Before drawing any conclusions from fig. 5.12., the copolymeric nature of the sample must be considered. The composition distribution in random copolymers has received a theoretical treatment by Scott[23]. He found that most random copolymers that have a significant contribution distribution (*i.e.* "blockiness"), should be expected to separate into two (or more) phases, relating the interaction parameter to the Hildebrand solubility parameters:

$$\chi_{AB} = (V_r / RT)(\delta_A - \delta_B)^2 \qquad \textbf{[5.22]}$$

Krause *et al*[24] demonstrated how to calculate the interaction parameters between random copolymers and homopolymers or other random copolymers. Following a complex argument, they arrive at the solubility parameter of copolymer *C* being given by:

$$\delta_C = \sum \delta_i \phi_i^C \qquad \textbf{[5.23]}$$

where δ_i is the solubility parameter of the homopolymer that corresponds to monomer *i* in the random copolymer and the summation is taken over all the different repeat units of the copolymer. The interaction parameter is then calculated using equation 22.

The most obvious way to establish the random nature of a copolymer is to record the NMR spectrum. It has been said on a number of occasions that NMR does not give an effective means of characterisation for the materials in this work due to the complications of the polydisperse side chain. However, the thermal properties

of polymers are also characteristic of their structure. A block copolymer of two immiscible components is likely to display two glass transition temperatures at the respective temperatures of the block components. However, in this case, a single glass transition temperature was recorded for MW96/40 at the weighted average of the T_g's of its components. One must therefore assume that there is no significant "blockiness" present in the sample, and the reservations of Scott may be neglected, *i.e.* MW96/40 behaves as a homopolymer.

By considering fig. 5.12, we see that all the χ-values obtained from the fitting of the SANS data lie above the spinodal line, with the exception of that from the 2% blend. This would suggest that the blends are thermodynamically unstable with respect to demixing at all these compositions. However, it has been stated that the scattering intensity from phase separated blends is infinite. Clearly, were this the case, no fits to the data could be achieved. Therefore, it is suggested that the discrepancies between the data and the fits to the data have considerable significance. The plots of the residuals maintain that the RPA overestimates the scattering intensity, particularly at lower values of Q. Figure 5.9 reinforces this argument by pointing out the relative sensitivity of the fitting routine as a function of Q, the greatest sensitivity being found at lower values. It seems likely, therefore, that the RPA analysis has overestimated the size of the interaction parameters, particularly for the blends with higher fractions of fluoropolymer. This overestimation will bring the values of χ down nearer to the spinodal value.

This result ties in well with the findings of the differential scanning calorimetry described in chapter 4 [*q.v.*]. Here, the sigmoidal dependence of the T_g with

composition was interpreted as being characteristic of incipient phase separation in the blend.

It is interesting to consider the length scale over which any inhomogeneity exists. The simplest observation to make is that the samples themselves are optically clear, which suggests that the size of a given phase is less than the wavelength of visible light *i.e.* phase size<~400nm. This conclusion is also corroborated by the results from the DSC, which finds a single glass transition temperature for all the compositions studied. The length scale associated with the processes of the glass transition are of the order of μm.

At this point, it is instructive to look at the other fitting parameter which was used in the RPA analysis, notably the radius of gyration of the fluoropolymer. The dependencies of this parameter on the two variables composition and temperature are shown in figures 5.13. and 5.14., respectively:

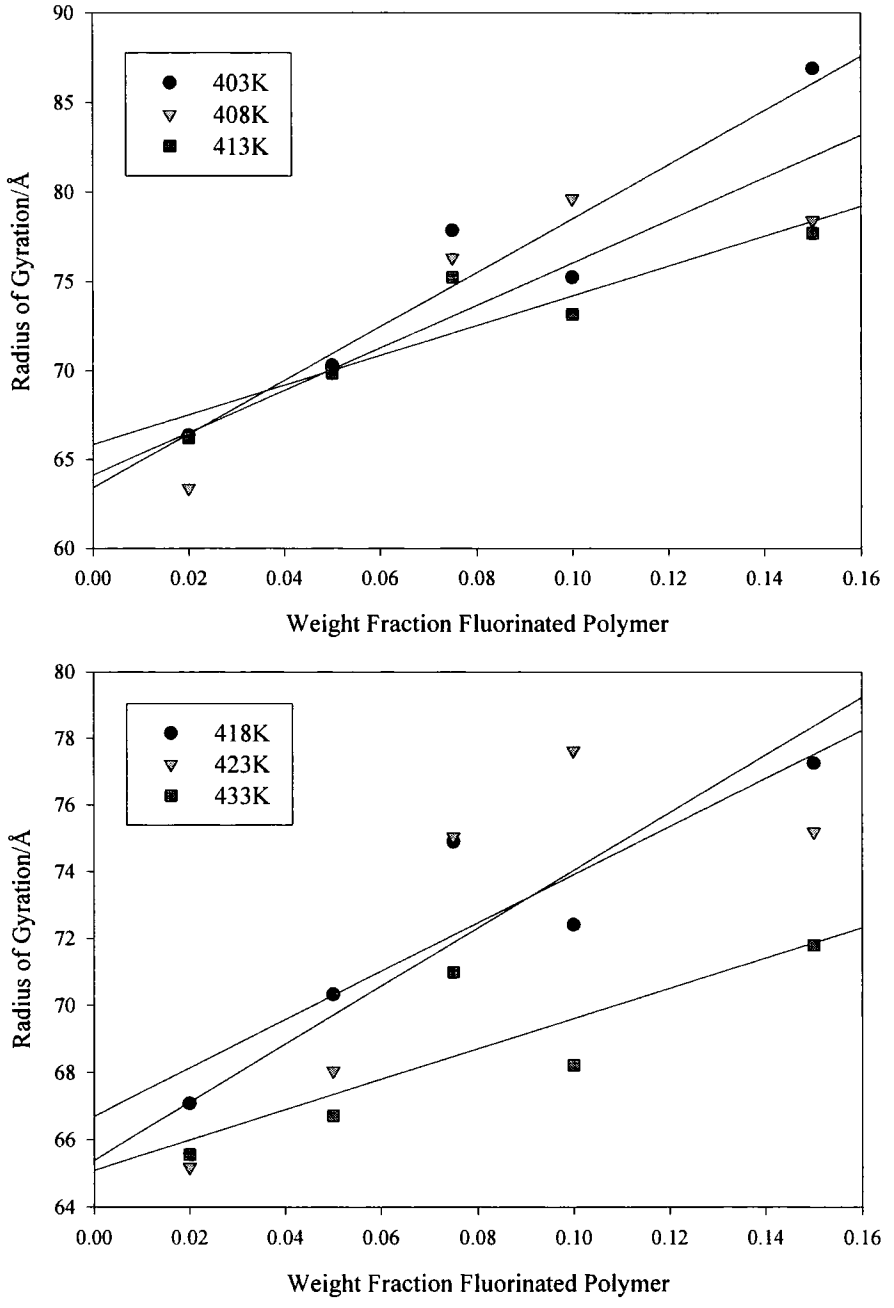

Figure 5.13 Radius of Gyration as a Function of Composition

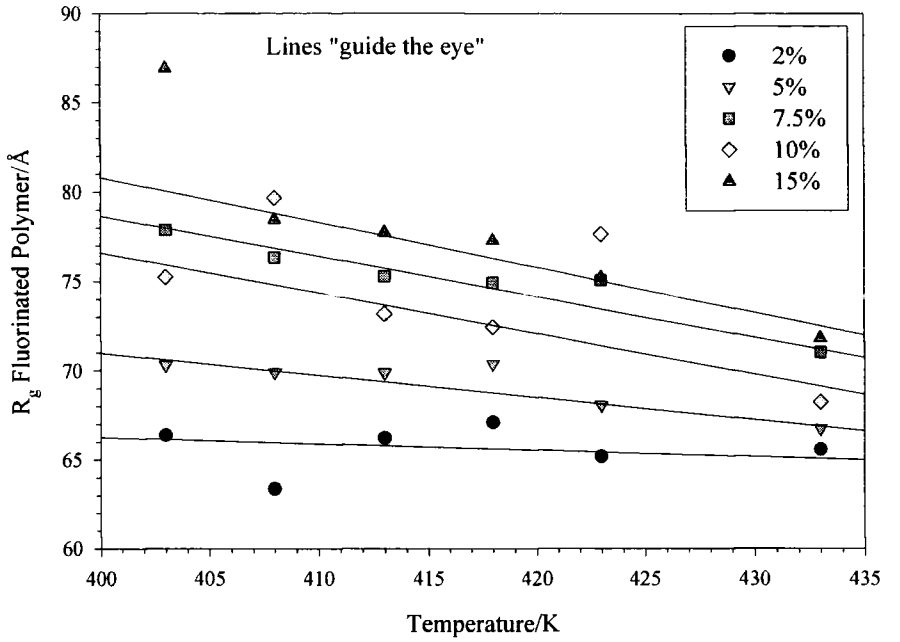

Figure 5.14 Radius of Gyration as a Function of Temperature

The large amount of data represented on figs 5.13. and 5.14. requires a little clarification. From fig 5.13., it can be seen that the general trend is an increase in the radius of gyration of the fluoropolymer with increasing fluoropolymer content.

Figure 5.14. shows the radius of gyration of MW96/40 as a function of temperature at a given concentration. For the blends with the lowest fluoropolymer content, the radius of gyration of the fluoropolymer is comparatively insensitive to temperature. However, at higher concentrations, there is a marked reduction in the radius of gyration as the temperature increases. Before any conclusions can be drawn on the physical state of the blend, it is instructive to look at the form of the scattering bodies.

The free form fitting method described earlier has been found to be wholly inadequate in fitting these data. Whilst the fits look superficially good, careful analysis reveals large discrepancies between the data and the fitted value, and especially at higher Q. It is this Q-regime which is sensitive to the shape of the

scattering bodies, so it is critical that the fit in this region is good. In the light of the observations on the free-form fitting approach, this analysis was discontinued in favour of the simpler (if somewhat crude) method of plotting the data on logarithmic axes. A typical plot of log(I(Q)) *vs.* log(Q) is shown in figure 5.15, below:

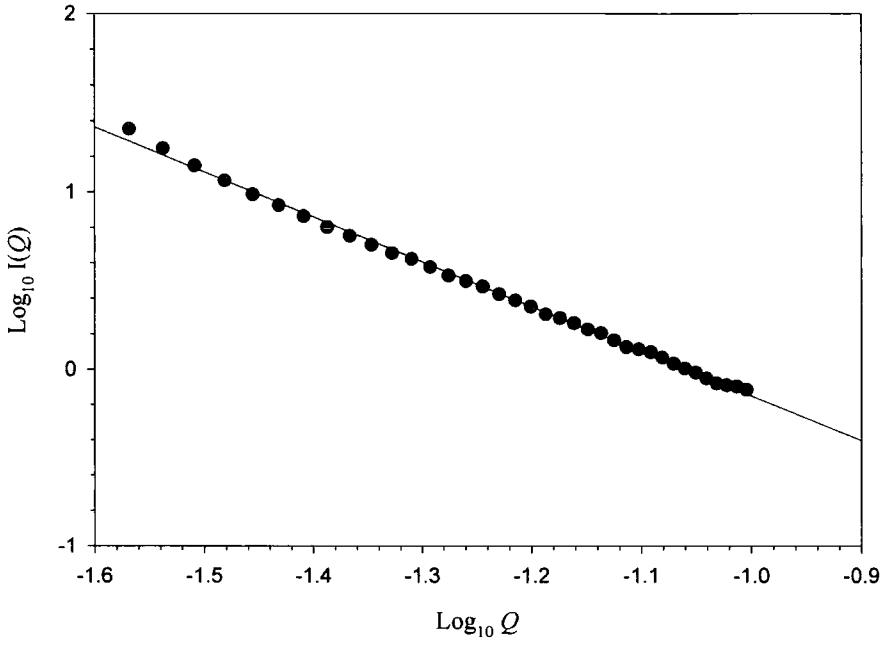

Figure 5.15 Log-Log Treatment: 10% Fluoropolymer, 423K

Collecting values of α from each blend at each temperature, one arrives at figures 5.16 and 5.17, showing the dependence on composition and temperature, respectively:

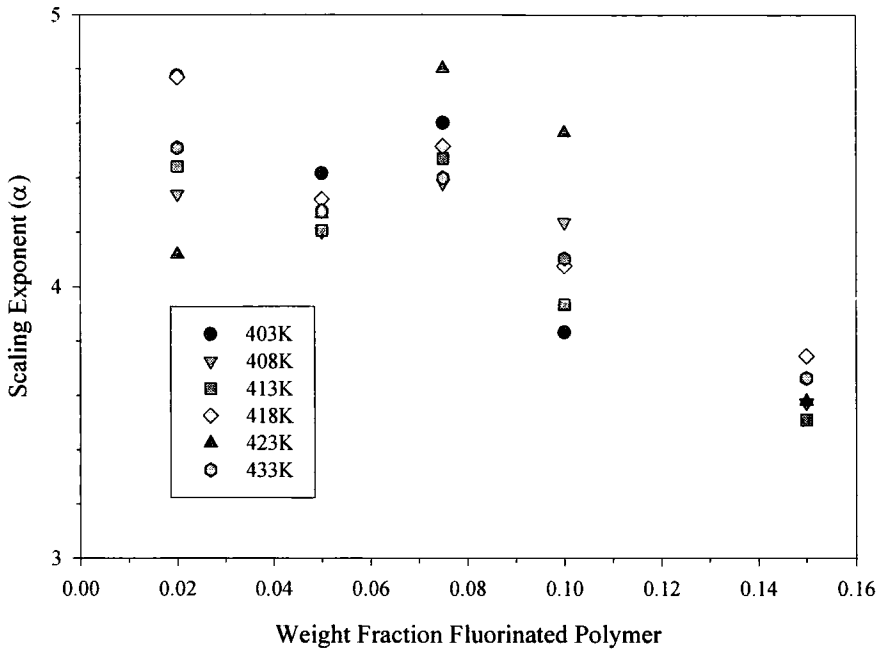

Figure 5.16 Scaling Exponent *vs.* Composition

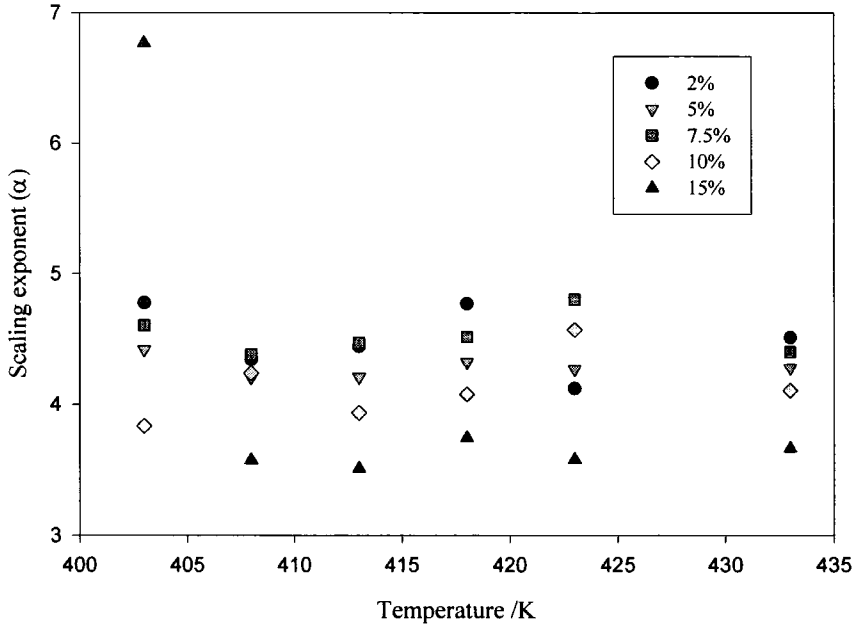

Figure 5.17 Scaling Exponent *vs.* Temperature

Looking at the two figures above, one concludes that the value of the scaling exponent forms a broad band around $\alpha = 4$. Considering the values given in table 5.4. this is indicative of a 3-dimensional scatterer such as a sphere

The Log-Log approach relies on there being a significant linear portion of data for it to give accurate values. Such a linear portion has been found typically to be encompassed by $0.03 \leq Q \leq 0.12$, and over this region, the correlation coefficient, $r^2 > 0.99$ ($r^2 = 1$ is a perfect straight line).

The findings of the log-log analysis have considerable implications when considering the results from the RPA fitting of the data. The RPA assumes a Gaussian form for the polymer chain, with the corresponding scaling exponent of 2. Where there is variation from this value, errors are going to be incurred due to the inaccurate assumptions being made.

Notwithstanding the limitations of the log-log approach, it does give a qualitative idea of the behaviour of the scaling exponent. It can be said with reasonable confidence that the value of the scaling exponent lies some distance from the expected value of 2 for the Gaussian chain model used in the RPA, and therefore the conclusions to be drawn from this analysis are also called into question. In the light of these analyses and observations, it seems necessary to propose a different physical picture for the state of the (deuterated, read also fluorinated) polymers in this blend.

5.6. Conclusions

In the light of the shortcomings of the analyses, assigning a physical explanation to these observations is a tentative process. None the less, there are a number of possible processes which may explain the observed facts.

The most obvious of these processes are the accepted mechanisms of polymer phase separation, *i.e.* "nucleation and growth" or spinodal decomposition. Whilst these processes have the same end result (phase separation), they occur by different mechanisms.

The name "nucleation and growth" is fairly self explanatory. This process is prevalent in metastable regions of the phase diagram, in which any localised concentration fluctuations tend to decay to the equilibrium position. For phase separation to occur, this tendency must be overcome, and this is achieved when a large fluctuation is found. This *nucleus*, once formed, can grow by normal diffusion processes[25,26].

This is in contrast to *spinodal decomposition*, which takes place inside the spinodal region. Here, a polymer blend is unstable to phase separation, so an infinitesimal fluctuation in blend composition sees no thermodynamic barrier, and thus, separation should occur by a continuous and spontaneous process. Since the mixture is initially uniform, this spontaneous reaction must occur by a diffusional flux against the concentration gradient, *i.e.* by "uphill" diffusion with a negative diffusion coefficient[27,28].

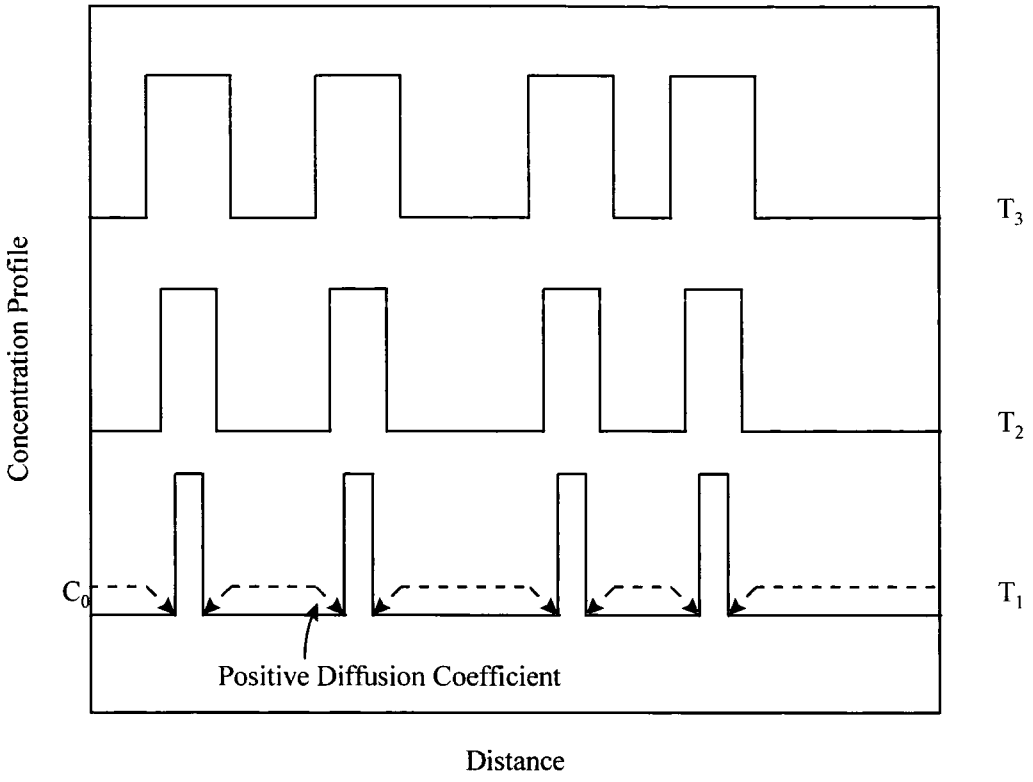

Figure 5.18 Schematic of "Nucleation and Growth"

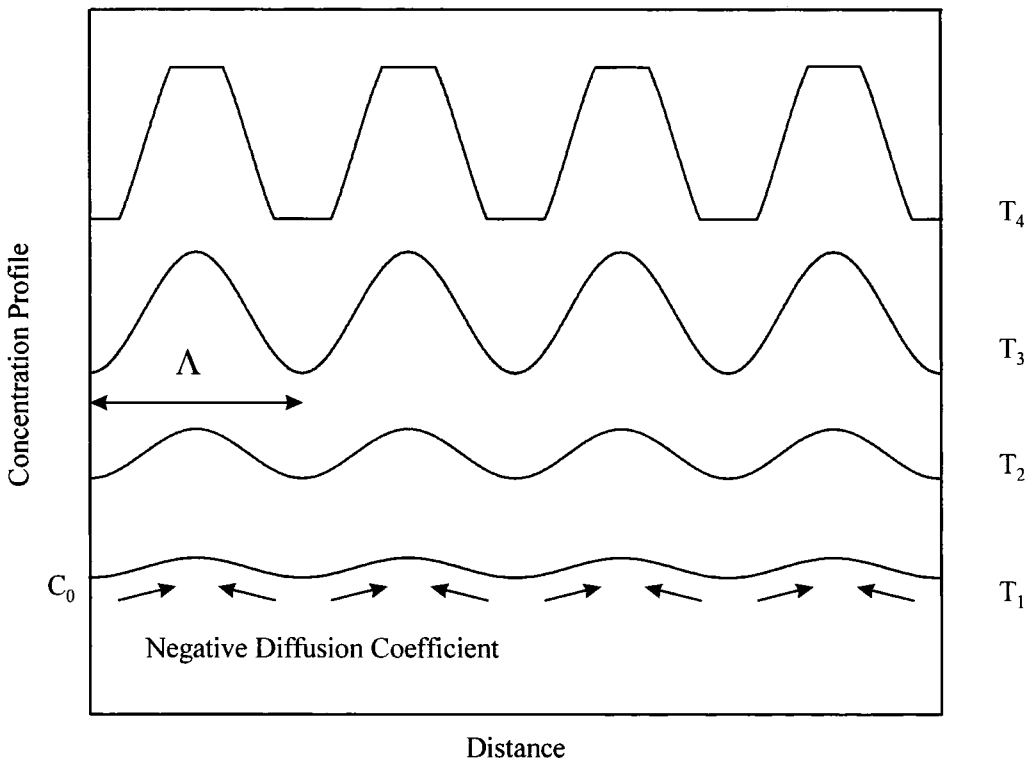

Figure 5.19 Schematic of Spinodal Decomposition

Looking back at the findings from this chapter, we can see that the nucleation and growth behaviour is incompatible with the observations. With a positive diffusion coefficient, one would expect to see the radius of gyration (size) of the scattering particles to increase with temperature as diffusion became increasingly favoured.

Secondly, spinodal decomposition can also be ruled out, as this is a thermodynamically favoured process within the boundaries of the spinodal curve. Were this the mechanism at work here, one could only expect to see an increase in the size of the scatterers as more material separated into individual phases.

However, there is a physical explanation which does fit in with the observed facts, and this is aggregation of the fluoropolymer. Micellisation (aggregation) is inherent in low molecular weight surfactant molecules, but it has also been observed for a number of polymers and copolymers, especially block copolymers when blended with a homopolymer which is only miscible with one of the blocks[29-34]. These systems undergo complex (and potentially reversible) microphase separation with a wide range of morphologies as a function of concentration.

The composition dependence of the particle size may simply be explained by the fact that a higher concentration of fluoropolymer favours the formation of larger aggregates. The interactions which favour the formation of aggregates are likely to be hydrogen-bond like, which are thermally labile. At higher temperatures, a larger proportion of fluoropolymer chains remain unassociated, and the size of the scattering particles is therefore reduced.

Further evidence for the possibility of such an explanation comes from Jouannet *et al*[35], in which inter- and intramolecular interactions between fluorinated side chains and ester functionalities are postulated to explain the immiscibility of a fluoroalkyl methacrylate - methyl methacrylate copolymer with methyl methacrylate homopolymer. The system discussed is not entirely different from the one in the current study, so similar reasoning could be applied to this system. The vicinal protons (α-to the CF_2 group) are highly acidic, and may partake in a hydrogen bonding kind of interaction. Similarly, the protons of the -CFH- groups of the side chain are electron deficient. The nature of these interactions will be further discussed when more evidence has been considered.

5.7. References

1)Hopkinson, I.; Kiff, F. T.; Richards, R. W.; King, S. M.; Munro, H. *Polymer* **1994**, *35*, 1722-1729.

2)Hasegawa, H.; Sakurai, S.; Takenaka, M.; Hashimoto, T.; Han, C. C. *Macromolecules* **1991**, *24*, 1813.

3)Shibayama, M.; Yang, H.; Stein, R. S.; Han, C. C. *Macromolecules* **1985**, *18*, 2187.

4)King, S. M. *LOQ Homepage*; http://ndafleetwood.nd.rl.ac.uk/largescale/LOQ/loq.htm.

5)Han, C. C.; Bauer, B. J.; Clark, J. C.; Muroga, Y.; Matsushita, Y.; Okada, M.; Qui, T. C.; Chang, T. H.; Sanchez, I. C. *Polymer* **1988**, *29*, 2002-2014.

6)Krishnamoorti, R.; Graessley, W. W.; Balsara, N. P.; Lohse, D. J. *Journal of Chemical Physics* **1994**, *100*, 3894.

7)Kumar, S. K. *Macromolecules* **1994**, *27*, 260.

8)Londono, J. D.; Narten, A. H.; Wignall, G. D.; Honnell, K. G.; Hsieh, E. T.; Johnson, T. W.; Bates, F. S. *Macromolecules* **1994**, *27*, 2864-2871.

9)Londono, J. D.; Wignall, G. D. *Macromolecules* **1997**, *30*, 3821-3824.

10)Muthukumar, M. *Journal of Chemical Physics* **1986**, *85*, 4722.

11)Riedl, B.; Prudhomme, R. E. *Polymer Engineering and Science* **1984**, *24*, 1291-1299.

12)Zhikuan, C. *Polymer Communications* **1984**, *25*, 21-23.

13)Higgins, J. S.; Benoit, H. *Polymers and Neutron Scattering*; Clarendon Press: Oxford, 1994.

14)De Gennes, P. G. *Scaling Concepts in Polymer Physics*; Cornell University Press:, 1979.

15)Debye, P. *Journal of Physical Colloid Chemistry* **1947**, *51*, 18.

16)Fetters, L. J.; Lohse, D. J.; Colby, R. H. *Chain Dimensions and Entanglement Spacings*; in *Physical Properties of Polymers Handbook*, Mark, J.E.; Ed.; AIP Press: New York, 1997, pp 335-341.

17)Guinier, A.; Fournet, G. *Small Angle Scattering of X-rays*; John Wiley & Sons: New York, 1955.

18)Benmouna, M.; Briber, R.; Hammouda, B. *Macromolecular Theory and Simulations* **1997**, *6*, 197-235.

19)Hammouda, B. *Advances in Polymer Science* **1993**, *106*, 87-133.

20)Hammouda, B.; Briber, R. M.; Bauer, B. J. *Polymer* **1992**, *33*, 1785-1787.

21)Hammouda, B. *Journal of Non-Crystalline Solids* **1994**, *172*, 927-931.

22)Hammouda, B.; Bauer, B. J.; Russell, T. P. *Macromolecules* **1994**, *27*, 2357-2359.

23)Scott, R. L. *Journal of Polymer Science* **1952**, *9*, 423.

24)Krause, S.; Smith, A. L.; Duden, M. G. *Journal of Chemical Physics* **1965**, *43*, 2144.

25)Balsara, N. P.; Lin, C.; Hammouda, B. *Physical Review Letters* **1996**, *77*, 3847-3850.

26)Muller, G.; Schwahn, D.; Springer, T. *Physical Review E* **1997**, *55*, 7267-7282.

27)Nishi, T.; Wang, T. T.; Kwei, T. K. *Macromolecules* **1975**, *8*, 227.

28)Reich, S. *Physics Letters* **1986**, *114A*, 90.

29)Adedeji, A.; Jamieson, A. M.; Hudson, S. D. *Macromolecules* **1995**, *28*, 5255-5261.

30)Adedeji, A.; Hudson, S. D.; Jamieson, A. M. *Macromolecules* **1996**, *29*, 2449-2456.

31)Hu, W. C.; Koberstein, J. T.; Lingelser, J. P.; Gallot, Y. *Macromolecules* **1995**, *28*, 5209-5214.

32)Laurer, J. H.; Ashraf, A.; Smith, S. D.; Spontak, R. J. *Langmuir* **1997**, *13*, 2250-2258.

33)Polance, R.; Nichols, K. L.; Jayaraman, K. *Polymer* **1994**, *35*, 5051-5056.

34)Prahsarn, C.; Jamieson, A. M. *Polymer* **1997**, *38*, 1273-1283.

35)Jouannet, D.; Pham, T.-N.; Pimbert, S.; Levesque, G. *Polymer* **1997**, *38*, 5137-5147.

Chapter Six

Surface Energetics

6.1. Introduction

The surface (or more generally, interfacial regions) of a material are of considerable technological importance. The way a material interacts with its operational environment is largely determined by its surface properties and, similarly, the interfacial regions of a multi-component system make a significant bearing on the physical and chemical properties.

It is, therefore, of great interest to determine the interfacial properties of a system, and a vast array of techniques is now available. In the interests of brevity, the reader is referred to standard texts on the subject.[1-3]

Many techniques described therein are specifically applied to crystalline materials (metals, inorganics), and in that respect are of distinctly limited utility where polymers are concerned. However, *X*-ray Photoelectron Spectroscopy (XPS)[4-8], Auger Electron Spectroscopy (AES)[9,10] and Secondary Ion Mass Spectrometry[11-16] (SIMS, dynamic and static) have all found considerable application in the characterisation of polymer surfaces and in near surface depth profiling. Of particular relevance to this work are the techniques of contact angle measurement, Neutron Reflectometry (NR) and Rutherford Backscattering Spectrometry. These techniques will be discussed in detail below, but by way of an introductory overview, contact angle measurements are used to determine the surface energy of a particular system by studying the way a fluid of known surface energy spreads over the surface.

Neutron Reflectometry and Rutherford Backscattering Spectrometry (RBS) are similar to one another in that they both determine the *near surface behaviour*. These techniques enable the detection of *surface segregation*, and also look at its

depth profile as any *surface excess* decays to the bulk concentration. The techniques are, none the less, complimentary. NR requires the fitting of mathematical models to the data to extract the information contained therein, a process which is inherently model-dependent and open to several interpretations. RBS, on the other hand, gives a more direct picture of the surface profile at the expense of resolution.

Similarly, research into ways of modifying the interfacial properties of a material is sustained at the high level commensurate with the technological importance given to this field. Plasmas in particular have found a wide number of applications, as they allow the modification of surface morphology and/or functionality without altering the properties of the bulk material *i.e.* they are *surface specific*. Additional advantages include the absence of solvent in any of the process stages[17,18].

More traditional "wet" chemistry still fulfils a significant role in surface modification[19], and perhaps this is particularly so where surface fluorination is desired. Academia and industrial concerns world-wide continue to seek ways of introducing fluorine into surface coatings in order to exploit a number of benefits such a process can bring. Most notable of these benefits are the lowering of surface energy and vapour permeability, combined with improved solvent resistance and possible lubrication effects.

Should a material prove to be resistant to fluorination itself, an enormous variety of fluorinated coating technology is available. The ubiquitous non-stick pan serves as an excellent mirror to the advances in fluoropolymer technology, reflecting, as it does, the fluoropolymer story from its inception to the current state-of-the-art.

It was in 1951 when DuPont first began to market poly(tetrafluoroethene) (PTFE) as a coating material for use as protection against harsh industrial environments. The coating was supplied as a dispersion in a chromic/phosphoric acid; PTFE is insoluble in practically all solvents except at elevated temperature. The strong acids react on baking to give oxides of chromium and phosphorus to key the PTFE coating into the pre-roughened surface of the substrate.

These harsh processing conditions were necessary as PTFE is neither solution nor melt processable. Over the 1960's and '70's, an enormous research effort was expended to prepare melt processable fluoropolymers, which cumulated in hexafluoropropene (HFP) copolymers with tetrafluoroethene and the development of hexafluoropropene oxide (HFPO). The state-of-the-art for PTFE-based coatings is now considered to be a mixture of PTFE, PHFP and PHFPO as copolymers or blends, with the addition of other polymeric materials to enhance the binding of the coating to the substrate.

When these coatings are baked, the fluorinated polymers undergo *surface segregation*, a thermodynamic process which seeks to minimise the surface energy of the system. As the fluoropolymers have very low surface energies, their concentration is enriched at the surface. Similarly, the binder materials with

a relatively high surface energy are enriched at the coating/substrate interface, improving adhesion.

This surface segregation behaviour is inherent in mixed polymer systems, and a fuller discussion of the phenomena will be presented later.

It remains for the issue of solution processability to be addressed. It is of concern to both consumers and manufacturers to reduce the costs incurred in the processing of fluorinated materials, and one way in which this may be achieved is by the preparation of fluorinated analogues of common functional polymers such as poly(styrene) and various polyacrylics. Whilst these materials do not possess all the properties of the perfluoropolymers (most notably the thermal and chemical resistance), they do provide a simple route into the desirable surface properties. In favourable cases, the solution processability of these materials means that they may be blended with cheaper polymers to give bulk, and the surface segregation behaviour means that a fluorinated surface will still be presented to the outside world.

6.2. Surface Thermodynamics[20]

The interface or surface is a region of finite thickness, usually less than 1μm, in which the composition and energy vary from one bulk phase to the other. The pressure in the interfacial zone is therefore inhomogeneous, having a gradient perpendicular to the interfacial boundary *c.f.* the homogeneous, isotropic bulk phase. It follows that no net energy is expended in transporting matter reversibly within the bulk phase, but energy is expended in creating an interface by

transport of matter to the interfacial zone. The reversible work (energy) required to create a unit interfacial (surface) area is the interfacial (surface) tension.:

$$\gamma = \left(\frac{\partial G}{\partial A}\right)_{T,P,n} \qquad \textbf{[6.1]}$$

where γ is the interfacial tension, G the Gibbs free energy of the total system, A the interfacial area, T the absolute temperature, P the pressure and n the total number of moles of matter in the system.

6.2.1. The Guggenheim Model

If two bulk phases α and β are separated by an interfacial layer σ of thickness t, for a two component system at equilibrium, we have:

$$\mu_1^{\alpha} = \mu_1^{\beta} = \mu_1^{\sigma} = \mu_1 \qquad \textbf{[6.2]}$$

$$\mu_2^{\alpha} = \mu_2^{\beta} = \mu_2^{\sigma} = \mu_1 \qquad \textbf{[6.3]}$$

where μ is the chemical potential. The variations in the Gibbs free energy are given by:

$$dG^{j} = -S^{j}dT + V^{j}dP + \mu_1 dn_1 + \mu_2 dn_2 \qquad \textbf{[6.4]}$$

$$dG^{\sigma} = -S^{\sigma}dT + V^{\sigma}dP + \gamma dA + \mu_1 dn_1 + \mu_2 dn_2 \qquad \textbf{[6.5]}$$

where S is the entropy, V the volume, n the number of moles of material and j = α, β (the bulk phases).

The integral forms of the above equations are:

$$G^j = n_1\mu_1 + n_2\mu_2 \qquad \textbf{[6.6]}$$

$$G^\sigma = \gamma A + n_1^\sigma \mu_1 + n_2^\sigma \mu_2 \qquad \textbf{[6.7]}$$

Dividing eqn 7 by A gives:

$$f^\sigma = \gamma + \Gamma_1\mu_1 + \Gamma_2\mu_2 \qquad \textbf{[6.8]}$$

where f^σ = G^σ/A, the specific surface free energy and Γ_i = n_i^σ/A, the surface concentration of component i.

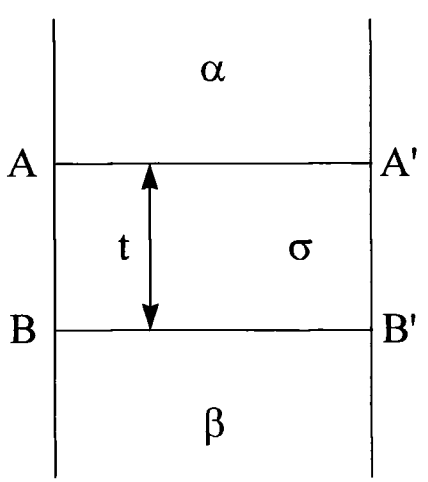

Figure 6.1 The Guggenheim Model for an Interface.

Surface tension is the excess specific surface free energy, *i.e.*

$$\gamma = f^\sigma - \left(\Gamma_1 n_1 + \Gamma_2 n_2\right) \qquad \textbf{[6.9]}$$

Equation 9 defines the distinction between the surface tension and the specific surface free energy.

6.2.2. Surface Segregation

The example of surface segregation given above was for PTFE and other perfluoropolymers, but according to a number of workers[21,22], this phenomenon is inherent in polymer-polymer systems.

The surface is characterised by two parameters, ϕ_1 and z^*, where ϕ_1 is the surface volume fraction of the component enriched at the surface and z^* is the surface excess. These parameters are shown schematically in fig 6.2.

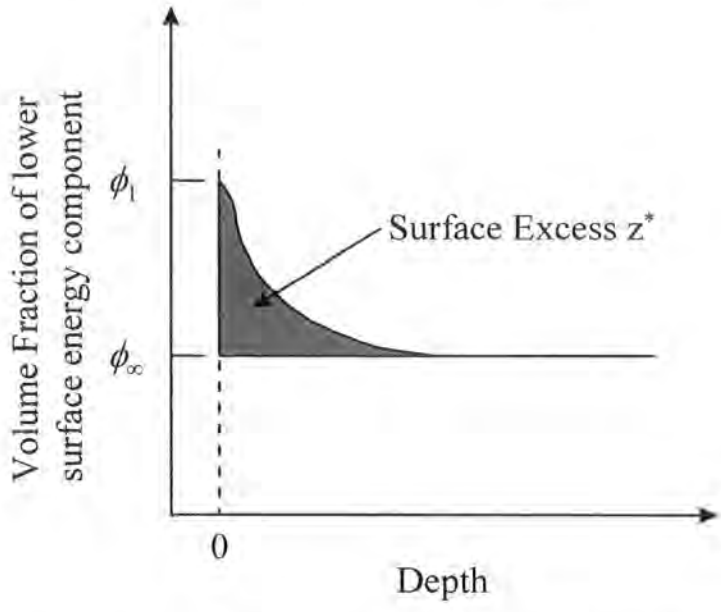

Figure 6.2 Parameters defining the surface of a Polymer Blend.

ϕ_∞ is the bulk volume fraction of component 1.

These authors go on to derive analytical expressions for ϕ_1 and z^* by assuming a mean field and considering the perturbations to such a field caused by the presence of a surface. The full expression for the composition profile $\phi(z)$ is arrived at by minimising the free energy of the system as a whole, taking into

account the free energy to be gained by forming a low energy surface and that expended in the creation of the surface layer, [*q.v.*]. This function reads:

$$-\frac{df_s}{d\phi_1} = \mu_1 + g\phi_1 = \pm\frac{a}{3}\sqrt{\frac{Q(\phi_1,\phi_\infty)}{\phi_1(1-\phi_1)}} \qquad \textbf{[6.10]}$$

Here, $Q(\phi_1,\phi_\infty)$ is the function:

$$Q(\phi_1,\phi_\infty) = G(\phi) - G(\phi_\infty) - \Delta\mu(\phi - \phi_\infty) \qquad \textbf{[6.11]}$$

where $G(\phi)$ is the free energy of mixing of the blend per lattice site, a is the statistical segment length and $\Delta\mu$ is the exchange chemical potential $\partial G/\partial\phi$ evaluated at the bulk volume fraction ϕ_∞. The effect of the surface is represented by a bare surface energy, of the form

$$f_s(\phi_1) = -\mu_1\phi_1 - \frac{g}{2}\phi_1^2 \qquad \textbf{[6.12]}$$

The difference in surface energy of the two components is given by $\mu_1 + g/2$ for a Flory-Huggins lattice cell, where μ_1 represents a surface chemical potential favouring component 1 at the surface. The parameter g expresses the way in which interactions of the blend are affected by the surface, and is related to the Flory-Huggins interaction parameter, χ (per segment). In many blends, the size

of g is small relative to the difference in surface energy, and in these instances, g may be ignored.

The composition profile is given by:

$$z = \frac{a}{6}\int_{\phi_z}^{\phi(z)} \frac{d\phi}{\phi(1-\phi)Q(\phi,\phi_\infty)^{1/2}} \qquad \textbf{[6.13]}$$

It is especially worthy of note to mention that the shape of the volume fraction profile is entirely determined by the bulk thermodynamics of the blend; the difference in surface energy between the components affects only the surface composition.

The integrated surface excess z^* is given by

$$z^* = \int_0^\infty [\phi(z) - \phi_\infty]dz \qquad \textbf{[6.14]}$$

which may be directly calculated by

$$z^* = \frac{a}{6}\int_{\phi_\infty}^{\phi_1} \frac{d\phi}{\phi(1-\phi)Q(\phi,\phi_\infty)^{1/2}} \qquad \textbf{[6.15]}$$

While these equations in themselves may be used to evaluate the surface parameters of a blend, Jones & Kramer go on to develop simpler analytical expressions.

They start by assuming a Flory-Huggins form [*q.v.*] for the free energy of mixing for a polymer blend the components of which have equal degrees of polymerisation N, and furthermore define an additional parameter χ_b:

$$\chi_b = \frac{1}{N(1-2\phi_\infty)}\ln\left(\frac{1-\phi_\infty}{\phi_\infty}\right) \qquad \textbf{[6.16]}$$

χ_b is the value of χ on the coexistence (binodal) curve.

Using equation 16 and the Flory-Huggins expression, equation 11 may be recast

$$Q(\phi,\phi_\infty) = (\chi_b - \chi)(\phi - \phi_\infty)^2 + \frac{1}{N} f(\phi,\phi_\infty) \qquad \textbf{[6.17]}$$

$$f(\phi,\phi_\infty) = \phi\ln\phi + (1-\phi)\ln(1-\phi) - \ln(1-\phi_\infty) + \frac{\phi(1-\phi) - \phi_\infty^2}{(1-2\phi_\infty)}\ln\frac{(1-\phi_\infty)}{\phi_\infty} \qquad \textbf{[6.18]}$$

If $|\chi|N$ is large, which is the case in many miscible polymer blends, and also that ϕ_∞ is not too close to 0 or 1, the second term in equation 17 may be neglected. This simplifies the expression to

$$Q(\phi,\phi_\infty) = (\chi_b - \chi)(\phi - \phi_\infty)^2 \qquad \textbf{[6.19]}$$

Using this simplified expression allows the explicit evaluation of the surface volume fraction and integrated surface excess by substituting into equations 10 and 15, respectively.

Employing such a tactic for the surface volume fraction, the following expression results

$$\phi_1 = \frac{\phi_\infty + t}{1+t} \qquad \textbf{[6.20]}$$

where

$$t = 9\left(\frac{\mu_1}{a}\right)^2 \frac{1}{\chi_b - \chi} \qquad \textbf{[6.21]}$$

t is a measure of the driving force for surface segregation represented by a reduced surface energy difference.

Thus, the surface volume fraction may be expressed in terms of the bulk volume fraction ϕ_∞ and a single reduced parameter t, which accounts for the difference in surface energies between the two polymers, their molecular weight and their thermodynamics of mixing embodied in the interaction parameter, χ.

For the integrated surface excess: using equation 19 and substituting into equation 15, the following is obtained:

$$z^* = \frac{a}{6}\frac{1}{\sqrt{\chi_b - \chi}} \int_{\phi_\infty}^{\phi_1} \frac{d\phi}{\sqrt{\phi(1-\phi)}} \qquad \textbf{[6.22]}$$

This integration may be done analytically, to yield:

$$z^* = \frac{a}{3}\frac{1}{\sqrt{\chi_b - \chi}}\left(\arcsin\sqrt{1-\phi_\infty} - \arcsin\sqrt{1-\phi_1}\right) \qquad \textbf{[6.23]}$$

Using these expressions, Jones goes on to demonstrate the effects of the various parameters on the surface volume fraction and surface excess in their hypothetical blend. Figure 6.3 shows the surface volume fraction varying as a function of t, the reduced surface energy difference, for different values of ϕ_∞.

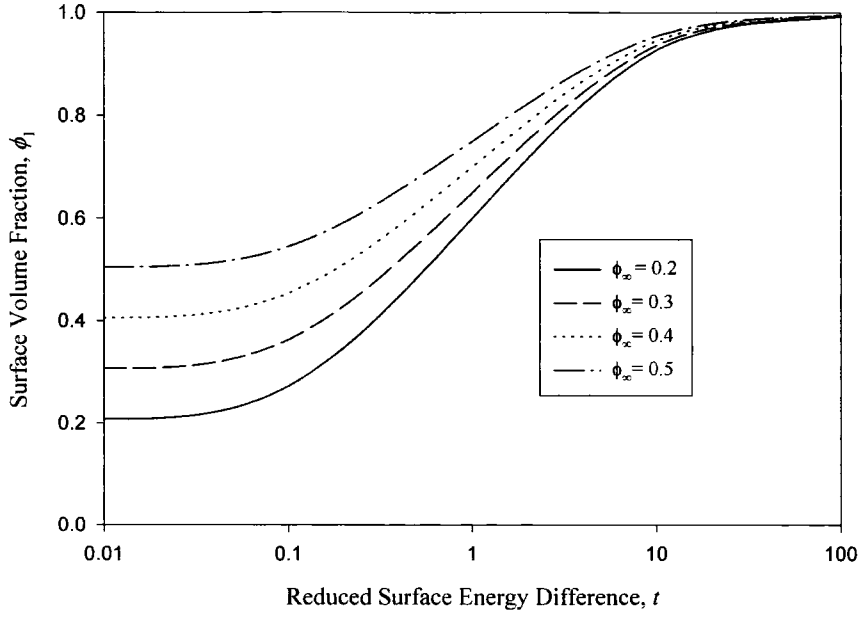

Figure. 6.3 Surface volume fraction as a function of reduced surface energy difference, t, for different values of the bulk volume fraction ϕ_∞

Of more practical importance is the dependence of ϕ_1 and z^* on the measurable parameters $\Delta\gamma$ (the difference in surface energy between two components of a blend) and the interaction parameter χ. Such dependencies can be examined using equations 20 and 23 by substituting for t. To do this, μ_1 is related to $\Delta\gamma$ as follows:

$$\mu_1 = \frac{b^3}{k_B T}\Delta\gamma \qquad \textbf{[6.24]}$$

where b is the size of the Flory-Huggins lattice cell, k_B is Boltzman's constant and T is the temperature. b should have the units of Å and $\Delta\gamma$ mJ.m^{-2}.

For poly(styrene), we obtain $\Delta\gamma = 3.54\mu_1$, and for polymers with a degree of polymerisation = 500, the curves of figure 6.4 may be generated.

From the first set of curves, it is clear that there only needs to be a small difference in the surface energies of the blend components for there to be complete enrichment of the low surface energy component at the air interface. The surface excess is also insensitive to the difference in surface energies, it rapidly saturating at small values. Therefore, it remains once more to emphasise that the surface properties of a (miscible) polymer blend are almost entirely determined by the bulk thermodynamics of the blend, a feature embodied in the Flory-Huggins interaction parameter.

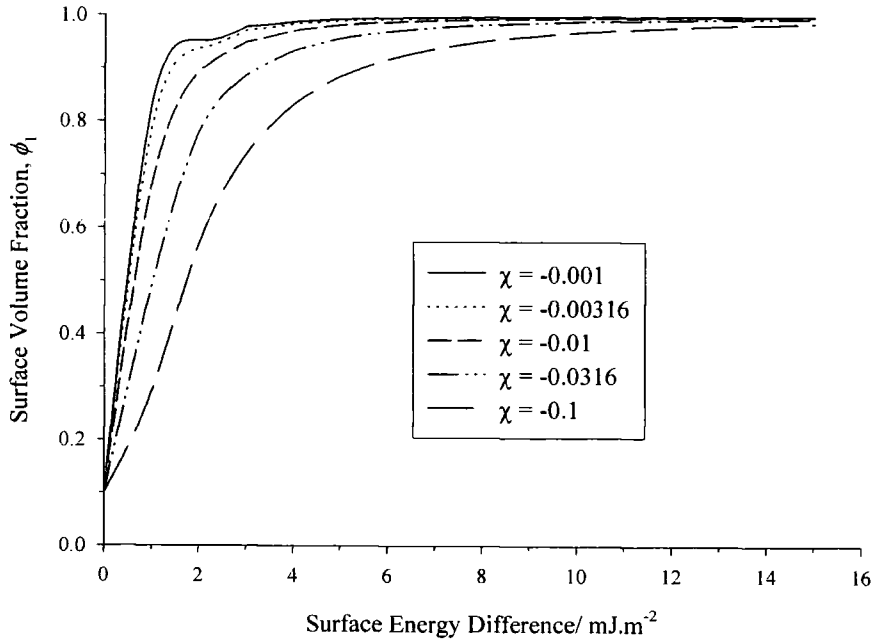

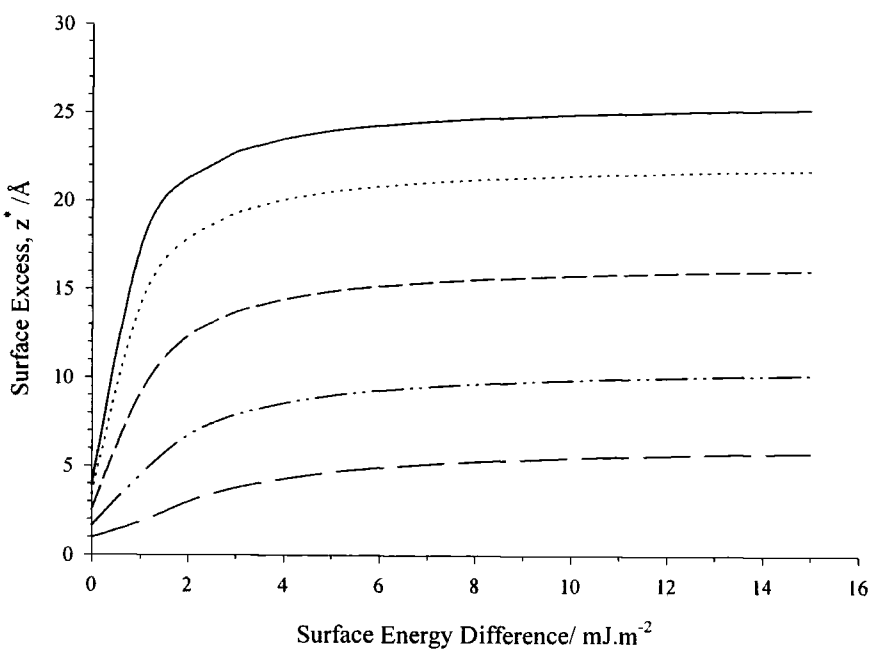

Figure 6.4 Surface Volume Fraction (ϕ_1) and Surface Excess (z^*) as a function of the difference in surface energy of two components of a miscible polymer blend. The legend on the top axes apply to both.

6.3. Contact Angle Equilibrium

A liquid in contact with a solid will exhibit a *contact angle*. If the system is at rest, a static contact angle will be observed. The system at rest may be in stable equilibrium, the lowest energy state, or in a metastable equilibrium. Stable equilibrium is obtained if the surface is *smooth*, *homogeneous*, *planar* and *non-deformable*. The contact angle found in these circumstances is denoted θ_e, the equilibrium or Young's contact angle. If, however, the substrate is rough or compositionally inhomogeneous, the system may reside in a metastable state and the observed contact angle is also metastable. Metastable contact angles are seen to vary with drop volume, external mechanical energy such as vibration and how the liquid drop is formed (advancing or receding the liquid front on the substrate). If the angle is formed by advancing the liquid front over the surface, it is denoted the advancing contact angle θ_a. If the liquid front recedes from the surface, the receding contact angle, θ_r, is observed. θ_a is usually greater than θ_r, with the exception of when the system is in static equilibrium, where $\theta_a = \theta_r$.

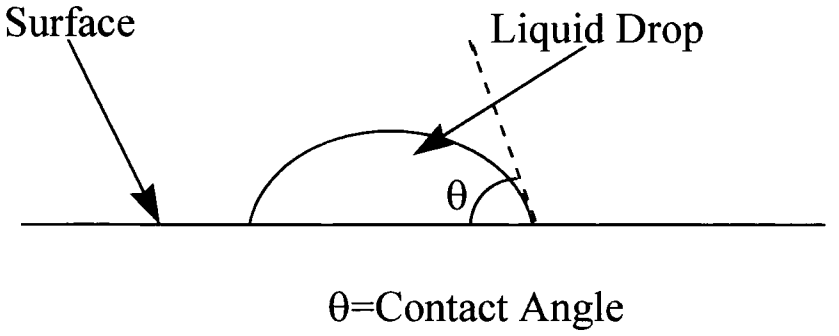

Figure. 6.4 Schematic of Contact Angle Measurement

The equilibrium contact angle on a rough surface is *Wenzel's* angle θ_W, and the equilibrium contact angle on an inhomogeneous surface is *Cassie's* angle θ_C. These angles are seldom observed, as they correspond to the lowest energy state

on that surface. More commonly, the system resides in a metastable state and thus exhibits a metastable contact angle. In this instance, advancing and receding contact angles are different, known as *hysteresis.* The extent of hysteresis is given by $\theta_a - \theta_r$.

If a liquid drop has a steady contact angle on a horizontal planar substrate, and the surface is found to be smooth and homogeneous, the addition of a small volume of liquid will cause the liquid front to advance, after which the same contact angle will re-establish. Similarly, if a small volume of liquid is removed, the liquid front will recede, but the same contact angle will be observed. If the surface is rough and/or inhomogeneous, addition of liquid will increase the height of the drop without moving its periphery. As the critical amount of liquid is exceeded, the front will advance suddenly. The contact angle at the critical point is the *maximum advancing contact angle.* The converse is true when liquid is removed, and the contact angle at the critical point is the *minimum receding contact angle.*

Both advancing and receding contact angles can be observed in the same drop if the substrate is tilted. When the drop width is very large, the Laplace equation[23] gives:

$$\sin\theta_a - \sin\theta_r = \frac{g\rho z_0^2}{2\gamma} \qquad \textbf{[6.25]}$$

where g is the acceleration due to gravity, ρ is the liquid density, z_o the vertical distance between the top and bottom of the drop on a horizontal surface and γ the surface tension of the liquid. The contact angles are related to the angle of tilt by:

$$mg \sin\alpha = L\gamma(\cos\theta_a - \cos\theta_r) \quad \textbf{[6.26]}$$

where m is the mass of the drop, α is the angle of tilt and L the drop length. At the tilt angle where the drop just starts to roll down the tilted plane, the angle measured at the front of the drop is the maximum advancing contact angle, and that measured at the rear the minimum receding contact angle. If no hysteresis is observed, the drop will roll down the plane at the slightest tilt of the substrate.

Techniques using contact angle measurements have been described by a number of workers[24-30]

Fowkes[27] adds to work by Zisman[30], who compiled a large number of data on the works of adhesion of pure liquids on polymer surfaces. In a previous work[26], Fowkes describes the partitioning of the work of adhesion and the surface free energies of pure organic liquids into a van der Waal's (dispersion) and a polar (acid-base) contribution:

$$\gamma_L = \gamma_L^{\,d} + \gamma_L^{\,ab} \quad \textbf{[6.27]}$$

$$W_{SL} = W_{SL}^{\,d} + W_{SL}^{\,ab} \quad \textbf{[6.28]}$$

where

$$W_{SL}{}^{d} = 2(\gamma_L{}^{d}\gamma_S{}^{d})^{1/2} \quad \textbf{[6.29]}$$

and

$$W_{SL} = \gamma_L(1+\cos\theta) = 2\left(\gamma_L^{d}\gamma_S^{d}\right)^{1/2} + 2\left(\gamma_L^{ab}\gamma_S^{ab}\right)^{1/2} \quad \textbf{[6.30]}$$

The acid-base contribution to the work of adhesion of a liquid to a polymer surface is often a hydrogen bond.

6.4. Experimental Procedure

Contact angle measurements were performed on a Ramé-Hart contact angle goniometer, fitted with an environmentally controlled chamber. The chamber helps to exclude dust, as well as allowing experiments to be done at a known (elevated) temperature. The contact angle is measured on a sessile drop, formed by depositing an amount of test liquid onto a polymer-coated microscope slide. Before a measurement can be made, it must be ensured that the goniometer stage is level with respect to both axes. This is achieved as described in the manufacturer's instructions. The environmentally controlled chamber is then fitted, and the sample clamped in the holder. In order to ensure the atmosphere in the chamber is saturated with the vapour of the test liquid, an amount of the liquid is poured into a quartz cell, which is then inserted into the chamber. The test liquid (ultra-high quality water, CH_2I_2) is dispensed from a syringe onto the

surface of the sample, and then left to allow the system to equilibrate. The contact angle is measured by aligning the cross-wires tangentially with the drop profile at the base of the drop.

6.4.1. Sample Preparation

Polymer samples were deposited onto glass microscope slides from solution, the concentration of which depended on the molecular weight of the polymer. It generally varied between 3-5% w/v. Two techniques have been tried: static solvent casting and spin casting.

Static solvent casting, with the solvent just evaporated first at room temperature then *in vacuo* overnight, was found to give a poor, uneven surface. Many defects, such as those produced by escaping solvent bubbles and dust are seen on the surface, which are manifest in a non-equilibrium contact angle being observed. Spin casting, on the other hand, gives a uniform film comparatively free from such defects. Effects resulting from solvent bubbles may be eliminated by heating the sample above its T_g, *i.e.* annealing the films.

The annealing process is considered to be important. Katano *et al*[31] describe the difference in surface energy of a number of fluoroalkyl (meth)acrylates according to their thermal treatment. On heating above a certain temperature (dubbed the "critical" temperature), the contact angle of the polymer film depended on the rate at which the film had been cooled, and in what environment. If the blend was annealed, *i.e.* cooled slowly from above the critical temperature, the maximum contact angle was observed. In contrast, quenching by immersing the film in

water caused a reduction in the contact angle which was attributed to a surface rearrangement.

Clearly, such an added complication is undesirable, and to prevent any such difficulties, the all samples were annealed above their glass transition temperatures before slow cooling to room temperature.

6.5. Results & Discussion

POLYMER	TEST LIQUID	CONTACT ANGLE/° @298K
PMMA	Water	79.4
	CH_2I_2	42.0
PTFEMA	Water	95.4
	CH_2I_2	78.3

Table 6.1 Contact Angle Measurement Results

Using equation 30, and assuming the atmosphere to be saturated with the vapour of the test liquid, the works of adhesion of the two polymers are calculated to be **86.2mJ. m^{-2}** and **88.6mJ. m^{-2}** for PMMA, and **65.9mJ. m^{-2}** and **61.1mJ. m^{-2}** * for PTFEMA (water, CH_2I_2 respectively). These correspond to surface energies of 39.6mJ.m^{-2} and 25.4mJ.m^{-2} for PMMA and PTFEMA by the geometric mean method. Accepted literature values for PMMA are around 41mJ.m^{-2}, and Katano [31] gives the surface energy of PTFEMA as being 27mJ m^{-2}.

* *N.B.* Some authors report surface energies in units of mN.m^{-1} or, in older papers, Dyne.cm^{-1}; these are the same as mJ.m^{-2}

It is worthy of note that the work of adhesion for PTFEMA measured using water is greater than that found with methylene iodide. Ellison *et al*[25] note that test liquids with a hydrogen bonding capability, *e.g.* water, are seen to spread more than those with no such capability on a $-CF_3$ or $-CF_2H$ surface. They propose the formation of hydrogen bonded complexes on the surface, raising the work of adhesion accordingly. They report an equilibrium contact angle of water on a $-CF_3$ surface[†] of 102°, giving a work of adhesion of $57.5 mJ.m^{-2}$.

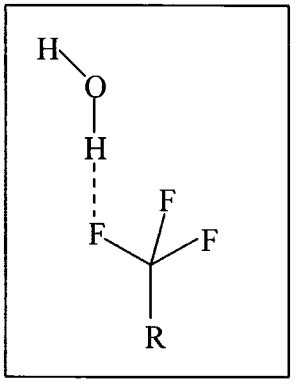

Figure 6.5 Hydrogen Bond to CF_3 Surface

6.5.1. P(MeTelMA)

This work has failed to establish a surface energy for P(MeTelMA), for the simple reason that no reproducible contact angle has been measured. What has been observed is a spread of contact angles, using water as test liquid, ranging from around 85° (which is larger than that for PMMA, *q.v.*) to around 68-70° (considerably smaller than PMMA).

There are a number of possible causes of this effect: the film may be too thin, allowing the contact angle to be affected by the glass substrate, the polymer may be contaminated resulting in surface heterogeneity, the surface may be rough or,

[†] $CF_3 (CF_2)_8COOH$

perhaps there is a secondary interaction between the polymer and the substrate. Their individual contributions will now be considered:

The thickness of the film is unlikely to affect the contact angle of the material. It is common practice to measure the contact angle of monolayers of surfactant molecules, and such a sample will clearly be thinner than the samples under study here.

Contamination of the polymer surface is a more significant possibility. Samples were prepared in a regular fume hood without any facilities to exclude dust or similar contaminants from the surface. Notwithstanding this fact, other samples have been successfully prepared in the same manner, and in the light of this, adventitious contamination can be ruled out. Contamination during the preparation of the polymer itself is also unlikely. The solvents used were of high purity and every care was taken to purify monomers before use. However, given the mixed nature of the monomer, it is impossible to ensure all contamination has been eliminated.

The effects of surface roughness have already been discussed extensively. There are no reasons why the P(MeTelMA) surface should be any rougher (or, indeed, smoother) than any other sample studied. Surface roughness has been investigated using a Tencor Instruments Alpha Step apparatus, which is used to study surface topography and thickness. The results from this clearly show that the roughness of the P(MeTelMA) films are no greater or less than the PMMA films used successfully in previous experiments.

The possibility of a secondary interaction between the substrate and the sample has been investigated for the PMMA:Glass system by Briggs *et al*[24]. They find a

different contact angle at the air:film interface to that at the film:glass interface, and interpret these findings in terms of a surface restructuring by orientation of the polar groups towards the film:glass interface. Their theory is backed up by evidence surface analysis by *X*-ray Photoelectron Spectroscopy and Secondary Ion Mass Spectrometry. Using both of these techniques, they finds an enrichment of the carboxylate functionality at the film:glass interface.

In the current work, it seems possible that the hydrofluoro- groups could find favourable interactions at the high energy glass surface, especially noting that before coating, the glass was scrupulously cleaned with permanganic acid thus increasing the number of oxidised functionalities at the surface. This effect could be the solid state analogue of the interactions postulated by Ellison *et al*, *q.v.*

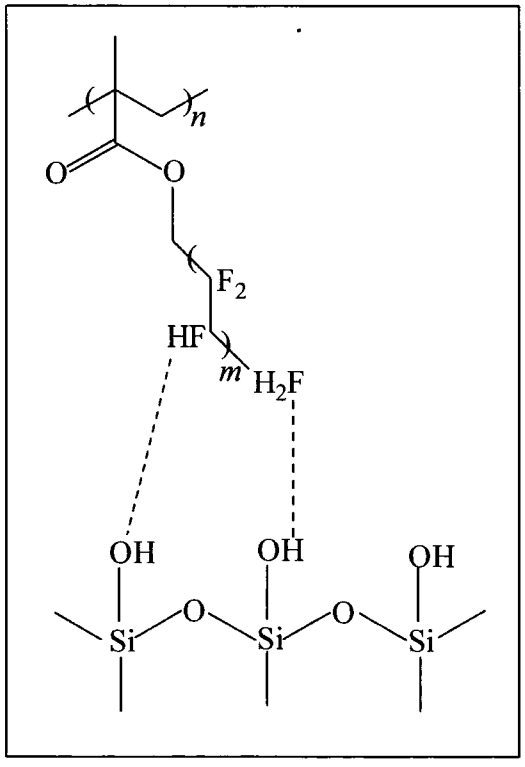

Figure 6.6 Interaction between Fluorinated Sidechain and Glass Substrate

Fowkes[27] also hints at a possible explanation. By adsorption of a test acid or base from solution onto a polymer surface and measuring its contact angle, the Langmuir adsorption isotherm can be determined and the number of surface functionalities calculated. Using this approach on PMMA, Fowkes found that most of the ester functionalites of the PMMA are buried in self-associated clusters. The highly polar fluoroalkyl group could have a similar effect, either associating in its own right, or causing greater association of the ester functionality by increasing its polarisation[32].

6.5.2. P(EthTelMA)

In contrast to the behaviour of the P(MeTelMA), a stable contact angle was obtained with a number of liquids for P(EthTelMA). A slightly different technique was used to determine the surface energy of the polymer, as that used earlier relied on just two measurements, *i.e.* the contact angles with water and methylene iodide. In this treatment, a number of homologous liquids are used and the contact angle of the liquid is determined as before. If suitable homologues have been chosen, the cosines of their contact angles will lie in a rectilinear region, which is then extrapolated to $\cos\theta = 1$. The dropline onto the *x*-axis from this point gives the *critical surface energy*[33-35]. This procedure is illustrated for P(EthTelMA) in fig 6.7.

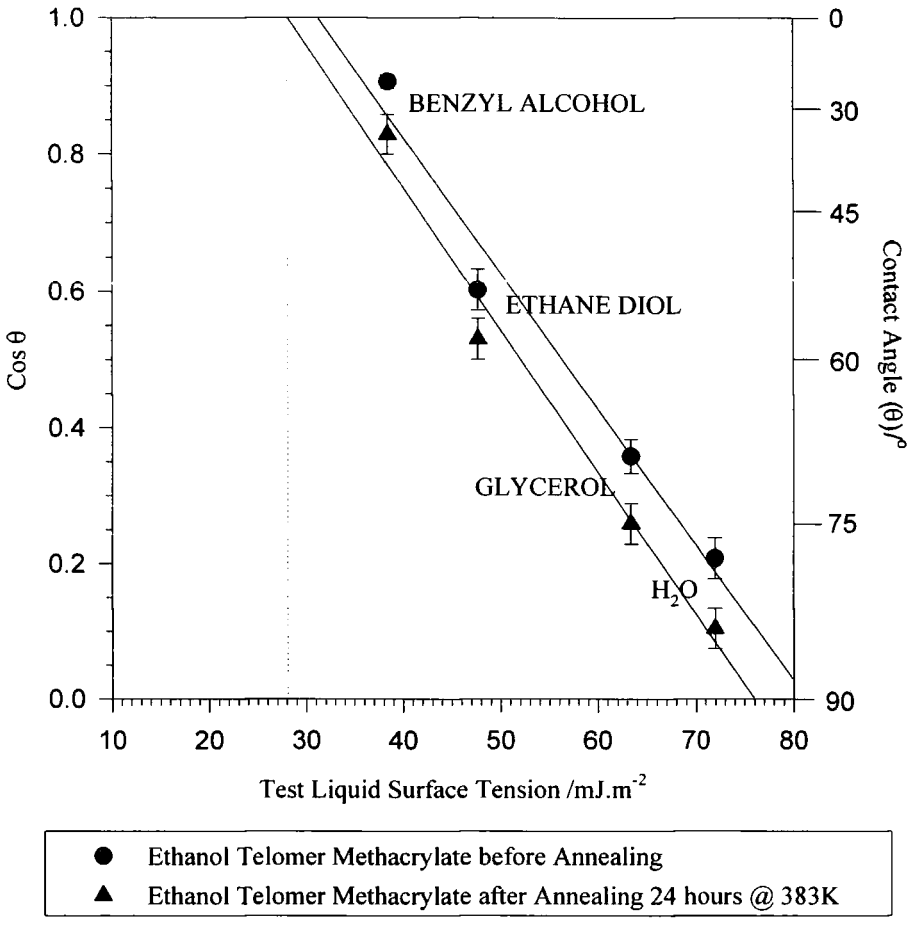

Figure 6.7 Determination of the Critical Surface Energy of P(EthTelMA)

It is clear from the graph that annealing the polymer has the effect of reducing the its surface energy; more low energy groups have migrated to the surface during the annealing procedure.

That P(MeTelMA) has a larger surface energy than PMMA, compared with the low energy surface of P(EthTelMA) is a most striking difference between these two seemingly very similar polymers. The explanation which fits in best with these observations is the one offered by Fowkes, *i.e.* self-association of functional groups in the polymer. It seems that this self-association is more favourable in the P(MeTelMA) than the P(EthTelMA). It seems that there are two possible contributory factors here:

1. The additional steric demands made by the extra methyl group of the ethanol telomer sidechain. This seems unlikely as there is a rather more bulky fluoroalkyl group, which makes the steric bulk of the methyl group relatively insignificant.

2. An electronic effect. Methyl groups are known to be electron-donating. Therefore, the carbonyl of the P(EthTelMA) is likely to be more electron rich than that in the methanol telomer-functionalised polymer. This being the case, agglomeration is likely to be less favoured in P(EthTelMA), and relatively enhanced in the P(MeTelMA) case.

The final part of this study involved the examination of blends of the polymers. Without having gained satisfactory data on the P(MeTelMA) system, the PMMA:P(MeTelMA) was excluded from this study leaving the PMMA:P(EthTelMA) blend.

6.5.3. Polymer Blends

Contact angle measurements have been performed on polymer blends containing the ethanol telomer methacrylate polymer with PMMA, in compositions 5:1, 2:1, 1:1, 1:2 and 1:5. Polymers were mixed in THF solution, before spin casting onto a prepared microscope slide[†]. Finally, samples were dried *in vacuo* to remove last traces of solvent.

The resulting films were studied in three states; un-annealed, annealed for 24 hours and annealed for 48 hours. The annealing temperature was 423K, *in vacuo*.

6.5.3.1. Results and Discussion

The following contact angles were observed on the un-annealed samples, using water[‡] as the test liquid. Composition is expressed PMMA:P(EtTelMA)

Blend Composition	**5:1**	**2:1**	**1:1**	**1:2**	**1:5**
Contact angles/°	83,79,83,84	83,84,83,**66**	84,83,83,84	81,77,77,78	82,82,77,76

Table 6.2 Contact Angles of Unannealed PMMA:P(EthTelMA) Blend

Noting the contact angles observed with water on the pure homopolymers, *viz.* 79°, 85° for PMMA, P(EtTelMA) respectively, one may conclude that the surface of the blends consists mainly of the fluorinated polymer, as expected. That there are patches of PMMA may be attributed to incomplete segregation, or other effects such as agglomeration of the fluorinated side chains.

[†] cut to size and cleaned in Permanganic acid, rinsed, dried.
[‡] Triply distilled, UHQ.

On annealing for 24 hours, the following results were obtained:

Blend Composition	**5:1**	**2:1**	**1:1**	**1:2**	**1:5**
Contact Angle /°	82,84,81,83	78,77,77,77	85,87,76,76	85,85,86,85	86,86,85,86

Table 6.3 Contact Angles PMMA:P(EthTelMA): Annealed 24Hours@423K

From these results, it can clearly be seen that annealing aids the progress of the fluorinated polymer to the surface, its presence being reflected in the larger contact angle. That the 2:1 blend in isolation displays a contact angle similar to that of PMMA is something of a mystery.

A possible explanation for the smaller contact angle in the 2:1 blend may also be manifest in the samples after 48 hours of annealing. The contact angles displayed by these samples show a large variation, and indicate the absence or depletion of a fluorinated surface.

Blend Composition	**5:1**	**2:1**	**1:1**	**1:2**	**1:5**
Contact Angle/°	81,81,73,71	73,75,80,80	77,76,76,75	80,77,81,81	81,80,77,77

Table 6.4 Contact Angle PMMA:P(EthTelMA): Annealed 48hours@423K

That the contact angle is **reduced** by lengthy annealing would suggest some kind of surface rearrangement is taking place, or more likely in this system, that some kind of decomposition is taking place. See Fig 6.8, below.

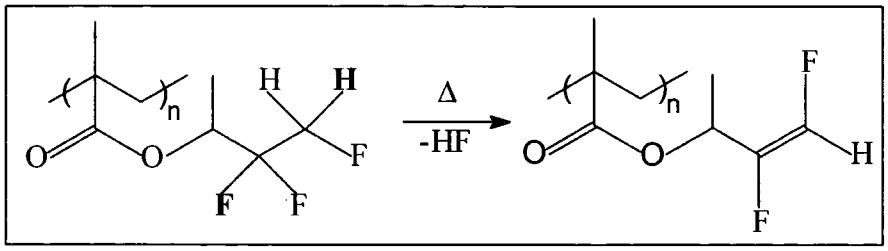

Figure 6.8 Proposed Decomposition Route

Evidence for this type of composition is seen in the TGA of the polymer blend; at 150°C, the 5:1 blend displays a 2% weight loss over 15 hours. This suggests that while both polymer backbones are stable, decomposition corresponding to the loss of HF from the side chains is taking place. That the side chain resulting from the dehydrofluorination is more polarisable means that the interaction between the surface and the test liquid become stronger, hence the reduction in the contact angle of the surface. Effects similar to this have already been discussed in the context of the monomer and polymer synthesis. See the respective chapters for more details.

A final point to take from the analysis of the above data is that the contact angle is relatively insensitive to the bulk concentration of the fluorinated polymer in the blend. This is to be expected in the light of the work of Jones (*q.v.*). Figure 6.9 illustrates this point graphically:

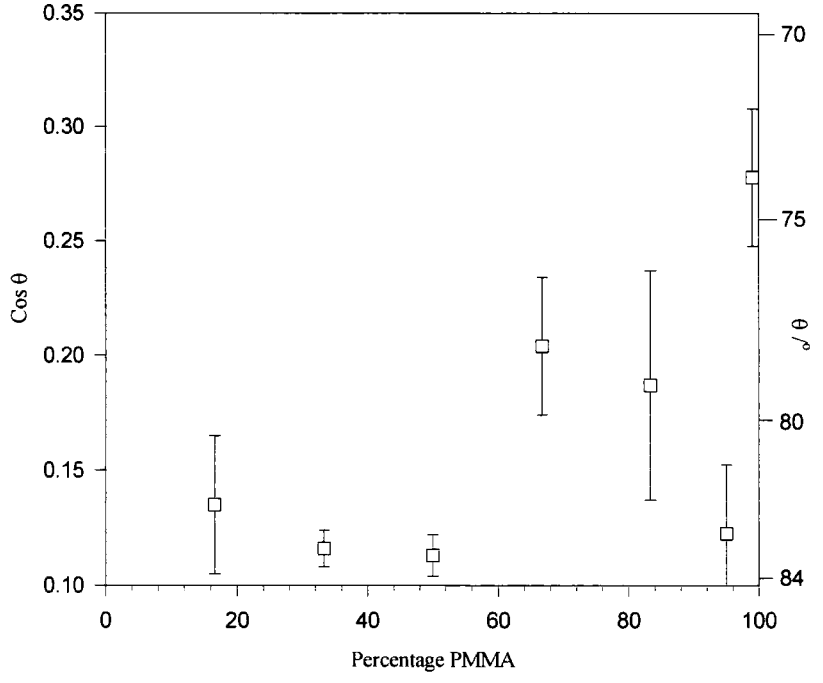

Figure 6.9 Variation of Contact angle with Composition PMMA:P(EthTelMA)

To summarise, the contact angles of PMMA and PTFEMA have been established and have been found to be in reasonable agreement with values reported in the literature. Furthermore, investigations have been made on the new fluoropolymers. This work has been unable to establish a reliable value for the surface energy/ work of adhesion of P(MeTelMA), but the surface energy of P(EthTelMA) has been established using the procedures of Fox and Zisman.

The surface energetics of blends of PMMA with P(EthTelMA) have also been investigated by contact angle methods, and these find that the surface of the blend is enriched in the fluorinated polymer, as would be expected from the Gibbs adsorption isotherm and, more latterly, the work of Jones *et al.*

6.6. References

1)Woodruff, D. P.; Delchar, T. A. *Modern Techniques of Surface Science*; 2 ed.; Cambridge University Press: Cambridge.

2)Wallis, J. M. *Methods of Surface Analysis: Techniques and Applications*; Cambridge University Press: Cambridge, 1989.

3)Czanderna, A. W.; Hercules, D. M. *Ion Spectroscopies for Surface Analysis*; Plenum Press: New York, 1991.

4)Forsyth, N. M.; Coxon, P. *Surface and Interface Analysis* **1994**, *21*, 430.

5)Gengenbach, T. R.; Chatelier, R. C.; Griesser, H. J. *Surface and Interface Analysis* **1996**, *24*, 611-619.

6)Sabbatini, L.; Zambonin, P. G. *Journal of Electron Spectroscopy and Related Phenomena* **1996**, *81*, 285-301.

7)Davies, M. C.; Lynn, R. A. P.; Hearn, J.; Paul, A. J.; Vickerman, J. C.; Watts, J. F. *Langmuir* **1995**, *11*, 4313-4322.

8)Shard, A. G.; Davies, M. C.; Tendler, S. J. B.; Nicholas, C. V.; Purbrick, M. D.; Watts, J. F. *Macromolecules* **1995**, *28*, 7855-7859.

9)Kikuma, J.; Konishi, T.; Sekine, T. *Journal of Electron Spectroscopy and Related Phenomena* **1994**, *69*, 141-147.

10)Cumpson, P. J. *Journal of Electron Spectroscopy and Related Phenomena* **1995**, *73*, 25-52.

11)Affrossman, S.; Bertrand, P.; Hartshorne, M.; Kiff, T.; Leonard, D.; Pethrick, R. A.; Richards, R. W. *Macromolecules* **1996**, *29*, 5432-5437.

12)Brant, P.; Karim, A.; Douglas, J. F.; Bates, F. S. *Macromolecules* **1996**, *29*, 5628-5634.

13)Briggs, D.; Fletcher, I. W.; Reichlmaier, S.; Agulosanchez, J. L.; Short, R. D. *Surface and Interface Analysis* **1996**, *24*, 419-421.

14)Spool, A. M.; Kasai, P. H. *Macromolecules* **1996**, *29*, 1691-1697.

15)Weng, L. T.; Bertrand, P.; Lauer, W.; Zimmer, R.; Busetti, S. *Surface and Interface Analysis* **1995**, *23*, 879-886.

16)Sauer, G.; Kilo, M.; Hund, M.; Wokaun, A.; Karg, S.; Meier, M.; Riess, W.; Schwoerer, M.; Suzuki, H.; Simmerer, J.; Meyer, H.; Haarer, D. *Fresenius Journal of Analytical Chemistry* **1995**, *353*, 642-646.

17)Tressaud, A. *Modification of the Surface Properties of Inorganic Materials by Plasma-Enhanced Fluorination*; Fluorine in Coatings II, Munich 1997 Paints Research Association, 1997.

18)Nicholls, J. *UltraThin PTFE and PVDF Coatings Deposited using Plasma Assisted Physical Vapour Deposition*; Fluorine in Coatings II, Munich 1997 Paints Research Association, 1997.

19)Barsamian, G. *Applied Chemistry of Fluorine: from Fluorination of Substances to Surface Fluorination of Materials*; Fluorine in Coatings II, Munich 1997; Paints Research Association, 1997.

20)Wu, S. *Polymer Interface & Adhesion*; Marcel Dekker: New York, 1982.

21)Jones, R. A. L.; Kramer, E. J. *Polymer* **1993**, *34*, 115-118.

22)Sakellariou, P. *Polymer* **1993**, *34*, 3408-3415.

23)Bikerman, J. J. *Physical Surfaces*; Academic Press: New York, 1970.

24)Briggs, D.; Chan, H.; Hearn, M. J.; McBriar, D. I.; Munro, H. S. *Langmuir* **1990**, *6*, 420-424.

25)Ellison, A. H.; Fox, H. W.; Zisman, W. A. *Journal of Physical Chemistry* **1953**, *57*, 622.

26)Fowkes, F. M. *Journal of Adhesion* **1972**, *4*, 155.

27)Fowkes, F. M.; Kaczinski, M. B.; Dwight, D. W. *Langmuir* **1991**, *7*, 2464-2470.

28)Park, I. J.; Lee, S.-B.; Choi, C. K. *Journal Of Applied Polymer Science* **1994**, *54*, 1449-1454.

29)Strange, M. ; MSc Thesis; University of Durham: Durham, 1978.

30)Zisman, W. A. in "Contact Angle and Wettability", Fowkes, F.M. Ed.; ACS: Washington, DC, 1964; Vol. 43.

31)Katano, Y.; Tomono, H.; Nakajima, T. *Macromolecules* **1994**, *27*, 2342-2344.

32)Jouannet, D.; Pham, T.-N.; Pimbert, S.; Levesque, G. *Polymer* **1997**, *38*, 5137-5147.

33)Fox, H. W.; Zisman, W. A. *Journal of Colloid Science* **1950**, *5*, 514.

34)Fox, H. W.; Zisman, W. A. *Journal of Colloid Science* **1952**, *7*, 109.

35)Fox, H. W.; Zisman, W. A. *Journal of Colloid Science* **1952**, *7*, 428.

Chapter Seven

Neutron Reflectometry

7.1. Introduction

As stated in the previous chapter, neutron reflectometry is a technique which enables the characterisation of the *near surface* and *interfacial* properties of a material[1-3]. In such an experiment, a neutron beam is played onto a surface with glancing incidence, and the *reflectivity*† of the sample is measured as a function of the scattering vector, Q, normal to the interface or surface. The reflectivity so obtained may be related via the *scattering length density*, and therefore the *neutron refractive index*, to the surface volume fraction and depth profile of the material under study.

7.2. Reflectivity Theory[4]

Reflectivity is defined as $I_r(Q)/I_0(Q)$, where $I_r(Q)$ is the reflected intensity, $I_0(Q)$ is the incident intensity and $Q = \left(\frac{4\pi}{\lambda}\right)\sin\theta$ (λ is the neutron wavelength and θ is the angle of incidence of the beam on the surface). Some of these terms are illustrated in fig 7.1:

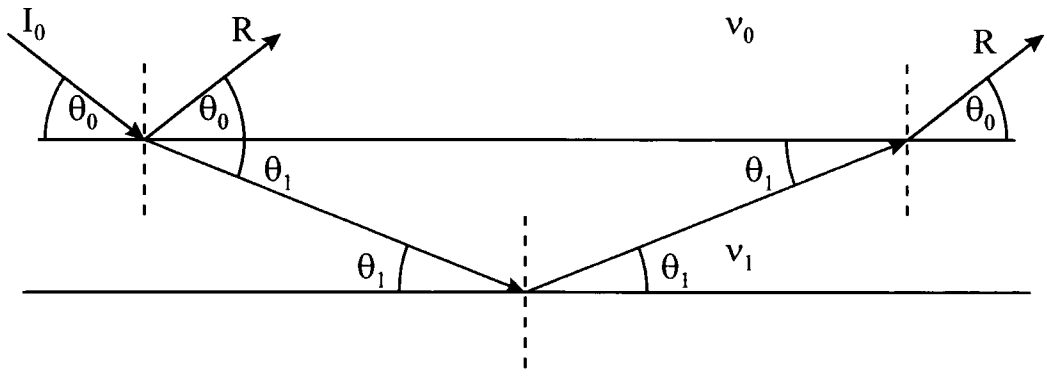

Figure 7.1 Schematic of Scattering Experiment

ν_0 and ν_1 represent the *neutron refractive index* in medium 0 and 1 respectively.

† *N.B.* Reflectivity is the property of a material which is measured by a reflectometry experiment.

The neutron refractive index is given by:

$$\nu = 1 - \lambda^2\left(\frac{\delta_b}{2\pi}\right) + i\lambda\left(\frac{\delta_a}{4\pi}\right) \qquad \textbf{[7.1]}$$

where λ is the wavelength of the incident radiation, δ_b is the bound scattering length density and δ_a is the neutron absorption cross section density. The scattering length density is defined as the average scattering length per unit volume, and is given by:

$$\delta = \frac{\rho N_A}{M}\sum b_i \qquad \textbf{[7.2]}$$

Here, ρ is the bulk density, N_A is Avogadro's number and M is the molar mass of the material. For polymers, M is equal to the molar mass of the repeat unit. A further simplification can be made when considering polymers, in that δ_a for their most common constituents (*i.e.* carbon, hydrogen and oxygen) are small, and the complex term in equation 1 may normally be neglected.

It is important to note that the scattering length density appears to the first power only in equation 1, making its sign significant. It was mentioned in chapter 5 that scattering length densities vary irregularly across the periodic table, and even between different isotopes of the same nuclei. As in small angle neutron scattering, deuterium labelling plays a significant part in the design and successful execution of a reflectometry experiment. The widely differing

scattering length densities of ^{1}H and ^{2}D can be utilised to highlight the position and nature of the interface under study.

The scattering length density is an additive property, *i.e.* $\delta_N(z) = \phi_D(z)\delta_D + (1-\phi_D(z))\delta_H$, where δ_D and δ_H are the scattering length densities of the deuterated and hydrogenous polymers, $\phi_D(z)$ is the volume fraction of the deuterated polymer as a function of depth. It is by this relation that the depth profile of a sample can be deduced.

7.2.1. Model Fitting

The major difficulty in using neutron reflectivity is that there are no exact methods by which the reflectivity can be directly related to the scattering length density profile, *i.e.* $R(Q)$ to $\delta_N(z)$. Therefore, data extraction normally involves the fitting of a model to the data.

Such a model can be obtained by noting that the reflectivity of neutrons from a surface is directly analogous to the reflectivity of electromagnetic radiation. For a wave passing from one medium of refractive index ν_0 to a medium of refractive index ν_1, Snell's law relates the angles of refraction to the refractive indices. For angles as defined in figure 7.1, Snell's law[‡] reads:

$$\nu_0 \cos\theta_0 = \nu_1 \cos\theta_1 \qquad [7.3]$$

[‡] For optics, Snell's law is normally expressed in terms of sines, not cosines. This is simply due to different conventions when defining the angles of incidence.

Typical values of the neutron refractive index are slightly less than 1 ($1-\nu$ is of the order of 10^{-6}). The critical angle, below which total external reflection occurs, is given by:

$$\cos\theta_c = \nu_1 \qquad \textbf{[7.4]}$$

Since θ is small, cosθ can be expanded to $1-\left(\theta_c^2/2\right)$. Therefore, substituting into equation 1, we obtain:

$$\theta_c = \lambda\left(\frac{\delta_N}{\pi}\right)^{1/2} \qquad \textbf{[7.5]}$$

Below the critical angle, the reflectivity is unity, *i.e.* $I_0(Q) = I_R(Q)$. Above the critical angle, for a single sharp interface between media 0 and 1, the reflectivity is given by:

$$R = \left|\frac{\nu_0 \sin\theta_0 - \nu_1 \sin\theta_1}{\nu_0 \sin\theta_0 + \nu_1 \sin\theta_1}\right|^2 \qquad \textbf{[7.6]}$$

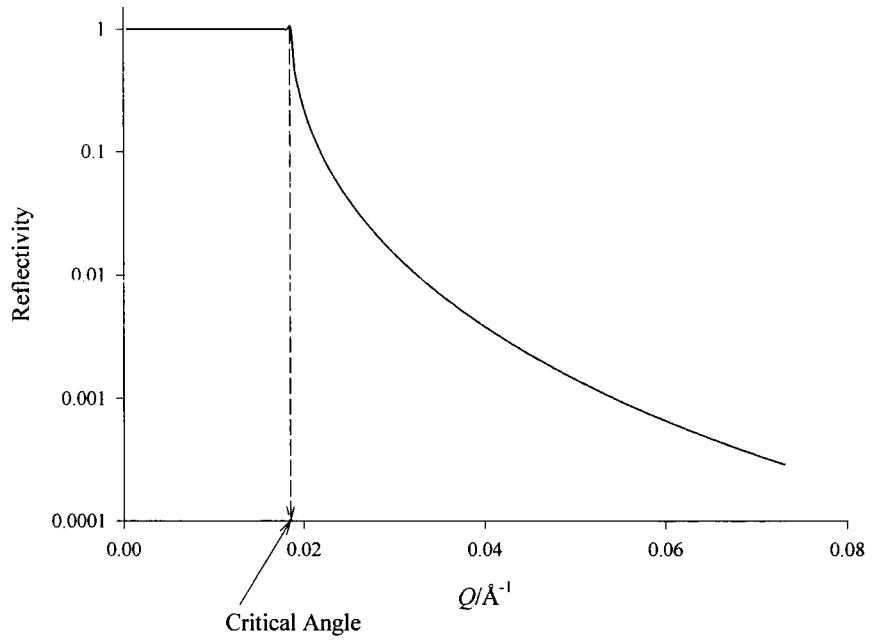

Figure 7.2 Fresnel Reflectivity computed from equation 6

In general, equation 6 can be extended for more than two layers. *E.g.*, for three layers:

$$R = \left| \frac{r_{01} + r_{12} \exp(2i\beta)}{1 + r_{01} r_{12} \exp(2i\beta)} \right|^2 \qquad [7.7]$$

where r_{ij} is defined as

$$\frac{\nu_i \sin\theta_i - \nu_j \sin\theta_j}{\nu_i \sin\theta_i + \nu_j \sin\theta_j} \qquad [7.8]$$

and

$$\beta = \left(\frac{2\pi}{\lambda}\right) \nu_1 d_1 \sin\theta_1 \qquad [7.9]$$

Examination of equation 7 reveals that β is the optical path of the neutron beam in a given medium, and the exponential term characterises the diminishing intensity of the multiply reflected waves.

This approach can be applied to calculate the reflectivity from a series of interfaces by assuming the sample to be made up of a number of discrete layers, each with their own scattering length density δ_i[5]. This is shown schematically in figure 7.3:

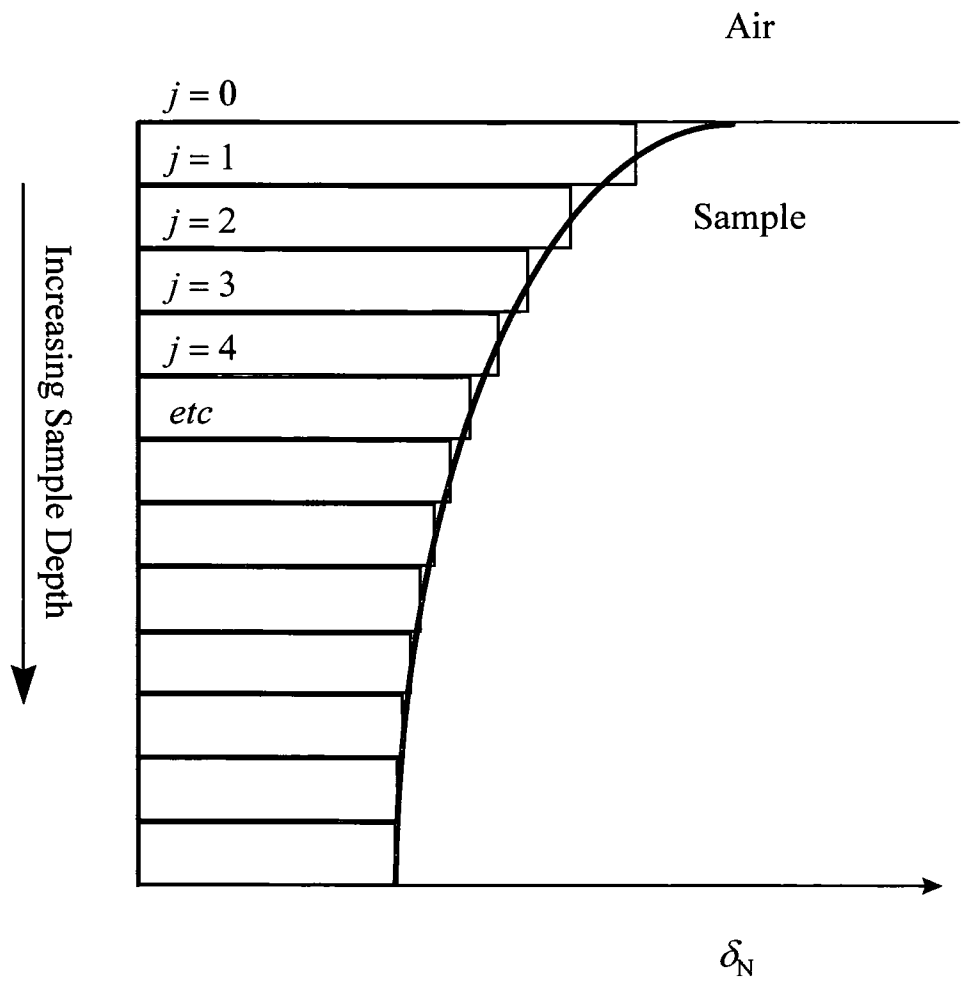

Figure 7.3 Schematic of Multilayer Approach to SLD Profile

The properties of a given layer are amenable to treatment by matrix algebra, the characteristics of the *j*th layer being given by:

$$M_j = \begin{bmatrix} \cos\beta_j & -\left(i/\kappa_j\right)\sin\beta_j \\ -i\kappa_j \sin\beta_j & \cos\beta_j \end{bmatrix} \qquad \textbf{[7.10]}$$

where $\kappa = \nu_j \sin\theta_j$.

The reflectivity is then given by the product of these matrices:

$$M = [M_1]\,[M_2]\,[M_3]\,\ldots\,[M_n] \qquad \textbf{[7.11]}$$

which results in a 2 x 2 matrix:

$$M = \begin{bmatrix} M_{11} & M_{12} \\ M_{21} & M_{22} \end{bmatrix} \qquad \textbf{[7.12]}$$

The reflectivity is then given by

$$R = \left| \frac{\left(M_{11} + M_{12}\kappa_s\right)\kappa_a - \left(M_{21} + M_{22}\right)\kappa_s}{\left(M_{11} + M_{12}\kappa_s\right)\kappa_a + \left(M_{21} + M_{22}\right)\kappa_s} \right|^2 \qquad \textbf{[7.13]}$$

where subscript *a* refers to the outer (air) medium and *s* to the final (substrate) medium.

This matrix technique is well suited to modelling the reflectivity from samples with complex layer structures, especially if a computer is used. However, it does not allow values of the scattering length profile $\delta(z)$ to be extracted from a set of

data. Therefore, for the correct conclusions to be made from neutron reflectivity experiments, it is necessary to have additional supporting evidence for any proposed structure. Such a technique (contact angle measurement) has already been described in chapter 6, and chapter 8 will go on to describe Rutherford backscattering spectrometry (RBS). By judicious use of the data so derived, it is usually possible to discount a large number of alternative structures proposed by the fitting processes to arrive at a credible and reliable conclusion.

While Fresnel's law describes the reflectivity from an ideal bulk surface, there are other aspects of thin film samples to be considered. The first is the so-called "*keissig fringes*," and the second point considers interfacial roughness.

7.2.2. Keissig Fringes

Reflectivity data from comparatively thin samples such as those used in this work have an added feature caused by the interference of neutrons reflected at the air-polymer interface with those reflected at the polymer-substrate interface. The measured reflectivity for an ideal sample is given by the Fresnel response modulated by the periodic interference pattern.

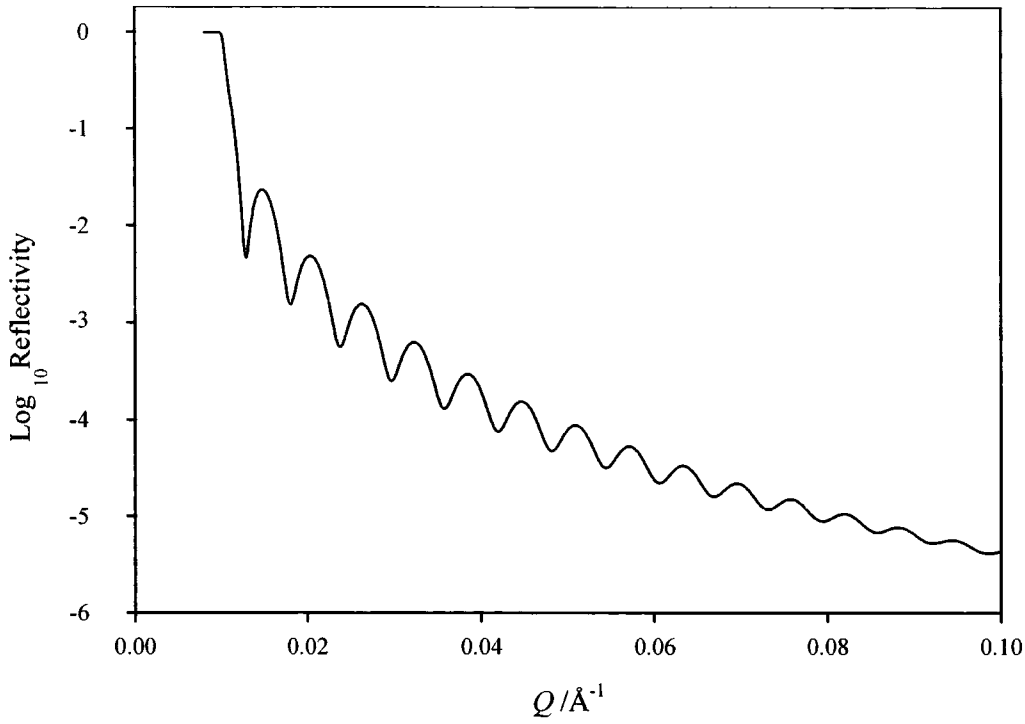

Figure 7.4 Calculated reflectivity profile showing Keissig Fringes for generic polymer of scattering length density 1.5×10^{-6} and thickness 1000Å

The periodicity of these fringes may be analysed to obtain the thickness of the film.

7.2.3. Surface and Interfacial Imperfections

Finally, considerations due to surface and interfacial imperfections should be addressed. Beam divergence and long range surface undulations contribute to the reflectivity in a similar way. However, if the surface displays localised roughness, this will modify the specular reflectivity in a manner indistinguishable from that produced by a diffuse interface. This is expressed as:

$$I(\lambda) = I_0(\lambda)\exp\left(-q_0 q_1 \langle\sigma\rangle^2\right) \qquad \textbf{[7.14]}$$

where $I(\lambda)$ and $I_0(\lambda)$ are the reflected intensity with and without surface roughness, $\langle\sigma\rangle$ is the root mean square roughness, $q_0 = 2k \sin\theta_0$ and $q_1 = 2k \sin\theta_1$.

7.3.Experimental

The experiments described in this work were performed on the CRISP reflectometer at the ISIS facility, Rutherford-Appleton laboratory, near Oxford. A diagram of the reflectometer is shown in figure 7.5.

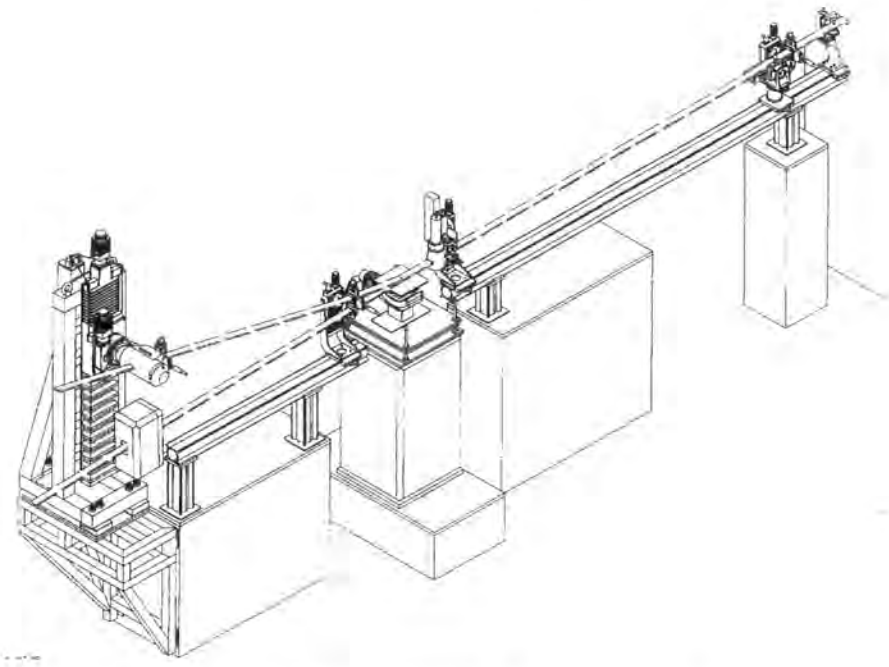

Figure 7.5 The CRISP Reflectometer, RAL

7.3.1. Neutron Reflectometry

Samples [*q.v.*] are placed on a vibrationally-isolated table before they are aligned with the aid of a laser. The alignment procedure ensures the sample to be level, then the geometry and collimation of the beam is optimised using a number of slits placed in the beam path. The instrument views the 20K hydrogen moderator, giving an effective wavelength of 0.5-6.5Å at an operating frequency of 50Hz. As ISIS is a pulsed neutron source [*q.v.*], it is necessary to define properly the pulsewidth, and this is achieved with a number of choppers further up beam. Further frame overlap suppression is provided by the nickel-coated silicon wafer

frame overlap mirrors, which reflect neutrons of wavelength greater than 13Å out of the main beam. See figure 7.6.

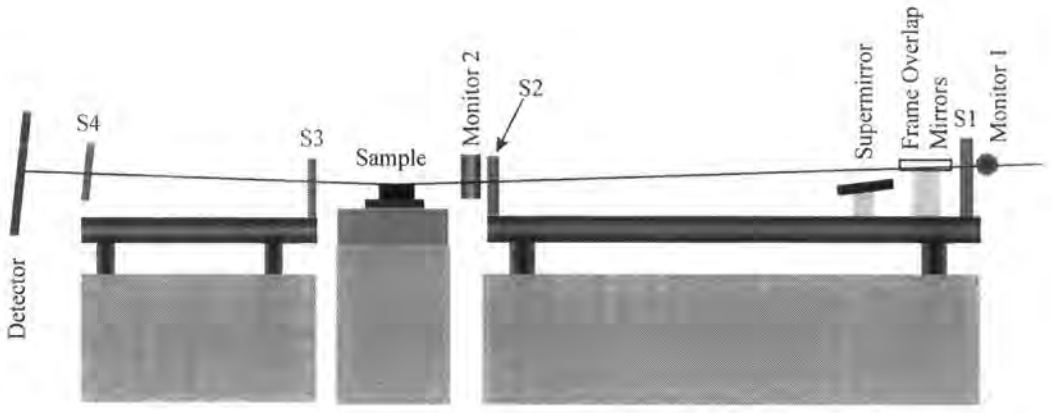

Figure 7.6 CRISP Geometry

7.3.2. Sample Preparation

To minimise the effects of roughness on the recorded reflectivity profile, solid samples should be optically flat. In practice, this is achieved by using a polished flat of crystalline silicon (a "block"). These blocks are ~50mm diameter x. 5mm thick.

The aim of this experiment was to establish the equilibrium structure of the surface of solution blended polymers. This required PMMA and MW96/40 [*q.v.*] to be blended in solution in MEK at 5,10,15, and 20% MW96/40 w/w, and spun cast onto the silicon blocks such as to achieve a film thickness of ~1000Å.

Film thicknesses were measured using a Tencor Instruments Alpha Step apparatus. This apparatus drags a sharp needle across the sample, and the deviation of this needle is measured to give the sample topography. By scratching the polymer film through to the silicon substrate, the maximum deviation corresponds to the sample thickness.

7.3.2.1. Annealing Procedures.

For the first experiment, it was necessary to ensure the equilibrium structure of the blend had been attained. This was achieved by annealing the samples *in vacuo* at 413K over a period of 4 days.

7.4. Results & Discussion

A reflectivity profile for a typical low concentration sample is shown in figure 7.7. Reflectivity before and after annealing is shown. Similarly, figure 7.8 shows the reflectivity from a sample with a high concentration of fluoropolymer.

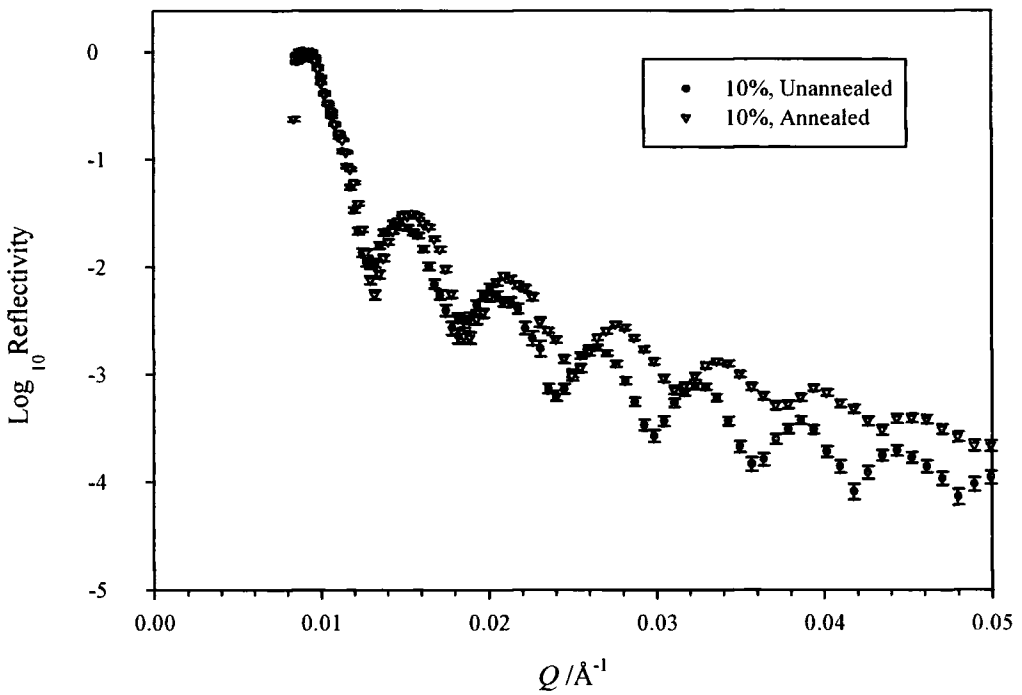

Figure 7.7 Reflectivity from 10% 96/40 Blend

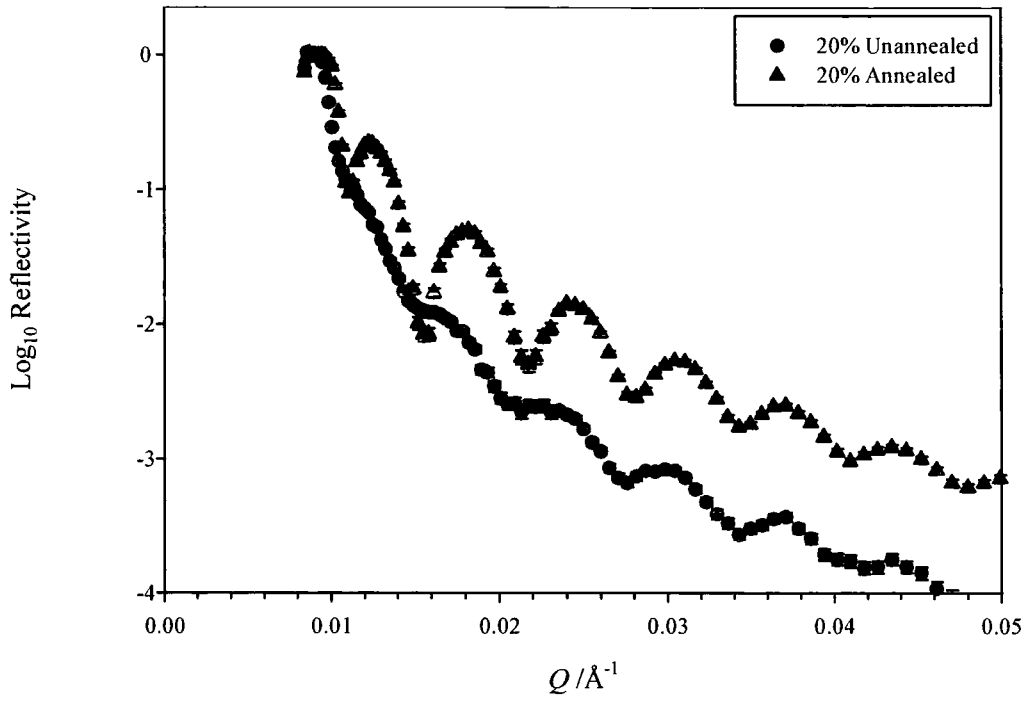

Figure 7.8 Reflectivity from 20% 96/40 Blend

There are a number of points to raise in the comparison of figures 7.7 and 7.8. The most notable is the increase in reflectivity with an increase in fluoropolymer content. This observation is an obvious one; the more polymer there is with a higher refractive index, the greater the reflectivity will be. Secondly, the increase in reflectivity with annealing should be noted. This suggests an increase in the concentration of the higher refractive index polymer at the surface, *i.e.* surface segregation of the fluoropolymer is apparently taking place[6]. Lastly, one sees the increase in amplitude of the keissig fringes with annealing in the higher concentration samples. This is indicative of the formation of a sharp interface within the sample, which may be due to the migration of the fluoropolymer to the air-polymer interface.

That surface segregation is inferred by this cursory glance at the data seems to be in conflict with the findings of the previous chapter, where a small, unstable

contact angle was reported. Clearly, it is necessary to look at these data more carefully, and consider the results of the fitting of the data to a number of models.

7.4.1. Fitting Procedures

During the course of this work, a number of fitting programs have been used in order to gain the most reliable physical picture of the characteristics of these materials.

First, a model independent fitting routine called MODELI was used. This program attempts to generate a scattering length density profile by adjusting the heights of a number of cubic spline functions. The profile so produced is then used to fit the reflectivity data.

PCMULF fits by splitting the scattering length profile into a number of layers, then changing the thickness and the scattering length of a given layer to optimise the fit. A gaussian roughness can be included in each layer to account for either surface roughness or a diffuse interface.

Finally, a maximum entropy routine called VOLFMEM was used. Such routines are favoured in cases where one has little *a priori* knowledge of the profile under investigation[7]

The results from the VOLFMEM program will be considered first. This program has been successfully applied to fit a large number of data, and in this respect has been used as a kind of standard.

7.4.1. As-Prepared Films

Figure 7.9 shows a typical fit to data from the VOLFMEM routine.

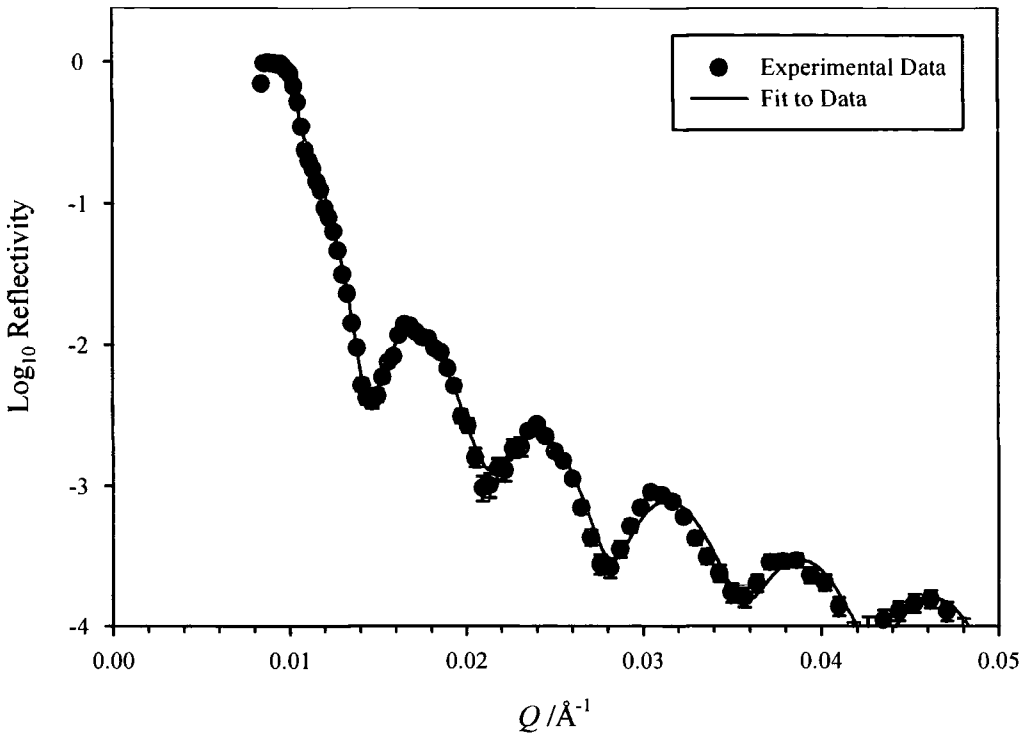

Figure 7.9 15% 96/40, Unannealed

From fits to the data, VOLFMEM calculates directly the volume fraction profile of the sample, and the results of this procedure are collated in figure 7.10.

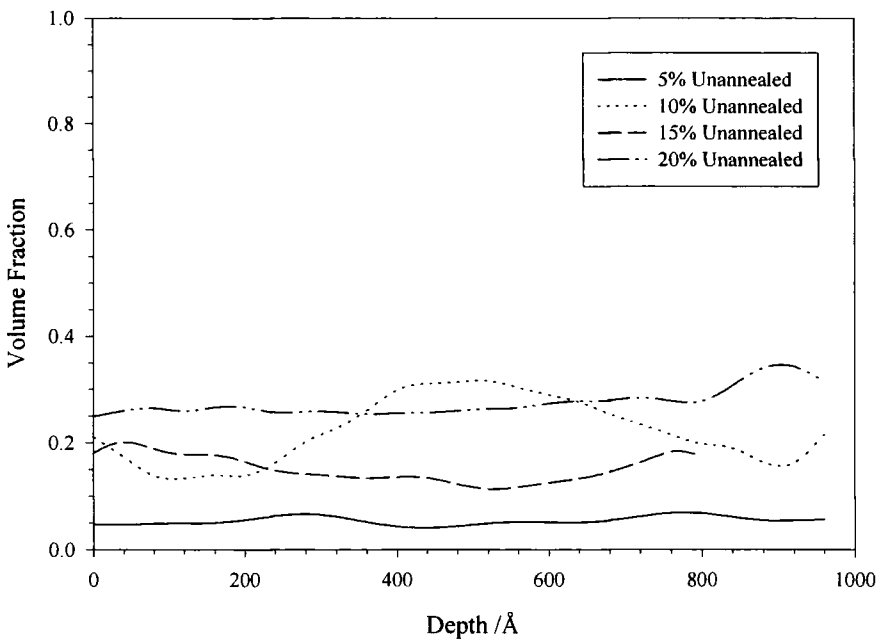

Figure 7.10 Volume Fraction Profiles from VOLFMEM 5, 10, 15 & 20% 96/40 Unannealed

We see from the above that, in the most part, the volume fraction profiles of the unannealed films are well described by a single, uniform layer with a volume fraction which is approximately consistent with the known composition of the blend.

The volume fraction profiles of the 10% blend should be considered separately, as this does not seem to fit in with this uniform layer picture.

However, before further judgement is passed on these apparent anomalies, one should consider the results of other fitting routines so as to ensure that the features of the above profiles are real and not artefacts of the VOLFMEM procedure.

The *scattering length density profiles* from the PCMULF program are shown in figure 7.11:

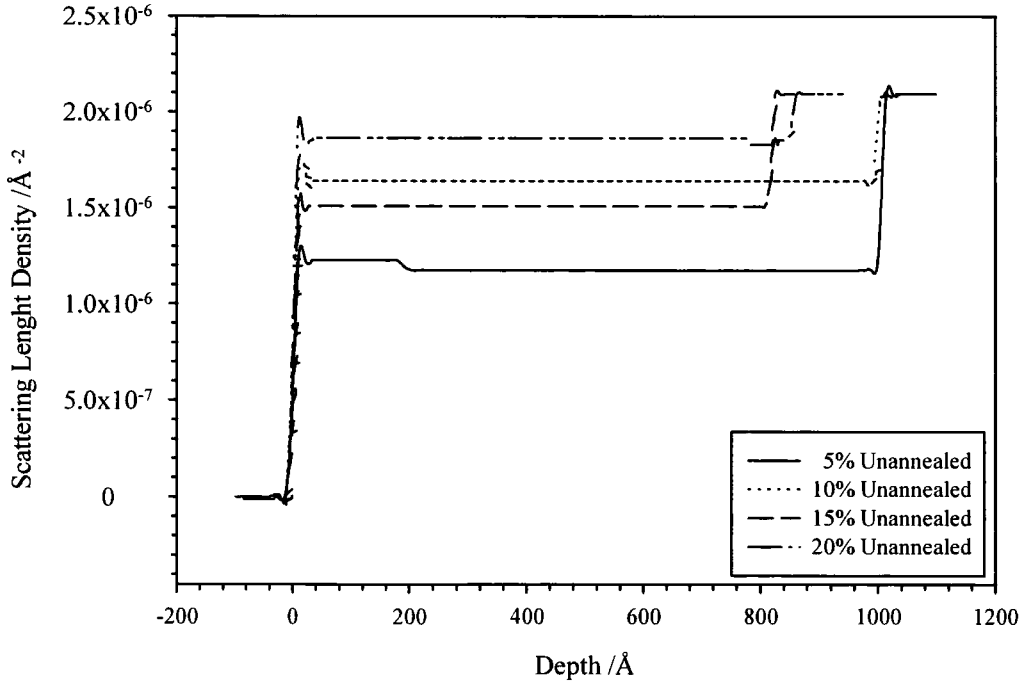

Figure 7.11 Scattering Length Density Profiles from PCMULF

5, 10, 15 & 20% 96/40

Knowing the scattering length density of the constituent polymers, one can extract the volume fraction profile from the corresponding scattering length density profile:

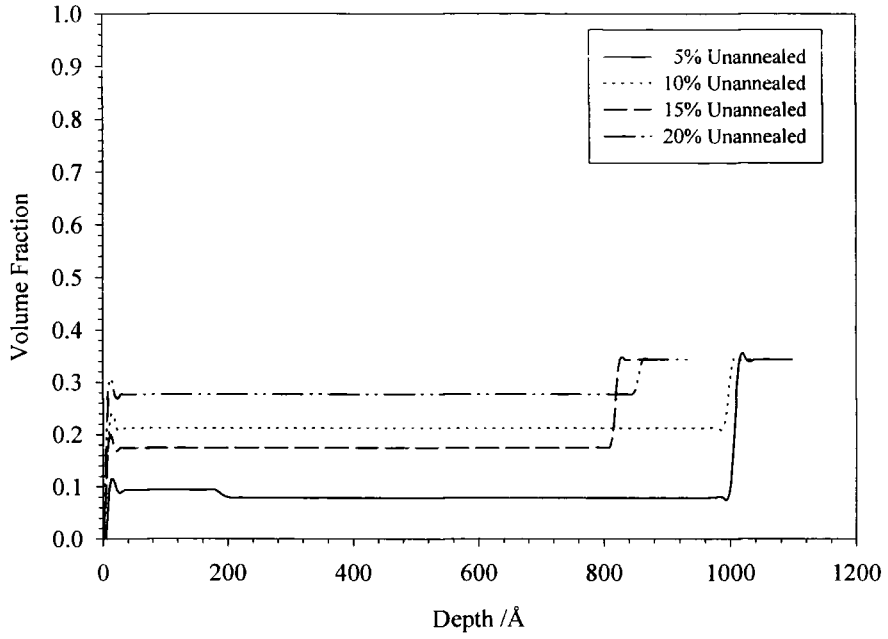

Figure 7.12 Volume Fraction Profiles from PCMULF

5, 10, 15 & 20% 96/40

The first thing to note from figure 7.12 is that the volume fraction profiles do not coincide with the value expected from the known composition of the blend. This feature is caused by the change in the density of the constituent polymers which may occur on blending. Equation 2 shows clearly that the scattering length density is directly proportional to the bulk density of the material.

Secondly, the volume fraction profile of the 10% fluoropolymer sample is uniform like the rest. This is in contrast to the profiles generated from the VOLFMEM routine, where segregation to both the surface and the substrate was suggested. This again may be an artefact of the PCMULF routine, and a third fitting technique should be looked at before any conclusions may be drawn.

MODELI is such a routine. As described above, this program assumes no *a priori* knowledge of the scattering length density profile of a given sample, and in this respect, may be used as an independent judge of the "correctness" of the profiles shown above. Figure 7.13 shows the fit to a set of data and the volume fraction profile which results:

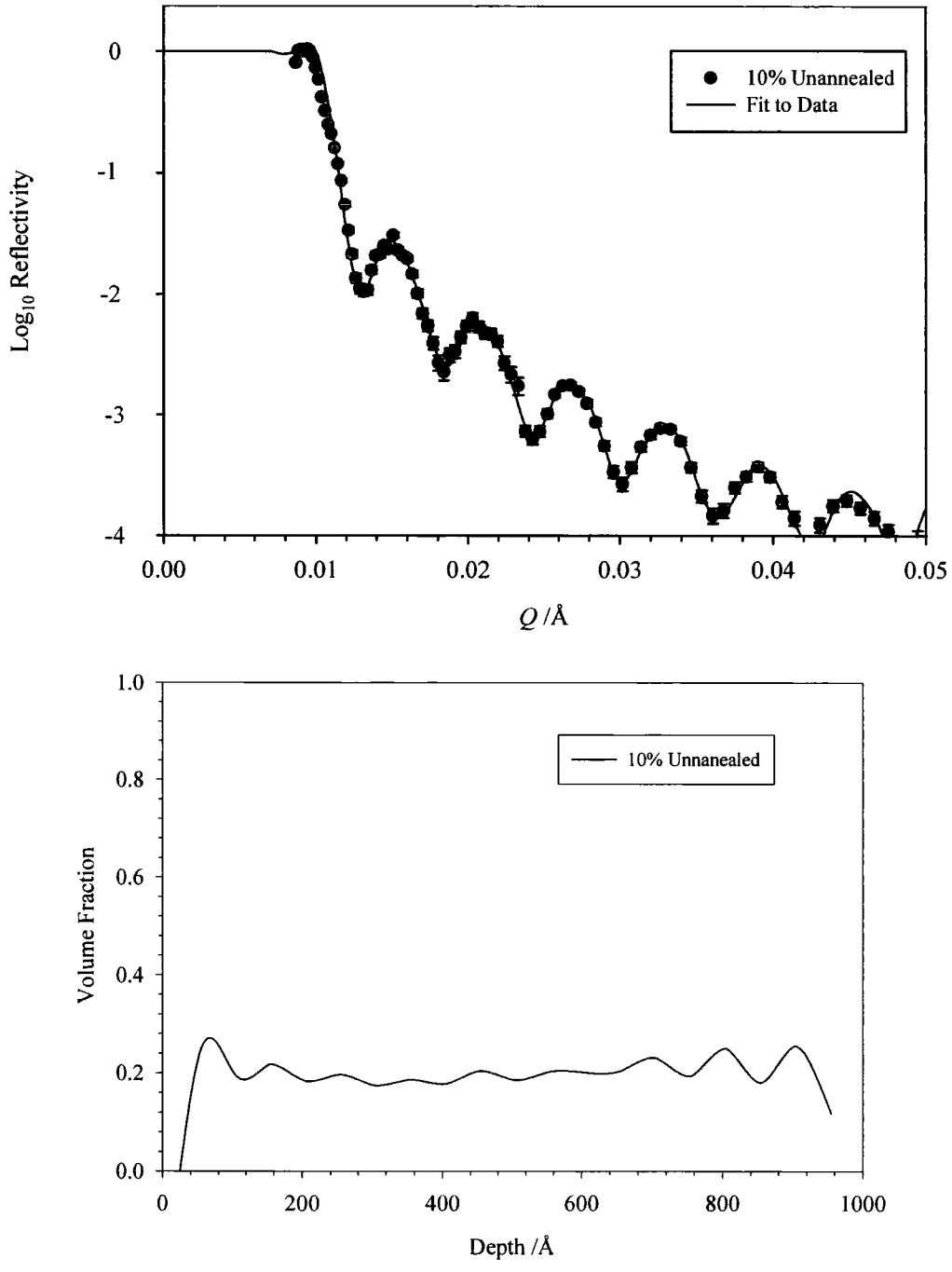

Figure 7.13 MODELI Fit & Volume Fraction Profile: 10% 96/40

From figure 7.13, we see that the profile obtained for the 10% blend is essentially uniform, perhaps with signs of segregation to the surface and substrate. However, there is no indication of the gross fluctuations in the volume fraction profile which are observed in the VOLFMEM results. Therefore, it seems likely that the true picture for this sample, and the other unannealed blends, is best represented by a film of uniform scattering length density and therefore uniform volume fraction throughout.

7.5.2. Annealed Films.

Turning to the annealed systems, an altogether more complex picture is found. Fits and volume fraction profiles from each of the techniques are shown in figures 7.14 to 7.16:

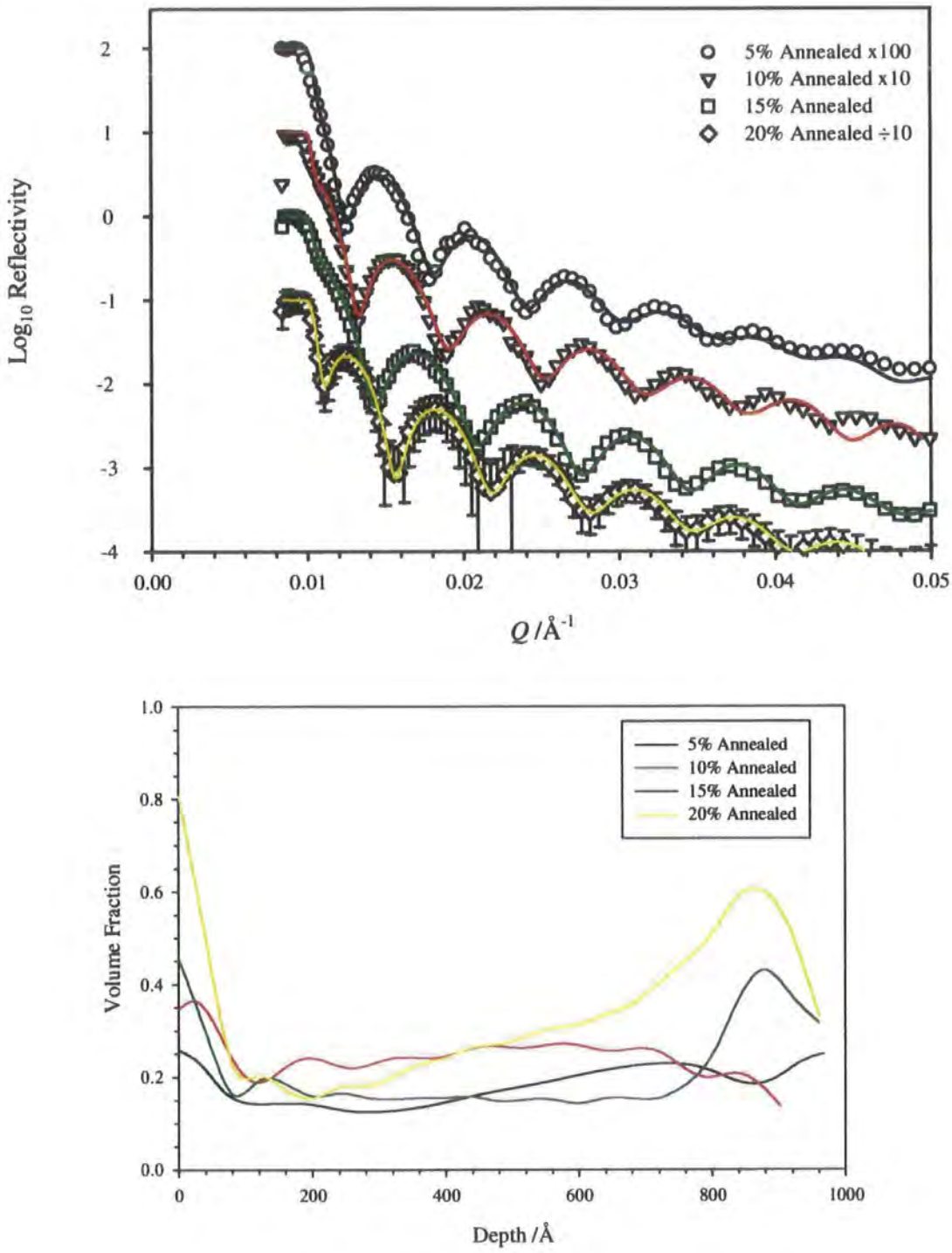

Figure 7.14. Fits and Volume Fraction Profiles: Volfmem

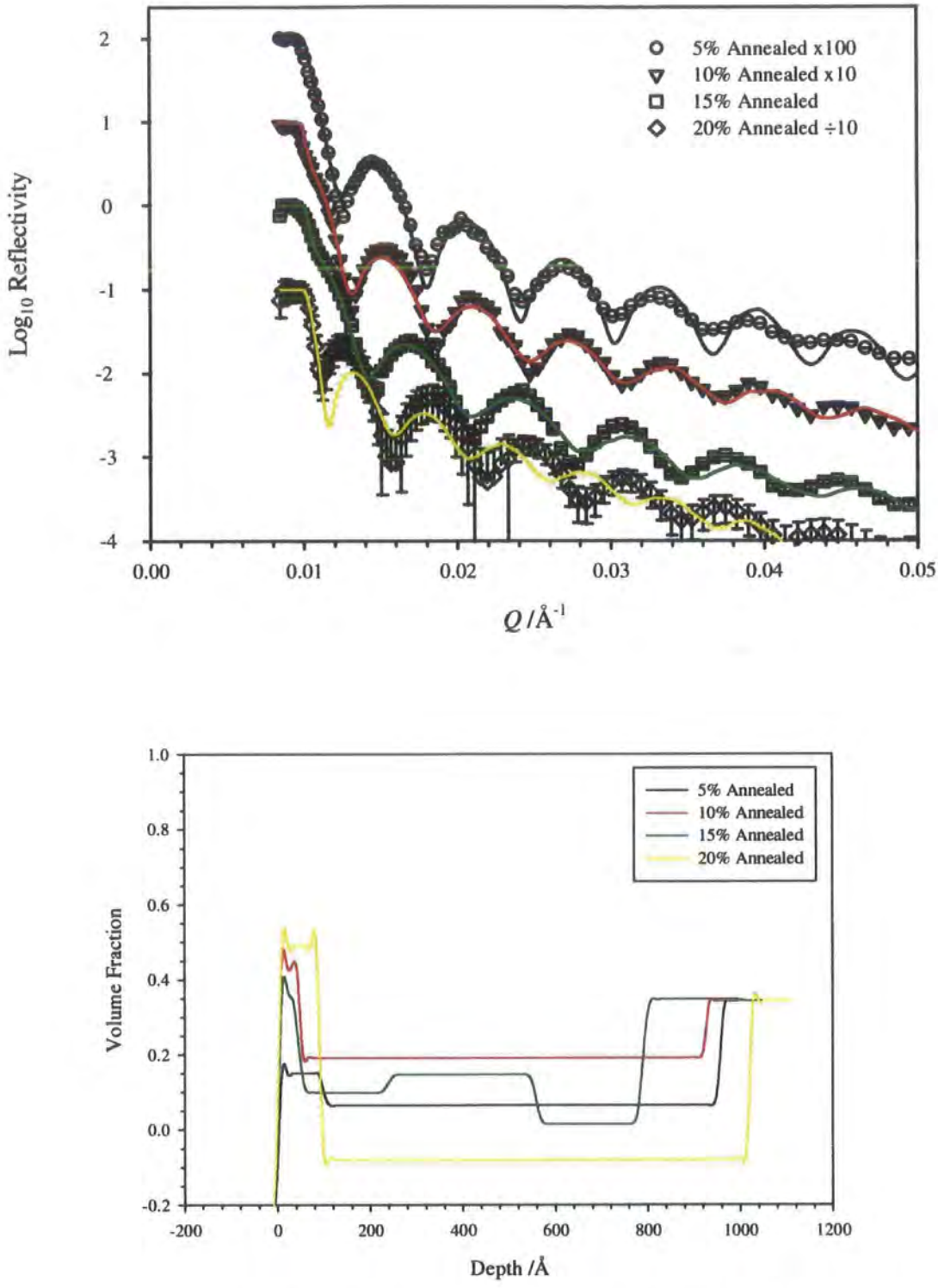

Figure 7.15. Fits and Volume Fraction Profiles: PCMULF

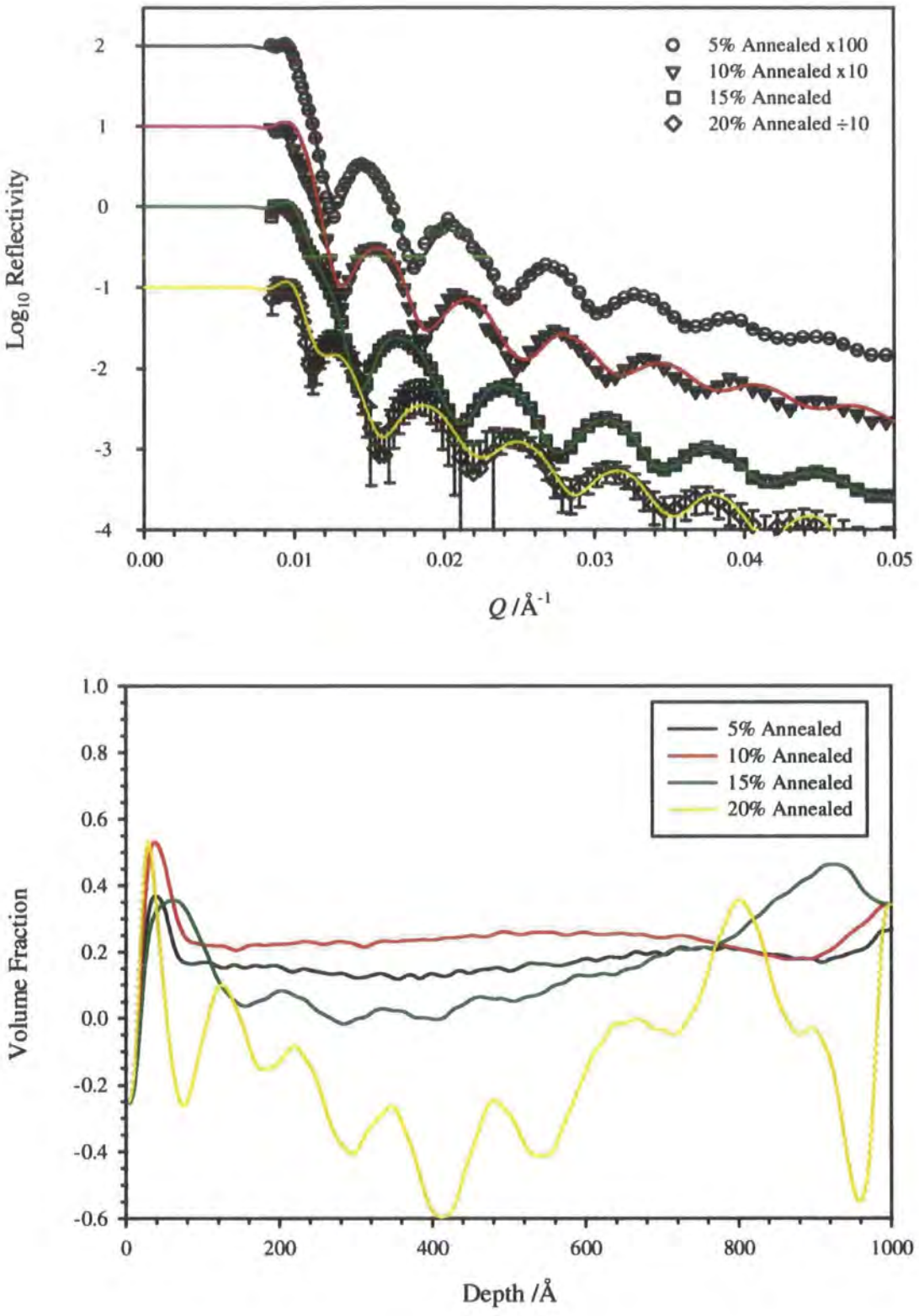

Figure 7.16. Fits and Volume Fraction Profiles: MODELI

We see from figure 7.14 that the VOLFMEM program has been reasonably successful, with only the fit to the 10% sample showing any large discrepancy from the experimental data.

From 7.15, we see that PCMULF has been rather less successful in fitting the data, with large discrepancies between the data and the fit at high concentrations. The fits to the data at lower concentrations are better as a whole, although the effects of instrument resolution are shown in the increased damping of the keissig fringes in the 5% sample.

Finally from 7.16, we see that MODELI has made a reasonable attempt to fit the data. The volume fraction profiles so produced show the surface segregation behaviour which was observed in the results from the VOLFMEM routine, with the most notable exception of the data from the 20% sample. Clearly, the routine has found a possible fit to the data, but the nature of reflectivity profiles means that the solution found by the fitting routine is not unique, and therefore not necessarily the right one.

With this conspicuous exception, the fits to the data have resulted in reasonable volume fraction profiles. Segregation of the higher refractive index polymer (the fluoropolymer) is observed in all cases, and at higher concentrations, one also sees enrichment of the fluoropolymer at the polymer-substrate interface.

All the profiles show higher than expected volume fractions, which was also seen in the unannealed samples. This is connected with the density of the film: a decrease in film density will make the scattering length density smaller, which in turn will require a higher polymer concentration to generate the observed reflectivity profile.

7.4.4. Surface Segregation

That surface segregation is implied from these results is in apparent contradiction with the results from contact angle measurements (see chapter 6). However, before any conclusions can be drawn from this particular section, it is necessary to theorise over the causes of the apparent reduction in scattering length density which is reflected(!) in the volume fraction profiles.

The surface properties of a material are governed by the balance between the bulk properties and the inherent tendency for a component of polymer mixtures to be adsorbed preferentially at the air-film interface[8]. We have already seen in chapter 5 that the materials studied here have an endothermic (unfavourable) enthalpy of mixing, which one would expect to favour the separation of the sample into two phases. However, the temperature dependence of the interaction parameter also points at a more complex behaviour than a lower critical solution temperature-driven phase separation[9], and the aggregation of the fluorinated polymers was mooted as a possible explanation[10]. Such aggregation behaviour is in response to thermodynamic forces which favour self-association of the fluoropolymer, and discourage inter-association between the fluoropolymer and the matrix. At a first glance, one could assume that this self-association behaviour would bring about an increase in the local density of the polymer.

However, one must also consider the packing of these aggregates and the differing free volume effects which result from repulsions between the fluoropolymer and the PMMA matrix. Considering the evidence from the previous chapter on contact angle analysis, we can postulate that the surface of

these materials displays long rang compositional inhomogeneities, a feature which is reflected in the wide range of contact angles recorded [*q.v.*]

To conclude, neutron reflectivity has been used to study the near surface depth profile of blends of PMMA and the fluorinated copolymer 96/40. It is suggested that there is a migration of fluorinated polymer to the air-polymer interface which is further enhanced by annealing the blends above their glass transition temperature. At higher concentrations, adsorption of the fluoropolymer to the polymer-substrate interface is also observed.

However, one should bear in mind the reservations which must arise due to the poor quality of some of the fits to the data, and also note the inherent difficulties, such as loss of phase information, which arise from the neutron reflectivity experiment.

Aggregation of the fluorinated polymer is used to explain the unrealistic (impossible) volume fraction profiles which have been generated by the data fitting routines in some instances, and may also help to explain the lack of success of the fitting routines in the first place.

7.5. References

1)Penfold, J.; Thomas, R. K. *J. Phys.: Condens. Matter* **1989**, *2*, 1369-1412.

2)Bucknall, D. *Materials World* **1995**, *3*, 593-595.

3)Richards, R. W. *Small angle neutron scattering and neutron reflectometry in polymer characterisation* in "*Polymer Characterisation*"; Hunt, B.J., James, M.I. Eds.; Blackie: Glasgow, 1993, pp 222-260.

4)Higgins, J. S.; Benoit, H. *Polymers and Neutron Scattering*; Clarendon Press: Oxford, 1994.

5)Lekner, J. *Theory of reflection of electromagnetic and particle waves*; Martinus Nijhoff: Dordrecht, 1987.

6)Geoghegan, M.; Jones, R. A. L.; Sivia, D. S.; Penfold, J.; Clough, A. S. *Physical Review E* **1996**, *53*, 825-837.

7)Sivia, D. S.; Hamilton, W. A.; Smith, G. S. *Institute of Physics Conference Series* **1990**, 223-231.

8)Jones, R. A. L.; Kramer, E. J. *Polymer* **1993**, *34*, 115-118.

9)Jong, L.; Pearce, E. M.; Kwei, T. K.; Hamilton, W. A.; Smith, G. S.; Kwei, G. H. *Macromolecules* **1992**, *25*, 2619-2623.

10)Jouannet, D.; Pham, T.-N.; Pimbert, S.; Levesque, G. *Polymer* **1997**, *38*, 5137-5147.

Chapter Eight

Rutherford Backscattering Spectrometry

8.1. Introduction

The previous chapter discussed the technique of neutron reflectivity and, in that discussion, it was stated that it was desirable to obtain an independent analysis of the surface depth profile such that the results from model fitting could be interpreted correctly. This work has attempted to gather such information using Rutherford backscattering spectrometry (RBS).

This technique is based on the works of Geiger, Marsden and Rutherford in the early years of this century, in which α-particles were directed towards a thin gold foil. When backscattering was observed, the nuclear model of the atom was confirmed, and Rutherford, expressing his amazement at such an observation, likened backscattering to "*firing a 15-inch shell at a piece of tissue paper and it coming back and hitting you*".

Backscattering spectrometry is, in essence, just as simple. When a bulk sample is bombarded with a beam of high energy particles, the vast majority of them become implanted in the material and do not escape. Similarly in a thin sample, most particles pass straight through without undergoing any interaction. However, a small fraction of incident particles undergo a direct "collision" with a nucleus in the upper few micrometers of the sample. This is because the diameter of atomic nuclei is of the order of $1x10^{-15}$m while the internuclear distance is around $2x10^{-10}$m. These "collisions" do not involve the actual coming together of the nuclei; the process is more accurately modelled using the classical physics principles of electrostatics.

See figure 8.1.:

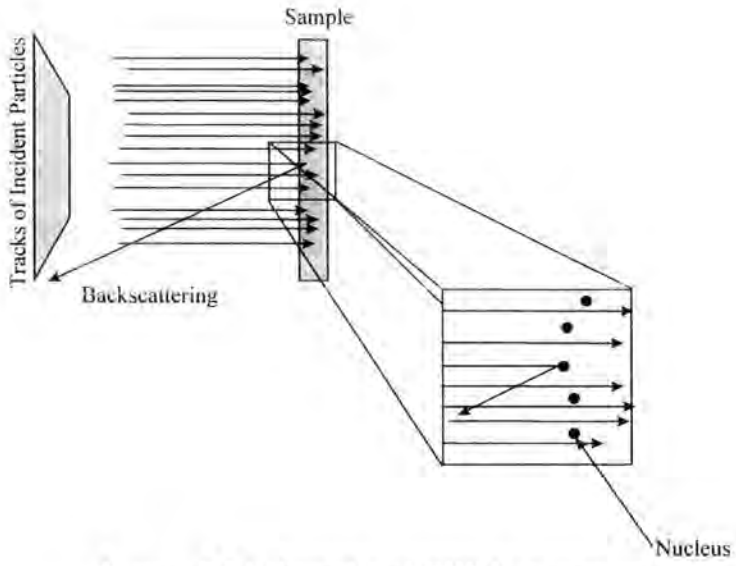

Figure 8.1 Schematic of RBS Experiment

8.2. Physical Basis of Backscattering Spectrometry

The energy measured for a particle backscattered at a given angle depends on two processes. Particles lose energy as they pass through the sample both before and after a collision, and will also lose energy during the scattering event itself. The former energy loss mechanism is characterised by the *stopping cross section* of the material. Losses from the latter process are due to *kinematic* considerations. These energy loss processes will now be discussed individually.

8.2.1. The Stopping Cross Section, ε

The stopping cross section of a material is related to the energy loss per unit length, dE/dx, the "stopping power" of the material. As particles of the analysing beam travel through a dense medium, they interact with the electron cloud of the atoms which lie in its path. They also undergo numerous small angle collisions with nuclei lying on its route. These are termed *electronic* and *nuclear stopping*, respectively, and their contributions are additive. Put simply, the electronic

stopping process is likened to friction between the projectile and the electron cloud of the sample. The nuclear contribution is only significant at very small particle velocities, at which energy can be transferred from the projectile to the nucleus of a target atom by electrostatic interaction between the screened charges of the two particles. Such interactions can be viewed as elastic collisions between two free particles, with the exception of the last few collisions when chemical binding energies (~10eV) must be considered. The respective contributions of electronic and nuclear stopping are considered to be independent of one another.

dE/dx is given by the Bethe-Bloch formula:

$$\frac{dE}{dx} = Nz_2\left(z_1e^2\right)^2 f\left(\frac{e}{m_1}\right) \qquad \textbf{[8.1]}$$

where N is the number of atoms per unit volume, $z_{1,2}$ is the charge on the analysing particle and target atom, respectively, and e is the electronic charge. $f(e/m)$ is a function which depends only on the target, not the type of projectile. dE/dx is an energy loss per unit length.

We also define the *stopping cross section*, ε:

$$\varepsilon = \left(\frac{1}{N}\right)\frac{dE}{dx} \qquad \textbf{[8.2]}$$

which has the dimensions of energy loss per atom per unit length.

To illustrate the difference between ε and dE/dx, consider two targets made up of the same number of atoms per unit area. Assume that, in one case, the atoms are closely packed and form a high volume density. In the other target, the atoms are loosely arranged and form a sponge-like structure of low volume density. As energy loss is assumed to be an atomic process independent of their packing, the energy ΔE transferred to the target must be the same in both cases. A larger value of dE/dx will be assigned to the denser target because the energy loss has occurred over a shorter length that in the less dense sample. However, $(1/N)dE/dx$, *i.e.* ε, is the same for both samples.

Theoretical predictions of the factor $f(e/m_1)$ are both complicated and inaccurate. In arriving at a solution to the theoretical problem, a number of simplifying assumptions must be made. The simple picture of scattering from a cloud of free electrons neglects the fact that electrons are bound to atomic nuclei. The ionisation energy has to be accounted for, and the scattering process becomes an inelastic one. The exact solution for the average energy transferred to an electron must be computed for every possible energetic state of an electron in the target, which will clearly depend on the populations of electron energy levels.

It is fortunate to note, therefore, that a considerable effort has been given to the tabulation of such data; extensive listings may be found in Chu *et al*[1]

8.2.2. The Scattering Cross Section, σ.

It has already been mentioned that only a very small number of projectiles incident on the sample undergo any kind of interaction which results in a backscattering event, but just how many is very small?

This question is addressed and answered by the scattering cross section, σ. Consider a beam of fast particles impinging on a thin, uniform target, which is significantly wider than the beam. At an angle θ to the direction of incidence, let an ideal detector count every particle scattered in the direction of the solid angle it subtends at the target, ΔΩ. If the total number of particles incident on the target is P, and the number of these particles which go on to hit the detector is ΔP, then the *differential scattering cross section* $d\sigma/d\Omega$ is given by:

$$\frac{d\sigma}{d\Omega} = \left(\frac{1}{Nt}\right)\left[\frac{\Delta P/\Delta\Omega}{P}\right] \qquad \textbf{[8.3]}$$

where N is the volume density of atoms in the target and t is its thickness. Nt is the number of atoms per unit area, or the areal density. The definition implies that ΔΩ is sufficiently small such that θ is well defined. t is also required to be small so the energy loss of particles is also small, and therefore the energy of the particles is virtually the same at any depth in the target. Finally, the total number of particles P must be large, so the quotient $\Delta P/P$ is well defined.

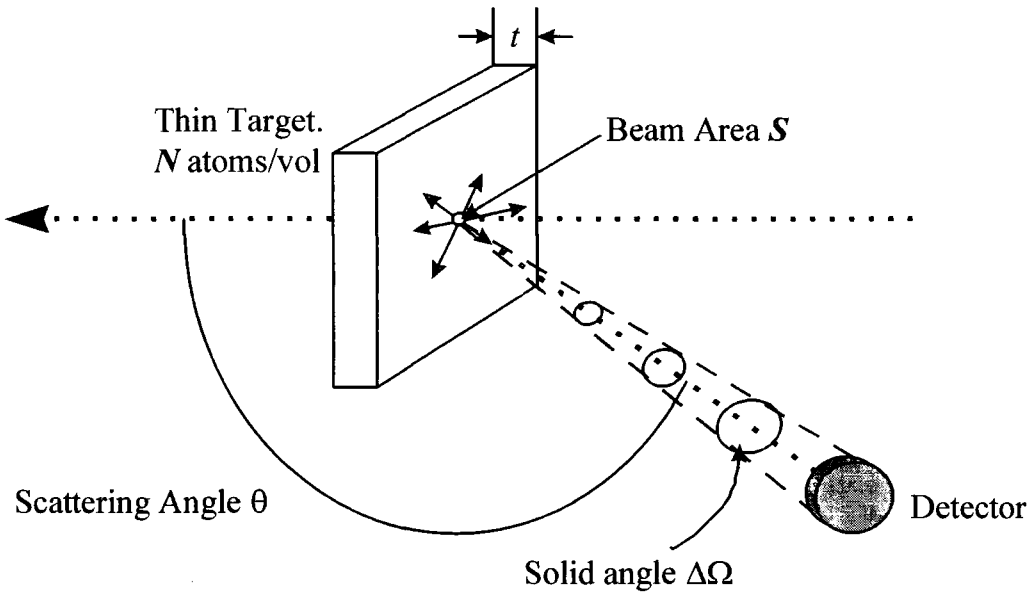

Figure 8.2 Schematic showing defining features of the Scattering Cross Section

The differential scattering cross section $d\sigma/d\Omega$ has dimensions of area, the interpretation of which when divided by the area of the incident beam is the probability that a scattering event will result in a signal at the detector, *i.e.* an atomic nucleus presents an area $d\sigma/d\Omega$ to the beam of incident particles. It is assumed that $d\sigma/d\Omega$ is small, and that the atoms of the target are randomly distributed in such a manner that their scattering cross sections do not overlap.

Unlike the stopping cross section [*q.v.*], the scattering cross section can be calculated exactly within a given physical model. In the majority of cases, the force which results in a backscattering event can be represented as a Coulombic repulsion between the two nuclei. This assumes that the distance of closest approach is large compared to nuclear dimensions ($\sim 10^{-15}$m), but small compared to the Bohr radius a_0 = 0.53Å. In this model, $d\sigma/d\Omega$ is given by the Rutherford formula:

$$\frac{d\sigma}{d\Omega} = \left[\frac{Z_1 Z_2 e^2}{4E\sin^2(\theta/2)}\right]^2 \qquad \textbf{[8.4]}$$

Here, Z_1 is the atomic number of the projectile particle with mass M_1, Z_2 is the atomic number of the target atom with mass M_2, e is the electronic charge (e = 1.609x10^{-19}C) and E is the energy of the projectile immediately before scattering.

This expression is valid when the projectile mass $M_1 << M_2$. Other formulas go on to give a general case, but these are beyond the scope of this text. The interested reader is referred to Chu's book[1]

8.2.3. The Kinematic Factor

Having discussed the features of the path taken by the analysis beam, and the likelihood of there being a scattering event, one must now consider what actually happens at the scattering centre itself. The scattering process is considered to be an elastic collision similar to that when billiard balls strike each other. In making this assumption, two conditions must be satisfied:

1) The particle energy E_0 must be much larger than the binding energy of the atoms in the target. Since chemical bonds have an energy of the order of 10eV, E_0 must be much greater than that.
2) Nuclear reactions and resonances must be absent. This imposes an upper limit on the projectile energy. Nuclear processes depend on the nature of the projectile species and the target atoms.

To formulate an expression for the energy exchange on scattering, one considers the conservation of energy and momentum. The geometry and terms for the following discussion are defined in figure 8.3., below:

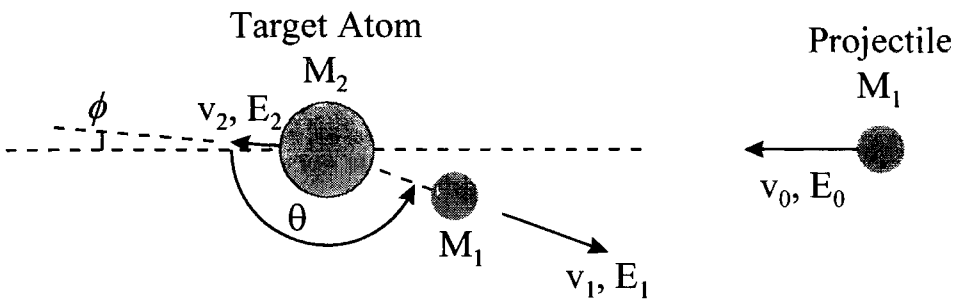

Figure 8.3 Schematic of Elastic Collision

Let v_0 be the size of the velocity of particle M_1, giving it an energy before the collision $E_0 = ½ M_1 v_0^2$. The target atom M_2 is considered to be stationary at this time. After the collision, M_1 has an energy $E_1 = ½ M_1 v_1^2$, and M_2 has an energy $E_2 = ½ M_2 v_2^2$.

Conservation of energy and momentum parallel and perpendicular to the direction of incidence are expressed by the equations:

$$\frac{1}{2} M_1 v_0^2 = \frac{1}{2} M_1 v_1^2 + \frac{1}{2} M_2 v_2^2 \qquad \textbf{[8.5]}$$

$$M_1 v_0 = M_1 v_1 \cos\theta + M_2 v_2 \cos\phi \qquad \textbf{[8.6]}$$

$$M_1 v_1 \sin\theta = M_2 v_2 \sin\phi \qquad \textbf{[8.7]}$$

Eliminating both ϕ and v_2, one finds

$$v_1/v_0 = \frac{\left[\left(M_2^2 - M_1^2 \sin^2\theta\right)^{1/2} + M_1 \cos\theta\right]}{\left(M_1 + M_2\right)} \qquad \textbf{[8.8]}$$

The *kinematic factor* is defined as the ratio of the energy after the collision to that before the collision, *i.e.*

$$K \equiv E_1/E_0 \qquad \textbf{[8.9]}$$

we obtain:

$$K_{M_2} = \left[\frac{\left(M_2^2 - M_1^2 \sin^2\theta\right)^{1/2} + M_1 \cos\theta}{M_1 + M_2}\right]^2 \qquad \textbf{[8.10]}$$

From this expression, we can see that the kinematic factor depends only on the ratios of the masses of the projectile and target atoms, and the scattering angle. In fact, for $\theta \rightarrow 180°$,

$$K_{M_2} = \left(\frac{M_2 - M_1}{M_1 + M_2}\right)^2 \qquad \textbf{[8.11]}$$

RBS is ideally suited for determining the concentration of trace elements heavier than the major constituents of the substrate. Its absolute sensitivity for light elements is poor, but the resolution between lighter atoms is great relative to

heavier ones, *e.g.* RBS can usually resolve C from N, or P from Si, but cannot resolve Fe from Ni. For a 2MeV beam, the response from a typical RBS instrument for a given element would appear as in figure 8.4.:

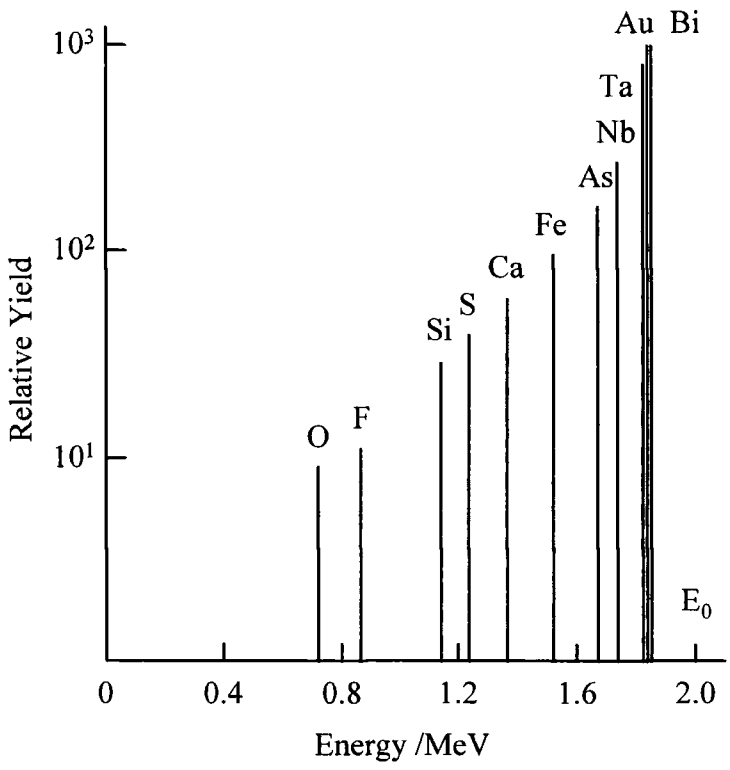

Figure 8.4 Typical Instrument Response

8.3. RBS and Polymers

It is interesting to note that Rutherford backscattering has found comparatively little use in the field of polymers.[2-8]. This is due to the comparative lack of sensitivity of the technique towards lighter elements typical of those found in organic polymers *i.e.* hydrogen, carbon and oxygen. Indeed, He^{++} will not scatter backwards from H or He atoms in a sample. Elements as light as or lighter than the projectile element will instead scatter at forward trajectories with significant energy. Thus, these elements cannot be detected using classical RBS. However,

the resolution of RBS is greater for lighter elements than heavier ones, so some of the detrimental effects from the loss of absolute sensitivity could be compensated for by these gains in resolution. The work that has been done has given a valuable insight into the interfacial properties of a number of polymer-polymer systems, and fluorine detection has featured quite strongly in these[5,9].

8.4. Experimental

8.4.1. Sample Preparation

Two attempts were made at gathering the backscattering spectrum of the polymers used in this study. In the first instance, films of blends of PMMA and 96/40 [*q.v.*] were spun cast from solution in a similar manner to that used to prepare samples for neutron reflectivity. The thicknesses of the films were also similar to those seen in the reflectivity experiments *i.e.* ~1000Å. The concentration range explored ranged from 5, 10, 20, 30 to 50% w/w 96/40 (fluoropolymer). The substrates used were silicon wafers which had been scored with a diamond-tipped glass cutter and broken to a suitable size for the RBS sample holder.

For the second set of experiments, polymer samples were pressed in a way analogous to that used to prepare samples for SANS. The concentration of fluoropolymer in these samples ranged from 5-40% in 5% intervals. The sample thickness was ~0.5mm.

It is important to note than the fluoropolymer used in the second set of experiments is not the same as was used in the first. The first set of experiments used the copolymer which was used in the SANS and neutron reflectivity

experiments, such that a direct comparison between the NR and RBS could be obtained. These samples were found to have an insufficient amount of fluorine present for RBS to detect. Therefore, the samples for the second set were from the fluorinated homopolymer (sample code 95/45), which has a higher fluorine content.

A selection of samples from each concentration was annealed at 413K for 48 hours. The remaining samples were untreated to act as a control.

8.4.2. Backscattering Spectrometry

The backscattering experiments described here took place on two occasions at the ion beam facility at the University of Surrey, Guildford. 1.8MeV α-particles were used as the analysis beam, and the take-off angle was set at 165°.This geometry optimises the resolution of the technique as well as giving maximum depth penetration.

In order to prevent the polymer samples from charging up in the beam current, it was necessary to apply a thin film of gold to act as an electrical conductor. This was achieved by placing the samples in a plasma chemical vapour deposition apparatus.

Finally, due to the high energy of the beam and the comparative lack of stability of polymeric samples to ion beam radiation, samples were cooled on a liquid nitrogen cold finger during irradiation in the beam.

Data analysis was performed on site by using a computer program called "RUMP". The results of these analyses are given below.

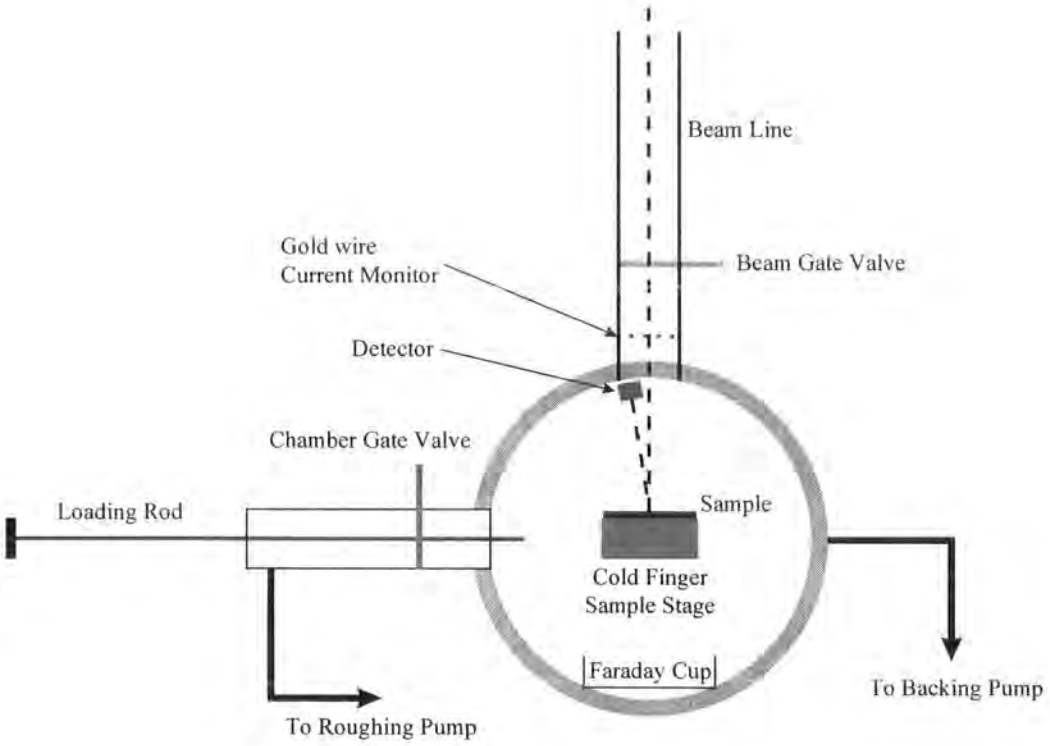

Figure 8.6 Sample Chamber of Backscattering Spectrometer

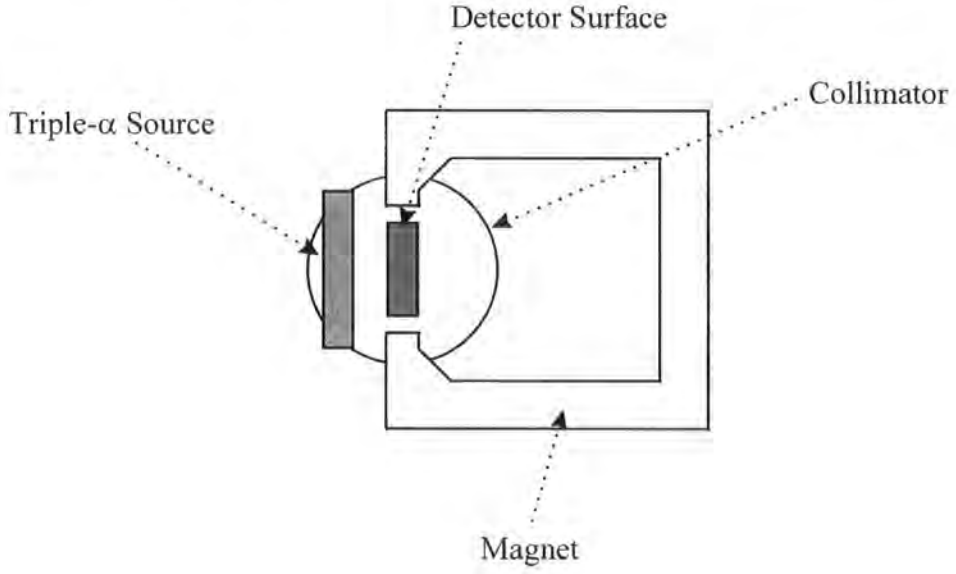

Figure 8.7 Close-up of the Detector (Plan view)

8.5. Results & Discussion

As stated earlier, two attempts were made at recording the RBS spectrum of the polymer blends studied in this work. The first experiment, in which the copolymer (96/40) featured as the fluorinated component, did not give sufficient resolution of the fluorine signal to make any quantitative assessment of the surface composition.

When the degree of fluorination was increased by the use of the fluorinated homopolyer (95/45), a better resolved signal was obtained. A typical spectrum, and its enlargement to show the region of interest, is given in figures 8.8 and 8.9 respectively:

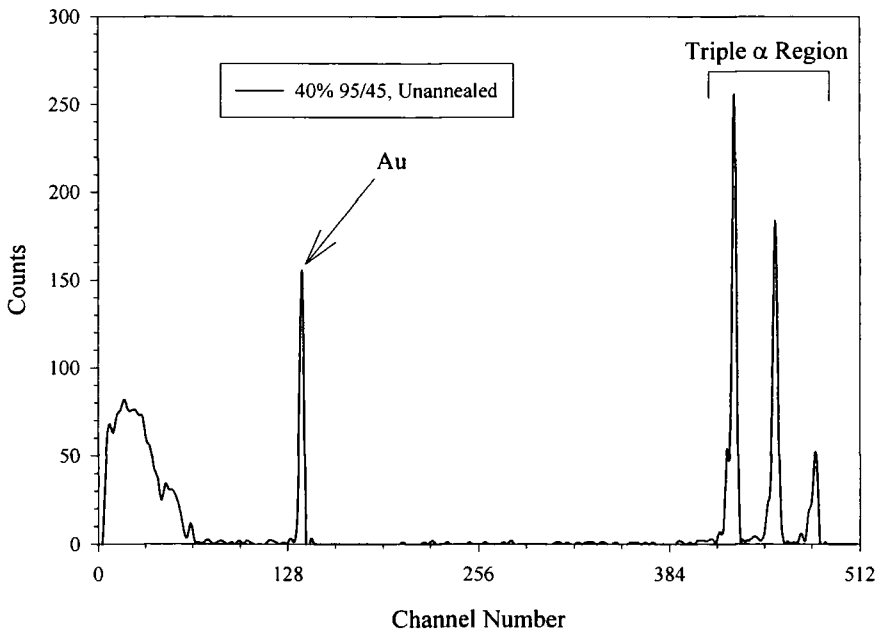

Figure 8.8 RBS spectrum

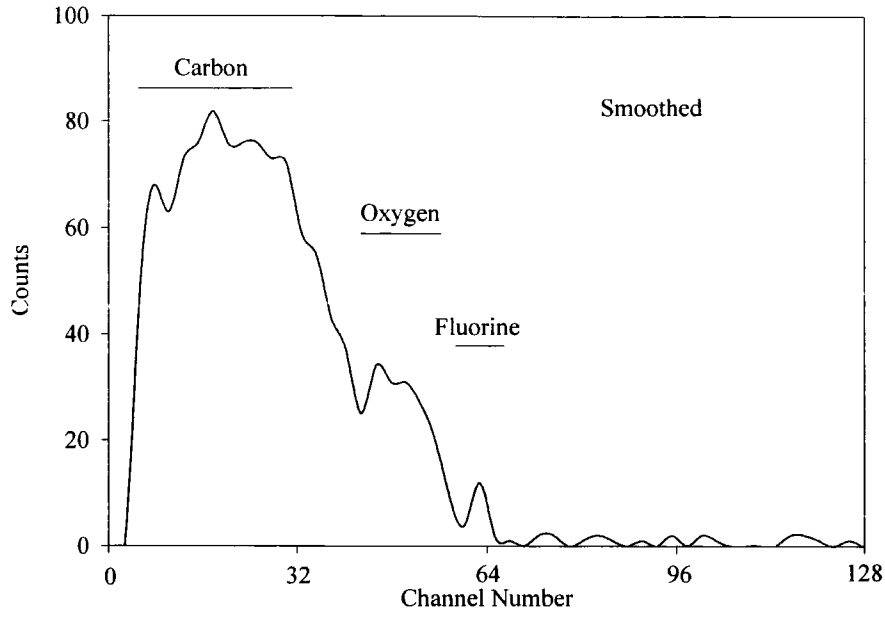

Figure 8.9 Enlargement of Fig 8.8 to show region of interest

There are a number of important features in figure 8.8 which must be discussed. The most prominent signals in the spectrum are the three lines labelled "Triple α region". These come from a calibration source near to the detector consisting of three radionucleides, ^{239}Pu, ^{244}Cm and ^{241}Am, all of which decay by α-emission to give peaks at known energies.

The second point of interest is the strong peak due to the gold which was deposited on the a sample surface to prevent the sample from charging.

Thirdly, one should note the relative intensities of the peaks. Peaks resulting from the polymer (see fig 8.9) are small relative to those from the gold coating; this reflects the difference in yield between the lighter and heavier elements (see fig 8.4).

Finally, the absolute intensity of the signal from the polymer should be considered. Of particular note is the signal from the fluorine, which, in spite of being present in a relatively high concentration, is still very small.

8.5.1. Comparison of Unannealed and Annealed Samples.

The main objective of the RBS experiments was to establish evidence for or against the surface segregation of the fluorinated polymers in blends with PMMA, such that this could be compared with the results from the neutron reflectivity studies discussed earlier. Were surface segregation going to occur, its development would normally be accelerated by annealing. Therefore, by comparing annealed and unannealed samples, one can gain an insight into the surface segregation behaviour of a given system.

The RBS spectrum of the polymer region of the 40% 95/45 blend with PMMA is shown in figure 8.10., with lower concentrations being shown in 8.11 and 8.12.

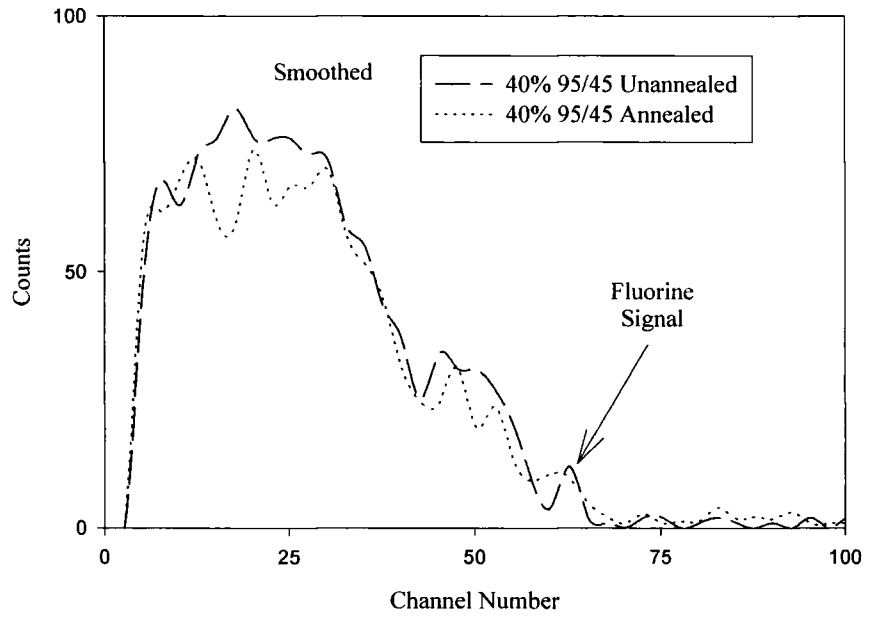

Figure 8.10 Comparison of Unannealed and Annealed Samples by RBS

40% 95/45

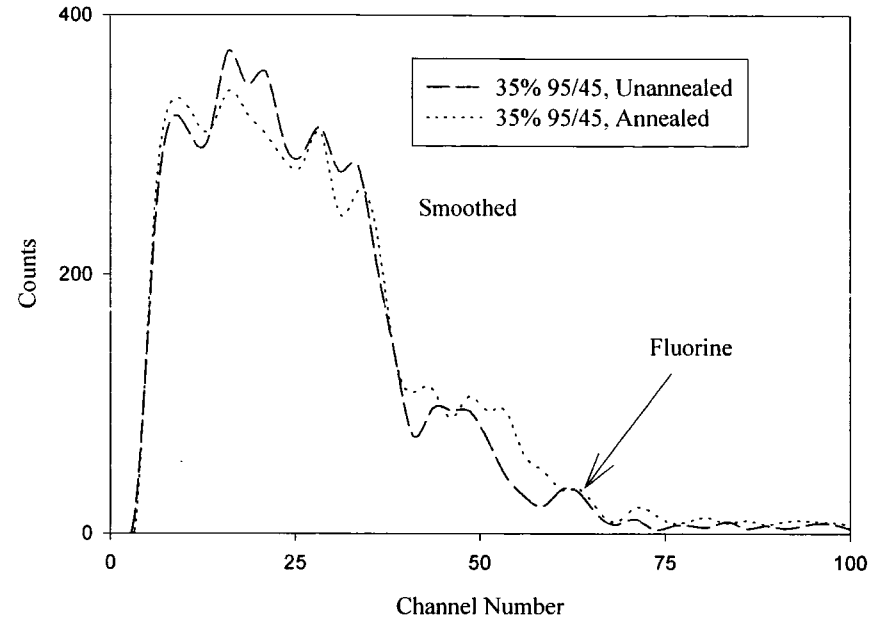

Figure 8.11 Comparison of Unannealed and Annealed Samples by RBS

35% 95/45

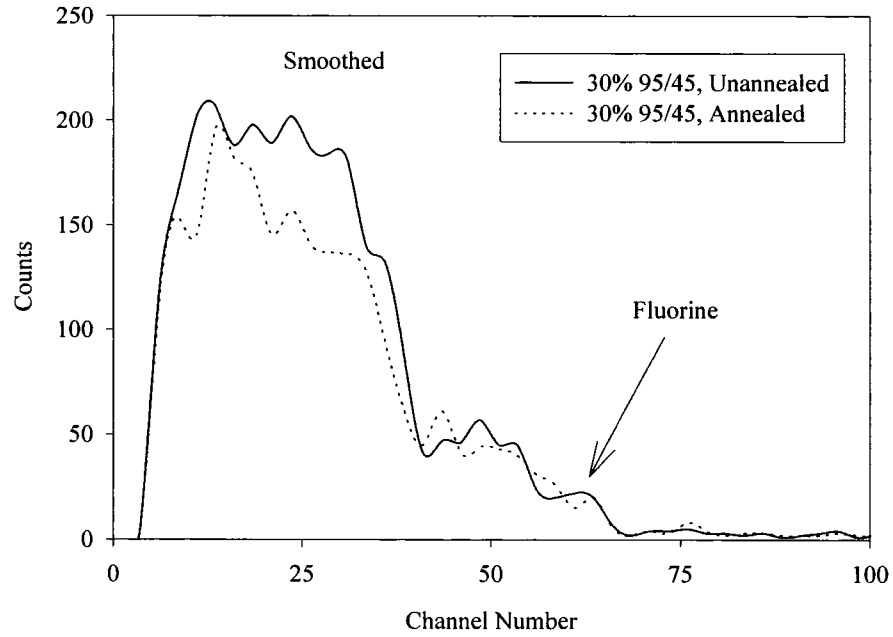

Figure 8.12 Comparison of Unannealed and Annealed Samples by RBS

30% 95/45

The main point to notice from figs 8.10 to 8.12 is that the spectra from before and after annealing are essentially the same, taking into account differences due to

different counting times. The undulations in the spectra are artefacts from the smoothing of the data.

Secondly, increases in counting times were necessary for the blends with lower concentrations of fluoropolymer, as these appear to approach the limits of sensitivity of the technique. Because of this, no spectra were recorded at fluoropolymer concentration less that 30% w/w.

8.6. Conclusions

Although the sensitivity of the technique towards light atoms is comparatively poor, the qualitative conclusions are likely to be sound. Indeed, quantitative depth profiling of surface fluorinated high- and low-density polyethylene has been successfully performed and reported by Karwacki and Bauman[10]. Therefore, the evidence from this technique suggests that no surface segregation behaviour occurs in this system. The breadth of the fluorine signal suggests that the fluorine is located uniformly throughout the sample.

8.7. References

1)Chu, W.-K.; Mayer, J. W.; Nicolet, M.-A. *Backscattering Spectrometry*; Academic Press: New York, 1978.

2)Faldi, A.; Genzer, J.; Composto, R. J.; Dozier, W. D. *Polymer Materials Science And Engineering* **1994**, *71*, 284-285.

3)Geoghegan, M.; Jones, R. A. L.; Clough, A. S.; Penfold, J. *Journal of Polymer Science Part B, Polymer Physics* **1995**, *33*, 1307-1311.

4)Green, P. F.; Palmstroem, C. J.; Mayer, J. W.; Kramer, E. J. *Macromolecules* **1985**, *18*, 501-7.

5)Hwang, S. S.; Ober, C. K.; Perutz, S.; Iyengar, D. R.; Schneggenburger, L. A.; Kramer, E. J. *Polymer* **1995**, *36*, 1321-1325.

6)Kramer, E. J.; Green, P. F.; Palmstroem, C. J. *Polymer* **1984**, *25*, 473-480.

7)Rafailovich, M. H.; Solokov, J.; Jones, R. A. L.; Krausch, G.; Klein, J.; Mills, R. *Europhysics Letters* **1988**, *5*, 657-662.

8)Valenty, S. J.; Chera, J. J.; Smith, G. A.; Katz, W.; Argani, R.; Bakhru, H. *Journal of Polymer Science, Polymer Chemistry edition* **1984**, *22*, 3367-3381.

9)van der Grinten, M. G. D.; Clough, A. S.; Shearmur, T. E.; Bongiovanni, R.; Priola, A. *Journal of Colloid and Interface Science* **1996**, *182*, 511-515.

10)Karwacki, J., E.J.,; Bauman, S. M. *Journal of Vacuum Science & Technology A* **1993**, *11*, 514-520.

Chapter Nine

Conclusions & Suggestions for Further Work

9.1.Conclusions

This work has been centred on the production and characterisation of a new family of fluoroalkyl methacrylate polymers and their blends with poly(methyl methacrylate). Partially fluorinated sidechains prepared from the telomerisation of trifluoroethene were attached to the methacrylate backbone using various synthetic methodologies.

These techniques are discussed in chapter 2, and include the use of trifluoroacetic anhydride, phosphorus pentoxide and acid and base catalysed transesterification, routes which have enjoyed a varying degree of success.

The trifluoroacetic anhydride route was highly successful in the production of a number of model compounds which were synthesised before a particular methodology was used to prepare the target monomers. However, when this route was applied to the target compounds, *i.e.* the target esters of the telomeric alcohols, this method failed to give a satisfactory yield.

The synthesis of esters using P_4O_{10} to absorb the water produced in the reaction was found to be unsuccessful on the small scales of reaction used here. However, this procedure may be more successful on a larger scale where powerful stirring is available.

Acid and base promoted transesterification reactions between the new fluoroalcohols and methyl methacrylate have also been tried, with the acid-catalysed reaction being found to be the more successful way of preparing the target monomers. This seems reasonable in that the fluoroalcohols themselves are somewhat acidic. Therefore, it is better to promote loss of methanol from the methacrylate ester than encourage the fluoroalcohol to deprotonate forming a stabilised alkoxide ion.

Monomers were characterised by the standard techniques of synthetic organic chemistry, FT-IR and NMR (^{1}H, ^{13}C, ^{19}F). Typical spectra are reproduced in the appendix. Assignment of spectra was complicated by the large number of absorbencies from the telomeric sidechain; the dispersity in length and the possibility of head-tail isomers make the rigorous identification of products essentially impossible. Partially fluorinated materials are not generally amenable to characterisation by mass spectrometry due to the electronic properties of fluorine. As a result, mass spectrometry has not been employed as a characterisation technique in this work.

One the target monomers had been prepared and characterised, a number of polymerisation techniques were used to prepare the desired polymeric materials. Initial attempts to perform the reaction in the bulk with free radical initiators generally yielded intractable samples due to secondary crosslinking. Reactions in solution were more successfully applied, although the yields were small and disappointing. Radical initiated reactions in emulsion and suspension were also explored. The emulsion reactions, when successful, were found to proceed very quickly to very high molecular weights. Reactions in suspension were less successful on the small scale used here, although they have been applied on a regular basis to methacrylate polymers on a pilot plant-scale reaction[1].

Apart from the radical-initiated reactions, anionic initiators were also investigated in an attempt to prepare polymers with a well defined molecular weight (low polydispersity). These techniques were generally unsuccessful, with essentially no polymer being recovered from these reactions. The labile protons of the fluorinated

sidechain are suspected of quenching the initiator residue in a competitive reaction to the desired polymerisation.

Once the polymers had been prepared, the solid state properties of both the pure materials and their blends with PMMA were studied by a number of methods. The first of these was differential scanning calorimetry, which was used to study the phase behaviour through the thermal properties of the materials. All the polymers were found to be amorphous.

The phase behaviour of the blended samples was elucidated by studying their glass transition as a function of composition. Single glass transition temperatures were recorded for the blends of both methanol- and ethanol telomer based polymers with PMMA over the full composition range. It is of particular interest to note that both methanol telomer derived polymer shows a sigmoidal dependence of T_g with composition, whereas the ethanol telomer variant shows the more common negative deviation from linearity.

A number of expressions which model T_g-composition behaviour were considered, and particularly that proposed by Kwei[2]. This expression has been used with some success to reproduce the T_g-composition dependencies, and using the interpretations of Lin[3], the phase behaviour of the blends was characterised by the two fitting parameters of the Kwei equation. This approach showed the PMMA:P(MeTelMA) system to be in a state of inchoate microphase separation, whereas the PMMA:P(EthTelMA) system is essentially homogeneous on the lengthscale studied by this technique.

Further to the use of Kwei's expression, the work of Lu and Weiss[4] was examined with the aim of extracting the Flory-Huggins interaction parameter directly from the DSC data. This approach reveals a small favourable interaction at low concentrations, which becomes a large unfavourable interaction at higher concentrations. This behaviour appears to be the same for both methanol and ethanol-telomer based systems, although the magnitudes of the interactions are different for the different systems.

While DSC provides information on the state of a system on the micrometer scale, SANS gives information on the molecular level. The scattering recorded from a blend system was fitted with an expression (DeGennes' random phase approximation)[5] which characterises the shape of the scattering body and the strength of interactions within the sample. Of particular interest is the ability to selectively observe one type of scatterer by the use of isotopic labelling and contrasting.

Using this technique, the properties of a methanol telomer-derived polymer have been investigated. In the concentration regime studied, a small unfavourable interaction is found, in contrast with that found at corresponding concentrations by DSC.

However, one should note that the systems under study in these two experiments are not directly comparable, the DSC study being focused on blends of homopolymers, and the SANS experiments on a PMMA:7:1 copolymer (MMA:MeTelMA) blend. In terms of simple solution theories, this should not make any difference, as these theories treat interactions as being between near neighbours only. In this representation, the copolymer can be considered to be analogous to a blend of PMMA with P(MeTelMA) at very low concentrations of fluoropolymer.

It is also necessary to look at the dimensions of χ which is derived from these different approaches. From the analysis of the DSC data using Lu and Weiss, one arrives at a χ-value which has units of mol^{-1}, whereas from SANS, the effective interaction parameter is dimensionless, defined in terms of a reference volume which corresponds to the volume of a polymer repeat unit. By converting the value of χ from DSC to have the same dimensions as that derived from SANS, we see a much smaller discrepancy (of the order of a factor of 10).

Further explanation may be derived by looking at the results from a free form expression which was used to check the validity of the results from the random phase approximation analysis. These fits suggest that, at high concentration, the scattering bodies have a spheroidal form rather than the gaussian chain which is assumed by the random phase approximation. The gaussian form factor assumed in the random phase approximation, in contrast to the more realistic spheroidal form, means that the interaction parameter is overestimated by the random phase approximation.

One possible explanation for these observations is the formation of clusters or aggregates. If one notes that the interaction parameter for this blend is unfavourable to mixing, and that aggregation or micellisation behaviour is known in block copolymer systems where one block is immiscible with the matrix, such an explanation seems plausible.

The shape of the aggregates depends on the strength of the interaction. Where the interaction between heterochains is modest, and the interaction between like chains is relatively large, the number of contacts is maximised by the formation of linear structures as shown in figure 9.1:

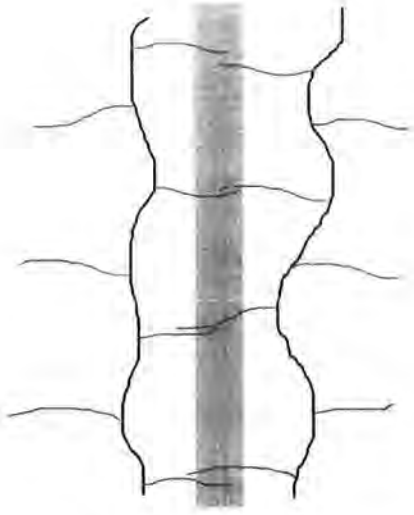

Figure 9.1 Ladder-like Aggregate

Such a structure could well develop in a three-dimensional manner, a process which is likely to lead to phase separation in the blend and also crystallinity in the pure polymer, *c.f.* crystallinity in nylons. Neither of these features have been observed.

This leaves the intramolecular interaction, whose origins are essentially the same as those of the homochain intermolecular interaction except the donor and acceptor sites reside on the same molecule. Such interactions are optimised by the aggregate adopting a spheroidal geometry, which is represented in two dimensional form in figure 7.18:

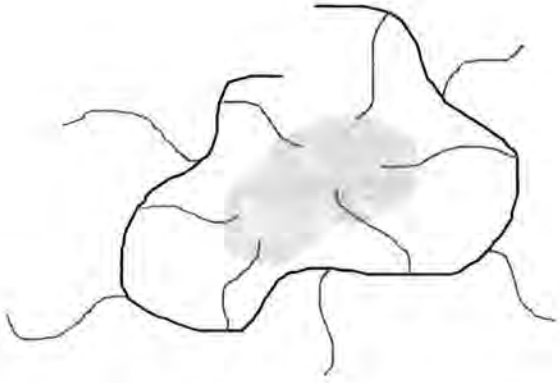

Figure 9.2 Spheroidal Aggregate

Clearly, it is necessary to speculate on the nature of the interaction responsible for this aggregation behaviour. The work of Jouannet[6] has been mentioned several times, and

this could provide two possible candidates. These workers cite the high electronegativity of fluorine atoms being influential over vicinal protons of CF_3- or -CF_2- groups, which render them amenable to the possibility of *inter* or *intra*molecular secondary bonding. Studies on PMMA:Poly(vinylidene fluoride) (PVDF) have shown that the interactions between these two miscible polymers are hydrogen bonds between the acidic vicinal protons of the PVDF and the carbonyl of the PMMA[7]. There is the possibility for a similar interaction in this system. The fluorinated sidechain has a number of highly acidic protons, which can fulfil the role of an acceptor to electrons donated by the carbonyl group of the PMMA.

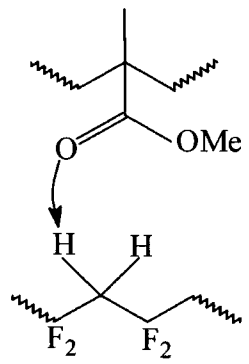

Figure 9.3 Hydrogen-bonding interaction in PMMA:PVDF

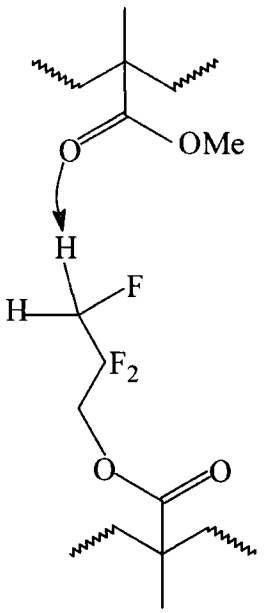

Figure 9.4 Corresponding Interaction between PMMA and *n*=1 MeTelMA

Coleman *et al* have explored such interactions using FT-IR spectroscopy[8]. Such a technique could be applied here, but for the fact that both of the blends' constituent polymers have carbonyl functionalities. These appear in a similar region of the IR spectrum, masking any effects due to secondary bonding.

As a final consideration for this type of interaction, one should consider it in terms of intramolecular bonding. Here again, Jouannet postulates the formation of rings with the acidic protons immediately adjacent to the ester-type oxygen of the ester. These can interact with the carbonyl group within the same monomer residue, forming a five-membered ring, or equally with the carbonyl of the adjacent monomer residue. This is, indeed, a possibility, but the longer sidechains studied here would exert a strenuous steric demand on the system, and the theory does not rationalise the findings of the SANS experiment, *i.e.* the fluorinated polymer exists in a spheroidal conformation. None the less, such an interaction could exist independent of the critical interaction. To overcome these reservations, one can consider an interaction between

the terminal H's and F's of the sidechain. The associative properties of HF molecules are well known. Indeed, the strength of these interactions is such that HF exists as a hexamer even in the gas phase [see, for example, Greenwood & Earnshaw[9]]. The highly polar -CH_2F and CF_2H groups at the end of the sidechains could partake in an interaction similar to HF in liquid or gas phase:

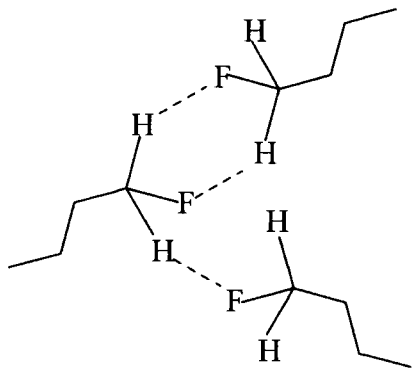

Figure 9.5 Proposed Hydrogen bonding interaction between terminal sidechain functionalities

On a larger scale, this would produce an aggregate looking like the schematic shown in figure 9.2.

It seems reasonable, therefore, to assume that the nature of this system is described by spheroidal inclusions of fluoropolymer embedded in a matrix of PMMA. A combination of the homochain interactions can lead to the formation of larger aggregates at higher concentrations, and the strength of the interaction is such that the clusters break up and shrink in diameter at higher temperatures.

That the fluorinated polymer might form aggregates could have a profound effect on the surface behaviour of these materials, and this has been investigated using a number of techniques. The first of these, contact angle measurements, showed an interesting contrast between the behaviour of the methanol- and ethanol telomer based

systems. The ethanol telomer-based systems displayed the expected behaviour, having a larger contact angle (lower surface energy) than PMMA, and was found to be enriched at the surface of films prepared from the blended polymers.

On the other hand, the contact angle behaviour of the methanol telomer based systems was found to be irreproducible, and generally smaller than that for PMMA. That such a material be enriched at the air-polymer interface *per se* is contrathermodynamic; the lower surface energy component should always be expected to be enriched at the surface[10,11].

The existence of these aggregate structures also helps to explain this low contact angle. The simplest possible explanation within this theory is that the surface under the test liquid is likely to display compositional inhomogeneity, which will result in a smaller, non-equilibrium, contact angle. Also, even if these structures are enriched at the air-polymer interface, the tying up of a number of polar sites in aggregation means that the fluorinated surface is less tightly packed and sites are available for external polar interactions such as those postulated by Ellison *et al*[12].

The surface behaviour of these systems is further described in chapters 7 and 8, where efforts to characterise the near surface depth profile are discussed.

Chapter 7 concentrates on the technique of neutron reflectivity. Thin films of a methanol telomer-based polymer blended with PMMA were studied by this method. Using a number of fitting routines, the data were analysed and the depth profiles extracted. We see that the fluorinated polymer is indeed enriched at the air-polymer interface, and this enrichment is enhanced by annealing the blends above their T_g. At

higher concentrations, the polymer-substrate interface is also enriched in fluoropolymer.

However, it is notable that the volume fraction profiles produced from these analyses are only correct in a qualitative manner only. In one instance, volume fractions less than zero are found, and in others, the concentration of polymer at the near surface exceeds the total concentration of the fluorinated polymer available in the entire film. The aggregation behaviour of the fluoropolymer may also be responsible for these effects, as it will effect the packing of the film at both the surface and in the bulk film.

Finally, chapter 8 considers the use of Rutherford backscattering spectrometry as a second depth profiling tool. This technique has a lower resolution than neutron reflectivity, but has the distinct advantage of giving the depth profile directly, without the need for model fitting or similar complex data analysis. RBS was used to study films of pure methanol telomer-derived polymer (contrast the copolymer used in the NR study) in blends with PMMA at concentrations up to 40% w/w. From these experiments, one must conclude that there is no increase in the surface concentration of fluoropolymer with annealing, a finding which seems to be at odds with those from the NR experiment. However, at the concentrations studied, it is possible that the surface is already saturated with fluoropolymer, in which case one would simply expect the layer to become thicker. Results from small angle neutron scattering show that the size of the aggregates increases with concentration. If this growth takes place by more polymer adsorbing onto the outside of the aggregate in a radial manner, it will take increasingly large amounts of polymer for a single aggregate to grow further.

9.2. Suggestions for further work

The single greatest problem which this work has encountered is the characterisation of the species present in a given batch of monomer or polymer. This problem has meant that large quantities of monomer and polymer were prepared so that, as much as possible, like was compared with like.

This problem need not have arisen until late into the project, or perhaps not at all, by noting one simple experimental fact. By far the greatest product in terms of yield in the telomerisation reactions of methanol and ethanol with trifluoroethene is the simple adduct[13], and this adduct and subsequent esters could have been characterised absolutely before any further study was undertaken. This strategy could have equally been applied even if the ultimate goal of the project was to study the properties of the longer telomeric esters, as a basic set of characterised compounds would have been available for comparison. However, the technological driving force behind this work maintained that it was more desirable to study polymers with the longer, telomeric sidechains, and this technology-based opinion prevailed over the more scientific one offered above.

While the synthesis of the telomeric esters also proved difficult at the time, this problem has been solved by other workers[14].

Apart from a more systematic approach to the synthesis and characterisation of the pure telomeric ester-derived polymers, the most obvious area for further investigation is the extended study of the aggregation behaviour of these systems. It should be emphasised that the existence of these aggregates is simply a theory to explain the

observations made during this work, and there is little, if any, direct experimental evidence for their existence. Small angle neutron scattering, in combination with the more rigorous synthetic techniques called for above, could be used to gather further information on this interesting property of this system.

If this aggregation behaviour is demonstrated to be correct, a number of interesting properties could be investigated. Considerable interest has been registered in the use of fluorinated materials as surfactants in super critical fluid technology. Fluoropolymers are known to be miscible in supercritical CO_2 ($scCO_2$), in contrast to many hydrogenous monomers and polymers[15]. Therefore, not only may these materials be polymerisable in supercritical CO_2, they may also act as surface active materials which enable the polymerisation of $scCO_2$-phobic materials in an emulsion-like process. Careful selection of fluorosurfactants has already enabled $scCO_2$ technology to be applied to the polymerisation of a number of commercially important vinyl monomers[16,17], a development with clear industrial and environmental importance.

Surfactants are also used in emulsion and suspension polymerisations, technology which is currently employed to a number of vinyl monomer systems. The use of these materials in such an environment could aid the polymerisation of other fluorinated materials which may be stabilised in the interior of the aggregates.

Partially fluorinated materials could also feature heavily in another field of science which is showing enormous growth and continuing vast potential, notably biocompatibility. At present, many contact lenses are prepared from fluoroalkyl

methacrylate systems because of their favourable optical and biocompatible properties. There biocompatibility could be further enhanced by the increased wettability by polar liquids offered by the materials developed in this work, whilst perhaps retaining some of the optical properties required for this application. Given the amphiphilic behaviour observed here, the lipophobic properties for which fluoropolymers are also known may also be observed by these systems.

9.3. References

1)Chisholm, M. S., Personal Communication.

2)Kwei, T. K. *J. Polym. Sci.: Polym. Lett. Ed* **1984**, *22*, 307-313.

3)Lin, A. A.; Kwei, T. K.; Reiser, A. *Macromolecules* **1989**, *22*, 4112-4119.

4)Lu, X.; Weiss, R. A. *Macromolecules* **1992**, *25*, 3242-3246.

5)De Gennes, P. G. *Scaling Concepts in Polymer Physics*; Cornell University Press:, 1979.

6)Jouannet, D.; Pham, T.-N.; Pimbert, S.; Levesque, G. *Polymer* **1997**, *38*, 5137-5147.

7)Leonard, C.; Halary, J. L.; Monnerie, L. *Polymer* **1985**, *26*, 1507-1513.

8)Coleman, M. M.; Painter, P. C. *Hydrogen Bonded Polymer Blends*; Coleman, M. M.; Painter, P. C., Ed.; Pergamon: London, 1995; Vol. 20, pp 1-59.

9)Greenwood, N. N.; Earnshaw, A. *Chemistry of the Elements*; Pergamon Press: Oxford, 1984.

10)Wu, S. *Polymer Interface & Adhesion*; Marcel Dekker: New York, 1982.

11)Jones, R. A. L.; Kramer, E. J. *Polymer* **1993**, *34*, 115-118.

12)Ellison, A. H.; Fox, H. W.; Zisman, W. A. *Journal of Physical Chemistry* **1953**, *57*, 622.

13)Gilani, A. H. S. ; Gilani, A. H. S., Ed.; University of Durham,: Durham,, 1997.

14)Powell, R. L., Personal Communication.

15)Johns, K. *Supercritical Fluids for Coatings from analysis to Xenon: A brief Overview*; Johns, K., Ed.; Paint Research Association: Munich, 1997.

16)Adamski, F. A.; Beckman, E. J. *Macromolecules* **1994**, *27*, 312-314.

17)Watkins, J. J. *Macromolecules* **1995**, *28*, 4067-4074.

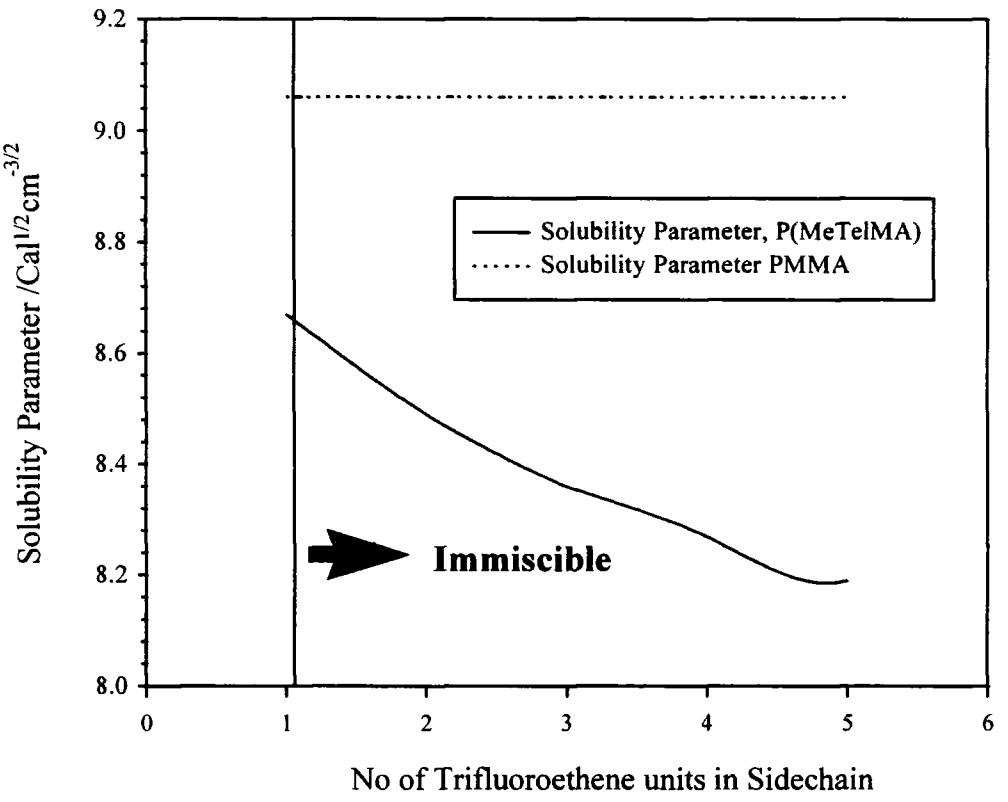

Solubility Parameter Calculation to Predict Miscibility between PMMA and P(PeTelMA) with different lengths of sidechain

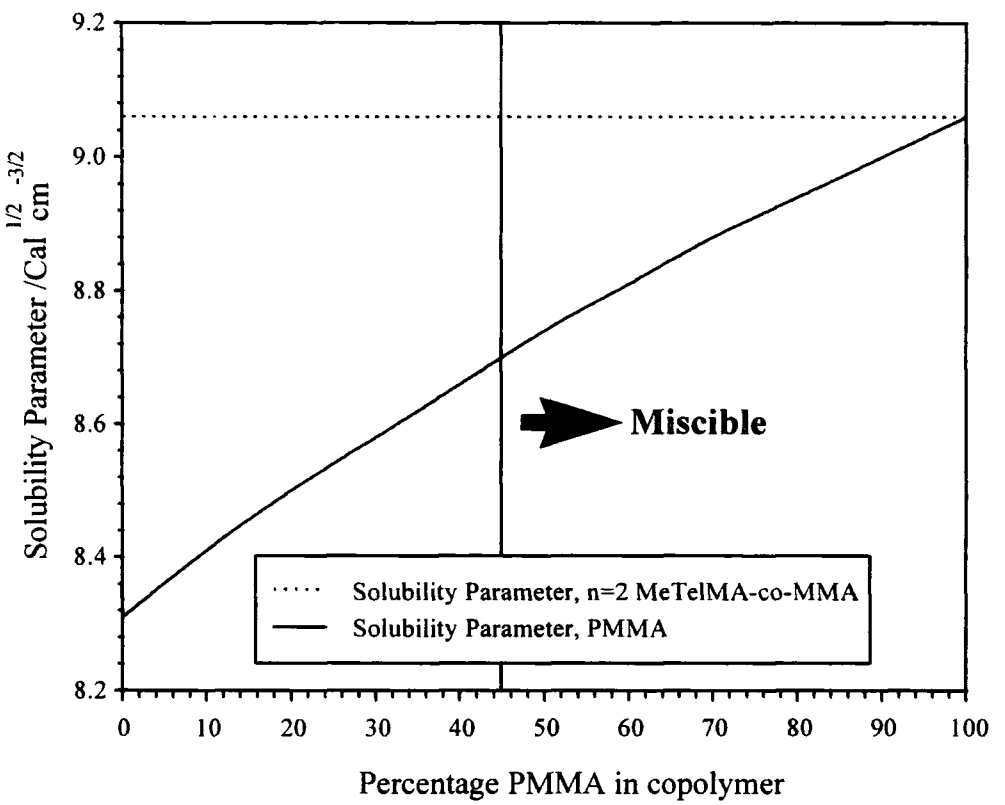

Solubility Parameter Calculation to Predict Miscibility between PMMA and n=2 P(MeTelMA). The compositions where miscibility is predicted lie to the right of the vertical line

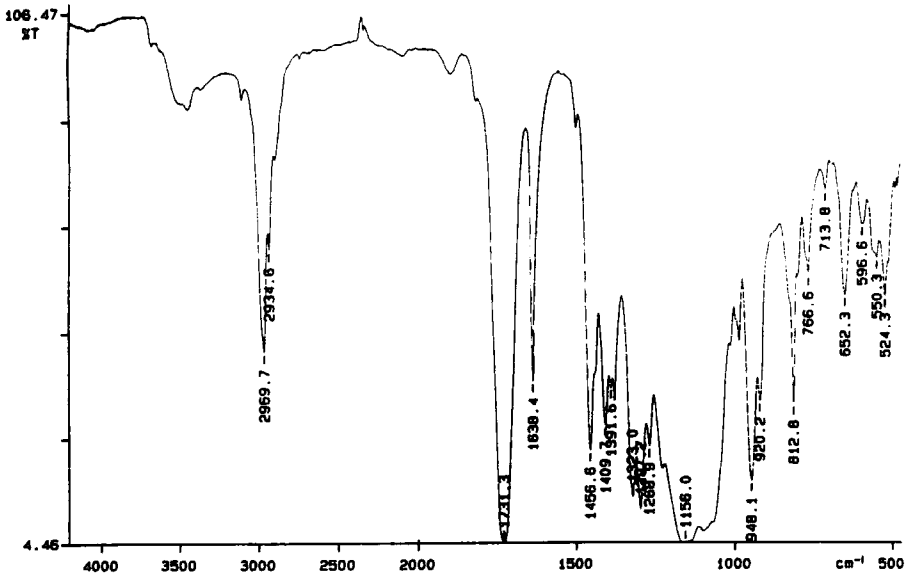

Methacrylate ester of Methanol-derived Telomer, MeTelMA

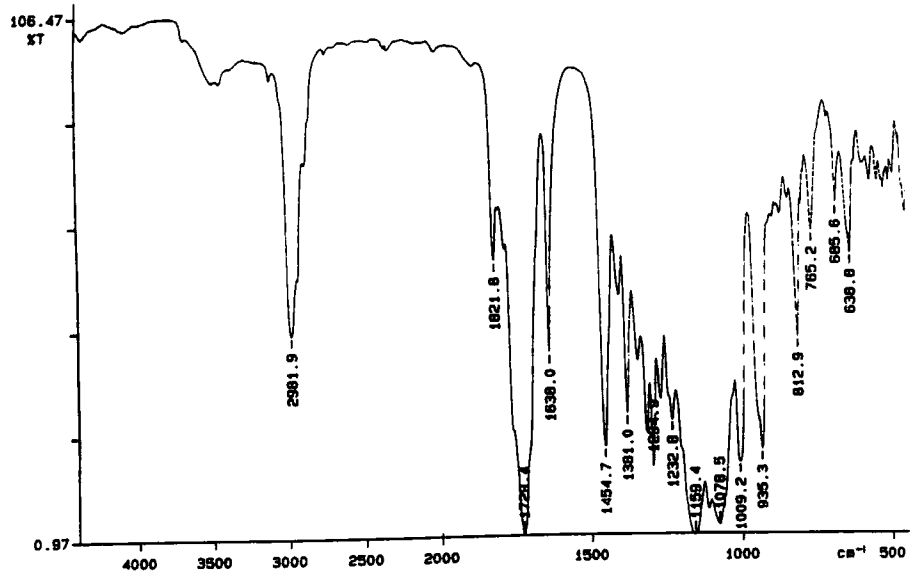

Methacrylate ester of Ethanol-derived Telomer, EthTelMA

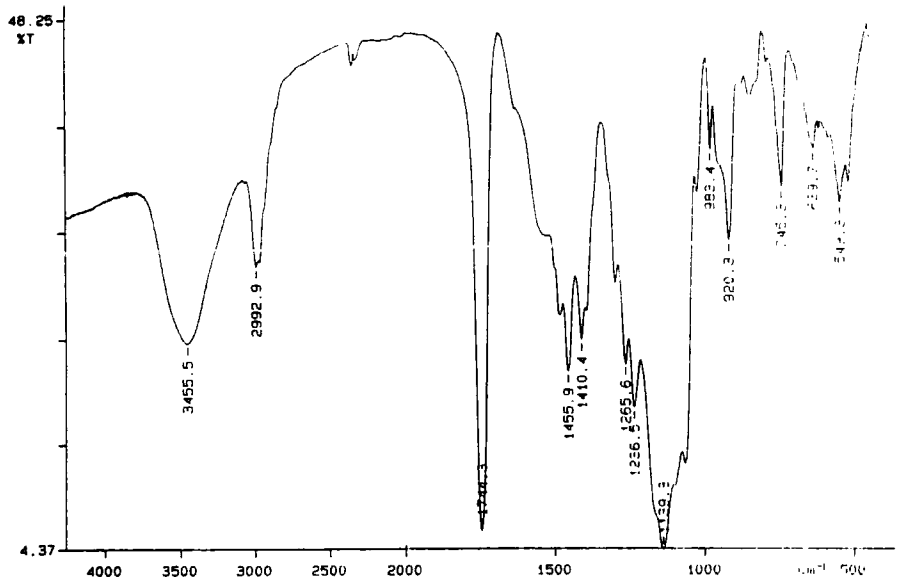

Poly(MeTelMA)

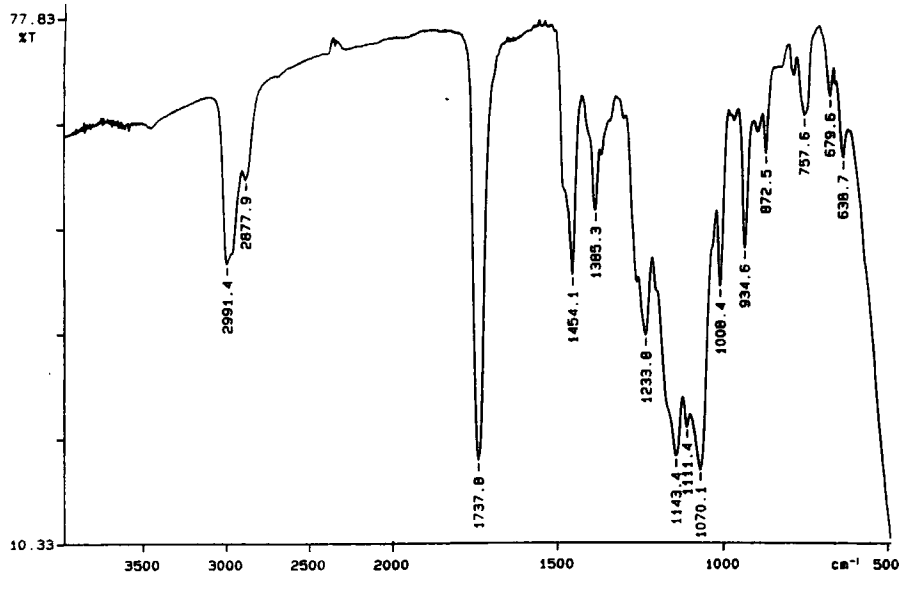

Poly(EthTelMA)

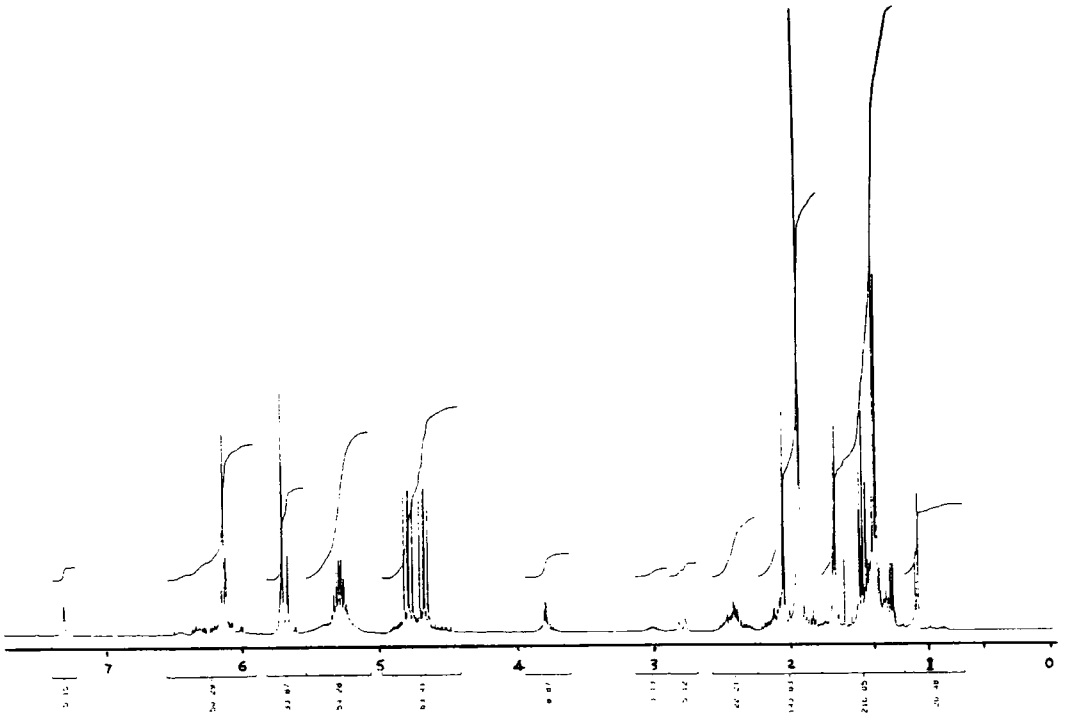

^{1}H NMR, MeTelMA

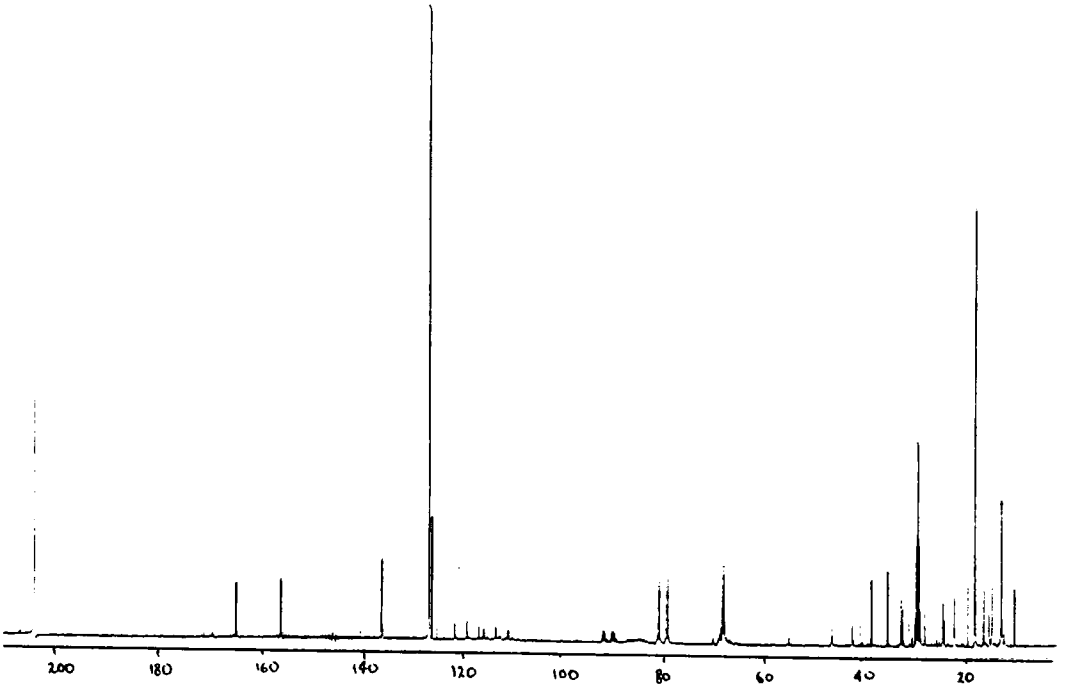

^{13}C NMR, MeTelMA

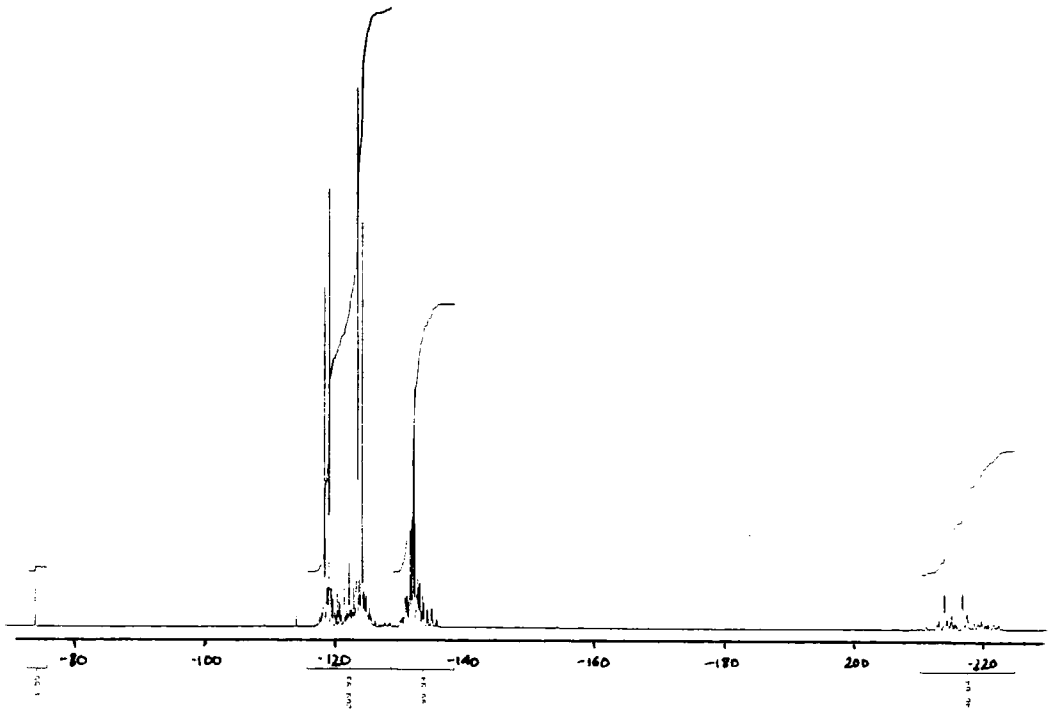

^{19}F NMR, MeTelMA

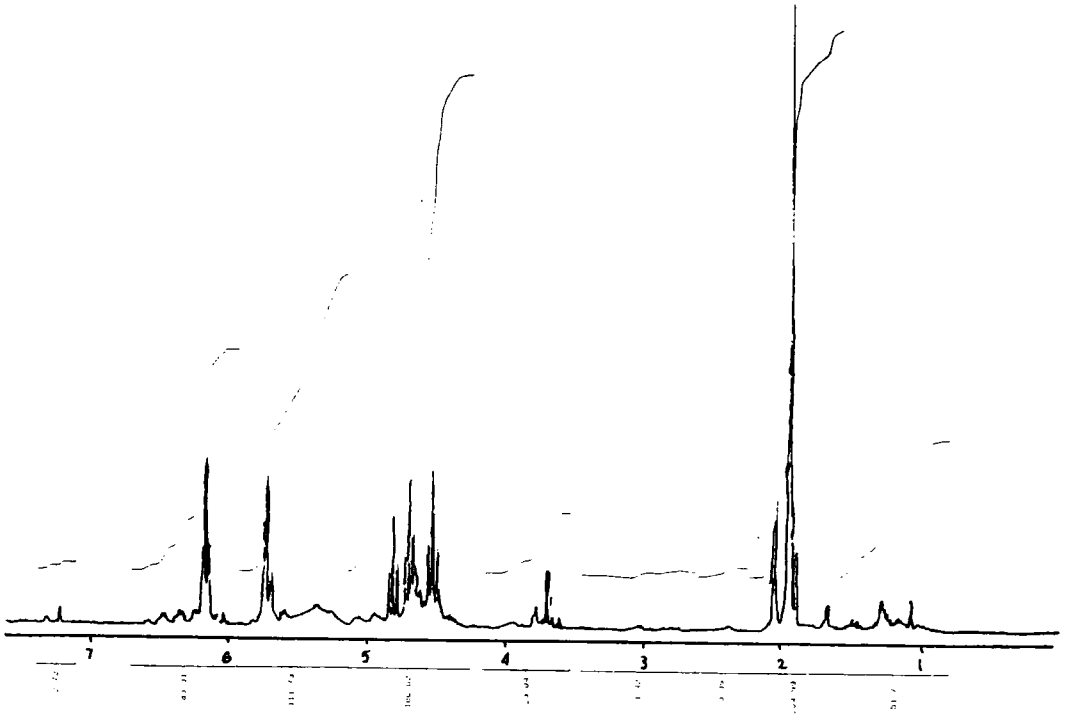

^{1}H NMR, EthTelMA

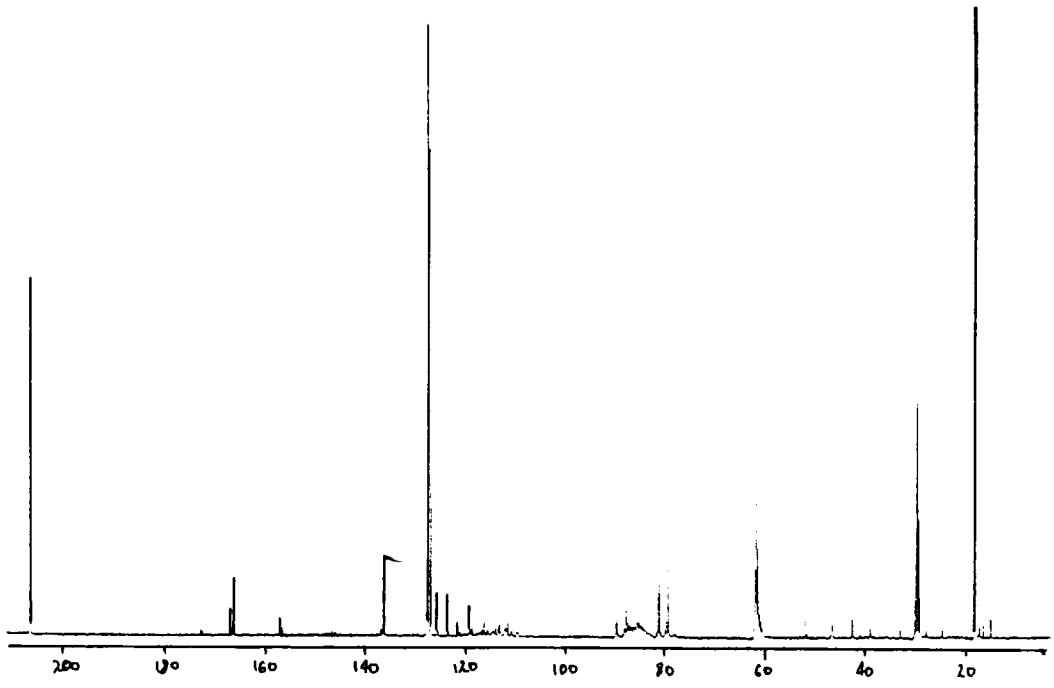

^{13}C NMR, EthTelMA

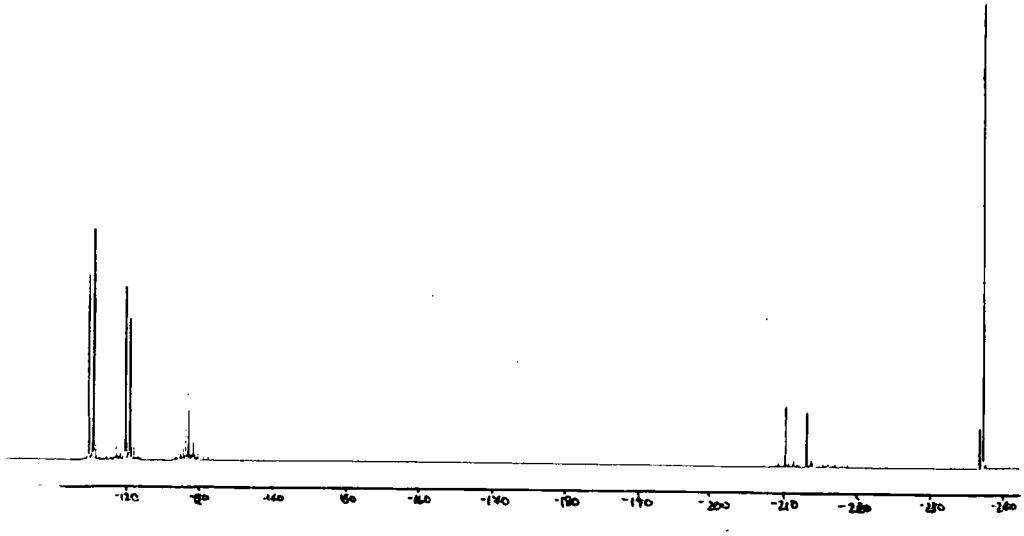

^{19}F NMR EthTelMA

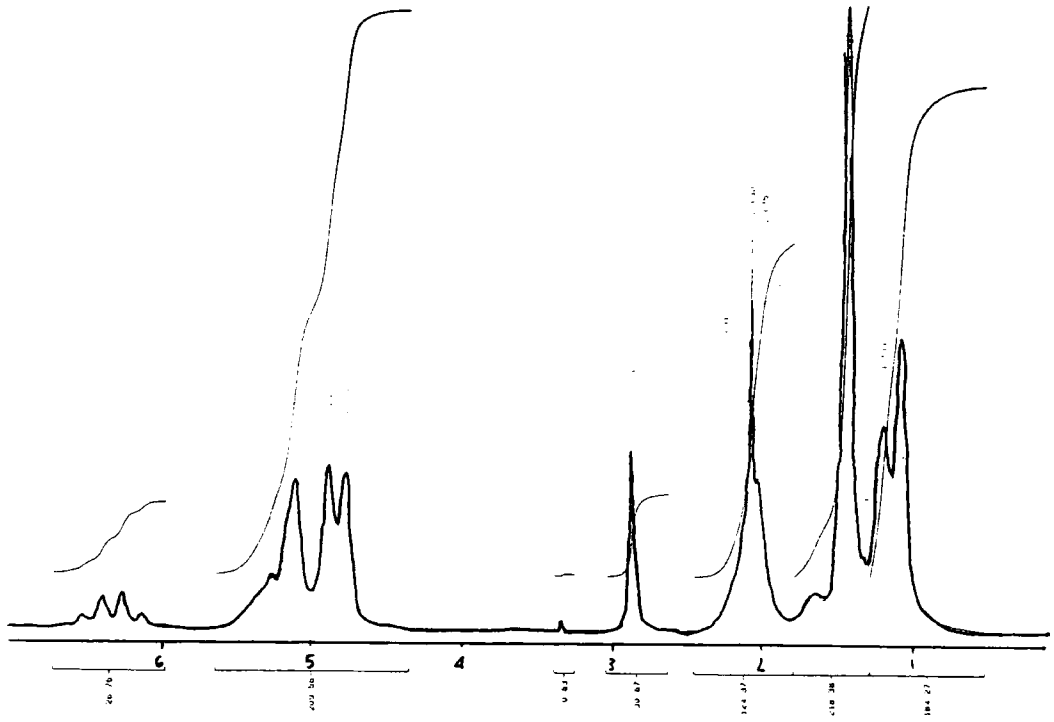

^{1}H NMR Telomeric Ester-derived Methacrylate Polymer

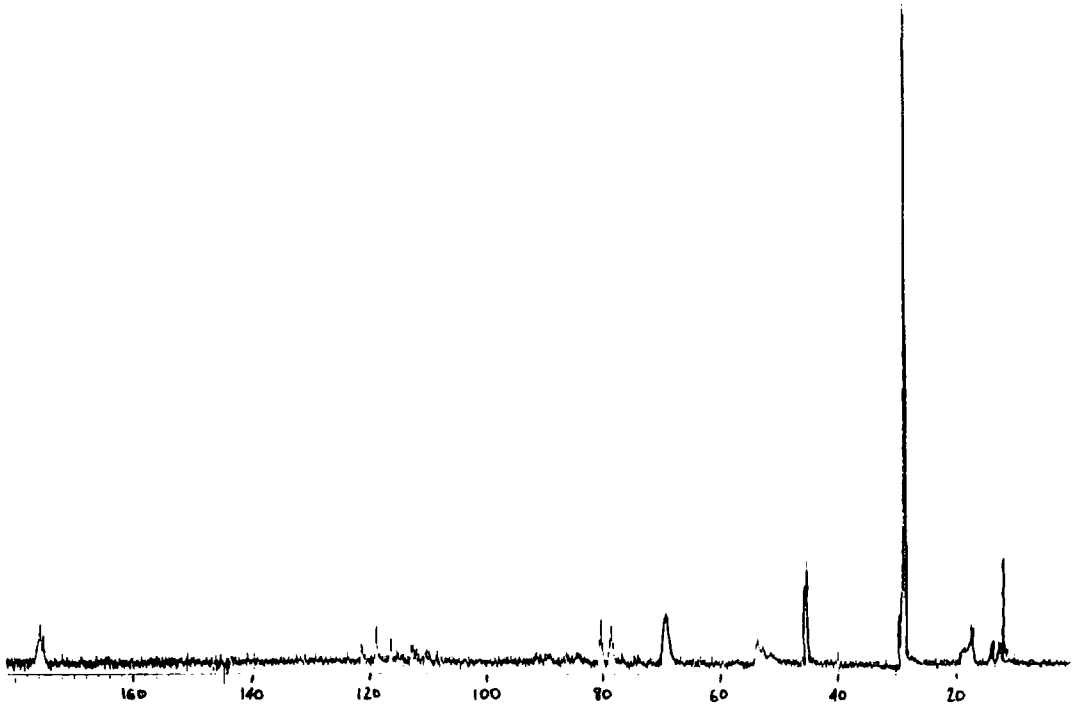

^{13}C NMR Telomeric Ester-derived Methacrylate Polymer

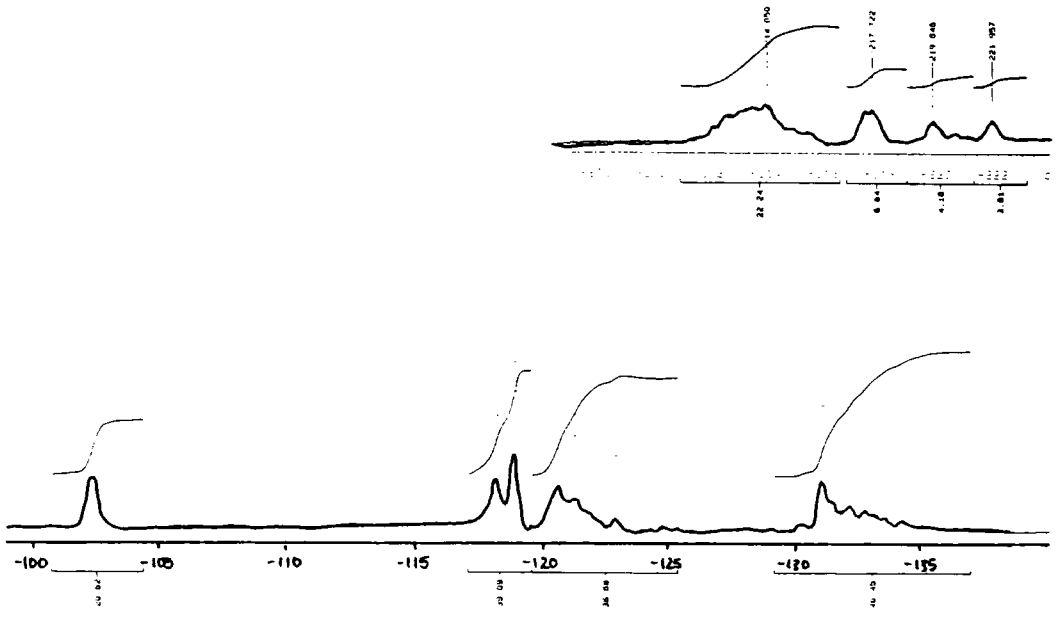

^{19}F NMR Telomeric Ester-derived Methacrylate Polymer

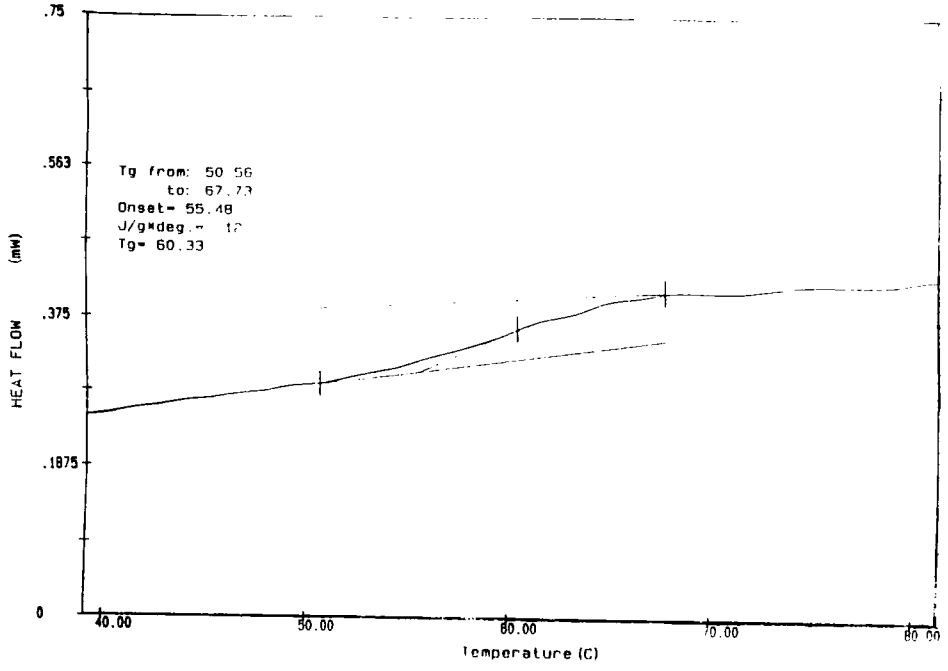

Poly(MeTelMA)

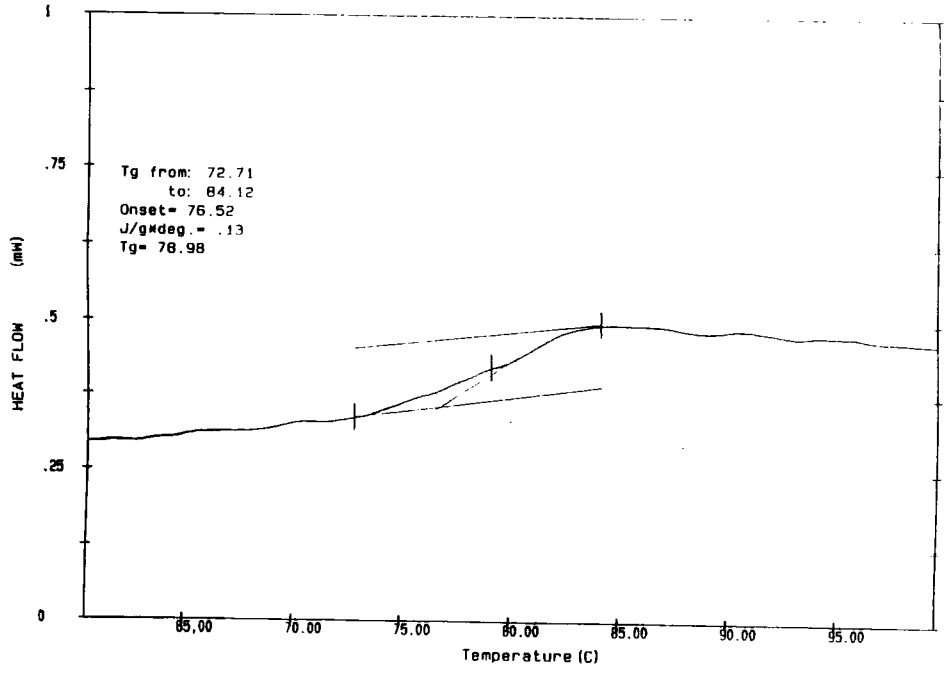

Poly(EthTelMA)

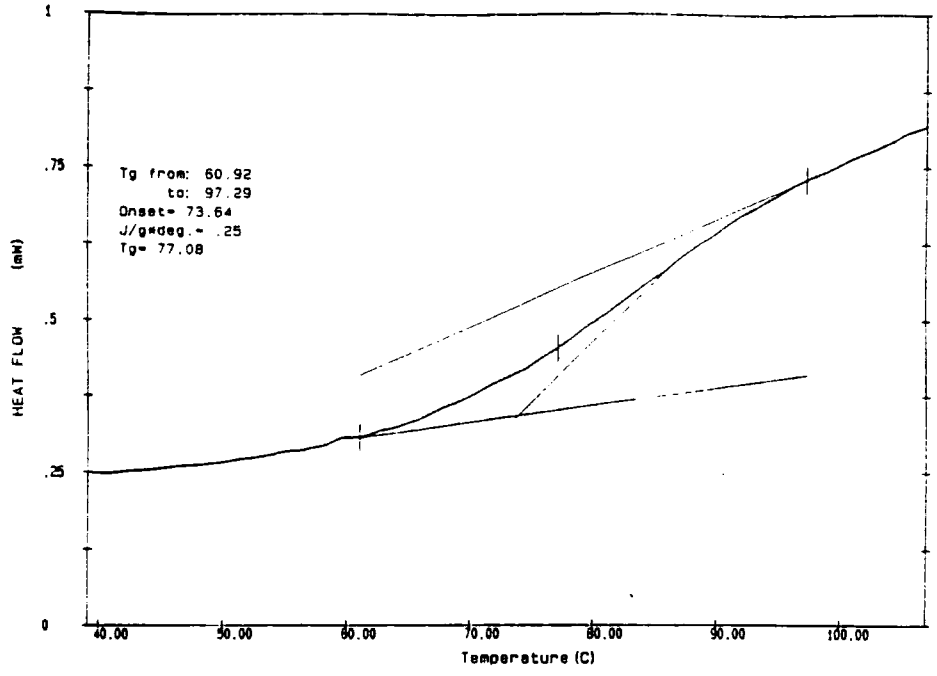

PMMA:P(MeTelMA) 1:5 Blend

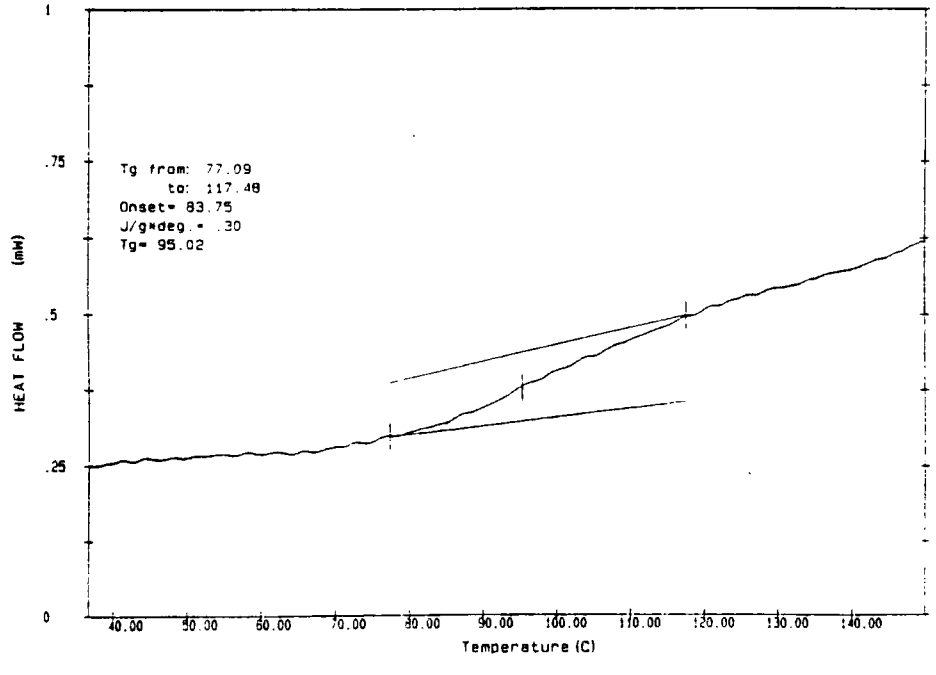

PMMA:P(EthTelMA) 1:1 Blend

Lectures & Colloquia Attended

1994

October 5 Prof. N. L. Owen, Brigham Young University, Utah, USA
Determining Molecular Structure - the INADEQUATE NMR way

November 2 Dr P. G. Edwards, University of Wales, Cardiff
The Manipulation of Electronic and Structural Diversity in Metal Complexes - New Ligands

November 9 Dr G. Hogarth, University College, London
New Vistas in Metal-imido Chemistry

November 23 Dr J. M. J. Williams, University of Loughborough
New Approaches to Asymmetric Catalysis

December 7 Prof. D. Briggs, ICI and University of Durham
Surface Mass Spectrometry

1995

January 18 Dr G. Rumbles, Imperial College, London
Real or Imaginary Third Order Non-linear Optical Materials

February 1 Dr T. Cosgrove, Bristol University
Polymers do it at Interfaces

February 8 Dr D. O'Hare, Oxford University

Synthesis and Solid-state Properties of Poly-, Oligo- and Multidecker Metallocenes

March 1 Dr M. Rosseinsky, Oxford University

Fullerene Intercalation Chemistry

May 30 Prof P. Calvert University of Arizona, USA

Freeforming: Chemical Methods for the processing of polymers, ceramics & composites

November 17 Prof. David Bergbreiter, Texas A&M, USA

Design of Smart Catalysts, Substrates and Surfaces from Simple Polymers

November 22 Prof. I Soutar, Lancaster University

A Water of Glass? Luminescence Studies of Water-Soluble Polymers.

1996

January 10 Dr Bill Henderson, Waikato University, NZ

Electrospray Mass Spectrometry - a new sporting technique

January 17 Prof. J. W. Emsley , Southampton University

Liquid Crystals: More than Meets the Eye

January 31 Dr J. Penfold, Rutherford Appleton Laboratory,

Soft Soap and Surfaces

February 28 Prof. E. W. Randall, Queen Mary & Westfield College

New Perspectives in NMR Imaging

March 12 RSC Endowed Lecture - Prof. V. Balzani, Univ of Bologna

Supramolecular Photochemistry

October 22 Professor B. J. Tighe, Department of Molecular Sciences and Chemistry, University of Aston

Making Polymers for Biomedical Application - can we meet Nature's Challenge?

Joint lecture with the Institute of Materials

October 23 Professor H. Ringsdorf (Perkin Centenary Lecture), Johannes Gutenberg-Universitat, Mainz, Germany

Function Based on Organisation

October 29 Professor D. M. Knight, Department of Philosophy, University of Durham.

The Purpose of Experiment - A Look at Davy and Faraday

November 12 Professor R. J. Young, Manchester Materials Centre, UMIST

New Materials - Fact or Fantasy?

Joint Lecture with Zeneca & RSC

November 18 Professor G. A. Olah, University of Southern California, USA

Crossing Conventional Lines in my Chemistry of the Elements

November 20 Professor J. Earnshaw, Deptartment of Physics, Belfast

Surface Light Scattering: Ripples and Relaxation

November 27 Dr Richard Templer, Imperial College, London

Molecular Tubes and Sponges

December 3 Professor D. Phillips, Imperial College, London

"A Little Light Relief" -

December 4 Professor K. Muller-Dethlefs, York University

Chemical Applications of Very High Resolution ZEKE Photoelectron Spectroscopy

1997

January 22 Dr Neil Cooley, BP Chemicals, Sunbury

Synthesis and Properties of Alternating Polyketones

February 19 Professor Brian Hayden, University of Southampton

The Dynamics of Dissociation at Surfaces and Fuel Cell Catalysts

March 11 Dr A. D. Taylor, ISIS Facility, Rutherford Appleton Laboratory

Expanding the Frontiers of Neutron Scattering

March 19 Dr Katharine Reid, University of Nottingham

Probing Dynamical Processes with Photoelectrons

Conferences & Courses Attended

1995

January	IRC Polymer Physics Introduction Course, University of Leeds
April	MACRO Group UK Meeting, Loughborough University

1996

August	Neutron & Muon Beam Users Meeting, Rutherford-Appleton Laboratory, Oxfordshire.

1997

February	Fluorine in Coatings II, Munich, Germany.